Fluid Dynamic Studies in Support of an Industrial Ebullated Bed Hydroprocessor

Dominic Pjontek

Thesis submitted to the
Faculty of Graduate and Postdoctoral Studies
in partial fulfillment of the requirements for the degree of
Doctor of Philosophy

In

Department of Chemical and Biological Engineering
Faculty of Engineering
University of Ottawa

Abstract

Commercial ebullated bed hydroprocessors, such as the LC-Finer[SM], are used for the production of synthetic crude oil by upgrading bitumen extracted from the Alberta oil sands. The objective of this thesis was to investigate the impact of an increased vacuum distillation tower bottoms feed fraction on the reactor fluid dynamics (e.g., bed and freeboard phase holdups, bubble characteristics and local fluidization behaviour). Industrial conditions were simulated in a high pressure gas-liquid-solid fluidization system based on dimensional and geometric similitude. Considering important geometric characteristics and matching dimensionless groups, base-case conditions resulted in an ebullated bed of nitrogen, 0.5 wt.% aqueous ethanol, and aluminum cylinders (average lengths and diameters of 7.5 and 3.2 mm, respectively) operating at 6.5 MPa and a gas-to-liquid superficial velocity ratio of 0.78.

The proposed scale-down method resulted in high gas holdup conditions similar to industrial measurements. The use of the Sauter mean diameter to account for particle size and shape at the simulation conditions was investigated by comparing glass spheres with diameters of 4 and 1.5 mm to aluminum cylinders with equivalent volume-to-surface area ratios. Local bubble characteristics, including gas holdups, bubble rise velocities, and chord lengths, were then investigated under various operating conditions using a monofibre optical probe. Overall fluid dynamics were studied when increasing the liquid viscosity and varying the gas and liquid superficial velocities due to their relevance for industrial ebullated bed hydroprocessors. Freeboard and bed region gas holdup relations were studied and correlations were developed for gas and solid holdups at the simulation conditions based on the dimensionless groups.

Mesophase generation in hydroprocessors due to undesired secondary reactions was also considered for an increased vacuum residue feed fraction. Adding a dispersed immiscible liquid phase which preferentially wetted the particles was therefore experimentally studied at non-simulating conditions using nitrogen, biodiesel, glycerol and various particles, where fluidization behaviour and phase holdups were considerably affected due to particle clustering. A study on the impacts of particle size, shape and material demonstrated the influences of fluid and particle properties, specifically the relative surface energies and viscous forces, on agglomeration due to interparticle liquid bridging.

Résumé

Les hydroprocesseurs à lit fluidisé triphasé commerciaux, tel que le LC-Finer^{SM}, sont utilisés pour la production de pétrole brut synthétique par la valorisation du bitume extrait des sables bitumineux de l'Alberta. L'objectif de cette thèse est d'étudier l'impact d'une augmentation de résidus de distillation sous vide dans l'alimentation sur la dynamique des fluides du réacteur (par exemple, les rétentions de phases dans le lit et au-dessus du lit, les caractéristiques de bulles et le comportement de fluidisation local). Les conditions industrielles ont été simulées dans un lit fluidisé gaz-liquide-solide à haute pression selon une analyse dimensionnelle. En considérant les caractéristiques géométriques importantes et des groupes adimensionnels équivalents, les conditions de base résultantes sont un lit triphasé d'azote, d'une solution aqueuse de 0.5 m% d'éthanol et de cylindres d'aluminium (longueur et diamètre de 7.5 et 3.2 mm, respectivement) opérant à 6.5 MPa avec un ratio de vitesses superficielles gaz-liquide de 0.78.

La méthode de mise à l'échelle proposée a entraîné des conditions à haute rétention de gaz semblables aux mesures industrielles. L'utilisation du diamètre surface-volume moyen pour modéliser la taille et la forme des particules aux conditions de simulation a été étudiée en comparant des sphères de verre avec des diamètres de 4 mm et de 1.5 mm à des cylindres en aluminium avec des rapports surface-volume équivalents. Les caractéristiques de bulles locales, y compris les rétentions de gaz, les vitesses de montée des bulles et les longueurs de cordes, ont ensuite été étudiées à diverses conditions d'opération en utilisant une sonde optique à monofibre. L'hydrodynamique global du lit fluidisé a été étudiée en augmentant la viscosité du liquide et en variant les vitesses superficielles du gaz et du liquide en raison de leur impact sur les hydroprocesseurs de lit triphasé industrielles. La relation entre les rétentions de gaz dans les régions au-dessus et dans le lit fluidisé a été étudiée et des corrélations ont été développées selon des groupes adimensionnels pour les rétentions de gaz et de solides aux conditions de simulation.

La génération de mésophase par des réactions secondaires indésirables dans les hydroprocesseurs lors d'une augmentation de résidus sous vide dans l'alimentation a aussi été considérée. L'ajout d'une phase liquide non miscible et dispersée qui mouille préférentiellement les particules a donc été étudié expérimentalement en utilisant de l'azote,

du biodiésel, de la glycérine et diverses particules. Le comportement de fluidisation et les rétentions de phases ont été considérablement affectés par l'agglomération des particules. Une étude sur les effets de la taille, de la forme et du matériel des particules a démontré l'influence des propriétés des fluides et des particules, plus spécifiquement des énergies de surface relatives et des forces visqueuses, sur l'agglomération suivant la formation de ponts liquides interparticulaires.

Statement of Contributions of Collaborators

I hereby declare that I am the sole author of this thesis. I have performed the experimental studies and subsequent data analysis and I have written all of the chapters contained in this thesis.

My supervisor, Dr. Arturo Macchi, and industrial collaborators, Craig McKnight and Jason Wiens from Syncrude Canada Ltd., provided continual support and guidance throughout this work. They also contributed with many helpful editorial comments and corrections.

Experiments related to the paper presented in Chapter 3 were performed with the help of Valois Parisien during the winter of 2012. He is a coauthor to the paper presented in the previous chapter.

Experiments and the literature review related to the paper presented in Chapter 5 were assisted by Jérôme Landry during the summer of 2010. He is a coauthor to the paper presented in the previous chapter.

The experimental system construction and contact angle measurements related to the paper presented in Chapter 6 were carried out with the help of Valois Parisien during the summer of 2011 and fall of 2013, respectively. Experiments for the previous chapter were performed with the help of Connor Farrell during the summer of 2013. They are coauthors to the paper presented in the previous chapter.

Acknowledgments

I would first like to express my sincere gratitude to my supervisor, Dr. Arturo Macchi, for giving me the opportunity to work on this project and for his continuous support, guidance and inspiration throughout my graduate studies. I truly appreciate our many discussions and his mentoring with respect to the various aspects of academic research.

I would like to thank Syncrude Canada Ltd. for believing in this project and for their generosity in sponsoring the work. I would like to particularly thank Craig McKnight, Jason Wiens, Larry Hackman and Kevin Reid from Syncrude Canada Ltd. for their insight, support and guidance throughout this research program.

I would like to thank the National Science and Engineering Research Council for providing me with financial support and for funding this research project. I would also like to thank the Canadian Foundation for Innovation and the Ontario Innovation Trust for financially supporting this project.

I would like to sincerely thank Valois Parisien for his assistance during experiments and/or various research tasks related to the local bubble characteristics and particle agglomeration studies. I would also like to thank my fellow group members, particularly Patrick Plouffe, Denis Myre, Jérôme Landry, Connor Farrell and André Guerra for their help.

I would also like to thank the technical staff in the Department of Chemical and Biological Engineering, Louis Tremblay, Franco Ziroldo and Gérard Nina, for their assistance during the high pressure system maintenance as well as for their guidance during the construction and design of the fluidization column for the agglomeration studies.

I am very grateful to my fellow friends and classmates for their support and for making the work environment amusing. Lastly, I would like to thank my family, particularly my parents Bob Pjontek and Lisette Fournier and my brother Nicolas Pjontek, for their constant love and support during my studies.

Table of Contents

List of Figures

List of Tables

Chapter 1

Introduction

Three-phase fluidized bed reactors promote contact between gas, liquid and solid phases, thus facilitating heat and mass transfer. Examples of industrial applications are encountered in catalytic hydroprocessing of heavy oil residues, Fischer-Tropsch synthesis, coal liquefaction, and waste water treatment (Fan, 1989). Reviews and books currently available in the literature summarize many aspects of three-phase fluidization (Fan and Yang, 2003; Fan, 1989; Fan et al., 1999; Wild and Poncin, 1996; Yang et al., 2007). Most research on the fluid dynamics and heat/mass transfer characteristics of gas-liquid-solid fluidized beds have been completed under ambient operating conditions using single-component liquids (Wild and Poncin, 1996). However, the unit of interest for this thesis is an ebullated bed hydroprocessor which operates at elevated temperatures and pressures and contains a multi-component liquid, resulting in complex fluid dynamic behaviour.

The design of three-phase fluidized bed reactors is dependent on the momentum, heat and mass transfer as well as the reaction kinetics. For an ebullated bed reactor, there are many steps to consider for catalytic reaction modelling: (i) diffusion from the gas to the liquid, (ii) diffusion from the liquid to the solid surface, (iii) internal diffusion to the catalytic site, (iv) adsorption into the catalytic site, (v) reaction on the catalyst, (vi) desorption of the products, (vii) internal diffusion from the catalyst pores to the outer surface, and (viii) diffusion of the products from the surface to the bulk liquid. One of the key parameters for ebullated bed hydroprocessors is the liquid residence time as it directly affects the single pass conversion (McKnight et al., 2003). Studies have thus focused on the overall fluid dynamics, particularly the gas and liquid holdups, to improve the unit performance.

At this point, a distinction must be made between ebullated beds and slurry bubble columns, which are separate configurations of gas-liquid-solid fluidized beds used for residue upgrading. For an ebullated bed, liquid and gas flow co-currently through a contained bed of particles, where average particle diameters are typically in the 1 to 5 millimetre range. Due to their size, fluidization is achieved primarily due to the liquid flow. In a slurry bubble

column, the gas flows through a liquid containing suspended particles typically in the 5 to 150 μm range, where the superficial liquid velocity is much lower compared to the gas. Due to the smaller particle size, fluidization occurs due to gas flowing through the liquid, where local liquid flow and particle suspension is primarily induced by the bubble wakes.

1.1. Synthetic crude oil production via bitumen upgrading in Canada

Canada has one of the largest oil reserves in the world, recently estimated at 168 billion barrels in the oil sands which are recoverable using currently available technology (Ancheyta and Speight, 2007; CAPP, 2014). Canadian oil sands are found in three locations: the Athabasca, Peace River and Cold Lake areas in Alberta and Saskatchewan. Bitumen is recovered using mining techniques when the oil sands are located near the surface, while reserves at a depth of 70 meters or more are recovered using in-situ techniques such as steam assisted gravity drainage (CAPP, 2014). Once extracted, bitumen is a highly viscous and tar-like liquid which requires upgrading for transportation and conventional oil refining.

The Syncrude Project is a joint venture currently between seven companies (Canadian Oil Sands Limited, Imperial Oil, Suncor Energy, Sinopec, Nexen, Mocal Energy, and Murphy Oil). Syncrude produces a synthetic crude oil through mining, extraction and upgrading of bitumen from the Athabasca oil sands. The product is currently referred as Syncrude Crude Oil (SCO) and consists of light oil with no residual bottoms and low sulphur content (0.2 wt.%). During the upgrading process, bitumen is first extracted from the oil sands in froth flotation tanks and separated using centrifuges. The bitumen is then distilled at near atmospheric pressures into light gas oil and atmospheric tower bottoms (ATB). A portion of the ATB is sent to a second distillation tower operating under vacuum pressures, further separating into light and heavy gas oils as well as the remaining vacuum tower bottoms (VTB). The ATB and VTB are upgraded via hydrogen addition (e.g., hydroprocessing) and/or carbon rejection (e.g., fluid bed coking) technologies. Syncrude Canada Ltd. uses the LC-Finer^{SM} hydroprocessor to reduce the carbon-to-hydrogen ratio of the atmospheric and vacuum tower residues via a combination of thermal cracking and hydrogen addition. The remaining ATB and VTB as well as unconverted residues from the LC-Finer^{SM} are upgraded in the fluid coker units, where the large hydrocarbons are thermally

cracked and produce coke due to the carbon rejection. LC-Finer[SM] and fluid bed coker products are then sent to fixed bed hydrotreaters for nitrogen and sulphur removal to produce the synthetic crude oil.

1.1.1. LC-Finer hydroprocessor

This thesis focuses on the LC-Finer[SM] hydroprocessor, shown in Figure 1.1, which operates as a co-current ebullated bed. The "LC" stands for "Lummus and Cities Service", which were the companies initially involved in licensing the technology. The unit is designed for heavy vacuum residues based on the following advantages (Rana et al., 2007): (i) liquid recirculation and fluidized bed result in approximately uniform temperature distribution, (ii) catalyst addition and withdrawal allow for continuous operation, and (iii) flexible operation based on catalyst selection and/or multi-stage configurations.

The inlet gaseous hydrogen and liquid ATB/VTB mixture are heated separately and then fed into the plenum chamber below the grid (i.e., gas-liquid distributor plate) using a horse-shoe/shroud distributor assembly. The feed is mixed with the recycled fluid, mainly consisting of unconverted liquid and some entrained gas from the freeboard region, before flowing through the risers and bubble caps located in the grid plate. Doped alumina cylindrical catalysts are fluidized by the co-current gas and liquid flow, where liquid can be considered the continuous phase while the hydrogen and catalyst constitute the dispersed phases. Above the fluidized bed, the liquid is recirculated to the plenum chamber using a recycle pan and pump. The liquid recirculation provides the necessary flow to fluidize the catalyst particles while also maintaining temperature uniformity throughout the reactor, where the system is typically approximated as well-mixed and isothermal. Liquid flow is mainly adjusted by the rotational speed of the recycle pump to control the catalyst bed height. The inlet gas flow maintains the hydrogen partial pressure, thus ensuring adequate hydrogenation in the reactor. Catalyst addition/withdrawal rates are varied to sustain the catalytic activity and an optimal recycle pump speed (e.g., an increase bed inventory will reduce the required pump speed to maintain the desired ebullated bed height).

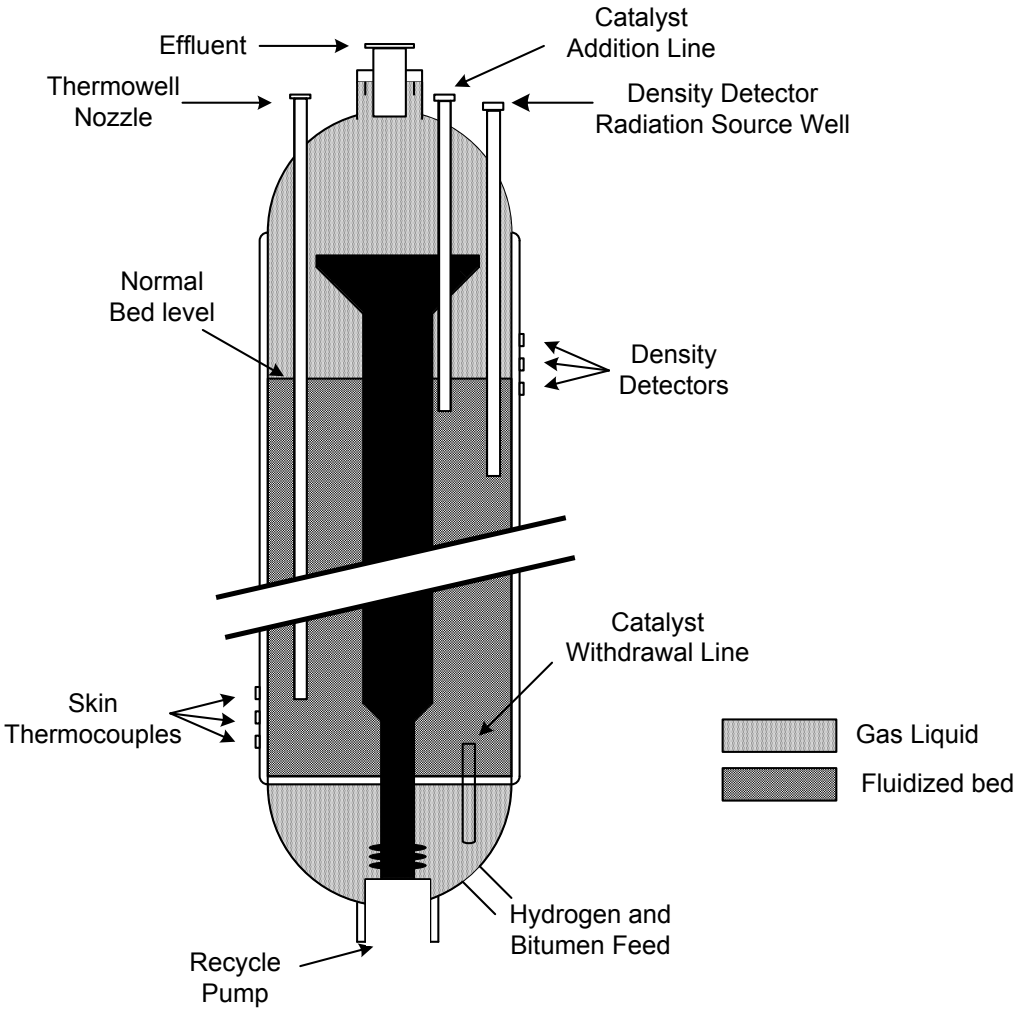

Figure 1.1. LC-Finer[SM] schematic (modified from McKnight et al., 2003).

Syncrude's LC-Finer[SM] operates at high temperatures and pressures of approximately 440°C and 11.7 MPa (McKnight et al., 2003), respectively, required for residue upgrading. It should be noted that the catalyst bed level is monitored using gamma-ray density detectors, shown in Figure 1.1. These measurement devices have also been used to estimate freeboard gas holdups, as shown in Figure 1.2, based on approximations for the gas and liquid densities at the reaction conditions. Unfortunately, gas holdups in the ebullated bed cannot be estimated using a similar method as it necessitates the catalyst inventory and density, which are not well known while the unit is operational.

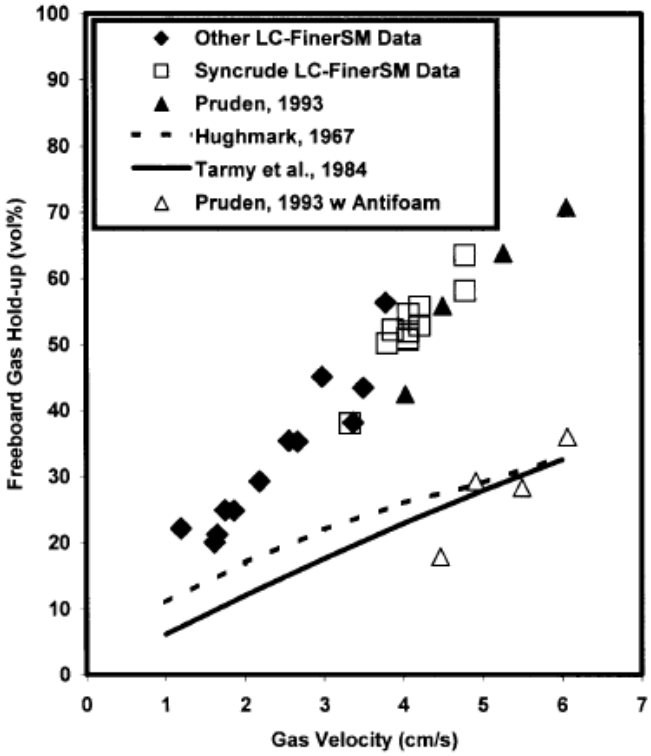

Figure 1.2. Commercial LC-Finer[SM] freeboard gas holdups compared with CANMET slurry bubble column pilot data and literature correlations (McKnight et al., 2003).

As the LC-Finer[SM] is limited by the reaction kinetics, its performance can be optimized by investigating the following fluid dynamic parameters:

- *Bed and freeboard gas holdups*
    - Residue conversion is highly dependent on liquid residence time, where minimization of the reactor gas holdup is desired.
    - Gas entrainment in the liquid recycle line reduces the liquid holdup and should be investigated at these conditions.
    - Bubble characteristics at industrial conditions are required for the recycle pan design and optimization to improve the freeboard gas-liquid separation.
    - The relation between freeboard and bed region gas holdups should also be studied as only the former can be currently measured in the industrial unit.

- *Fluidization behaviour*
    - Sufficient particle mixing is required to maintain catalytic activity and local temperatures throughout the ebullated bed.
    - A sharp interface between the ebullated bed and freeboard regions is desired to control the bed level, where liquid and solid properties as well as local bubble flow behaviour can influence the solid disengagement zone.
    - The gas-liquid distribution into the ebullated bed can affect the local bubble characteristics, fluidization behaviour, and radial distributions.
    - Local temperature increases may lead to undesired secondary reactions and potentially the formation of a carbonaceous mesophase.

This work thus advances the understanding of fluid dynamics at industrially relevant operating conditions. Experimental studies have been carried out to help optimize performance criteria (e.g., pitch conversion, hydrogen utilization, distillate product yields, and energy efficiency), which are related to the environmental impact of synthetic crude oil production.

1.2. Previous fluid dynamic studies relevant to hydroprocessing conditions

Ebullated bed fluid dynamics studies typically focus on the bubble characteristics (size and size distribution, shape, rise velocity, and radial profile), gas/liquid holdups and the bed void/expansion (i.e., solid holdup). Fan (1989) classified three major flow regimes for three-phase fluidized beds: bubbling, slugging, and transport. The slugging and transport regimes occur at relatively high gas velocities, which is not representative of the fluid dynamic behaviour in industrial hydroprocessors. Bubbling flow is generally separated into the dispersed/homogeneous or coalescing/heterogeneous regimes. Dispersed bubble flow occurs at relatively low gas flow rates and results in small bubbles with relatively uniform size. When increasing the gas flow rate in dispersed flow, the average bubble size remains approximately constant while the bubble population tends to increase. Beyond a transition gas velocity, the increased population leads to bubble coalescence, resulting in larger bubbles and a wider size distribution. Liquid circulation patterns and general mixing behaviour is

impacted by the wider size distribution as the larger bubbles rise faster and their induced wakes cause liquid back-mixing.

Much of the research on gas-liquid-solid fluidized beds has been completed under ambient operating conditions using air, water, and glass beads (Wild and Poncin, 1996). Such systems can differ significantly from hydroprocessors which have relatively low equilibrium surface tensions, reduced liquid viscosity, multi-component liquids, increased gas density and non-spherical particles. Freeboard gas holdup measurements and phase physical properties in the industrial unit indicated that the ebullated bed operates in the dispersed bubble flow regime at high gas holdups (i.e., generally above 25%). This behaviour is difficult to simulate in an aqueous system at ambient conditions as it typically result in lower gas holdups and spherical-cap bubbles with significant wakes (Fan, 1989). As a result, some studies related to industrial multiphase reactors have used pilot scale systems with similar phase physical properties and operating conditions or attempted to simulate high gas holdups by modifying the bubble coalescence behaviour with surface-active components.

Tarmy et al. (1984) and Ishibashi et al. (2001) measured the gas holdups in pilot scale coal liquefaction slurry bubble column reactors operating at pressures up to 20 MPa and temperatures up to 450°C. The previous studies observed high gas holdups, which were attributed to the large kinetic energy of the high pressure inlet gas and the presence of surface-active components. Ishibashi et al. (2001) observed a similar trend to the LC-Finer^{SM} freeboard gas holdups (refer to Figure 1.2) and established that the reactor was operating in dispersed bubble flow based on a drift flux analysis. Luo et al. (1999) studied the bubble characteristics in a slurry bubble column operating at pressures up to 5.62 MPa and using Paratherm NF heat transfer fluid. The authors discussed the impact of operating pressure on the bubble break-up behaviour, which affects the maximum stable bubble size. These experiments provided relevant observations on bubble characteristics at industrially relevant operating conditions, however larger solid particles and increased liquid flow rates must be considered for an ebullated bed.

Liquid recirculation in ebullated beds increases the cost of pilot scale equipment capable of reaching elevated pressures and/or temperatures, thus limiting the quantity of available literature studies. Fan et al. (1987) and Song et al. (1989) attempted to simulate the

fluid dynamic conditions of hydrotreating or coal liquefaction reactors using 0.5 wt.% aqueous t-pentanol in a cold flow system. The interfacial phenomena leading to bubble coalescence inhibition resulted in high gas holdups for the studied operating conditions due to the reduced bubble size and rise velocities. Even though gas holdups were in the range of hydroprocessing units, scaling between experimental and industrial units must account for other physical parameters (e.g., bed expansion/solid holdup, pressure effects, fluid distribution into the bed, relative gas and liquid velocities, etc.). Luo et al. (1997) studied pressure effects on the hydrodynamics and heat transfer in an ebullated bed at pressures up 15.6 MPa using Paratherm NF heat transfer fluid. The results provided valuable information on the fluid dynamic behaviour when increasing the pressure, nonetheless high gas holdups were not observed and the superficial liquid velocity was restricted ($U_L < 0.026$ m/s). Ruiz et al. (2005, 2004) carried out ebullated bed experiments in a 29.4 mm diameter column using 1.7 mm glass beads, diesel fuel and nitrogen at pressures up to 15 MPa. Increased gas holdups and reduced minimum liquid fluidization velocities were observed due to the modified bubble behaviour. However, the studied gas and liquid superficial velocities ranges (U_G and $U_L < 20$ mm/s) did not result in the high gas holdups observed in industrial units.

1.2.1. LC-Finer^{SM} fluid dynamic studies

Safoniuk et al. (1999) proposed a scale-down approach based on dimensional analysis and matching the following dimensionless groups to investigate the industrial fluid dynamics using a cold-flow experimental system with relaxed geometrical constraints:

$$M = \frac{g(\rho_L - \rho_G)\mu_L^4}{\rho_L^2 \gamma_{G-L}^3}, \quad Eo = \frac{g(\rho_L - \rho_G)d_P^2}{\gamma_{G-L}}, \quad Re_{L-S} = \frac{\rho_L d_P U_L}{\mu_L}, \quad \rho_S/\rho_L, \quad U_G/U_L \tag{1.1}$$

The previous method assumed that: (i) gas viscosity was negligible compared to the liquid viscosity, (ii) equilibrium liquid properties (e.g., gas-liquid surface tension) were sufficient to characterize bubble coalescence behaviour, (iii) gas density was much lower than the liquid and solid densities, hence it was only included in the buoyancy term, $g(\rho_L - \rho_G)$, and (iv)

wall effects could be relaxed above a given column-to-particle size ratio (d_C/d_P) in the dispersed bubble flow regime. At matching dimensionless groups for both systems, industrial freeboard gas holdups nearly doubled those obtained with the experimental unit (McKnight et al., 2003). The significant discrepancy was attributed to the following possible reasons: (i) internal gas recycle via the liquid return line in the industrial unit, (ii) inaccurate measurements of physical properties and phase holdups in the industrial unit, and/or (iii) inadequate and/or missing dimensionless groups. While the first and second considerations could have influenced the comparison, the large deviation was believed to be primarily due to difficulties when simulating high gas holdup conditions in the cold-flow unit.

Macchi et al. (2001) investigated the applicability of the previous scaling method by comparing single and multi-component liquids. Bubble coalescence behaviour of multi-component liquids can differ compared to pure liquids as the gas-liquid interfacial properties may not be well represented by the equilibrium surface tension. Bed expansion discrepancies were mainly observed at higher gas velocities, following the transition to coalesced bubble flow. Bed and freeboard gas holdups were greater for the multi-component liquid due to bubble coalescence inhibition. Macchi et al. (2003) also investigated the effect of gas density in a bubble column and ebullated bed using helium, air, carbon dioxide and sulphur hexafluoride (ρ_G ranging from 0.17 to 6.07 kg/m^3). Gas holdups increased in both configurations with the denser gases as the dispersed bubble flow regime was sustained for higher superficial gas velocities. Dargar and Macchi (2006) investigated multiple aqueous solutions with different surface-active compounds and observed similar gas holdups in a bubble column and ebullated bed, where surfactant type and concentration mainly affected the foam stability at the free surface.

Prior work therefore demonstrated that the scale-down of industrial high gas holdup conditions must also account for coalescence inhibition due to liquid mixtures and/or surface-active compounds as well as enhanced bubble break-up at elevated pressures.

1.3. Scale-down of hydroprocessing fluid dynamics using dimensional similitude

Fluid dynamic studies for an industrial ebullated bed hydroprocessor could be carried out at one of the following scales: (i) measurements in the commercial unit at industrial operating conditions, (ii) pilot scale system using the same phase physical properties and operating conditions, but for a reduced size, or (iii) laboratory system attempting to scale-down significant fluid dynamic characteristics. The first method is ideal as the phenomena of interest would be directly measured. However, this can be difficult as many of the required parameters for accurate measurements are not well known in the industrial hydroprocessor (e.g., catalyst inventory, catalyst density, gas recycle fraction, hydrogen consumption and product formation in the ebullated bed, etc.). In addition, deviations from steady-state operation are generally avoided, limiting the ranges of studied operating conditions. Pilot scale systems can thus be used for fundamental studies as it generally more straightforward to measure the fluid dynamic parameters of interest. Unfortunately, it was not economically feasible to build a pilot scale system capable of operating at industrial hydroprocessing conditions with similar physical and geometric characteristics. As a result, experiments were carried out in a gas-liquid-solid fluidization column (101.6 mm diameter) capable of reaching pressures up to 10 MPa with a relevant range of gas and liquid superficial velocities. Due to system limitations on gas and liquid phase properties (i.e., non-flammable and inorganic), phase physical properties and operating conditions had to be carefully selected to scale-down the industrial fluid dynamic conditions.

Scaling between industrial and experimental systems must consider overall and local behaviours. The proposed scaling method will use the Buckingham Pi theorem to form a set of dimensionless groups. The fluid dynamic scale-down must first considerer significant geometric characteristics of both systems to achieve geometric similarity. It must also be ensured that both systems are operating in similar fluid flow regime, resulting in kinematic similarity. Lastly, if geometric and kinematic similitude are achieved, dynamic similarity requires the identification of all significant physical properties for the studied phenomena. Failing to include an important variable can lead to inaccurate results, while the inclusion of an insignificant parameter may create unnecessary experiments, eventually demonstrating that it is negligible. Experimental results at equivalent dimensionless groups should result in equal dimensionless properties in both systems.

Considerations for geometric similitude and the formation of dimensionless groups are discussed in section 4.2.1. Nonetheless, a summary is provided to specify the major assumptions and resulting dimensionless groups for the scaling approach used in this thesis.

1.3.1. Geometric similarity

As the experimental gas-liquid-solid fluidization system was not designed solely to model the LC-Finer^{SM}, geometric similarity must be evaluated. When considering relevant geometric characteristic of the industrial unit, the following properties must be discussed:

- Gas-liquid separation above the ebullated bed (exit design)
    - Gas entrainment in the industrial recycle pan may contribute to the high freeboard gas holdups in the LC-Finer^{SM}.
    - The experimental system has a two stage separation, where tests have demonstrated negligible gas entrainment at simulation conditions.
    - Gas entrainment in the industrial liquid recycle can therefore be essentially simulated by increasing the gas flow rate in the experimental system.
- Gas-liquid distribution (entrance design)
    - For the LC-Finer^{SM}, feed liquid and gas are delivered in a horse-shoe/shroud distributor assembly and combined with the recycled liquid before passing through the risers and bubble caps located in the grid plate.
    - In the experimental system, gas is injected with the liquid using a porous pipe below the distributor, resulting in analogous energy dissipation when both fluids flow through the perforated distributor plate.
- Column diameter and internals (wall effects)
    - The impact of wall effects and the presence of an internal recycle line on global phase holdups can be neglected in industrial hydroprocessors based on their relatively large column diameters.
    - Strict equality of the column-to-particle or column-to-bubble diameter ratios were relaxed due to the dispersed bubble flow regime and small bubble diameters at high gas holdups.

1.3.2. Physical properties selected for dynamic similarity

Non-geometric dimensionless groups were obtained by considering all phase physical properties which potentially influence the fluid dynamics of an ebullated bed. These variables can be separated into particle, liquid, gas and system properties.

- *Solid properties*: average size, size distribution, average density, density distribution, sphericity, wettability, porosity, coefficient of restitution.
- *Liquid properties*: density, surface tension, rheology, foaming characteristics, conductivity, volatility.
- *Gas properties*: density, viscosity, solubility, diffusivity.
- *System properties*: gas superficial velocity, liquid superficial velocity, gravitational acceleration.

The ANN-DA approach proposed by Larachi et al. (2001) provided initial considerations for relevant physical properties due to the large database used to develop the phase holdup correlations (20500 experimental measurements for Newtonian liquids). The following was assumed for the scale-down of an ebullated bed operating at high gas holdup conditions (further discussed in section 4.2.2):

- Gas viscosity was assumed negligible as $\mu_G << \mu_L$.
- Pressure effects are considered by also including the gas density.
- Particle shape effects were accounted for using the Sauter mean particle diameter (studied in Chapter 2).
- Gas-liquid equilibrium surface tension was not included as it was shown inadequate when predicting gas holdups when bubble coalescence was sufficiently inhibited. A binary approach was used for coalescing or coalescence inhibiting liquids.

The following parameters were thus selected: liquid density (ρ_L), gas density (ρ_G), particle density (ρ_S), liquid viscosity (μ_L), gravitational acceleration (g) via the particle-liquid buoyancy term ($g(\rho_S - \rho_L)$), average particle size/shape using the Sauter mean diameter ($d_{SV} = d_V\phi$), gas superficial velocity (U_G), liquid superficial velocity (U_L) and a binary consideration for bubble coalescence behaviour (coalescing or coalescence

inhibition). The particle Sauter mean diameter was selected as the characteristic length and the fundamental dimensions were mass, length, and time. The Buckingham Pi theorem thus resulted in the following dimensionless groups:

$$\mathrm{Re}_{S-L} = \frac{\rho_L \, d_{SV} \, U_L}{\mu_L} \;,\; \mathrm{Ar}_{S-L} = \frac{\rho_L \, d_V^{\,3} \, g(\rho_S - \rho_L)}{\mu_L^{\,2}}$$
$$\frac{\rho_G}{\rho_L} \;,\; \frac{\rho_S}{\rho_L} \;,\; \frac{U_G}{U_L} \qquad (1.2)$$

In addition to the previous dimensionless groups, this approach requires equivalent bubble coalescence behaviour for matching systems (i.e., coalescing or significantly inhibiting coalescence). The dimensionless groups focus on matching inertial, viscous and buoyant forces between both systems. Examining the resulting dimensionless groups, systems with matching solid-liquid Reynolds and Archimedes numbers should exhibit equivalent liquid-solid fluidized bed characteristics, shown with empirical correlations for the terminal particle settling velocity and n index required for the well-known Richardson and Zaki (1954) correlation. Consequently, the scale-down approach for this thesis matches the liquid-solid fluidized bed properties while the high gas holdup behaviour is accounted for by sufficiently inhibiting bubble coalescence, enhancing bubble break-up characteristics, and matching the gas-liquid superficial velocity ratio.

1.3.3. LC-Finer^{SM} simulating conditions

Experimental system properties, shown in Table 1.1, were adjusted to match non-geometric dimensionless groups estimated for the LC-Finer^{SM}. Base-case simulation conditions resulted in an ebullated bed of nitrogen, 0.5 wt.% aqueous ethanol (required for significant bubble coalescence inhibition), and aluminum cylinders operating at a pressure of 6.5 MPa and a gas-to-liquid superficial velocity ratio of 0.78. For confidentially reasons, hydroprocessing physical properties and operating conditions cannot be provided. It should be noted that glass spheres were originally selected as the simulating particles. However, aluminum cylindrical particles obtained for the particle shape study (Chapter 2) were used for the final simulation due to the similar particle-liquid density ratio and relevant length-to-diameter ratio of hydroprocessing catalysts. The ratios of the non-geometric dimensionless groups for both systems are presented in Table 1.2.

Table 1.1. Simulating phase physical properties and operating conditions.

Parameter	Symbol	Range	Units
Superficial liquid velocity	U_L	0.09	m/s
Superficial gas velocity	U_G	0.07	mm/s
Pressure	P	6.5	MPa
Column diameter	d_C	101.6	mm
Liquid density	ρ_L	998 ± 2	kg/m^3
Liquid viscosity	μ_L	$(0.95 \pm 0.4) \times 10^{-3}$	$Pa \cdot s$
Gas density	ρ_G	73.7	kg/m^3
Particle density	ρ_S	2711 ± 8	kg/m^3
Sphericity	ϕ	0.81 ± 0.05	-
Sauter mean diameter	d_{SV}	3.9 ± 0.2	mm
Particle-liquid Reynolds number	Re_{S-L}	350	-
Particle-liquid Archimedes number	Ar_{S-L}	2.1×10^6	-
Gas-liquid density ratio	ρ_G/ρ_L	0.074	-
Solid-liquid density ratio	ρ_S/ρ_L	2.72	-
Gas-liquid superficial velocity ratio	U_G/U_L	0.78	-

Table 1.2. Ratios of the experimental system to the LC-Finer^{SM} dimensionless groups.

Non-geometric dimensionless group	$\Pi_{experimental}/\Pi_{LC-Finer}$
Particle-liquid Reynolds number	1.06
Particle-liquid Archimedes number	1.22
Gas-liquid density ratio	0.97
Solid-liquid density ratio	0.97
Gas-liquid superficial velocity ratio	1.02

1.4. Carbonaceous mesophase formation

Upgrading heavier feeds may lead to coke formation in hydroprocessors, which can cause fouling in the reactor and downstream equipment as well as reduced catalytic activity (Gray, 1994). Coke is generally defined as toluene insoluble materials and is believed to originate from the asphaltene fraction in the feedstock (Srinivasan and McKnight, 1994). An intermediate phase between vacuum residue and solid coke, commonly referred as carbonaceous mesophase, was initially identified by its optical anisotropy under polarized light (Brooks and Taylor, 1965). Some potential formation mechanisms have been discussed by previous authors (Bagheri et al., 2012; Gray and McCaffrey, 2002; Marsh and Latham, 1986; Wiehe, 1994), where mesophase likely forms due to an increased rate of thermal cracking relative to the hydrogenation rate. If the cracking rate of alkyl chains from polyaromatics cores increases relative to the rate of aromatic core hydrogenation, planar polyaromatic cores may oligomerize/coalesce to form initial mesophase domains. Bagheri et al. (2012) observed the in-situ formation of both small and large mesophase domains, shown in Figure 1.3, in a stirred hot-stage reactor at 440°C and 4.8 MPa.

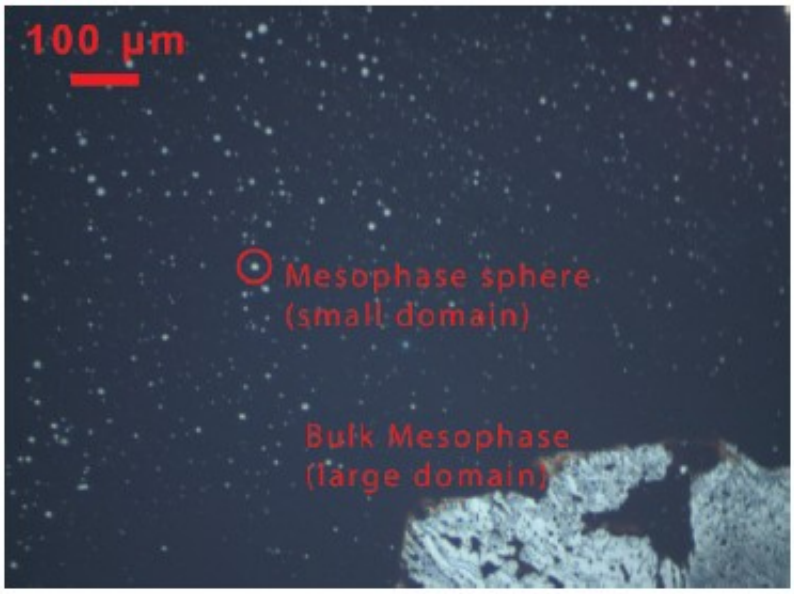

Figure 1.3. Photomicrograph of mesophase formed during cracking Athabasca vacuum residue under hydrogen at 4.8 MPa and 440^{o}C stirred at 140 rpm (Bagheri et al., 2012).

Mesophase may impact the fluidization behaviour of ebullated bed and slurry hydroprocessors due to particle clustering. Few studies are currently available in the open literature with regards to the effect of an additional immiscible liquid in three-phase fluidized beds. A recent review on dispersed liquid phases in gas-liquid reactions concluded the need for additional research due to the complexities in the hydrodynamic and mass transfer behaviour associated with the two immiscible liquid phases (Kaur et al., 2007). A better understanding of the impact of a dispersed immiscible liquid phase on the fluid dynamics of ebullated beds and slurry bubble columns could thus benefit hydroprocessing reactors.

1.5. Research objectives

The main objective of this doctoral thesis is to investigate the fluid dynamics of an ebullated bed hydroprocessor following an increased vacuum distillation tower bottoms feed fraction. The effects of gas and liquid superficial velocities will be continuously evaluated throughout the experiments due to their relevance for hydroprocessors. Entrained gas from the freeboard region in the commercial unit is recycled and mixed with the feed gas and liquid below the distributor plate. Consequently, the gas recycle fraction can be essentially studied by varying the inlet gas flow rate in the experimental system. The rotational speed of the industrial liquid recycle pump is used to control the ebullated bed height and is comparable to varying the experimental liquid superficial velocity. It should however be noted that varying the liquid superficial velocity in the experimental unit at the base simulation conditions would not account for potential changes to the entrained gas in the liquid recycle line. The following provides the scope of the present work:

1. Experimentally evaluate the proposed scale-down method for the LC-Finer^{SM} fluid dynamics. Obtaining an experimental system capable of simulating the high gas holdup conditions is crucial to model the industrial hydroprocessing fluid dynamics.

2. Investigate bubble properties above the ebullated bed at the simulation conditions. Bubble characteristics at industrial operating conditions are required for the optimization and design of the recycle pan.

3. Simulate the modified liquid properties due to the increased vacuum residue feed fraction. Deviations to the overall phase holdups and fluidization behaviour are required to predict the system response when varying the feed properties.

4. Study the potential impact of mesophase formation in gas-liquid-solid fluidized beds. Fluid dynamic deviations due to particle clustering can provide the necessary information to identify mesophase formation in an industrial unit.

1.5.1. Thesis structure

Base-case simulation conditions for the LC-Finer^{SM} are first investigated in Chapter 2. The Sauter mean particle diameter was selected as the characteristic length for the fluid dynamic scale-down. Chapter 2 presents a study which experimentally investigates whether the Sauter mean diameter can be used to account for particle shape effects in an ebullated bed. A comparison of two sets of spheres and cylinders with equivalent Sauter mean diameters is carried out. Overall gas, liquid and solid holdups in the bed and freeboard regions and fluidization characteristics are compared at varying bubble flow regimes by increasing the system pressure and/or adding a surfactant.

Bubble characteristics are then investigated in Chapter 3 using of a monofibre optical probe in a bubble column and the freeboard region of an ebullated bed at high gas holdup conditions. Global and local gas holdups as well as photos are compared to local measurements while varying gas/liquid flow rates, increasing the pressure and adding a surfactant. Results in the freeboard region of an ebullated bed are compared to bubble column results at equivalent operating conditions, relevant for future work.

The impact of a more viscous liquid on the overall fluid dynamic behaviour at the simulation conditions is studied in Chapter 4. A comparison of the overall phase holdups for two sizes of cylindrical particles (d_{SV} of 1.6 and 3.9 mm) at matching dimensionless groups provides a preliminary verification of the proposed scale-down method. The relation between freeboard and bed region gas holdups is also studied. Lastly, the proposed dimensionless groups are used to correlate the overall phase holdups under high gas holdup conditions.

The potential impact of mesophase formation is first studied in Chapter 5, where the overall fluid dynamics in a bubble column and ebullated bed were investigated following the addition of a dispersed immiscible liquid phase. Following the interesting clustering behaviour observed in the initial study, Chapter 6 examines the effects of particle size, shape and material using glass spheres and aluminum cylinders with equivalent volume to surface area ratios. Interparticle forces relevant to gas-liquid-liquid-solid fluidized beds are discussed, with an emphasis on the relation between fluid and particle properties with respect to attractive forces due to liquid bridging.

Experimental equipment and measurement techniques for each study are presented within the respective Chapters. Lastly, the thesis conclusions and recommendations for future research are presented in Chapter 7.

Nomenclature

Ar_{L-S}	particle-liquid Archimedes number
d_C	column inner diameter (m)
d_P	particle diameter (m)
d_{SV}	Sauter mean diameter (m)
d_V	volume equivalent diameter (m)
Eo	Eötvös number
g	gravitational acceleration (m/s^2)
M	M-group
Re_{L-S}	particle-liquid Reynolds number
U_G, U_L	gas and liquid superficial velocities (m/s)

Greek symbols

γ_{G-L}	gas-liquid surface tension (N/m)
μ_G, μ_L	gas and liquid dynamic viscosity (Pa s)
ρ_G, ρ_L, ρ_S	gas, liquid and solid densities (kg/m^3)
ϕ	sphericity

Chapter 2

Hydrodynamic comparison of spherical and cylindrical particles in a gas-liquid-solid fluidized bed at elevated pressure and high gas holdup conditions

Dominic Pjontek and Arturo Macchi

Chemical and Biological Engineering Department, University of Ottawa, 161 Louis Pasteur, Ottawa, Ontario, Canada, K1N 6N5

Abstract

Experiments were carried out to validate the use of spheres in lieu of cylinders when investigating the global hydrodynamic features of a co-current gas-liquid-solid fluidized bed. Two sizes of glass spheres with diameters of 4 and 1.5 mm were compared to aluminum cylinders with equivalent volume/surface area ratios (i.e., matching Sauter mean diameters). Lengths/diameters of the larger and smaller cylinders were 7.5/3.2 mm and 3.1/1.2 mm, respectively, which resulted in equal particle sphericity of 0.8 for both sizes. The particle properties of the larger particles led to the inertial settling flow regime ($Re_{LT\infty} > 500$) in water while the smaller particles were in the intermediate regime ($0.2 < Re_{LT\infty} < 500$). High gas holdup conditions were obtained by increasing the system pressure to 6.5 MPa and/or adding a surfactant. Atmospheric conditions were also studied for comparison. Experiments were conducted in a 101.6 mm diameter column with tap water or a 0.5 wt.% aqueous ethanol solution as the liquid phase. Global phase holdups measured from the dynamic pressure profiles characterized the hydrodynamic behaviour of the fluidized bed and studied the impact of particle shape. Standard deviations of the mean holdups aided the comparison and also examined the fluctuations of the bed interface. Liquid-solid fluidized bed experiments demonstrated that equivalent Sauter mean diameters resulted in comparable bed porosities. Gas-liquid-solid fluidized bed dynamics of equivalent size spherical and cylindrical particles were similar in the dispersed bubble flow regime whereas differences were observed in the presence of larger coalescing bubbles.

***This manuscript has been published**: Pjontek, D., Macchi, A., 2014. Hydrodynamic comparison of spherical and cylindrical particles in a gas–liquid–solid fluidized bed at elevated pressure and high gas holdup conditions. Powder Technol. 253, 657–676.

2.1. Introduction

Many industrial applications of gas-liquid-solid fluidized beds, e.g. the LC-Finer[SM] hydroprocessor used for resid upgrading (McKnight et al., 2003), employ extruded cylindrical catalysts. Most gas-liquid-solid fluidized bed experimental studies currently available in the open literature use spherical glass beads due to their ease of use, cost, and availability. Although some studies have used cylindrical extrudates (Ruiz et al., 2004; Song et al., 1989; Soung, 1978), the validity of simulating cylindrical particles with spheres in a gas-liquid-solid ebullated bed needs to be investigated.

Flow through a fixed bed of particles can provide a starting point in the literature when accounting for particle shape in a fluidized bed. The Ergun equation (Ergun, 1952) is one of the most widely used correlations to determine the pressure drop of a fixed bed.

$$\frac{\Delta P}{\Delta L} = 150\frac{\mu_F U_F}{d_{SV}^{\ 2}}\frac{(1-\varepsilon)^2}{\varepsilon^3} + 1.75\frac{\rho_F U_F^{\ 2}}{d_{SV}}\frac{(1-\varepsilon)}{\varepsilon^3} \tag{2.1}$$

Eq. (2.1) accounts for the shape of non-spherical particles by using the diameter of a sphere with an equal surface area to volume ratio, generally referred as the Sauter mean diameter (d_{SV}). Previous experiments have used the Ergun equation to measure the sphericity (ϕ) of irregular particles in a fixed bed at very low flow rates where viscous forces dominate (Subramanian and Arunachalam, 1980).

Drag on particles must also be considered where a particle's terminal settling velocity, when the force balance is equal to zero, is a key parameter for fluidized beds. The gravitational, buoyant and drag forces acting on a particle at its terminal velocity in a liquid are related as follows:

$$\frac{\pi}{6}(\rho_S - \rho_L) g\, d_V^{\ 3} = \frac{1}{2}\rho_L\, U_{LT\infty}^{\ 2}\, C_D\, A_P \tag{2.2}$$

Where the left hand side is the net gravitational force and the right hand side is the drag force. Examining the previous equation, the drag coefficient (C_D) and projected area (A_P) of the settling particle are required to determine the terminal velocity. Drag coefficients for spherical particles can be estimated via available correlations in the literature (Brown and Lawler, 2003; Haider and Levenspiel, 1989; Khan and Richardson, 1987; Turton and Clark,

1987) and the projected area of a sphere can be calculated. These parameters are not as easily determined for cylinders as the projected area and drag coefficient of a cylindrical particle depends upon its orientation. Lau et al. (2010) observed that the settling of a cylinder in the inertial regime ($Re_{LT\infty} > 500$) resulted in both horizontal and inclined orientations due to wall effects. Some drag coefficient correlations developed for cylinders estimated the projected area based on the diameter of an equal volume sphere while experimentally measuring the terminal velocities (Chhabra et al., 1999; Gabitto and Tsouris, 2008; Haider and Levenspiel, 1989). Although the estimated projected areas may not be accurate, the product of the interrelated drag coefficient and projected area is the parameter required to estimate the terminal velocity. Nonetheless, the orientation of a single cylinder falling in a tube differs from the orientations of many particles in a fluidized bed. The previous correlations used the particle sphericity to account for shape effects. The terminal velocity of cylindrical particles has thus been related using the volume equivalent diameter and particle sphericity.

In liquid-solid fluidized beds, the bed porosity (ε) of spherical particles can be estimated using the Richardson and Zaki (1954) empirical correlation.

$$\frac{U_L}{U_{LT\infty}} = k\,\varepsilon^n \tag{2.3}$$

The terminal free settling velocity of the particles ($U_{LT\infty}$), the wall effect factor (k) and the n index can be estimated for spheres using available correlations (Khan and Richardson, 1989; Turton and Clark, 1987). Gabitto and Tsouris (2008) experimentally demonstrated that the Haider and Levenspiel (1989) terminal settling velocity predictions for cylinders are relatively accurate for isometric particles with $\phi \geq 0.7$. Wall effects for cylindrical particles have been estimated by Chhabra (1995), where non-spherical particles usually experience smaller wall effects compared to spheres, with the exception of cylinders with a length over diameter ratio greater than 10. Unfortunately, no reliable set of correlations have been developed yet to estimate the n index for non-spherical particles (Epstein, 2003).

Another method to predict the bed porosity of non-spherical particles assumes that the liquid immobilizes around the surface irregularities, where the particles then behave as smooth spheres (Fouda and Capes, 1977; Steinour, 1944). This leads to an effective particle

volumetric concentration ($K\varepsilon_S$) based on a hydrodynamic volume factor K, defined as the liquid envelope and solid volume divided by the solid volume. Eq. (2.3) is modified as follows.

$$\frac{U_L}{U_{LT\infty}} = k\left(1 - K\,\varepsilon_S\right)^n \tag{2.4}$$

The effective volumetric concentration can be estimated by assuming that the settled bed porosity is equivalent to the bed porosity at minimum fluidization (Eastwood et al., 1969), which is related to the particle sphericity. The definition of the hydrodynamic volume factor results in effective particle diameters and densities to then estimate the bed porosities using correlations for spheres. The particle properties used to quantify shape and size when estimating bed porosities are again the volume equivalent diameter and sphericity.

The fluid dynamic characteristics of cylindrical particles in gas-liquid-solid fluidized beds have been experimentally studied by some authors. Soung (1978) studied the bed expansion of commercial cobalt-molybdenum cylindrical catalysts with n-heptane and nitrogen as the liquid and gas phases, respectively. A correlation was developed that accounted for particle shape via the product of sphericity (ϕ) and the diameter of a sphere with equivalent volume (d_V). Song et al. (1989) investigated the hydrodynamic characteristics of seven hydrotreating catalysts consisting of cobalt and molybdenum oxide on extruded porous alumina supports in water and a 0.5 wt.% aqueous t-pentanol solution. The Sauter mean diameter of the particles ranged from 1.51-1.90 mm. The authors discussed that particle shape effects were dependent on the bubble/particle size ratio. Bed void fractions for the water fluidized bed were compared to the Begovich-Watson (1978) correlation, which underestimated the experimental data. The fit was improved by adding particle sphericity, although its exponent prevents the direct use of the Sauter mean diameter. A separate bed porosity correlation was developed by Song et al. (1989) for the surfactant system using d_{SV} to account for particle size and shape. Minimum liquid fluidization velocities (U_{lmf}) and bed porosities of fresh and equilibrium hydrocracking catalysts were studied by Ruiz et al. (2004) in water, diesel or jet fuels as the liquid phase and air or nitrogen as the gas phase. Experimental U_{lmf} values were compared to many correlations and

the sphericity was successfully incorporated to improve the fit of the two correlations with the best initial predictions (Begovich-Watson (1978) and Ermakova et al. (1970)). Particle sphericity was again added to the Begovich-Watson (1978) correlation for bed porosity to improve the fit for the studied particles.

In summary, the previous gas-liquid-solid studies compared their experimental data obtained using non-spherical particles to correlations developed for spheres. Lack of fit was then corrected by adding the particle sphericity to the existing correlations and fitting the exponent using experimental data. The previous studies however did not directly compare spheres and cylinders in a single gas-liquid-solid fluidized bed to determine a methodology to account for particle shape. As some of the modified correlations did not directly substitute the Sauter mean diameter, it is difficult to conclude whether this parameter effectively accounts for particle shape when comparing the global fluid dynamic behaviour of spheres and cylinders. In addition, the gas holdups, an important parameter for ebullated beds, were only measured by Song et al. (1989).

Sinha et al. (1986) compared the gas-liquid-solid bed porosities of cylindrical and spherical particles using kerosene and heptane as the liquid phases and nitrogen as the gas phase. Although the authors concluded that the spheres and cylinders were equivalent, some experimental observations reveal that the effect of particle shape may not have been fully isolated in the study. The spheres and cylinders used in the study had an apparent size distribution, where the solid phase ordered itself axially based on size when operated as a liquid-solid fluidized bed. The author also mentioned that the pressure profiles along the length of the column were curved, implying that the bed densities were not constant. The previous observations and the exclusion of gas holdup measurements render it difficult to fully compare the fluidized bed behaviour of the studied spheres and cylinders.

The objective of this study is thus to experimentally investigate whether the Sauter mean diameter can be used to account for particle shape effects on the global hydrodynamics in a gas-liquid-solid fluidized bed. A comparison of two sets of spheres and cylinders with equivalent Sauter mean diameters was completed in the same experimental system. Particles were selected to minimize particle size and density distribution effects, hence focusing on shape effects. Global gas, liquid and solid holdups in the bed and freeboard regions and

fluidization characteristics are compared and discussed over relevant ranges of gas and liquid superficial velocities. Interactions between bubble characteristics and particle shape are studied by increasing the system pressure and/or adding a surfactant. The previous operating conditions also led to high gas holdup conditions which are relevant when studying the fluid dynamics of industrial gas-liquid-solid ebullated beds.

2.2. Experimental setup

Experiments were carried out in a gas-liquid-solid fluidization system (Figure 2.1), purchased from Zeton Inc. (Burlington, Ontario), which is capable of reaching pressures up to 10 MPa. The fluidization column is made of stainless steel with an inner diameter of 101.6 mm and a maximum expanded bed height of 1.8 m. Glass viewing windows with dimensions of 118.75 mm x 15.63 mm are located at heights of 244 mm, 603 mm, and 956 mm above the top of the distributor plate. At the top of the column, an expanded overflow section was designed as the primary gas-liquid separation stage. The liquid is conveyed into a partitioned liquid storage tank for further degassing and then recycled to the column. The system was pressurized using industrial grade nitrogen cylinders. National Instruments hardware and software are used for data acquisition.

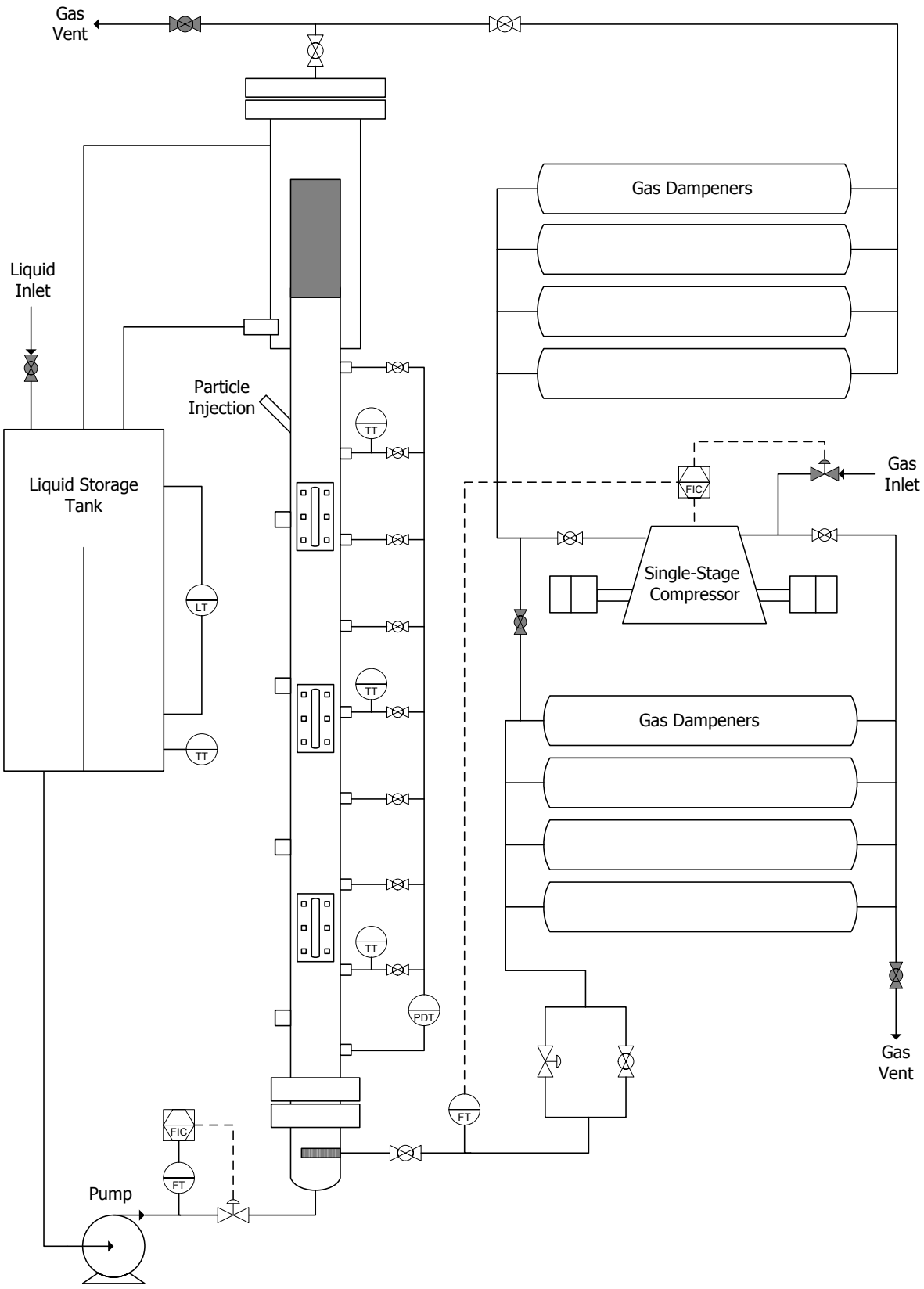

Figure 2.1. Schematic of the high pressure gas-liquid-solid fluidization system.

Global phase holdups were determined using a differential pressure transmitter (Rosemount, model: 1151DP3S22C6Q4). The reference pressure port for the dynamic pressure drop is located at 95 mm above the distributor plate. Subsequent pressure ports are equally spaced by a distance of 146 mm. A centrifugal pump (Kronto, model: HPGS 1x1x5C-A1) drives the liquid from a storage tank to the base of the column. A magnetic flow meter measures the liquid flow rate which is controlled by an automated needle valve. Gas is circulated via a single stage reciprocating compressor (Hydro-Pac, model: C01.5-10-100LX), where fluctuations in the gas flow are reduced by gas dampeners located at the compressor's inlet and outlet. A differential pressure transducer (Rosemount, model: 1151DP4522C6S4Q4) was used to measure the gas flow rate through orifice plates of varying size, depending on the operating pressure. The gas and liquid superficial velocities can be respectively varied between 0 to 0.4 m/s and 0 to 0.12 m/s. Gas is sparged in the plenum chamber of the column via a porous pipe with openings of 10 μm in diameter. The gas-liquid mixture then flows into the bed through a perforated distributor plate with 23 holes of 3.175 mm diameter. A mesh is used to prevent smaller particles from entering the plenum chamber.

System operating conditions for this study are summarized in Table 2.1. Errors in the operating conditions were estimated from measurement fluctuations during experiments, while errors on the fluid properties were estimated from repeated measurements. Liquid superficial velocities (U_L) for the ebullated bed were selected based on the liquid-solid fluidized bed experiments. Gas superficial velocities (U_G) were selected to observe the transition from dispersed to coalesced bubble flow at atmospheric conditions. The gas flow rate was also limited by the expansion of the fluidized bed to prevent particles from overflowing at the top of the column. The studied elevated pressure was selected based on previous experiments by Rudkevitch and Macchi (2008), where the effect of increased gas density on the hydrodynamics subsided at approximately 4 to 6 MPa. A value of 6.5 MPa was thus conservatively chosen to account for pressure effects on bubble characteristics. Water was used as a liquid phase since it is commonly used in experiments found in literature. A 0.5 wt.% aqueous ethanol (EtOH) solution was used to inhibit bubble coalescence and due to the effervescent foam produced at the free surface (Dargar and Macchi, 2006). The combined effects of elevated pressures and surface active compounds

are pertinent to industrial gas-liquid-solid fluidized beds, where gas holdups are considerably higher compared to atmospheric air-water systems (McKnight et al., 2003).

Table 2.1. Experimental operating conditions and fluid properties.

Parameter	Symbol	Range	Units
superficial liquid velocity	U_L	0 to 110 (± 1%)	mm/s
superficial gas velocity	U_G	0 to 140 (± 2%)	mm/s
pressure	P	0.1 and 6.5 (± ~1%)	MPa
column diameter	d_C	101.6	mm
temperature	T	24 ± 2	°C
liquid density	ρ_L	997 ± 1	kg/m^3
liquid viscosity	μ_L	(9.1 ± 0.4) x 10^{-4}	Pa · s
gas density	ρ_G	1.15 ± 0.03 and 73.7 ± 0.7	kg/m^3

2.2.1. Particle selection

Particle shape can be characterized using various parameters. The volume equivalent diameter (d_V) is the volume of a sphere with equal volume for a given particle. For cylinders, the volume equivalent diameter is calculated as follows:

$$d_V = \left(\frac{3}{2} {d_P}^2 L_P \right)^{\frac{1}{3}} \tag{2.5}$$

Particle sphericity (ϕ) is defined as the ratio of the surface area of a volume equivalent sphere to the surface of the studied particle, which can be calculated for a cylinder as follows:

$$\phi = \frac{d_V^{\,2}}{0.5 d_P^{\,2} + d_P L_P} \tag{2.6}$$

The Sauter mean diameter (d_{SV}) is the diameter of a sphere which has an equivalent volume/surface area ratio when compared to the cylindrical particles. It is the product of the volume equivalent diameter and sphericity.

It is hypothesized in this study that the Sauter mean diameter accounts for shape effects when comparing the fluid dynamics of gas-liquid-solid fluidized beds containing spheres or cylinders. Glass beads are commonly used in experiments found in the open literature and were thus selected as the spheres. The cylindrical particles were selected to minimize particle density and size distribution effects while attempting to match the spherical properties. The cost and manufacturing method of the cylinders led to the selection of aluminum as the material. Although the density is a slightly higher compared to the glass spheres, the manufacturing process (Pellets LLC) minimized variations in the diameter and length. Furthermore, the minor particle density difference mainly affects the bed expansion in a predictable manner.

Particle properties of the spheres and cylinders in this study are provided in Table 2.2. Errors for the cylindrical particles were estimated based on 100 particles, errors for the glass beads were based on the manufacturer specifications, and density errors were estimated from repeated measurements. The bed can expand or initially collapse at the introduction of gas depending on the particle properties and operating conditions (Epstein, 1976; Muroyama and Fan, 1985). Larger and smaller glass spheres with diameters of 4.0 and 1.5 mm allowed the comparison of bed expansion and collapse, respectively. Cylindrical particle dimensions depended on the manufacturing process, where aluminum wire with constant diameter was cut into specified lengths. The aluminum wire diameters were thus chosen to match the Sauter mean diameter of the spheres while maintaining the desired length/diameter ratio of approximately 2.5 which results in a sphericity of approximately 0.8. The studied spheres and cylinders are visually compared in Figure 2.2.

Table 2.2. Characteristics of equivalent spherical and cylindrical particles.

Parameter	L spheres	L cylinders	S spheres	S cylinders
material	borosilicate glass	aluminum 1100	borosilicate glass	aluminum 5356
density, ρ_S (kg/m^3)	2500 ± 9	2711 ± 8	2502 ± 4	2649 ± 9
diameter, d_P (mm)	4.0 ± 0.3	3.2 ± 0.03	1.5 ± 0.2	1.2 ± 0.07
length, L_P (mm)	-	7.5 ± 0.4	-	3.1 ± 0.1
d_V (mm)	-	4.9 ± 0.1	-	1.9 ± 0.1
d_{SV} (mm)	4.0 ± 0.3	3.9 ± 0.2	1.5 ± 0.2	1.6 ± 0.2
sphericity, ϕ	1.0 ± ~ 0	0.81 ± 0.05	1.0 ± ~ 0	0.80 ± 0.08

Figure 2.2. Visual comparison of the L spheres (a), L cylinders (b), S spheres (c), and S cylinders (d).

2.3. Measurement techniques

2.3.1. Global phase holdups

Global phase holdups were calculated by measuring the dynamic pressure drop, where the hydrostatic head of the liquid phase is subtracted, throughout the bed and freeboard regions. The bed height (h_B) was estimated from the intersection of the bed and freeboard dynamic pressure profiles, obtained by linear regression. Visual observations of the bed height were recorded when possible to corroborate the bed height obtained by the pressure drop method. Solid holdups (ε_S) were calculated knowing the mass of solids in the fluidized bed.

$$\varepsilon_S = \frac{4\,m}{\pi\, d_C^{\,2}\, h_B\, \rho_S} \tag{2.7}$$

Neglecting frictional drag on the wall and accelerations of the phases in the vertical direction, the gas holdups in the bed region (ε_G) were measured via the bed region dynamic pressure profile.

$$\varepsilon_G = \frac{\left(\Delta P/\Delta z\right) g^{-1} + (\rho_S - \rho_L)\,\varepsilon_S}{\rho_L - \rho_G} \tag{2.8}$$

The bed region liquid holdups (ε_L) were calculated knowing that the sum of phase holdups must give unity. The gas holdups in the freeboard region (ε_{G-FB}) were measured based on the dynamic pressure profile above the bed.

$$\varepsilon_{G-FB} = \frac{\left(\Delta P/\Delta z\right) g^{-1}}{\rho_L - \rho_G} \tag{2.9}$$

2.3.2. Statistical analysis

Standard deviations of the phase holdups were estimated to provide additional insight on the fluid dynamic behaviour of the bed and freeboard regions. Bars presented in the figures of this study provide the estimated standard deviations based on the method discussed in this section. The dynamic pressure drop was measured for 20 seconds at each pressure

port, for a minimum of three ports in the bed and three ports in the freeboard region based on the operating conditions, with a sampling rate of 20 Hz. Pooled variances (s_P^2) were estimated for the bed and freeboard regions as follows:

$$s_P^2 = \frac{\sum_{i=1}^{N}(m_i - 1)s_i^2}{\sum_{i=1}^{N}(m_i - 1)} \tag{2.10}$$

Where m is the number of data points for a given measurement and N is the number of pressure drops measured in the bed or freeboard. Phase holdups were calculated from the intercept (β_0) and slope (β_1) of the dynamic pressure profiles in the bed and freeboard region. The standard deviations of the intercept (s_{β_0}) and slope (s_{β_1}) were estimated as follows:

$$s_{\beta_0} = \sqrt{\frac{s_P^2 N}{N \cdot \left(\sum_{i=1}^{N} \Delta z_i^2\right) - \left(\sum_{i=1}^{N} \Delta z_i\right)^2}} \tag{2.11}$$

$$s_{\beta_1} = \sqrt{\frac{s_P^2 \left(\sum_{i=1}^{N} \Delta z_i^2\right)}{N \cdot \left(\sum_{i=1}^{N} \Delta z_i^2\right) - \left(\sum_{i=1}^{N} \Delta z_i\right)^2}} \tag{2.12}$$

Bed heights were determined via the intersection of the bed and freeboard region pressure profiles. The bed height standard deviation (s_{h_B}) were hence estimated using the following.

$$s_{h_B} = \sqrt{\left(\frac{s_{\beta_{0-FB}}}{\beta_{1-B} - \beta_{1-FB}}\right)^2 + \left(\frac{s_{\beta_{0-B}}}{\beta_{1-B} - \beta_{1-FB}}\right)^2 + \left(\frac{\beta_{0-FB} \cdot s_{\beta_{1-B}}}{\beta_{1-B} - \beta_{1-FB}}\right)^2 + \left(\frac{\beta_{0-B} \cdot s_{\beta_{1-FB}}}{\beta_{1-B} - \beta_{1-FB}}\right)^2} \tag{2.13}$$

Finally, the standard deviations of the solid (s_{ε_S}), gas (s_{ε_G}) and liquid (s_{ε_L}) holdups in the bed region were estimated as follows.

$$s_{\varepsilon_S} = \frac{4m}{\pi d_C^2 \rho_S h_B^2} s_{h_B} \tag{2.14}$$

$$s_{\varepsilon_G} = \sqrt{\left(\frac{s_{\beta_{1-B}}}{g(\rho_L - \rho_G)}\right)^2 + \left(\frac{\rho_S - \rho_L}{\rho_L - \rho_G} s_{\varepsilon_S}\right)^2} \tag{2.15}$$

$$s_{\varepsilon_L} = \sqrt{s_{\varepsilon_G}^{\,2} + s_{\varepsilon_S}^{\,2}} \tag{2.16}$$

The gas holdup standard deviation in the freeboard is estimated using Eq. (2.15), where the solid holdup standard deviation is equal to zero.

2.3.3. Minimum liquid fluidization velocity

The minimum liquid fluidization velocity (U_{Lmf}) is the superficial liquid velocity for a given superficial gas velocity where the bed is considered fluidized. The dynamic pressure drop was measured with a pressure port located in the bed region at constant gas flow rate while gradually lowering the liquid velocity. The minimum liquid fluidization velocity was estimated from the change in the dynamic pressure drop from the fluidized to the fix bed regime. An example is shown in Figure 2.3.

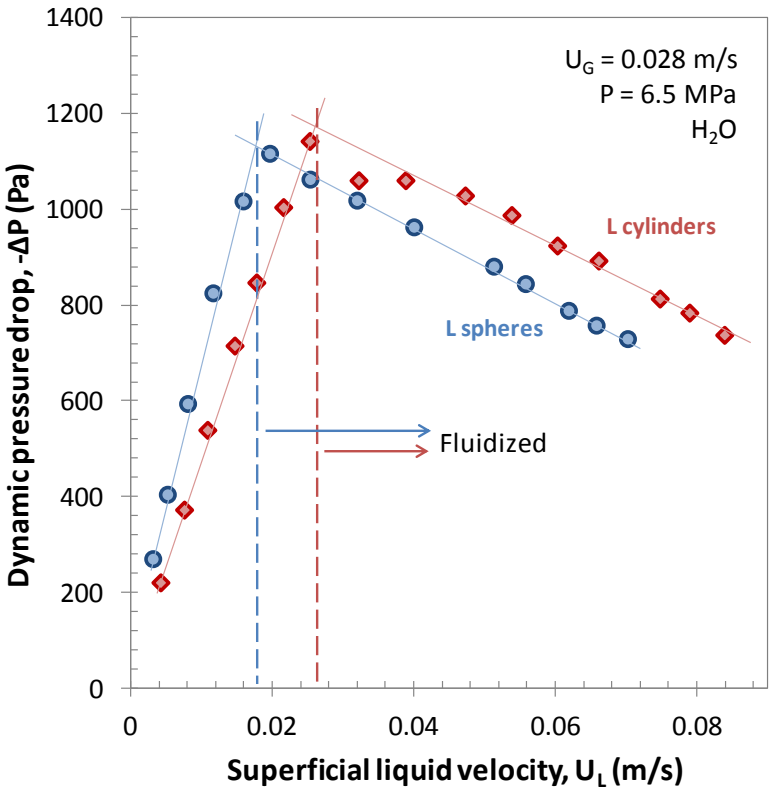

Figure 2.3. U_{lmf} measurement example for the 4 mm spheres and equivalent cylinders.

2.4. Liquid-solid fluidized bed

Hydrodynamics of the larger and smaller equivalent particles were first investigated in liquid-solid fluidized beds. Figure 2.4 shows the solid volumetric fractions for the large and small size sets of equivalent spheres and cylinders. Solid holdups over the range of studied liquid superficial velocities were comparable, implying similar liquid-solid fluidization behaviour for both particle shapes. It should be noted that the range of studied solid holdups for the cylindrical particles did not include the lower liquid velocities used with the spheres. The minimum fluidization characteristics differed between spheres and cylinders, where the cylinders generally required higher liquid flow rates to fluidize partially due to the greater particle density (further discussed in section 2.6). There was naturally no significant difference in bed void between the water and aqueous ethanol solution systems.

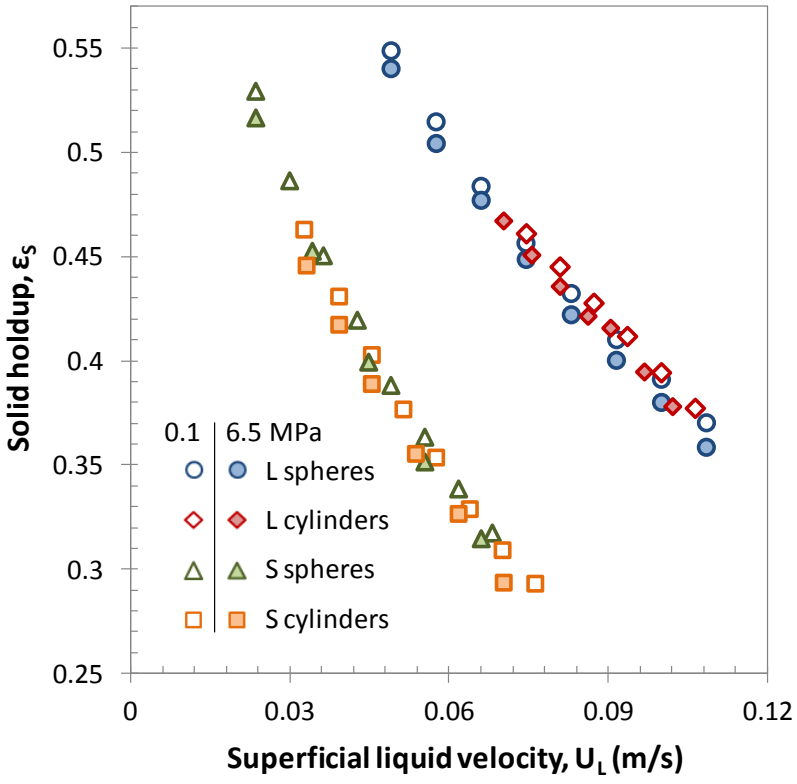

Figure 2.4. Solid holdups as a function of the superficial liquid velocity for L and S particles in water. Hollow and solid data points represent pressures of 0.1 and 6.5 MPa, respectively.

Experimental results were compared to bed porosity empirical correlations to evaluate if the models predict particle shape effects in a liquid-solid fluidized bed. The resulting parameters and average absolute relative errors (AARE) are provided in Table 2.3.

Table 2.3. Liquid-solid bed void fraction correlation parameters.

	Parameter	L spheres	L cylinders	S spheres	S cylinders
Linearization of Equation (2.3)	n	2.39	2.45	2.86	3.04
	U_{LT} (m/s)	0.325	0.342	0.201	0.216
	AARE (%)	0.4	0.2	0.1	0.2
Spherical correlations	n	2.44	2.43	2.58	2.53
	$U_{LT\infty}$ (m/s)	0.40	0.48	0.21	0.26
	k	0.83	0.81	0.91	0.90
	AARE (%)	0.4	5.9	3.7	11.7
Cylindrical correlations	$U_{LT\infty}$ (m/s)	-	0.31	-	0.18
	k	-	0.94	-	0.98
	AARE (%)	-	7.1	-	1.5
Assuming liquid immobilization	K	-	1.09	-	1.09
	ρ_{eff} (kg/m^3)	-	2575	-	2522
	d_{eff} (mm)	-	5.04	-	1.92
	n	-	2.43	-	2.53
	$U_{LT\infty}$ (m/s)	-	0.47	-	0.25
	k	-	0.81	-	0.89
	AARE (%)	-	1.4	-	4.9

The parameters of the Richardson and Zaki (1954) empirical correlation were estimated using the experimental data by linearizing Eq. (2.3) as follows:

$$\ln U_L = n \ln \varepsilon + \ln\left(U_{LT}\right) \tag{2.17}$$

The slope of Eq. (2.17) provided the n index and the intercept provided the settling velocity of a single particle, accounting for wall effects. The n index for spherical particles in the Newton flow regime ($Re_{LT\infty} > 500$), where inertial forces dominate, is typically between 2.3 and 2.4 (Khan and Richardson, 1989). This is observed for the L spheres ($Re_{LT\infty} = 1550$) and L cylinders ($Re_{LT\infty} = 1440$). The n index in the Stokes flow regime ($Re_{LT\infty} < 0.2$), where viscous forces dominate, is generally between 4.6 and 4.8. The Reynolds numbers for the settling S spheres and S cylinders ($Re_{LT\infty} = 330$ for both) indicate the transition between the Stokes and Newton flow regions. This is further confirmed by the n parameter obtained with the experimental data, which is between the typical values for both Stokes and Newton flow regions. The experimental data indicated that the settling velocities and n index values of the equivalent spheres and cylinders were similar.

The first set of correlations used for comparison assumes that cylindrical particles can be estimated as spheres, where the volume equivalent diameter is used as the characteristic length. The n index and wall effects required for Eq. (2.3) were calculated using the following relations (Khan and Richardson, 1989).

$$\frac{4.8 - n}{n - 2.4} = 0.043 Ar_L^{\,0.57}\left[1 - 1.24\left(d_V / d_C\right)^{0.27}\right] \tag{2.18}$$

$$k = 1 - 1.15\left(d_V / d_C\right)^{0.6} \tag{2.19}$$

The free settling velocity of a single particle was estimated using the correlation of Turton and Clark (1987), shown to provide adequate predictions for spheres (Brown and Lawler, 2003).

$$Re_{LT\infty} = \frac{d_V\, U_{LT\infty}\, \rho_L}{\mu_L} = Ar_L^{\,1/3}\left[\left(\frac{18}{Ar_L^{\,2/3}}\right)^{0.824} + \left(\frac{0.321}{Ar_L^{\,1/3}}\right)^{0.412}\right]^{-1.214} \tag{2.20}$$

The previous correlations provided a good fit for the large and small spheres (AARE of 0.4% and 3.7%, respectively). The estimated settling velocities, calculated as the product of $U_{LT\infty}$ and k, for the spheres were comparable to those obtained using the experimental data. The spherical correlations however under predicted the bed void for the large and small cylinders (AARE of 5.9% and 11.7%, respectively). The deviations likely resulted from an over prediction of the cylindrical free settling velocities. The n indexes for the smaller particles were underestimated using Eq. (2.18), likely as the particles are in the intermediate settling flow region ($0.2 < Re_{T\infty} < 500$).

A second comparison was completed using available correlations for cylindrical particles. The terminal free settling velocities were estimated using the Haider and Levenspiel (1989) empirical correlation for isometric non-spherical particles.

$$Re_{LT\infty} = \frac{d_V U_{LT\infty} \rho_L}{\mu_L} = Ar_L^{1/3}\left(\frac{18}{Ar_L^{2/3}} + \frac{2.335 - 1.744\phi}{Ar_L^{1/6}}\right)^{-1} \tag{2.21}$$

Wall effects for the cylinders were estimated using the following correlation, valid for cylinders where $L_P / d_P < 10$ (Chhabra, 1995).

$$k = 1 - 1.33 d_V / d_C \tag{2.22}$$

As previously mentioned, no correlation has been found in the open literature for the n index of cylinders. The n values previously determined assuming volume equivalent spherical particles were consequently used (refer to Eq. (2.18)). Estimated bed porosities for the smaller cylinders were comparable to the experimental results (AARE = 1.6%), however they over predicted the bed porosities of the larger cylinders (AARE = 7.1%). Wall effects were previously experimentally observed to be less significant for cylinders compared to spheres (Chhabra, 1995), agreeing with the estimated k values of Eq. (2.22).

The last correlation assumed liquid immobilization around the cylinders to form pseudo-spheres (Fouda and Capes, 1977). As shown in Eq. (2.4), a hydrodynamic volume factor (K) must be estimated. It was assumed that the settled bed porosity was equivalent to the void at minimum fluidization (Eastwood et al., 1969), which results in the following.

$$K = \frac{0.603}{1 - 0.415/\phi^{0.483}} - 0.03 \tag{2.23}$$

Required parameters for Eq. (2.4) (n, k and $U_{LT\infty}$) were estimated based on the correlations previously presented for spherical particles using the effective particle diameter ($d_{eff} = d_V K^{1/3}$) and effective density ($\rho_{eff} = [\rho_S + \rho_L(K-1)]/K$). Eq. (2.4) was then used to compare with the experimentally obtained bed porosities, where the parameters of interest for this comparison are provided in Table 2.3. Effective densities were comparable to the density of glass while the effective diameters were similar to the cylinders' volume equivalent diameters. Estimated settling velocities for this method were the closest to the experimentally measured values. The main difference when calculating the bed porosities were from the n index and wall effects. The estimated porosities for the larger cylinders were rather close (AARE = 1.4%) to the experimental results while the smaller cylinders had a slightly greater deviation (AARE = 4.9%).

In summary for the studied liquid-solid fluidized beds, experimental bed porosities demonstrated that the Sauter mean diameter effectively accounted for shape effects of cylinders when $\phi = 0.8$. Experimentally estimated settling velocities indicated that the drag forces on the studied spheres and cylinders were similar in the liquid-solid fluidized bed. Although drag coefficients are generally higher for a cylinder compared to a sphere (Haider and Levenspiel, 1989), changes to the cylindrical projected area due to particle orientation, as described by Lau et al. (2010), likely led to similar solid holdups. It was also visually observed as the cylinders had various orientations while fluidized. When trying estimate the bed porosity, correlations developed for cylindrical particles and the liquid immobilization approximation provided better predictions when considering the large and small cylinders. Prior to the inclusion of the gas phase, the equivalent spheres and cylinders resulted in similar liquid-solid fluidized bed hydrodynamics.

2.5. Gas-liquid-solid phase holdups

The fluid dynamic behaviour of the gas-liquid-solid fluidized bed was investigated by measuring global phase holdups in the bed region while varying parameters of interest.

Assuming the Sauter mean diameter is sufficient to account for particle shape effects, the measured holdups for equivalent particles should be comparable. In addition to the mean holdups, estimated standard deviations are shown on the figures using bars in this section to provide additional information on the hydrodynamic behaviour. Pressure effects and the addition of surfactant were also studied to determine the impact of bubble characteristics on general hydrodynamics and particle shape effects. Figure 2.5 provides the mean holdup average absolute differences (AAD) for the studied gas-liquid-solid operating conditions. Associated trends and experimental data are discussed in the following sections.

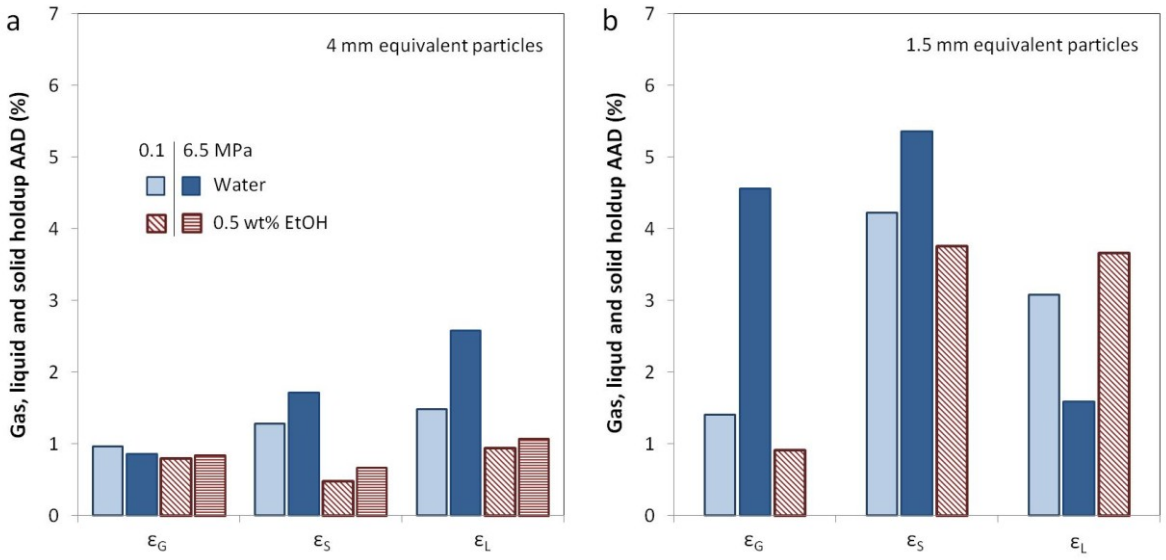

Figure 2.5. Bed region holdup average absolute differences between the cylindrical and spherical particles for the studied gas-liquid-solid operating conditions.

2.5.1. 4 mm equivalent particles (water)

Gas, liquid and solid holdups in the bed region for the 4 mm spheres and equivalent cylinders in water are presented in Figure 2.6. Gas holdups at atmospheric pressure (Figure 2.6a and 2.6b) show a transition from dispersed to coalesced bubble flow, noted by the change in slope at a gas velocity of approximately 60-70 mm/s for both liquid flow rates. Greater volumes of gas passing through the bed region at higher gas flow rates increase the likelihood of bubble coalescence. Gas holdups remained fairly constant following the

transition as larger bubbles have a lower residence time due to their increased rise velocities. Estimated gas, liquid and solid holdup standard deviations corroborate the presence of larger bubbles at gas flow rates above 70 mm/s, where small and evenly sized bubbles resulted in minimal variations to the measured dynamic pressure drops. Conversely, as bubble coalescence became more prominent, pressure fluctuations increased due to large and rapid changes to the fluid mixture's density. Solid holdup standard deviations provide a qualitative measure of the bed interface stability. It was visually confirmed that the bed interface experienced greater fluctuations in coalesced bubble flow. The system properties, mainly larger particle size, resulted in the dispersed bubble flow regime at low gas flow rates. Bed expansion at the introduction of gas was visually observed and is confirmed by the solid holdup reduction at low gas flow rates. The previous has been generally observed for particles above a given size range, typically greater than 2.5 mm for glass beads (Han et al., 1990). The net gravitational force of the larger particles was sufficient to enhance bubble break-up in the bed region, resulting in relatively evenly sized dispersed bubbles. Wake effects of the relatively small spherical bubbles have less of an impact on the bed hydrodynamics and increasing the gas flow rate thus generally resulted in greater bed porosity.

The liquid flow rate had a greater impact on the solid and liquid holdups for the studied operating conditions. The gas-perturbed liquid model (Zhang et al., 1998) assumes that the solid particles are fully supported by the liquid. The bed hence expanded at the higher liquid superficial velocity due to greater the drag on the particles, as shown in Figures 2.6c and 2.6d, where the increased bed porosity was mainly due to a greater liquid volume, shown in Figures 2.6e and 2.6f. The transition from dispersed to coalesced flow was influenced by the higher liquid velocity, resulting in an increased gas velocity and gas holdup at the point of transition. The previous observations are partially due to the gas injection method in the experimental system, where the gas is mixed with the liquid in the plenum chamber below to the distributor plate. The ensuing shear stresses on the bubbles passing through the distributor are a function of the liquid velocity. Bubble size is dictated by the various forces acting upon the gas-liquid interface. Shear stresses due to higher liquid velocities thus enhanced bubble break-up upon entering the bed.

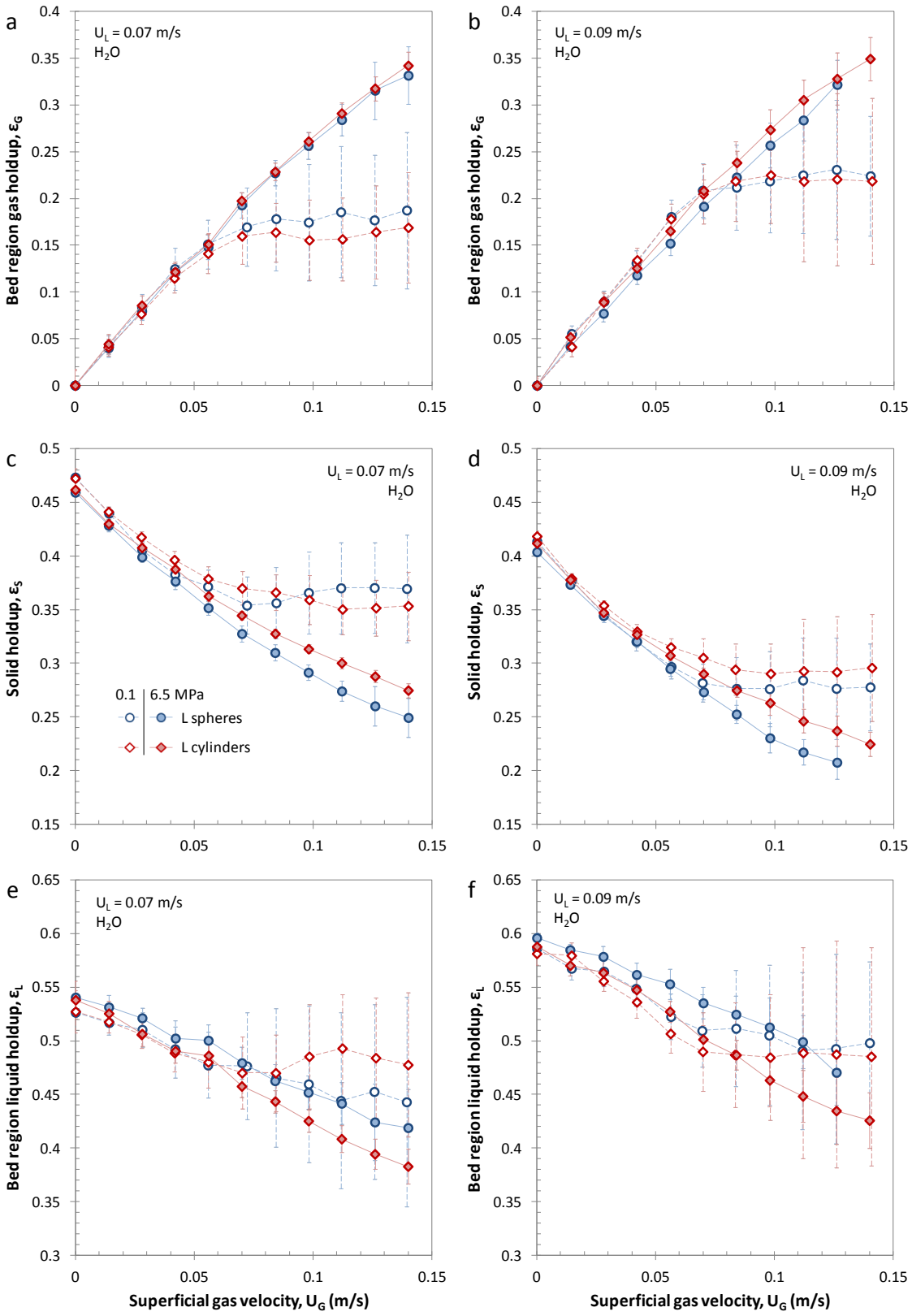

Figure 2.6. Gas, solid and liquid holdups in the bed region for the 4 mm spheres and equivalent cylinders at 0.1 and 6.5 MPa in water.

The effects of operating at elevated pressure, more specifically an increased gas density, are important to consider for industrial gas-liquid-solid fluidized beds. Bubble coalescence, bubble break-up and the maximum stable bubble size are each affected by the operating pressure. When considering bubble coalescence, three steps are commonly considered (Chaudhari and Hofmann, 1994):

1. approach of two bubbles to form a thin liquid between them,
2. thinning of the film by drainage of the liquid,
3. rupture of the film at a critical thickness.

Bubble collisions are highly dependent on wake effects (Fan and Tsuchiya, 1990), which are more prominent in the presence of large/coalescing bubbles. In addition, the thinning of the film is believed to be slower at elevated pressures due to lower surface tension and increased liquid viscosity (Fan et al., 1999). Bubble break-up and the maximum stable bubble size are a function of the forces at the bubble interface. When operating at higher pressures, increased bubble break-up and lower maximum stable bubble size may be due to the internal circulation of the gas (Fan et al., 1999). Higher gas densities result in a greater centrifugal force acting outwards on the bubble surface. As the internal centrifugal force exceeds the gas-liquid surface tension force, bubble break-up is enhanced and the maximum stable bubble size is reduced.

Solid data points in Figure 2.6 show the effect of pressure for the studied gas and liquid flow rates. The gas holdups at 6.5 MPa in the bed increased at a nearly constant rate for the studied gas flow rates. Elevated pressure therefore inhibited the transition from dispersed to coalesced bubble flow, which is in agreement with the theoretical expectations. It should also be noted that the estimated standard deviations at 6.5 MPa were relatively smaller than those at atmospheric pressure, corroborating the dispersed bubble flow regime at higher gas flow rates. As the gas holdups increased, the solid and liquid holdups were both reduced due to the greater bed porosity from the increased volume of gas.

The AAD comparison presented in Figure 2.5a demonstrates that the measured global holdups for the spheres and equivalent cylinders were similar in water at atmospheric and elevated pressure. Although the mean holdups occasionally differed, the standard deviations must be considered. Gas holdups were comparable prior to the transition from the dispersed

to coalesced flow. As larger bubbles were formed, gas holdups at superficial liquid velocities above 60-70 mm/s differed marginally while the standard deviations suggest that the discrepancy was minor. Gas holdups measured at the higher liquid flow rate, shown in Figure 2.6b, were quite similar. Solid holdups at 6.5 MPa showed that the cylindrical particles resulted in lower bed porosity which may be due to the slightly higher particle density, as shown in Table 2.2. Overall, the spheres and cylinders were comparable based on the hydrodynamic behaviour studied via the global phase holdups and their standard deviations. Bubble/particle size ratios must nonetheless be considered as differences primarily appeared following the transition from dispersed to coalesced bubble flow.

2.5.2. 4 mm equivalent particles (0.5 wt.% aqueous ethanol)

Surfactant was added to the liquid in an attempt to achieve the high gas holdups observed in some industrial gas-liquid-solid fluidized beds (McKnight et al., 2003). The molecular structure of a surfactant generally has both a polar and non-polar component. As a result, a small quantity of ethanol added to water coats the gas-liquid interface as the gas phase is non-polar and the liquid phase is polar. The added surfactant lowered the gas-liquid surface tension (0.072 N/m for water and 0.0685 N/m for the 0.5 wt.% aqueous ethanol solution); however its main impact on the ebullated bed hydrodynamics was bubble coalescence inhibition. As the polar ends of the surfactant molecule cover the outer surface of a bubble, a repulsion force is present between two approaching bubbles. Since this is the first step to bubble coalescence (Chaudhari and Hofmann, 1994), the ethanol solution resulted in smaller bubbles compared to the water system.

Global phase holdups obtained with the 4 mm equivalent particles using 0.5 wt.% aqueous ethanol are provided in Figure 2.7. Compared to the analogous results in water (Figure 2.6), the transition from dispersed to coalesced bubble flow is less apparent. Although the increase in the gas holdup was not entirely linear (refer to Figures 2.7a and 2.7b), the minor change in the slope at higher gas velocities suggests that only a small portion of the bubbles were coalescing. This is further confirmed when examining the low gas holdup standard deviations, indicating the presence of small dispersed bubbles. Solid holdups, shown in Figures 2.7c and 2.7d, reveal that increased gas velocity resulted in

greater bed expansions, as expected with dispersed bubble flow. The bed interface was visually observed to be stable, which is also confirmed via the relatively low solid holdup standard deviations. Increased liquid flow had a minor impact in the surfactant solution, where it mainly reduced the solid holdups due to greater bed expansion. The increased liquid holdups, shown in Figures 2.7e and 2.7f, and minor changes in the gas holdups at U_L of 0.09 m/s indicate that the expanded volume in the bed was primarily occupied by the liquid.

Pressure had less of an impact when surfactant was added to the system. Results at 6.5 MPa in Figure 2.7 were comparable to those obtained at atmospheric pressure. Elevated pressure and addition of surfactant have similar effects on bubble dynamics. Both hinder bubble coalescence, where elevated pressures modify the forces acting on a bubble and surfactants interact with the bubble interface. Bubble break-up in the presence of surfactant was again related to the gas injection method in the experimental system (refer to Figure 2.1). Shear stresses while passing through the distributor plate led to significant bubble break-up upon entering the bed. These small bubbles had a low tendency to coalesce due to the ethanol molecules at the gas-liquid interface, which resulted in the observed high gas holdups. In addition, the 4 mm particles have sufficient net gravitational force to enhance bubble break-up in the bed. Pressure effects have been previously shown to subside above a given pressure (Fan et al., 1999; Rudkevitch and Macchi, 2008). Pressure effects were thus minor in the surfactant system as the bubble sizes were already reduced due to shear stresses, bubble-particle interactions and surface active compounds at the gas-liquid interface.

The AAD for the global holdups in the surfactant solution (Figure 2.5) demonstrated that the spherical and cylindrical particles had nearly equivalent fluid dynamic behaviour at 0.1 and 6.5 MPa. This further demonstrates the importance of the bubble/particle size ratio when comparing spheres and cylinders in a gas-liquid-solid fluidized bed. The 4 mm spheres thus exhibited comparable hydrodynamics to the equivalent cylindrical particles when the system was operated under high gas holdup conditions through surfactant addition and/or elevated pressure.

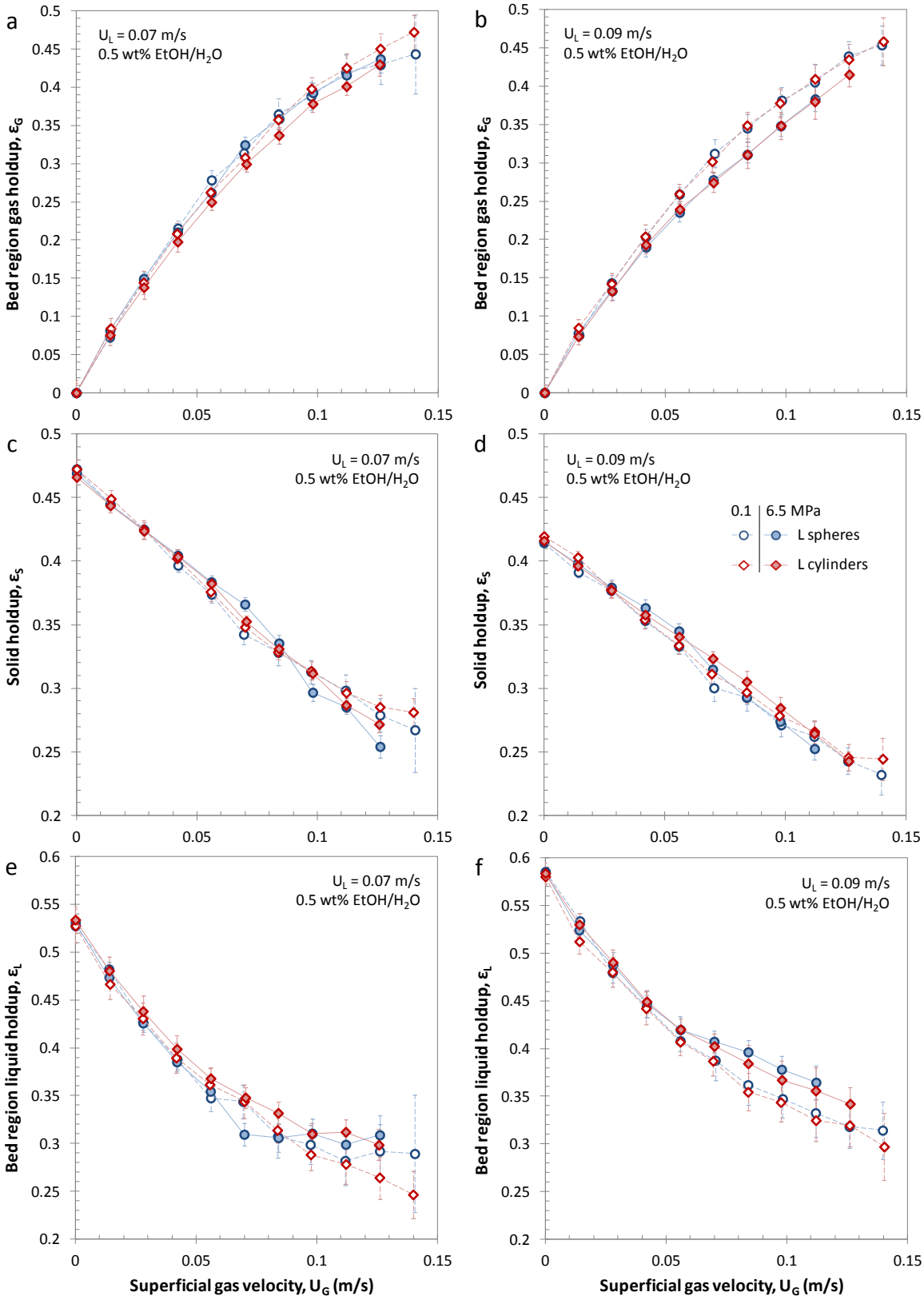

Figure 2.7. Gas, solid and liquid holdups in the bed region for the 4 mm equivalent particles at 0.1 and 6.5 MPa in the 0.5 wt.% aqueous ethanol solution.

2.5.3. 1.5 mm equivalent particles (water)

Bed region holdups for the 1.5 mm spheres and equivalent cylinders in water are shown in Figure 2.8. Relative to the 4 mm particles, a greater divergence was observed between the cylindrical and spherical particles for the studied operating conditions. The rate of increase for the gas holdup as a function of gas velocity (refer to Figures 2.8a and 2.8b) indicated a mostly consistent bubble flow regime. Coalesced bubble flow was visually observed in the bed region, which has been previously noted for particles in this size range (Han et al., 1990). Estimated standard deviations presented in Figure 2.8 show greater variation in the bed region due to the larger coalescing bubbles.

Solid holdups for the spherical particles, shown in Figures 2.8c and 2.8d, indicate that the bed contracted at the introduction of the gas phase. This behaviour is due to liquid entrainment in the wake of large rising bubbles. The entrained liquid thus reduced the effective amount of liquid in the bed, lowering the liquid flow rate available for fluidization. Cylindrical particles however did not exhibit the same bed contraction behaviour. At 0.1 MPa, the cylindrical solid holdups initially remained fairly constant while increasing the gas flow rate. The previous observation was likely due to particle stacking differences between the spheres and cylinders. For a given superficial liquid velocity, the liquid-solid fluidized bed measurements established that solid concentrations were similar for both spheres and cylinders. However, the loose bed packing porosities for the cylinders are known to be higher compared to spheres (Zou and Yu, 1996). The bed of cylinders may have thus been less likely to contract at the introduction of gas as the differences between the fluidized and static bed heights were smaller compared to the spheres at the studied liquid flow rates.

The superficial liquid velocity had a minor effect on the bed region gas holdups as it has less of an impact on larger coalescing bubbles. Increased liquid flow rate did however result in greater liquid holdups and generally lower solid holdups in the bed region. The superficial liquid velocity thus mainly affected the bed porosity via an increased liquid volume.

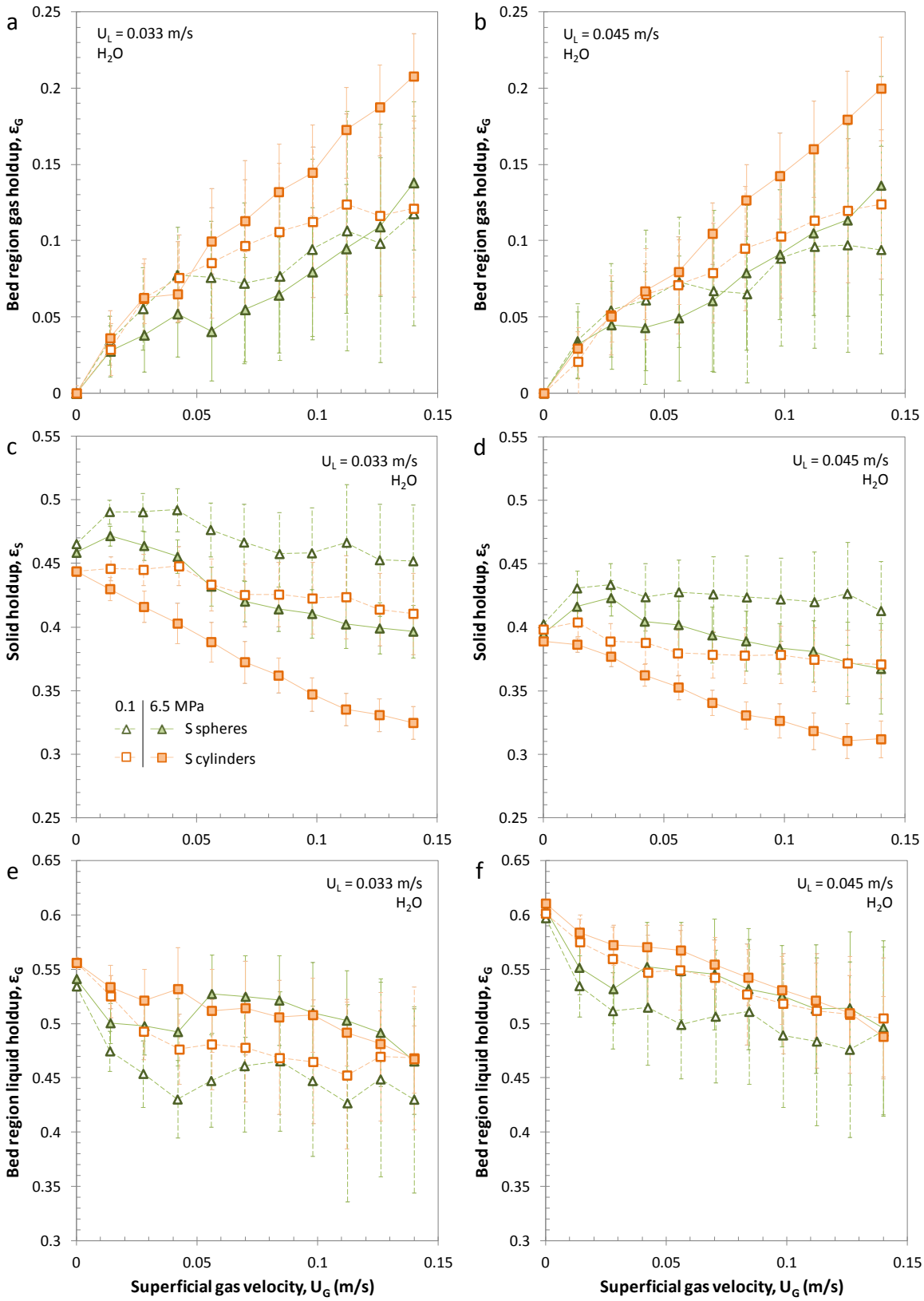

Figure 2.8. Gas, solid and liquid holdups in the bed region for the 1.5 mm spheres and equivalent cylinders at 0.1 and 6.5 MPa in water.

Pressure effects were less straightforward for the 1.5 mm particles compared to the larger 4 mm particles. It was expected that elevated pressures would increase the bed region gas holdups. However this was not generally observed as the bubbles in the bed region were still coalescing. Bed contraction can still be observed at high pressure in Figures 2.8c and 2.8d for the 1.5 mm spheres. This behaviour has been previously observed for spheres in a similar size range (Jiang et al., 1997). Figures 2.8c and 2.8d show that operating at 6.5 MPa had a consistent effect on the solid holdups, where elevated pressure resulted in lower solid concentrations compared to atmospheric pressure. As a result, it is believed that changes to bubble size and wake effects at elevated pressures had competing effects on the gas and liquid holdups. As the average bubble size was likely reduced at higher operating pressures, the liquid was less likely to be entrained by bubble wakes. This is confirmed by examining the spherical particle solid holdups at 6.5 MPa to the values with no gas flow, where bed expansion was eventually obtained at high pressure. As elevated pressures likely reduced the mean bubble size in the bed region, the reduced wake effects increased the liquid volume in the bed region, which is observed in Figures 2.8e and 2.8f. Based on the previous, the gas holdups appeared to increase or decrease at elevated pressures, depending on bubble shape and operating conditions.

The average absolute differences of the 1.5 mm equivalent particles (refer to Figure 2.5b) showed a larger discrepancy due to particle shape compared to the 4 mm equivalent particles. Gas holdups were generally greater for the cylinders while the solid holdups were higher for the spherical particles. The cylindrical particles generally did not exhibit the bed contraction behaviour observed with the spherical particles. Previous experiments suggested that particle shape effects were related to bubble size/shape (Song et al., 1989), which is in agreement with these results. Consequently, the Sauter mean diameter may not sufficiently account for particle shape effects in a fluidized bed with large coalescing bubbles and/or likely to exhibit bed contraction.

2.5.4. 1.5 mm equivalent particles (0.5 wt.% aqueous ethanol)

Global phase holdups with the added surfactant are presented in Figure 2.9 for the 1.5 mm equivalent particles. High pressure results were not completed due to operating

difficulties with the experimental system for this particle size. The high gas holdup conditions obtained due to combined effects of surfactant addition and elevated pressure resulted in bed expansions greater than expected for the smaller particles. Due to their size, particles flowed through the overflow section and partially blocked the liquid return line. The foam head then had the potential to cause liquid to enter the compressor, which must be prevented.

The 0.5 wt.% aqueous ethanol solution at atmospheric pressure resulted in the dispersed bubble flow regime at low gas flow rates ($U_G < \sim 0.06$ m/s). This is evident by the approximately linear increase in the gas holdup and the solid holdup reduction, implying that the bed was expanding. As the gas flow rate was further increased, bubbles in the bed region began to coalesce in the bed region. This can be further confirmed via the estimated standard deviation which increased following the transition from dispersed to coalesced bubble flow. Bed region phase holdups remained fairly constant following the bubble flow regime transition. Liquid velocity had a minor impact on the bed hydrodynamics at these conditions. At the lower gas velocities, liquid holdups increased and solid holdups decreased for the higher liquid flow rate, implying that the bed was expanding due to a higher liquid volume. The impact of liquid velocity however was relatively minor following the transition to coalesced bubble flow.

The comparison of the bed region holdups for the 1.5 mm equivalent particles in the aqueous ethanol solution is shown in Figure 2.5. Measured gas holdups for the spherical and cylindrical particles were very similar with the added ethanol. Both particles appeared to transition from the dispersed to coalesced flow at a gas flow rate of approximately 0.06 m/s. Differences in the solid and liquid holdups were nonetheless observed following the transition. Similar to the water system, solid holdups of the cylindrical particles were lower than the spherical particles. These results further emphasize that a relatively larger bubble to particle size ratio can lead to different global hydrodynamic behaviour when accounting for particle shape effects using the Sauter mean diameter.

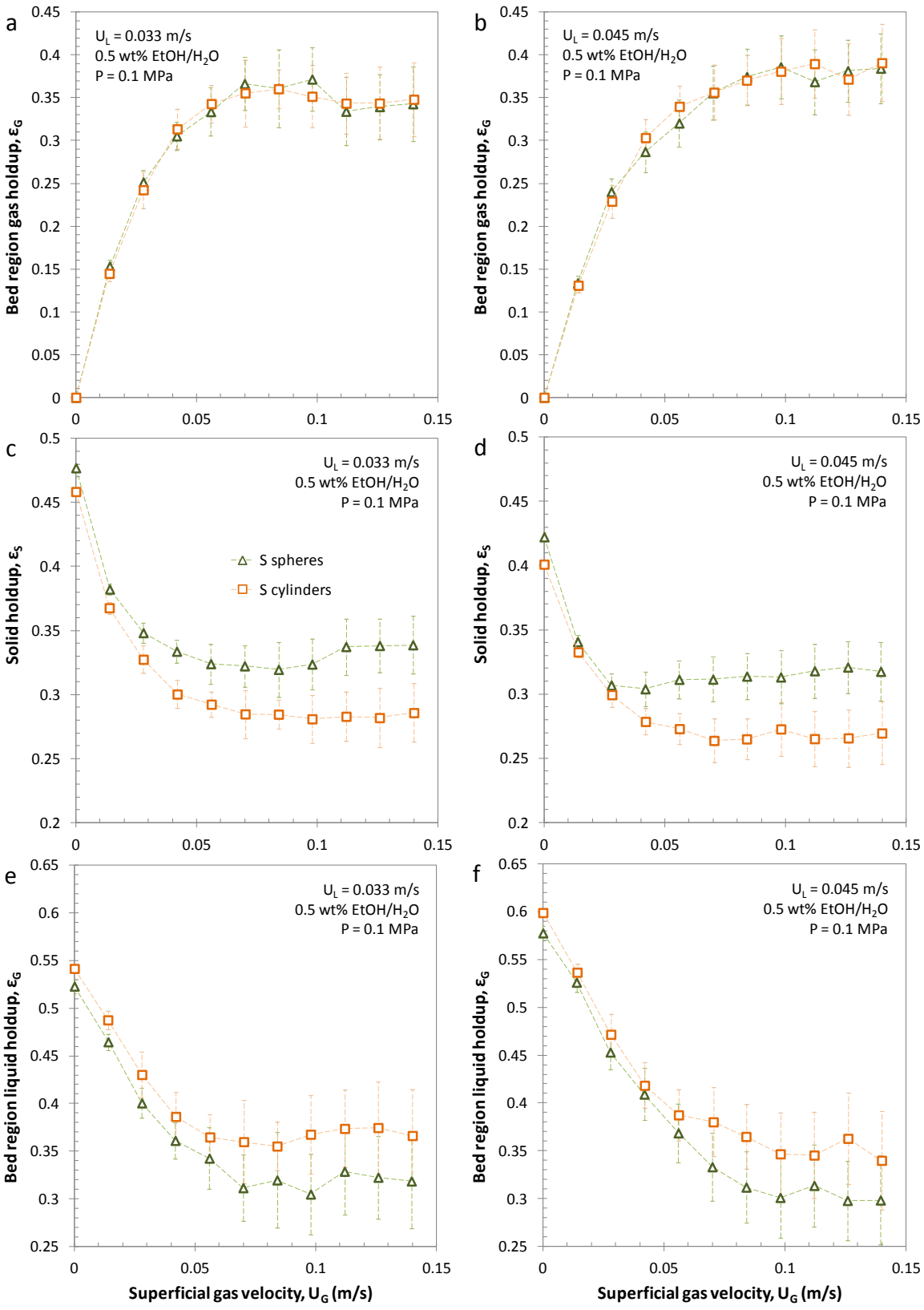

Figure 2.9. Gas, solid and liquid holdups in the bed region for the 1.5 mm equivalent particles at 0.1 and 6.5 MPa in the 0.5 wt.% aqueous ethanol solution.

2.5.5. Comparison with correlations

Experimental holdups at atmospheric pressure were compared to previously developed correlations which included a parameter for particle shape. Bed porosities for spherical particles have been previously correlated by Begovich and Watson (1978) using the following relation:

$$\varepsilon_{BW} = 3.93 \cdot U_L^{0.271} \cdot U_G^{0.0410} \cdot (\rho_S - \rho_L)^{-0.316} \cdot d_V^{-0.268} \cdot \mu_L^{0.0550} \cdot d_C^{-0.0330} \qquad (2.24)$$

Song et al. (1989) studied the hydrodynamics of various hydrotreating catalysts in water or a 0.5 wt.% aqueous t-pentanol solution. For the water system, bed porosities were correlated by incorporating the sphericity into Eq. (2.24), as shown below.

$$\varepsilon = \varepsilon_{BW} \cdot \phi^{-0.424} \qquad (2.25)$$

Similarly, Ruiz et al. (2004) correlated the bed void of other hydrotreating catalysts in diesel and jet fuels by modifying the Begovich and Watson (1978) as follows:

$$\varepsilon = \varepsilon_{BW} \cdot \phi^{0.378} \qquad (2.26)$$

Comparing the previous equations, it is observed that particle sphericity was seen to have opposing effects on the bed porosity, based on the sign of the exponents. Lastly, Song et al. (1989) also fitted the correlation for a 0.5 wt.% aqueous t-pentanol solution.

$$\varepsilon = 7.62 \cdot U_L^{0.204} \cdot U_G^{0.130} \cdot (\rho_S - \rho_L)^{-0.250} \cdot d_{SV}^{-0.175} \cdot \mu_L^{0.0600} \qquad (2.27)$$

The previous correlations were compared to bed void fractions obtained with the 1.5 and 4 mm equivalent particles for the water (Figure 2.10a) and surfactant system (Figure 2.10b). The original Begovich and Watson (1978) correlation was used to compare with the spherical particle data in the water system. Experimental data for cylindrical particles were only compared to correlations that accounted for particle shape. It should be noted that the spherical particles in the surfactant system were compared with Eq. (2.27) in Figure 2.10b. It was assumed that the hydrodynamics of the 0.5 wt.% aqueous t-pentanol solution were comparable to the 0.5 wt.% aqueous ethanol solution based on previous comparisons with various surfactants (Dargar and Macchi, 2006).

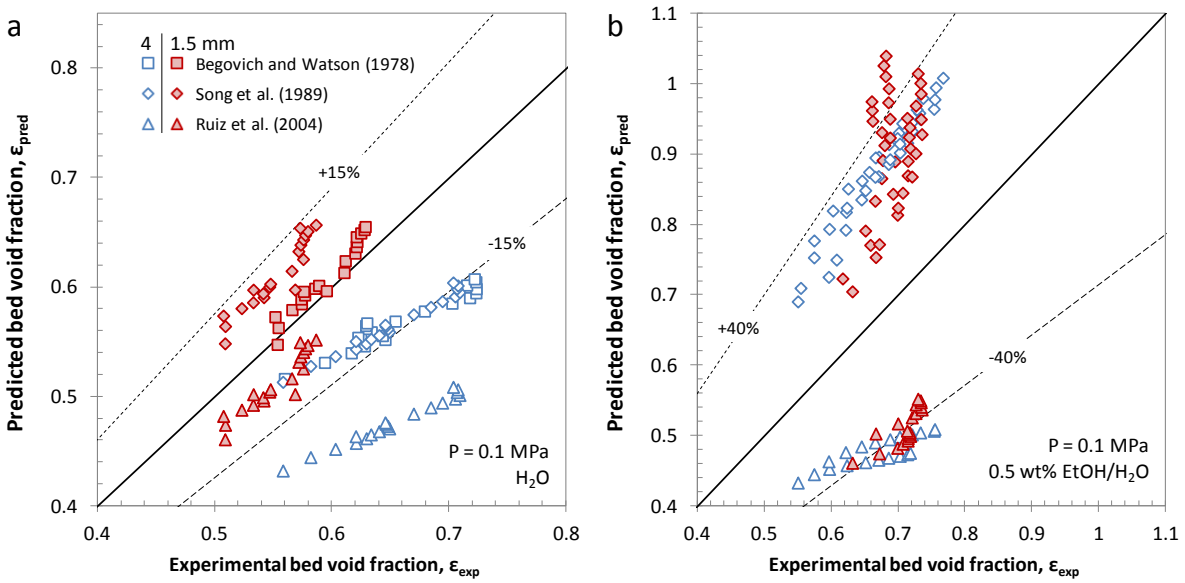

Figure 2.10. Comparison of bed void fractions for (a) water and (b) the 0.5 wt.% aqueous ethanol solution at atmospheric pressure.

Bed porosity predictions for the 1.5 mm particles water system were more accurate than for the 4 mm particles (Figure 2.10a). The Begovich and Watson (1978) correlation provided a good fit for the 1.5 mm spheres. Most of the predictions for the water system are within ± 20% of the experimental results, with the exception of Eq. (2.26) for the 4 mm cylinders. It is evident from Figure 2.10b that the correlations did not effectively predict the bed void fractions for the studied aqueous ethanol system.

Results were also compared to the Artificial Neural Networks and Dimensional Analysis (ANN-DA) approach of Larachi et al. (2001). The predictions were based on a large data set (20500 data for Newtonian liquids) and are said to account for bubble coalescence inhibition, elevated pressures and particle shape. The model requires the following parameters: superficial liquid velocity, liquid density, liquid viscosity, gas-liquid surface tension, gas density, gas viscosity, superficial gas velocity, volume equivalent diameter, particle sphericity, particle density, column diameter, and coalescence index (foaming or coalescing).

Bed porosity comparisons for the water and surfactant system are shown in Figure 2.11. The ANN-DA's predictions are generally within ± 20% for both systems, an

improvement over the modified Begovich and Watson correlations. It is interesting to note that the ANN-DA predicts different bed porosities for the 4 mm equivalent particles in both systems, while the experimental results generally overlap. The opposite is observed with the 1.5 mm particles, where the ANN-DA predictions primarily overlap but the experimental results show that the particle shape influenced the bed expansion.

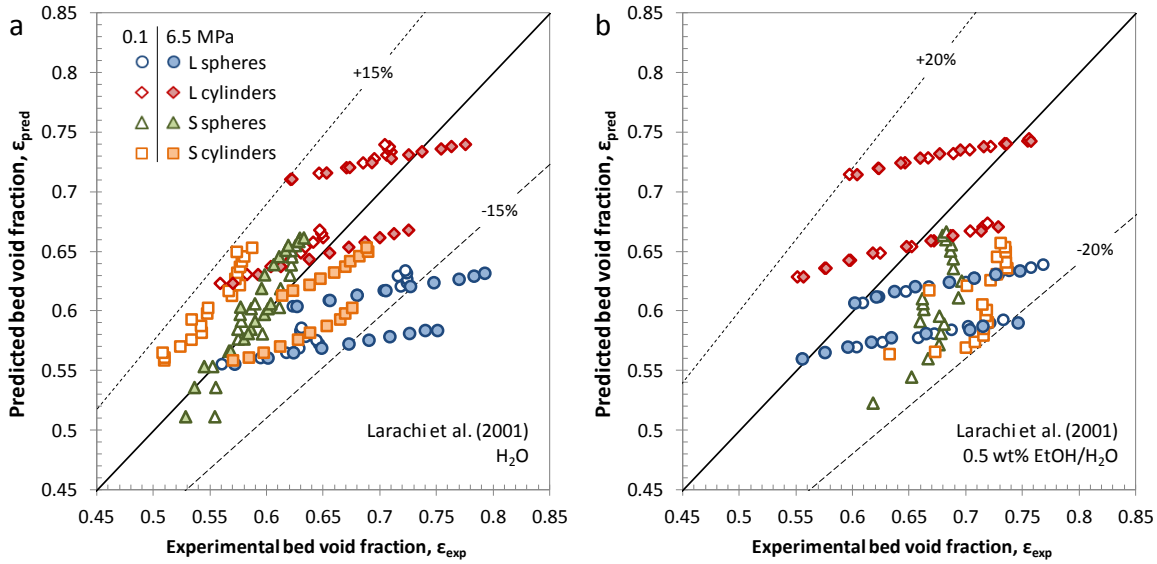

Figure 2.11. Comparison of bed void fractions for (a) water and (b) the 0.5 wt.% aqueous ethanol solution with the Larachi et al. (2001) ANN-DA.

Gas holdups are also predicted by the Larachi et al. (2001) ANN-DA and were compared with the experimental results in Figure 2.12. The gas holdup predictions have a larger associated error compared to the predicted bed porosities. The ANN-DA generally predicts similar gas holdups for the equivalent sets of particles, with the only exception being the 1.5 mm particles at 6.5 MPa in water. Gas holdups in the water system were over predicted for the 1.5 mm equivalent particles and under predicted for the 4 mm equivalent particles. For the surfactant system, predictions for the larger particles initially overestimated the gas holdups and eventually underestimate at higher gas flow rates. Predictions for the 1.5 mm equivalent particles in a foaming system underestimated the experimental gas holdups for the studied conditions.

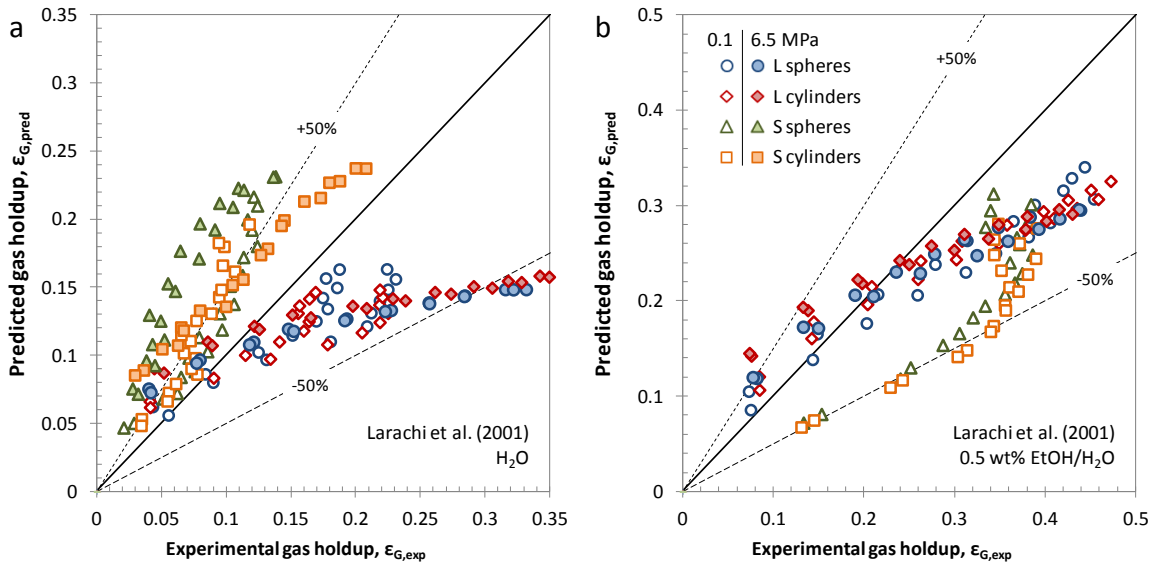

Figure 2.12. Comparison of bed gas holdups for (a) water and (b) the 0.5 wt.% ethanol-water solution with the Larachi et al. (2001) ANN.

Comparisons with the previous correlations reveal the difficulty when trying to account for particle shape in a gas-liquid-solid fluidized bed. Current models struggle to predict the effects of pressure, surfactant addition, and bed expansion/contraction for spheres alone. Some predictions seem to indicate that the Sauter mean diameter can sufficiently account for shape effects while others do not. These comparisons demonstrated the relevance of experimental measurements while trying to account for particle shape effects.

2.5.6. Freeboard gas holdups

Gas holdups in the freeboard region were measured to investigate the bubble characteristics above the bed. Figures 2.13 and 2.14 present the freeboard gas holdups for the 4 mm equivalent particles in water and the 0.5 wt.% aqueous ethanol solution, respectively. Compared to the equivalent bed region gas holdups (provided in Figures 2.6 and 2.7), the freeboard gas holdups are generally greater. This is mainly because there are no solid particles in the freeboard which reduces the interstitial velocity of the liquid, consequently increasing the bubble residence time. In addition, the 4 mm particles enhance bubble-break in the bed region, thus acting as an efficient gas-liquid distributor. Other gas holdup trends in

the freeboard are comparable to the bed region gas holdup trends discussed in sections 2.5.1 and 2.5.2.

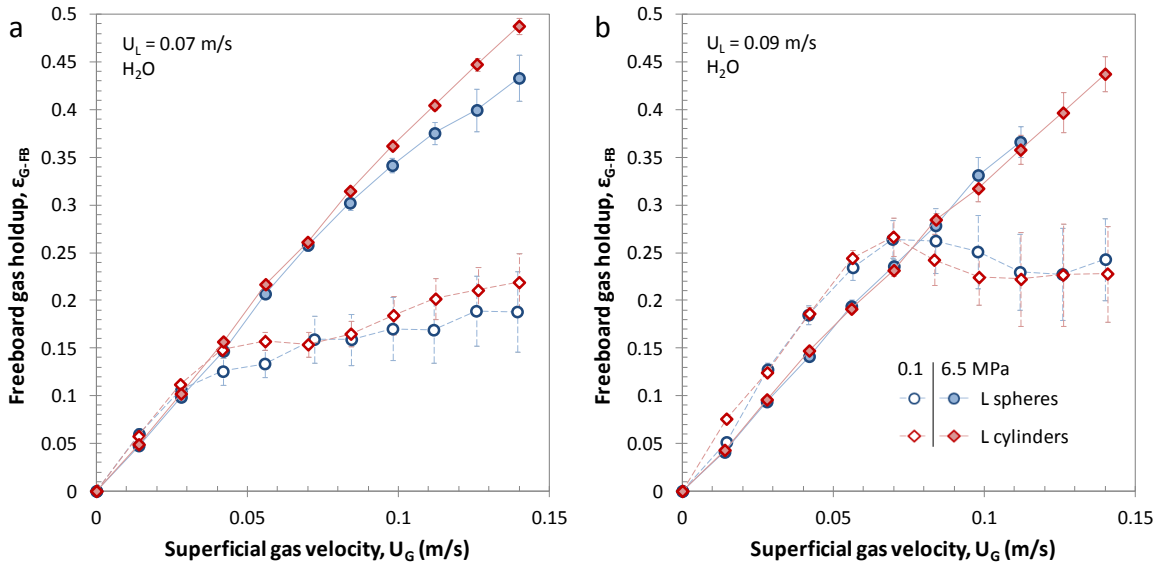

Figure 2.13. Freeboard gas holdups for the 4 mm equivalent spheres and cylinders at 0.1 and 6.5 MPa in water.

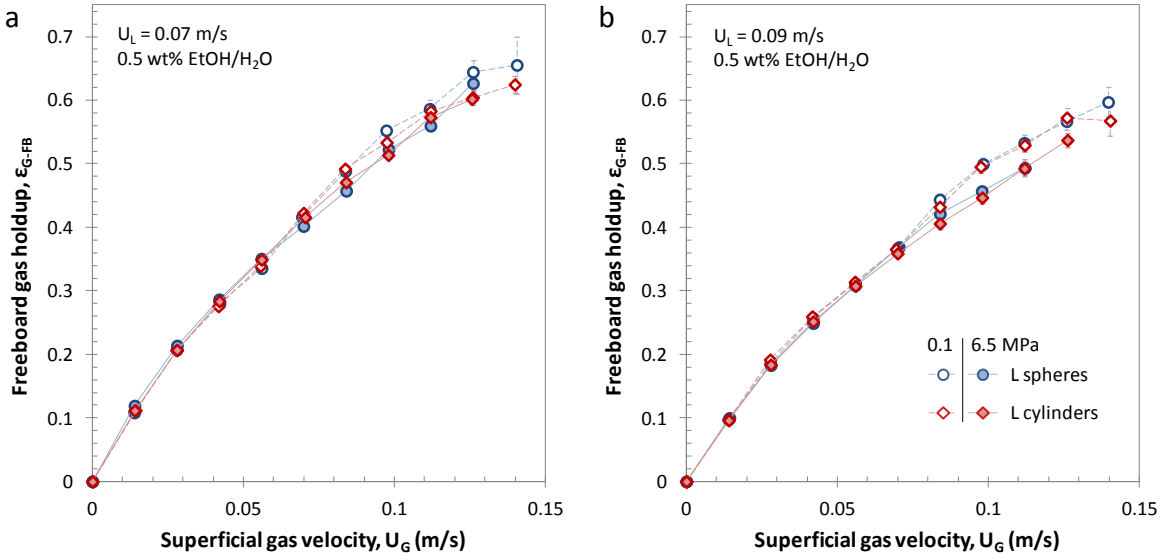

Figure 2.14. Freeboard gas holdups for the 4 mm equivalent spheres and cylinders at 0.1 and 6.5 MPa in the 0.5 wt.% aqueous ethanol solution.

Freeboard gas holdups for the 1.5 mm equivalent particles in the water and the 0.5 wt.% aqueous ethanol solution are provided in Figures 2.15 and 2.16, respectively. Unlike the 4 mm equivalent particles, there is a greater difference between the bed (Figures 2.8 and 2.9) and freeboard region gas holdup behaviour. As discussed in section 2.5.3, the 1.5 mm equivalent particles led to bubble coalescence in the bed region. Upon exiting the bed of smaller particles, the large bubbles were visually observed to break-up in the freeboard. Freeboard gas holdups at 6.5 MPa in the water system present a much larger difference when compared to bed region gas holdups. Increasing the pressure thus enhanced bubble break-up in the freeboard region (highest observed freeboard gas holdup ~ 47% at 6.5 MPa), while bubble coalescence due to the particle-bubble interactions was still significant (highest observed bed region gas holdup ≈ 20% at 6.5 MPa). Gas holdups in the freeboard for the aqueous ethanol solution followed similar trends to the bed region gas holdups, where the main difference was higher gas holdups in the freeboard as solid particles were no longer present.

Particle size was not expected to have a significant impact on the freeboard gas holdups. This is confirmed by comparing Figures 2.13 and 2.15, which show similar trends. The main differences between the freeboard holdups for both sets of particles are the bubble behaviour in the fluidized bed and the studied liquid velocities. Larger particles increased bubble break-up while the smaller particles led to coalescence in the fluidized bed. Although it is difficult to directly compare the freeboard holdups as the liquid velocities are not equal, larger particles showed a distinct transition from dispersed to coalesced flow at atmospheric pressure. It should be noted that freeboard measurements were limited by the height of the fluidization column. Experimental results thus provide information on the bubble behaviour in the region above the bed as limited by the studied system.

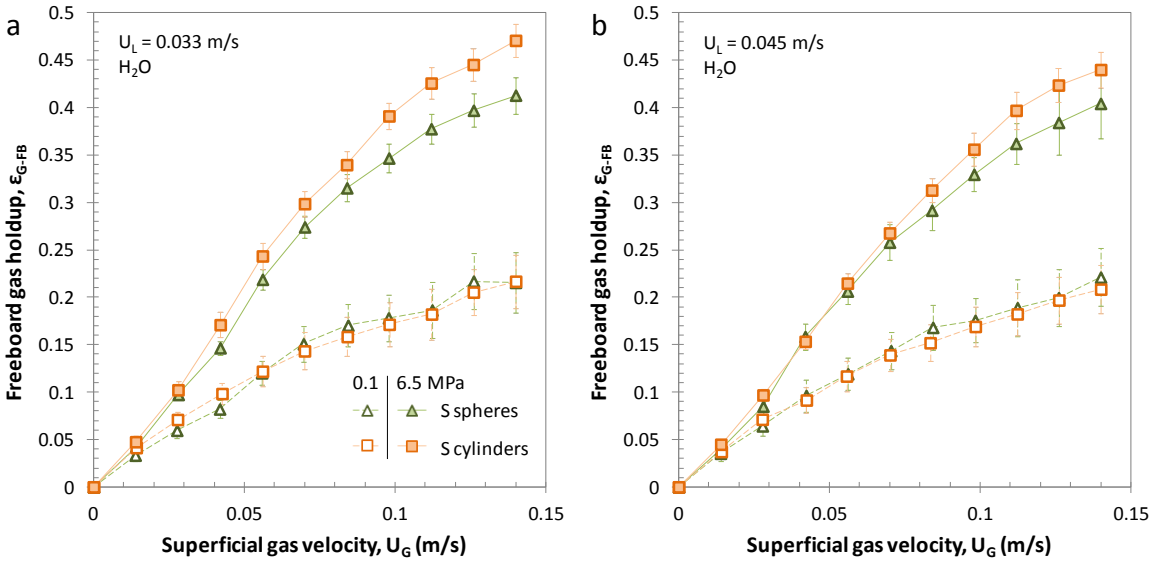

Figure 2.15. Freeboard gas holdups for the 1.5 mm equivalent spheres and cylinders at 0.1 and 6.5 MPa in water.

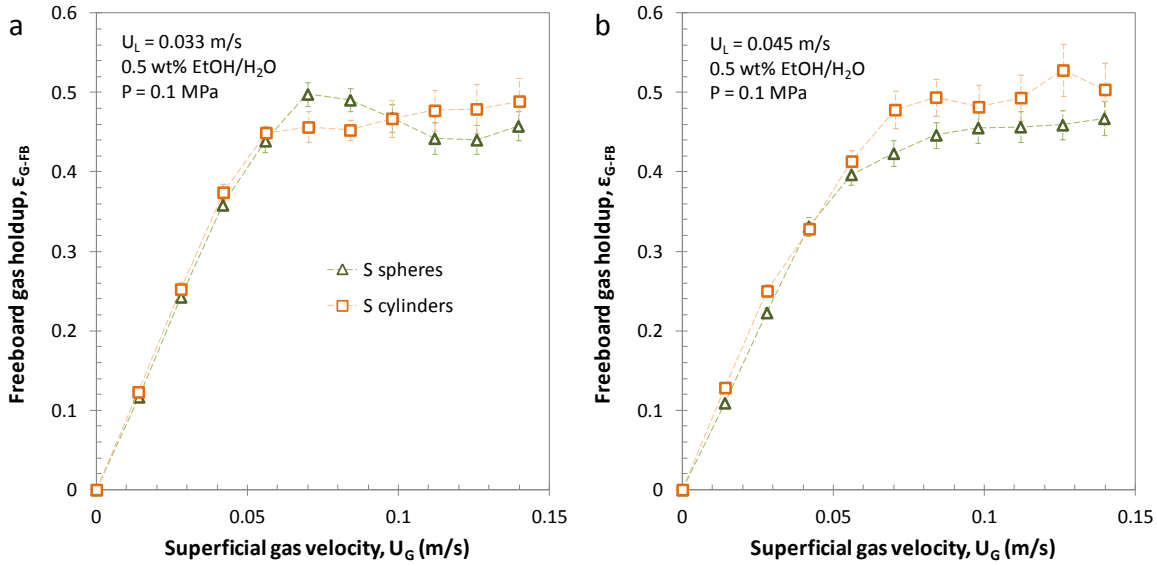

Figure 2.16. Freeboard gas holdups for the 1.5 mm equivalent spheres and cylinders at 0.1 MPa in the 0.5 wt.% aqueous ethanol solution.

Freeboard gas holdups for the studied gas-liquid-solid ebullated bed conditions were generally comparable for the spheres and cylinders, as shown in Figure 2.17. Divergence between spheres and cylinders mainly occurred between the 1.5 mm equivalent particles due to differences in the contraction/expansion behaviour in the bed region. The previous could likely be diminished if the freeboard region had a sufficient length to fully reach the stable bubbles sizes. Overall, hydrodynamics above the bed were not significantly affected by particle shape.

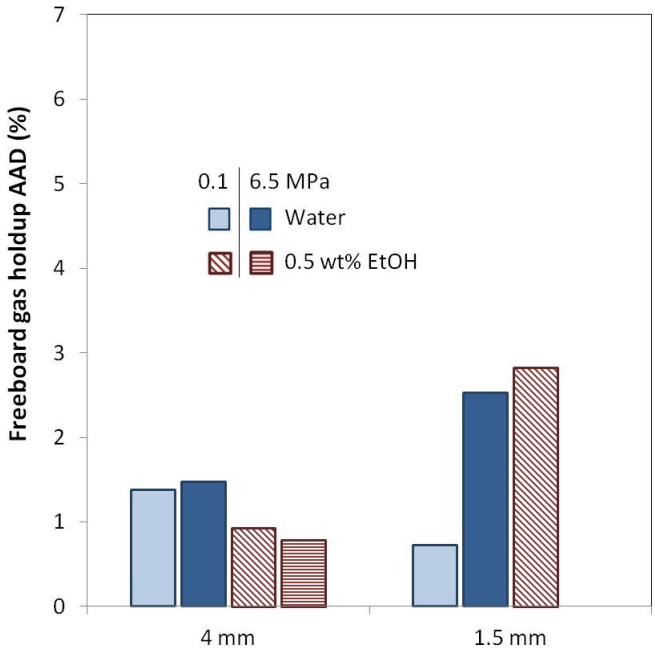

Figure 2.17. Freeboard gas holdup average absolute differences between the cylinders and spheres for the studied gas-liquid-solid operating conditions.

2.6. Minimum liquid fluidization velocity

Fluidization characteristics of the spherical and cylindrical particles were also compared by measuring the minimum liquid fluidization velocity. Previous experiments by Briens et al. (1997) have classified three fluidization regimes: fluidized bed, agitated bed, and compacted bed. For the previous definitions, a fluidized bed refers continuous particle movement in relation to each other, an agitated bed refers to particle movement primarily

due to gas bubbles passing through the bed, and compacted bed has no vertical or horizontal particle movement. It was demonstrated that the pressure gradient measurement technique discussed in section 2.3.3 measures the transition from the compacted bed to the agitated bed (Briens et al., 1997). The previous transition will be considered as the minimum liquid fluidization velocity for this study and will provide a comparison basis between the spheres and cylinders. Experimental results were compared to the gas-perturbed liquid model by Zhang et al. (1998):

$$\mathrm{Re}_{\mathrm{Lmf}} = \sqrt{\left[150\left(1-\varepsilon_{\mathrm{mf}}\right)/3.5\phi\right]^2 + \varepsilon_{\mathrm{mf}}{}^3\left(1-\alpha_{\mathrm{mf}}\right)^3 \mathrm{Ar'}_{\mathrm{L}}/1.75} - 150\left(1-\varepsilon_{\mathrm{mf}}\right)/3.5\phi \qquad (2.28)$$

Lee et al. (2003) noted that the best fit was obtained when the accounting for the gas-liquid mixture in the buoyancy, modifying the Archimedes number ($\mathrm{Ar'}_{\mathrm{L}}$), and when approximating the experimentally observed decrease in bed voidage at minimum fluidization ($\varepsilon_{\mathrm{mf}}$) with the addition of gas.

$$\mathrm{Ar'}_{\mathrm{L}} = \frac{\rho_{\mathrm{L}}\left(\rho_{\mathrm{S}} - \left(\rho_{\mathrm{G}}\,\alpha_{\mathrm{mf}} + \rho_{\mathrm{L}}\left(1-\alpha_{\mathrm{mf}}\right)\right)\right) g\, d_{\mathrm{P}}{}^3}{\mu_{\mathrm{L}}{}^2} \qquad (2.29)$$

$$\varepsilon_{\mathrm{mf}} = \varepsilon_{\mathrm{mf}}\big|_{U_{\mathrm{G}}=0}\left(1 - 0.34\left(1 - \frac{U_{\mathrm{lmf}}}{U_{\mathrm{lmf}}\big|_{U_{\mathrm{G}}=0}}\right) + 0.22\left(1 - \frac{U_{\mathrm{lmf}}}{U_{\mathrm{lmf}}\big|_{U_{\mathrm{G}}=0}}\right)\right) \qquad (2.30)$$

The gas holdup on a solids-free (α_{mf}) basis at minimum fluidization was estimated using the empirical relation of Yang et al. (1993):

$$\alpha_{\mathrm{mf}} = \frac{0.16\,U_{\mathrm{G}}}{\varepsilon_{\mathrm{mf}}\left(U_{\mathrm{G}} + U_{\mathrm{Lmf}}\right)} \qquad (2.31)$$

The bed void at minimum fluidization ($\varepsilon_{\mathrm{mf}}$) was difficult to measure as the bed height could not always be visually measured due to the stainless steel column. As a result, the bed void at minimum fluidization was estimated based on the approximation of Wen and Yu (1966):

$$\varepsilon_{\mathrm{mf}} \approx \frac{0.415}{\sqrt[3]{\phi}} \qquad (2.32)$$

Figure 2.18 compares the minimum liquid fluidization velocity of both sets of particles in the water system. Minimum liquid fluidization velocities of all particles decreased as expected with an increased gas flow rate until the values stabilized at higher gas velocities. The gas-perturbed liquid model predictions are generally comparable to the experimental data, with the exception of the larger cylinders. The model assumes that the solid particles are fully supported by the liquid, where the effective liquid velocity depends on the volume of gas occupying the bed. Differences between the gas-perturbed liquid model and the experimental results likely resulted due to inaccurate bed void assumption at minimum fluidization for the 4 mm particles. For both sets of particles, the minimum liquid fluidization velocities of the cylinders were predicted and visually observed to be higher than the spheres.

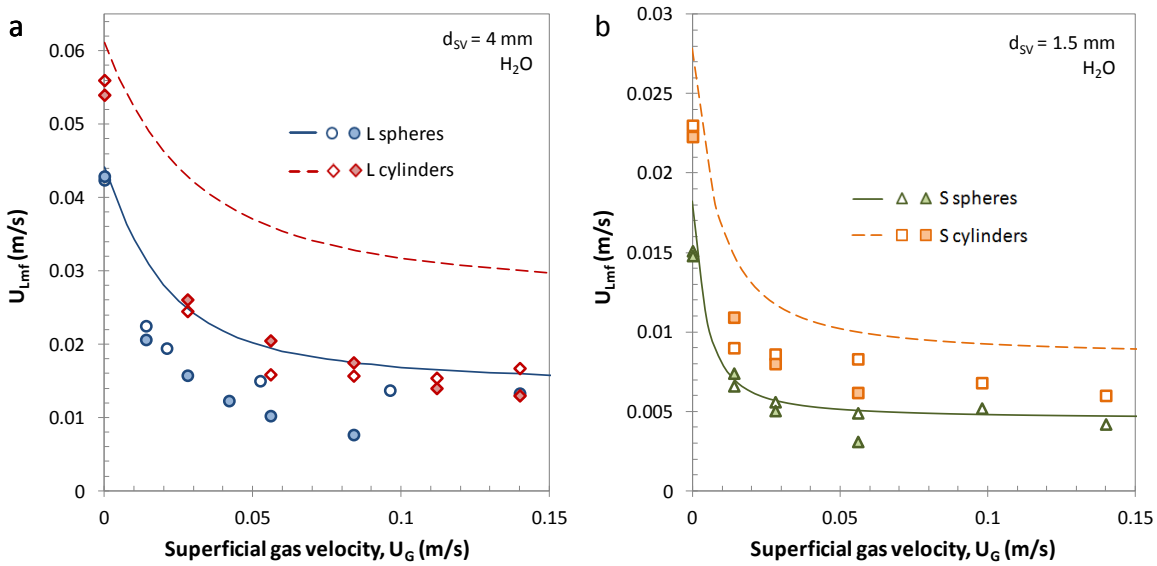

Figure 2.18. Minimum liquid fluidization velocity as a function of superficial gas velocity for the 4 (a) and 1.5 (b) mm equivalent particles in water. Hollow and solid data points represent pressures of 0.1 and 6.5 MPa, respectively. Lines are predictions (Zhang et al., 1998).

2.7. Conclusions

Liquid-solid and gas-liquid-solid hydrodynamics of 4 and 1.5 mm glass spheres were compared to aluminum cylinders with equivalent Sauter mean diameters. Liquid-solid fluidized bed porosity measurements showed similar hydrodynamic behaviour for the equivalent spheres and cylinders. Bed void correlations revealed the importance of the volume equivalent diameter and particle sphericity when studying cylinders.

The 4 mm equivalent particles showed comparable mean phase holdups in the gas-liquid-solid fluidized beds with water (phase holdup AAD < 2.6%), particularly when considering the estimated standard deviations. Phase holdups for the larger particles in the 0.5 wt.% aqueous ethanol solution were very similar (phase holdup AAD < 1.1%). Deviations between mean phase holdups of the spheres and the cylinders mostly occurred following the transition to coalesced bubble flow in the bed region.

Hydrodynamic similarity for the 1.5 mm equivalent particles in water (phase holdup AAD < 5.5%) differed from the observations with the larger particles. Gas holdups in the water system were generally greater for the cylinders while solid holdups were greater for the spherical particles. Cylindrical particles did not undergo the bed contraction observed with the spherical particles at the introduction of gas. For the surfactant solution, gas holdups were similar for the 1.5 mm equivalent particles ($AAD(\varepsilon_G) = 0.9\%$). Differences in the solid and liquid holdups were primarily observed in coalesced flow ($AAD(\varepsilon_S) \approx AAD(\varepsilon_L) = 3.7\%$), where solid holdups of the cylindrical particles were lower than the spherical particles.

Currently available correlations struggled to predict the effects of pressure, surfactant addition, and particle shape when comparing with the experimentally measured gas-liquid-solid holdups. Freeboard gas holdups for the studied gas-liquid-solid ebullated bed conditions were generally comparable as the hydrodynamics above the bed were not significantly affected by particle shape. The minimum liquid fluidization velocities of the cylinders were slightly higher than for the spheres at the studied gas flow rates.

In summary, the Sauter mean diameter accounted for particle shape effects in the liquid-solid fluidized beds. Shape effects were satisfactorily accounted for in the gas-liquid-solid fluidized bed using the Sauter mean diameter when the operating conditions led to small evenly dispersed bubbles. Discrepancies between equivalent spherical and cylindrical

particles were observed in the presence of large coalescing bubbles in the bed region. Further differences between spheres and cylinders were observed with the 1.5 mm particles as the cylinders did not undergo the bed contraction observed with the equivalent spheres. It is thus imperative to consider the particle-to-bubble size ratio when accounting for particle shape effects using the Sauter mean diameter.

Acknowledgments

The authors are grateful to Craig McKnight and Jason Wiens (Syncrude Canada Ltd.) for their valuable insights and would also thank Pellets LLC for manufacturing the aluminum cylindrical particles. The authors would like to acknowledge the Natural Sciences and Engineering Research Council of Canada, the Canadian Foundation for Innovation, the Ontario Innovation Trust and Syncrude Canada Ltd. for financial support.

Nomenclature

AAD	average absolute difference, $AAD = (1/n)\sum_{i=1}^{n} \left| y_{i,cylinder} - y_{i,sphere} \right|$
AARE	average absolute relative error, $AARE = (1/n)\sum_{i=1}^{n} \left| \left(y_{i,pred} - y_{i,exp} \right) / y_{i,exp} \right|$
A_P	projected area (m^2)
Ar_L	liquid Archimedes number, $Ar_L = \rho_L d_V^{\,3} (\rho_S - \rho_L) g / \mu_L^{\,2}$
Ar'_L	liquid Archimedes number accounting for gas-liquid mixture (refer to Eq. (2.29))
C_D	drag coefficient
d_C	column inner diameter (m)
d_{eff}	effective diameter (m)
d_P	particle diameter (m)
d_{SV}	Sauter mean diameter (m)
d_V	volume equivalent diameter (m)
g	gravitational acceleration (m/s^2)
h_B	bed height (m)

k	wall effect for bed expansion correlation
K	hydrodynamic volume factor
L_P	particle length (m)
m	mass of the particles (kg)
m_i	number of data points in the i'th measurement
n	index for bed expansion correlation
N	number of dynamic pressure drop mean values in the bed or freeboard
P	pressure (Pa)
$-\Delta P$	dynamic pressure drop (Pa)
$\Delta P/\Delta L$	pressure drop per unit of length in a fixed bed (Pa/m)
$Re_{LT\infty}$	liquid-particle Reynolds number based on terminal free settling velocity, $Re_{LT\infty} = U_{LT\infty}\,\rho_L\,d_P/\mu_L$
s	standard deviation
s_P^2	pooled variance
T	temperature (°C)
U_F	fluid superficial velocity (m/s)
U_G, U_L	gas and liquid superficial velocities (m/s)
U_{Lmf}	minimum liquid fluidization velocity (m/s)
U_{LT}	terminal settling velocity of a particle, accounting for wall effects (m/s)
$U_{LT\infty}$	terminal free settling velocity of a particle (m/s)
Δz	vertical distance between differential pressure taps (m)

Greek symbols

α_{mf}	gas holdup at minimum fluidization on a solids-free basis
β_0	dynamic pressure profile intercept
β_1	dynamic pressure profile slope
ε	bed void fraction
ε_G, ε_L, ε_S	gas, liquid and solid holdups in the bed region
ε_{G-FB}	freeboard gas holdup
μ_F	fluid dynamic viscosity (Pa s)

μ_L	liquid dynamic viscosity (Pa s)
ρ_{eff}	effective particle density (kg/m^3)
ρ_F	fluid density (kg/m^3)
ρ_G , ρ_L , ρ_S	gas, liquid and solid densities (kg/m^3)
ϕ	sphericity

Subscripts

B	bed
BW	Begovich and Watson (1978)
F	fluid
FB	freeboard
G	gas
L	liquid
mf	at minimum fluidization
P	particle
S	solid

Chapter 3

Bubble characteristics measured using a monofibre optical probe in a bubble column and freeboard region under high gas holdup conditions

Dominic Pjontek, Valois Parisien, Arturo Macchi

Centre for Catalysis Research and Innovation, Department of Chemical and Biological Engineering, University of Ottawa, 161 Louis Pasteur, Ottawa, Ontario, Canada, K1N 6N5

Abstract

Local bubble characteristics, including gas holdups, bubble rise velocities, and chord lengths, were measured using a monofibre optical probe manufactured to withstand elevated pressures. Previous studies have validated the use of single tip probes for simultaneous measurement of local bubble properties at atmospheric conditions; however no study has been currently reported for these probes at elevated pressures. Experiments were conducted in a 101.6 mm diameter column operating at pressures up to 9.0 MPa. Surfactant addition and operating pressure were studied to simulate high gas holdups observed in many industrial reactors containing liquid mixtures with surface-active compounds. Experiments were hence completed using two liquid phases: tap water and a 0.5 wt.% aqueous ethanol solution. Liquid and gas superficial velocities were varied between 0 - 90 mm/s and 0 - 150 mm/s, respectively. Radial profiles at atmospheric conditions validated the probe measurements in water. Local holdups, rise velocities and chord lengths were adequately measured in water up to 9.0 MPa. The probe struggled in the aqueous ethanol solution due to its physical constraints (i.e., tip diameter and sensing length) when compared to the significant bubble size reduction (chord lengths below 0.5 mm). Comparisons with fluidized bed freeboard measurements demonstrated that flow through the bed enhanced bubble breakup for a coalescing system, but had a negligible impact with the added surfactant.

***This manuscript has been published**: Pjontek, D., Parisien, V., Macchi, A., 2014. Bubble characteristics measured using a monofibre optical probe in a bubble column and freeboard region under high gas holdup conditions. Chem. Eng. Sci. 111, 153–169.

3.1. Introduction

Gas-liquid-solid flow is frequently encountered in chemical engineering processes. The fluid dynamic behaviour of these systems must be studied to predict heat and mass transfer, flow behaviour, and particle mixing. Bubble characteristics (e.g. bubble size distributions, bubble rise velocities, and local gas holdups) in industrial bubble columns and/or gas-liquid-solid fluidized beds are generally difficult to measure on-site due to their operating conditions. Vessels for such processes typically require materials that can withstand elevated temperatures and pressures, consequently limiting visual observations. The unit of interest for this study is the LC-Finer^{SM} hydroprocessor which operates at pressures and temperatures of approximately 11.7 MPa and 440°C, respectively (McKnight et al., 2003). The hydroprocessor's liquid recycle pan in the freeboard region was previously redesigned with the aid of CFD simulations, where the goal was to reduce the quantity of recycled gas (McKnight et al., 2003). The size of all bubbles for the simulation was assumed to be 1 mm based on a force balance. As computational times for CFD modeling are continually reduced and measurement techniques are improved, the objective of this study is to measure local bubble properties under high gas holdup conditions to improve future gas-liquid separation predictions and techniques.

Bubble characteristics in gas-liquid and gas-liquid-solid systems have been previously investigated using various measurement devices (Boyer et al., 2002). These techniques are commonly categorized as non-invasive or invasive, where the former do not interfere with the flow conditions inside the studied system. Non-invasive techniques can be used to measure some of the desired bubble parameters for this study. For example, global phase holdups in bubble columns operated at elevated pressures have been determined using differential pressure transducers via pressure profiles (Behkish et al., 2007; Jin et al., 2004; Rudkevitch and Macchi, 2008). Non-invasive techniques (e.g. dynamic gas disengagement, photography, radiography, NMR, particle image velocimetry, laser Doppler anemometry) have also been used to measure bubble size distributions or phase velocities (Chaouki et al., 1997). As discussed by Boyer et al. (2002) however, these techniques are limited by the operating conditions, low gas holdup requirements, and/or relative costs. Invasive techniques were thus examined to measure the desired bubble characteristics using the available experimental system under high gas holdup conditions.

Needle, heat transfer, and ultrasound probes are invasive measurement techniques which have been previously used to measure bubble properties in gas-liquid and/or gas-liquid-solid systems (Boyer et al., 2002). Ultrasounds probes measure the desired bubble properties based on the laws of ultrasound wave propagation, either through transmitted or reflected waves in a gas-liquid system. Unfortunately, the technique does not normally allow the simultaneous measurement of all desired bubble characteristics. Furthermore, the effectiveness is reduced at gas holdups above 10 - 20% due to repeated reflections/scattering of the signal (Broering et al., 1991; Macchi et al., 2001b). Gas holdups in a bubble column operating at elevated pressures were previously shown to exceed these limitations (Rudkevitch and Macchi, 2008), consequently restricting the use of ultrasound probes.

Heat transfer probes have been used to determine local gas holdups based on the heat exchanged between an electronically heated probe and the surrounding liquid medium. As a bubble interacts with the probe, the quantity of heat exchanged is reduced causing a noticeable signal change (Abel and Resch, 1978). By examining the magnitude and slope of the signal, Utiger et al. (1999) found that local bubble holdups determined with the heat transfer probe were comparable to those obtained with an optical probe. The main advantage for the heat transfer probes is the measurement of the liquid phase velocity and root mean square (RMS) fluctuations. Current heat transfer probes do not measure all desired bubble characteristics for this study.

Needle probes are capable of simultaneously measuring local gas holdups, bubble chord lengths and rise velocities. Two types of needles probes have been previously used for measurements in bubble columns: optical fibre and impedance/conductive probes (Boyer et al., 2002). Optical and impedance probes operate based on the differences in the refractive index or conductivity, respectively, of the liquid and gas phases. Signal fluctuations due to phase changes at the probe tip allow the measurement of local gas holdups and bubble frequency. Dual tipped probes were developed to measure the bubble chord length and rise velocities, where the distance between both probe tips is typically in the range of 0.5 - 5 mm (Chabot et al., 1998; Chaumat et al., 2007; Magaud et al., 2001; Moujaes, 1990; Shiea et al., 2013). Four-point optical probes were also developed and validated to improve bubble velocity vector measurements compared to dual tip configurations (Xue et al., 2008, 2003). Previous studies have shown that bubble size distributions become narrower while increasing

the pressure up to 15 MPa (Lin et al., 1998), where a notable fraction of bubbles diameters can be in the range of 1 mm and lower. The distance between multiple tips may consequently be an issue under high gas holdup conditions, where bubbles pierced by the front tip may be less likely pierced by subsequent tips. As shown in Table 3.1, few studies were found in the open literature where bubble characteristics were measured at elevated pressures and/or temperatures using an invasive device. In addition, these studies were conducted with no liquid flow which does not effectively simulate an ebullated bed reactor.

Table 3.1. Previous bubble characterization studies at elevated pressure and/or temperature using a probe.

Authors	Experimental System	Operating Conditions	Comments
Chabot and de Lasa (1993)	0.2 m bubble column ($U_L = 0$)	P = 0.1 MPa and T = 100 and 175°C	two spherical bulb optical fiber sensors
Soong et al. (1997)	0.10 m slurry bubble column ($U_L = 0$)	$P \leq 1.36$ MPa and $T \leq 265$°C	dual conductivity hot-wire probe
Luo et al. (1999)	0.102 m slurry bubble column ($U_L = 0$)	up to 5.6 MPa	U shape double tipped optical probe

An innovative monofibre optical probe developed by Cartellier (1992) eliminated the requirement that a bubble must be pierced by two consecutive tips to measure the rise velocity and chord length. Previous experiments demonstrated that the bubble rise velocity was inversely proportional to the signal rise time between the liquid and gas voltage levels when the probe was normal to the gas-liquid interface (Cartellier and Barrau, 1998a, 1998b). This relation is a function of the probe sensing length, a unique characteristic for each probe that must be determined prior to experiments. The monofibre optical probe's ability to simultaneously measure local gas holdups, bubble rise velocities and chord lengths has been validated at atmospheric conditions in a bubble column (Barrau et al., 1999; Cartellier, 1992) and in three-phase flow with particles of similar density to the liquid (Mena et al., 2008).

The main objective of this study is to investigate the use of a monofibre optical probe for bubble characterization in a bubble column and the freeboard region of an ebullated bed when operating under high gas holdup conditions (i.e., varying pressures up to 9.0 MPa, with and without the addition of a surfactant). In order to investigate the coalescing/heterogeneous and dispersed/homogeneous bubble flow regimes, data is gathered using water and a 0.5 wt.% aqueous ethanol solution, respectively. Radial profiles at low pressures are compared to globally measured values to provide a partial validation of the device. Global and local gas holdups as well as photos are compared to local holdups while varying gas/liquid flow rates, increasing the pressure and adding a surfactant. The impact of the previous parameters on bubble chord length distributions and rise velocities distributions are also discussed. Lastly, global and local measurements in the freeboard region of an ebullated bed are compared to bubble column results at equivalent operating conditions.

3.2. Experimental setup

Experiments were carried out in a gas-liquid-solid fluidization system (Figure 3.1) built by Zeton Inc. and capable of reaching pressures up to 10 MPa. The stainless steel fluidization column has an inner diameter of 101.6 mm and a maximum expanded bed height of 1.8 m. Glass viewing windows with dimensions of 118.8 mm x 15.6 mm are located at heights of 244 mm, 603 mm, and 956 mm above the top of the distributor plate. At the top of the column, an expanded overflow section was designed as the primary gas-liquid separation stage. Liquid is conveyed into a partitioned liquid storage tank for further degassing and then recycled to the column. The system was pressurized using industrial grade nitrogen cylinders. The optical probe can be inserted into the column using four ports located at heights of 168 mm, 460 mm, 752 mm and 1045 mm above the distributor plate. Global phase holdups were determined using a differential pressure transmitter, where the reference pressure port is located 95 mm above the distributor plate. Subsequent pressure ports are equally spaced by a distance of 146 mm. A centrifugal pump drives the liquid from a storage tank to the base of the column. Liquid flow is controlled by an automated needle valve and measured by a magnetic flow meter. Gas is circulated using a single stage reciprocating compressor, where fluctuations are reduced by gas dampeners located at the compressor inlet

and outlet. A differential pressure transducer was used to determine the gas flow rate through orifice plates of varying size, depending on the operating pressure. Gas is sparged in the plenum chamber of the column via a porous pipe with openings of 10 μm in diameter. The gas-liquid mixture then flows into the bed through a perforated distributor plate with 23 holes with diameters of 3.175 mm.

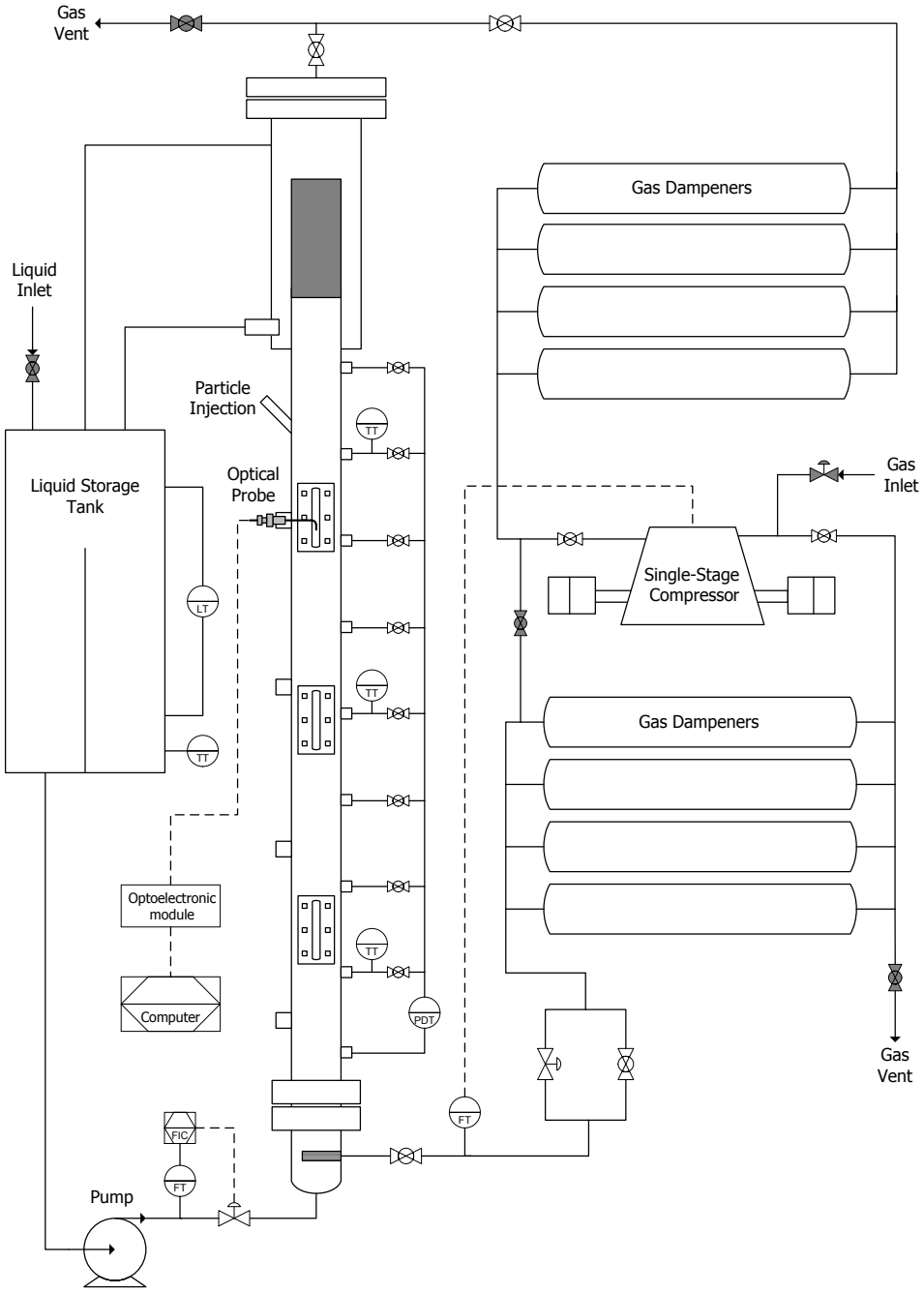

Figure 3.1. Schematic of the high pressure gas-liquid-solid fluidization system.

Experimental operating conditions, fluid and particle properties for this study are summarized in Table 3.2. For the previous table, uncertainties for the operating conditions were estimated from measurement fluctuations during experiments, uncertainties for the fluid properties and particle density were estimated from repeated measurements and uncertainties for the particle size were based on manufacturer specifications. Tap water was used as the liquid phase since it has been typically used with the monofibre optical probe. Surfactant addition was also studied as the hydrophilic and hydrophobic components of the molecular structure generally hinder bubble coalescence due to its accumulation at the gas-liquid interface. Increased gas holdups thus result from the subsequent surface tension reduction, repulsive forces between two approaching bubbles, increased drag due to surface tension gradients, and slower liquid drainage of two adjacent bubbles (i.e., Gibbs-Marangoni effect). Dargar and Macchi (2006) demonstrated that surfactant addition in water led to a considerable gas holdup increase in a bubble column and gas-liquid-solid fluidized bed; however, the type and concentration of surface active compound primarily impacted the stability of the foam layer at the free surface. A 0.5 wt.% ethanol (EtOH) aqueous solution was hence selected based on the previous study as it produced an effervescent foam at the free surface, thus facilitating liquid degassing before being recycled to the bottom of the column. The combined effects of elevated pressures and surface-active compounds are relevant to industrial gas-liquid-solid fluidized beds, where gas holdups are considerably higher compared to atmospheric air-water systems (McKnight et al., 2003). For the ebullated bed runs, borosilicate glass beads with an average diameter of 4 mm and particle density of 2500 kg/m^3 were used to minimize the probability of particles jetting from the bed interface, therefore minimizing the risk of damaging the probe in the freeboard region.

Table 3.2. Experimental operating conditions, fluid and particle properties.

Parameter	Symbol	Range	Units
superficial liquid velocity	U_L	0 to 91 (± 1%)	mm/s
superficial gas velocity	U_G	0 to 150 (± 2%)	mm/s
pressure	P	0.1 to 9.0 (± ~1%)	MPa
column diameter	d_C	101.6	mm
temperature	T	24 ± 2	°C
liquid density	ρ_L	997 ± 1	kg/m^3
liquid viscosity	μ_L	(9.1 ± 0.4) x 10^{-4}	Pa·s
gas density	ρ_G	1.15 ± 0.03 to 102 ± 1	kg/m^3
particle diameter	d_P	4.0 ± 0.3	mm
particle density	ρ_S	2500 ± 9	kg/m^3

3.3. Measurement techniques

During the experiments, local bubble properties were measured using a monofibre optical probe, global phase holdups were determined using a differential pressure transducer and photos were taken at selected conditions. Once the system reached steady state, all measurements were taken to ensure proper comparison between global and local values.

3.3.1. Monofibre optical probe

Optical probes distinguish the gas and liquid phases by measuring the intensity of a laser that is reflected at the probe tip when submerged in either phase. The laser is reflected and/or refracted at varying intensities depending on the tip geometry and the refractive indexes of the tip ($n_{glass} \approx 1.6$), gas ($n_{air} \approx 1$), and liquid ($n_{water} \approx 1.33$) phases. Since the gas has a lower refractive index compared to the liquid, light is reflected at a greater intensity

when the tip is submerged in gas. The resulting signal clearly distinguishes between the gas and liquid phases, allowing local bubble properties to be measured.

The single tip optical probe used in this study was custom-made by A2 Photonic Sensors for high pressure conditions. Two available probe geometries, 1C (conical) and 3C (conical-cylinder-conical), are presented in Figure 3.2. The primary difference between the configurations is the length of the sensing tip, where 1C and 3C probes are typically in the range of 50-100 μm and 200-500 μm, respectively. Due to their longer sensing lengths, 3C probes are generally more accurate and provide better precision due to their longer signal rise times (Cartellier and Barrau, 1998a). The 3C configuration also reduces the sensitivity to the bubble's impact angle at the tip. Nonetheless, the 1C probe's shorter sensing length ($L_S \approx 60$ μm for the studied probe) is better suited for small bubbles in the range of 0.5 - 1 mm and lower in diameter. As a result, the 1C probe geometry was selected to study the bubble characteristics under high gas holdup conditions. It should be noted that Mizushima et al. (2013) have demonstrated the use of a wedge shape monofibre probe; however the pre-signal noise resulting from the tip shape is greater compared to the 1C configuration.

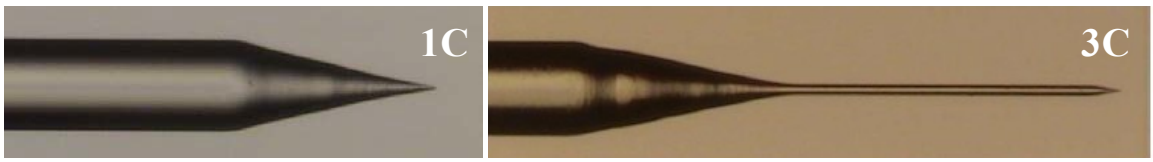

Figure 3.2. 1C and 3C optical probe tips (manufactured by A2 Photonic Sensors).

Monofibre optical probes can simultaneously measure local gas holdups, bubble velocities, and chord lengths by knowing the length of the sensing tip (L_S). This probe geometric characteristic must be determined through calibration prior to experiments, where an example of a calibration curve is provided by Mena et al. (2008). The probe's signal is measured via an optoelectronic module which emits the laser to the probe tip and converts the reflected optical signal into a digital signal. Figure 3.3 provides an example of a signal obtained with a 1C probe.

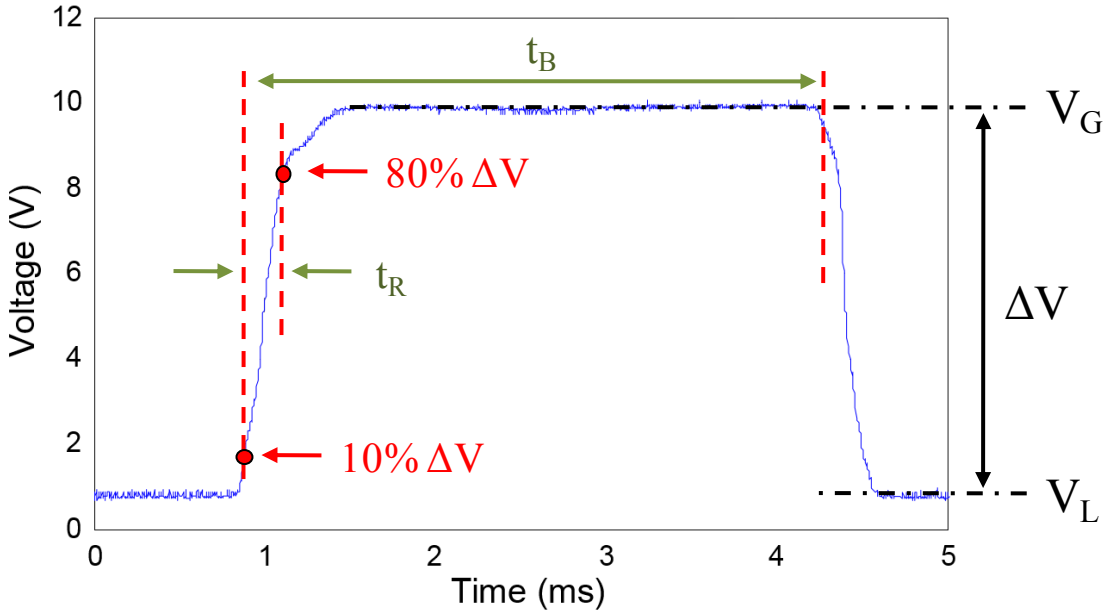

Figure 3.3. Signal example for a 1C probe (t_B: residence time, t_R: rise time, V_G: gas voltage, V_L, liquid voltage).

Local gas holdups (ε_G) are calculated as the ratio of the cumulated bubble residence times (t_B) on the probe tip over the total measurement time (t_T).

$$\varepsilon_G = \frac{\sum_i t_{Bi}}{t_T} \tag{3.1}$$

Bubble rise velocities (v_B) are estimated from the probe sensing length (L_S) and signal rise time (t_R), which is the time observed between selected lower and upper thresholds based on the gas and liquid voltage difference. Lower and upper threshold of 10% and 80% were used for these experiments based on recommendations from the manufacturer.

$$v_B = \frac{L_S}{t_R} \tag{3.2}$$

Knowing the rise velocity and residence time, the chord length (c_B) can be determined using the following relation:

$$c_B = t_B\, v_B \tag{3.3}$$

It should be noted that rise velocities and chord lengths in this study are only provided for fully detected bubbles (i.e., signals that exceeded the upper threshold). Bubble residence times used for local holdups however take into account all signals which exceeded the liquid voltage while accounting for signal noise.

The digital signal obtained by the optoelectronic module was analyzed by the SO5 software provided by A2 Photonic Sensors. Arrival times, rise times, and residence times were recorded for each bubble. Signals which do not reach the upper threshold are distinguished from fully detected bubbles. This may occur if the bubble is small relative to the probe sensing length or if the bubble is pierced off-center. Data acquisition was dependent on the number of bubbles measured for a set time limit. For all results, data was generally gathered for 60 seconds or more and with a minimum of 1000 bubbles to balance between repeatability and computational time of the properties. Nonetheless, most results in this study are based on a measurement of 100 seconds and over 1000 bubbles.

3.3.1.1. Optical probe measurement errors

It is crucial to consider potential sources of errors when characterizing bubbles using a 1C optical probe. Referring to Figure 3.3, measurement errors could influence the residence time (t_B) and rise time (t_R). Residence times detected by the probe can be influenced by multiple sources discussed by previous authors (Barrau et al., 1999; Enrique Juliá et al., 2005; Mena et al., 2008; Vejražka et al., 2010):

a) *blinding effect*: underestimation of bubble residence time for smaller bubbles due to improper dewetting at the probe tip,
b) *drifting effect*: bubble trajectory is altered prior to or during the piercing process, leading to an underestimated residence time,
c) *crawling effect*: overestimation of the residence time resulting from bubble deformation and/or deceleration at the probe tip.

Previous experiments by Barrau et al. (1999) in a bubble column obtained relative errors for the local gas holdups between -0.8 and -16%, where the poorest performance was observed with no liquid flow and/or at low gas fractions. Vejražka et al. (2010) obtained comparable relative errors to the previous study and demonstrated that bubbles were decelerated when

pierced at the center, leading to an overestimated residence time, while significant off-center piercing underestimated the residence times.

Rise time errors are primarily affected by the bubble's impact angle (β) with the probe tip. For 1C probes, the effect of β on the rise time is minor below 10° (Cartellier and Barrau, 1998b). Rise times however increased by approximately 45% at an impact angle of 30°. It was also shown that the influence of β is lower for a 3C probe (Cartellier and Barrau, 1998a), as the measured rise times were less affected due to the longer sensing length. It was not possible to measure β in the experimental system used in this study; qualitative observations of the flow pattern will nonetheless be discussed.

3.3.2. Global phase holdups

In the bubble column and ebullated bed, global phase holdups were determined by measuring the dynamic pressure drop, where the hydrostatic head of the liquid phase is subtracted, throughout the bed and freeboard regions. For the ebullated bed, the bed height (h_B) was estimated from the intersection of the bed and freeboard dynamic pressure profiles via linear regression. Global solid holdups (ε_S) were calculated knowing the solid mass (m) and density (ρ_S) in the fluidized bed.

$$\varepsilon_S = \frac{4\,m}{\pi\, d_C^{\,2}\, h_B\, \rho_S} \tag{3.4}$$

Neglecting frictional drag on the wall and accelerations of the phases in the vertical direction, the global gas holdups in the bed region (ε_G) were calculated using the measured bed region dynamic pressure profile.

$$\varepsilon_G = \frac{\left(\Delta P/\Delta z\right) g^{-1} + (\rho_S - \rho_L)\,\varepsilon_S}{\rho_L - \rho_G} \tag{3.5}$$

For the freeboard region above the bed or in the bubble column, the previous equation is simplified as follows to determine global gas holdups.

$$\varepsilon_G = \frac{\Delta P/\Delta z}{g\left(\rho_L - \rho_G\right)} \tag{3.6}$$

Phase holdup standard deviations for the bubble column, freeboard and ebullated bed could be estimated based on the method presented in Pjontek and Macchi (2014). Standard deviations were not included in the figures since their magnitudes were much smaller compared to the average values (e.g., average standard deviations for all water and 0.5 wt.% aqueous ethanol bubble column runs were 0.004 and 0.002, respectively).

3.3.3. Photography

Photos were taken through the sight glass available on the experimental system (refer to Figure 3.1) using a Nikon D3100 and a Nikon AF Micro-Nikkor 60mm f/2.8D lens. A 500 W halogen light was placed on the opposite side of the column. As a result of the column's cylindrical shape and the macro lens used, the photos in this study mainly provide information on the bubbles near the wall. Although the light intensity was observed to provide qualitative comparisons for the gas holdups, the camera shutter speed was varied depending on the operating conditions to minimize blurring due to the bubble rise velocities. Brightness of the photos provided in this study was hence adjusted to ensure clarity.

3.4. Bubble column results

3.4.1. Radial gas holdup profiles

The 1C optical probe performance was first investigated by measuring radial gas holdup profiles in a bubble column, where the results are presented in Figure 3.4. Measurements were taken in both water and the 0.5 wt.% aqueous ethanol solution while varying the gas and liquid superficial velocities to study the homogeneous and heterogeneous bubble flow regimes. The system was also operated at 1.0 MPa to study the initial radial profile changes when elevating the pressure.

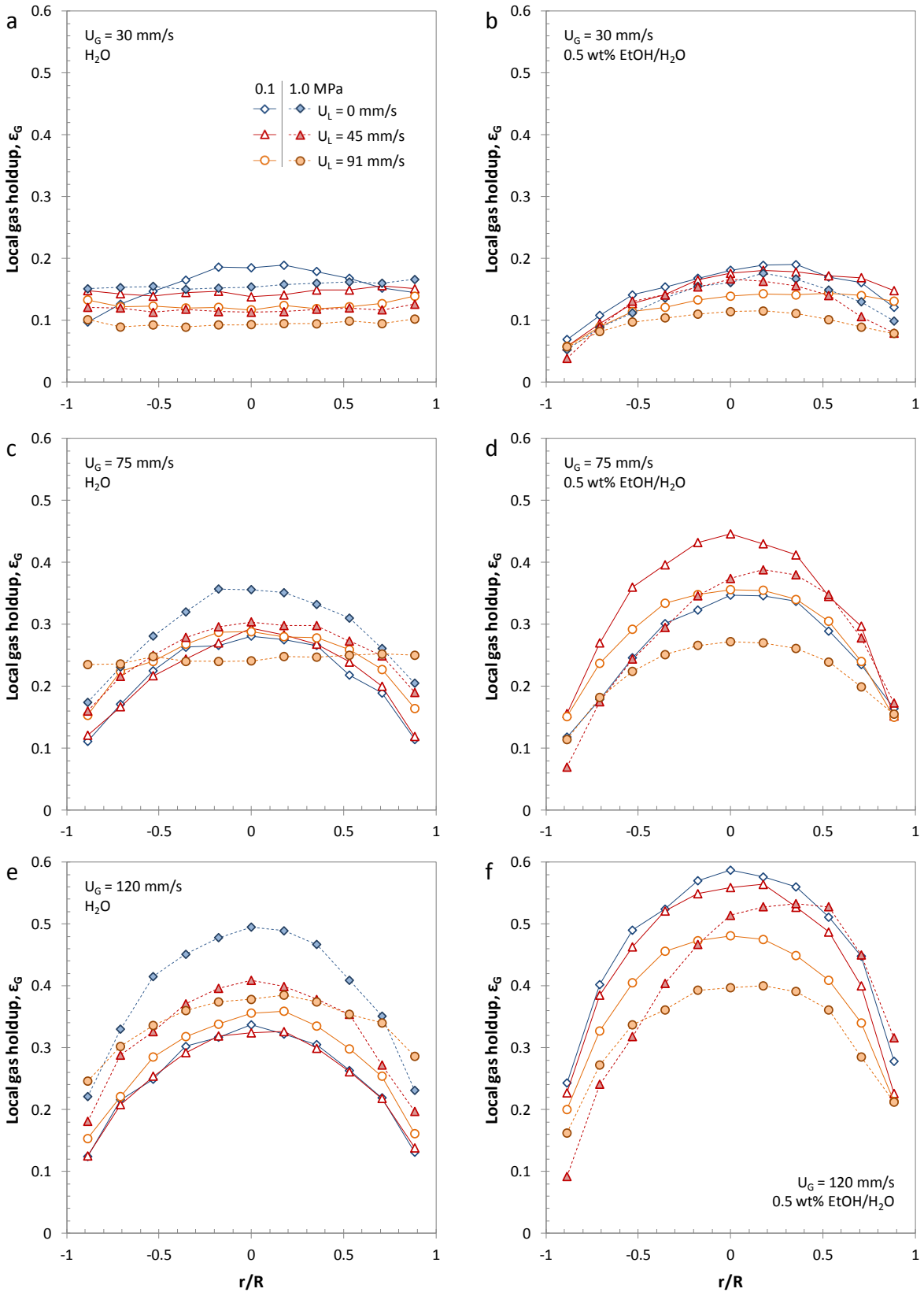

Figure 3.4. Radial gas holdup profiles in water and the 0.5 wt.% aqueous ethanol solution.

Local holdups obtained with the optical probe were compared to global holdups by integrating the radial measurements over the column cross sectional area:

$$\varepsilon_{G,global} = \frac{1}{\pi R^2} \int_0^R \varepsilon_{G,local} \, 2\pi r \, dr \tag{3.7}$$

Figure 3.5 shows that the integrated local measurements in the water system were within ± 20% of global measurements with an average relative error of 9.4%. Local measurements in the 0.5 wt.% aqueous ethanol under predicted the global values with an average relative error of 36.7%.

The visual comparison between the water and 0.5 wt.% aqueous ethanol provided in Figure 3.6 demonstrates the significant reduction in bubble size observed with the added ethanol. Measured bubble chord length distributions in water (Figure 3.11) and the 0.5 wt.% aqueous ethanol (Figure 3.13) are discussed in section 3.4.3. It was observed that surfactant addition increased the fraction of measured chord lengths below 1 mm at atmospheric pressure (approximately 80 to 95% for the selected gas and liquid flow rates) compared to measurements in water at similar operating conditions (approximately 25 to 30%). The comparison between local and global holdups with the added surfactant (Figure 3.5) demonstrates that the 1C optical probe was not properly detecting a fraction of bubbles below a particular diameter, where the 1C probe sensing length (approximately 60 μm) provides an estimated lower limit for chord length measurements. Significantly smaller bubble diameters are thus believed to have increased the blinding effect and resulted in the lower local gas holdup measurements. It is also important to consider the gas injection method when discussing bubble property changes due to adding a surfactant in the studied system. The gas first passes through a porous pipe placed below the distributor plate (refer to Figure 3.1). Afterwards, shear stresses acting on the bubbles due to both gas and liquid passing through the distributor enhance bubble breakup. Surfactant molecules at the gas-liquid interface then inhibited subsequent bubble coalescence when rising in the column, resulting in the size reduction observed in Figure 3.6.

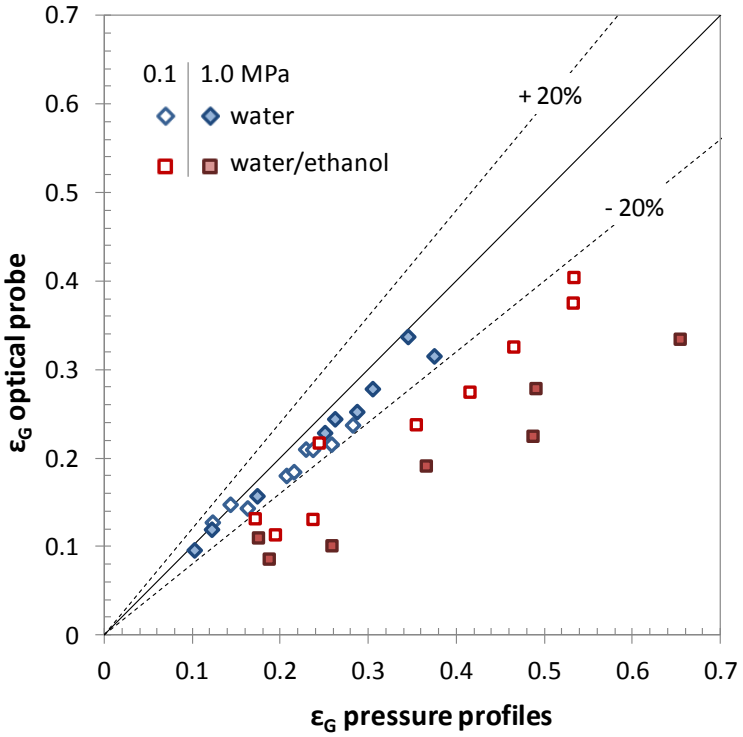

Figure 3.5. Comparison of global and integrated local gas holdups.

Gas holdups profiles measured in the water bubble using the optical probe followed expected trends. Increased gas flow rates resulted in overall higher void fractions and greater profile curvature from the column wall to the center. Flat profiles were obtained at the lowest superficial gas velocity of 30 mm/s (Figure 3.4a), as anticipated for well dispersed bubble flow. The formation of larger bubbles at higher gas flow rates led to increased curvature of the radial profiles, where maximum local gas holdups were at the center of the column (r/R = 0).

The impact of the superficial liquid velocity depended on the operating conditions. At a gas flow rate of 30 mm/s, liquid flow flattened the profiles and reduced the overall gas holdups due to well dispersed flow and increased bubble rise velocities. At increased gas velocities (Figure 3.4e), the highest gas holdups were observed at a liquid velocity of 91 mm/s. The previous observation may seem counter intuitive as higher liquid flow should increase the rise velocity for a constant bubble size. It can however be observed that liquid flow enhanced bubble breakup at the distributor and hence increased gas holdups due to greater bubble residence times in the column.

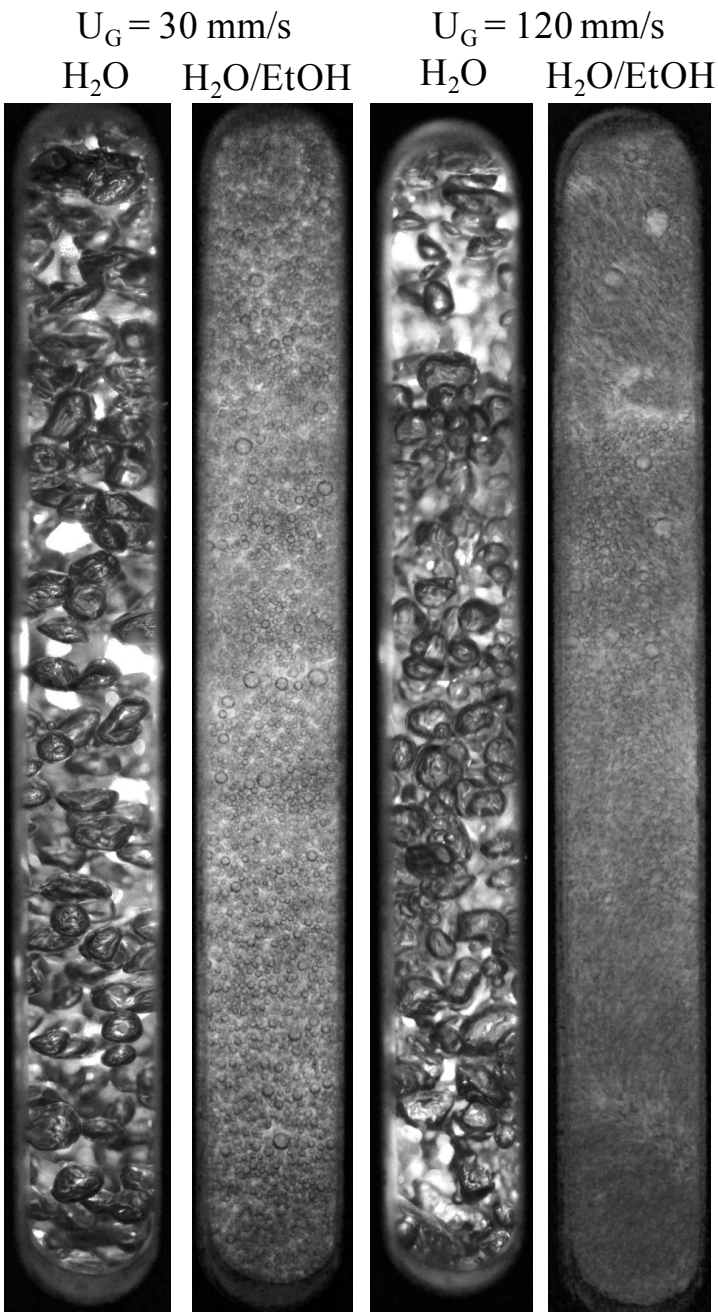

Figure 3.6. Photographic comparison of the water and 0.5 wt.% aqueous ethanol bubble columns at P = 0.1 MPa and U_L = 45 mm/s.

Fan et al. (1999) previously discussed that increasing pressure leads to enhanced bubble breakup due to the Kevin-Helmholtz instability and internal circulation of the gas, which is further discussed in section 3.4.2. Profiles at two operating conditions (U_G = 30

mm/s, U_L = 0 mm/s and U_G = 75 mm/s, U_L = 91 mm/s) changed from parabolic to flat when the pressure was increased from 0.1 to 1.0 MPa. In addition, mean gas holdups measured either locally or globally were generally greater at an operating pressure of 1.0 MPa. The previous observations are due to the enhanced bubble breakup and consequently smaller sizes, more narrow size distributions, decreased rise velocities and thus greater gas residence times in the column.

Trends in the 0.5 wt.% aqueous ethanol solution provide some insights into the limitations of the monofibre optical probe based on bubble size and flow patterns. Although radial profiles displayed comparable shapes to the water bubble column, it is believed that gas holdup profiles should have been less parabolic in the presence of surfactants due to the bubble size reduction. Ethanol addition increased global gas holdups; however the probe's measurements do not show the same increase. In addition, operating at 1.0 MPa resulted in higher global void fractions whereas the integrated radial profiles showed a decreasing trend. Modified bubble flow patterns were visually observed between water and the 0.5 wt.% aqueous ethanol. In the water bubble column, bubble flow paths were primarily in the vertical direction, whereas the smaller bubbles in the surfactant system were subject to liquid back mixing near the column wall. It should be noted that visual observations were completed through the sight glass on the column and were thus limited to the conditions near the wall under high gas holdups. A wide distribution of bubble velocity vectors with the added ethanol could explain the decreased local holdups measured as r/R approached unity. Higher void fractions at the center of the column indicates larger bubbles rising at the center, potentially causing the liquid back mixing observed near the wall and affecting the smaller bubbles observed in the surfactant solution (refer to Figure 3.6). Changes in bubble flow direction are thus believed to have inhibited the 1C probe measurements due to a combination of the blinding and drifting effects arising from a greater distribution of impact angles (β) and smaller bubble diameters.

3.4.2. Global and local gas holdups comparison

For these experiments, a balance between the total number of runs and probe locations had to be evaluated. Measuring profiles similar to those provided in section 3.4.1

would use a large quantity of pressurized gas cylinders as the system would have to be depressurized between each radial position change. Hence due to the experimental system design, safety considerations, and trends observed in section 3.4.1, it was decided to study the system at a larger number of operating conditions while measuring bubble characteristics at the center of the column (r/R = 0). This probe location provides relevant information when comparing global and local gas holdups. Global and local measurements for the water bubble column are provided in Figure 3.7.

The transition from dispersed/homogeneous to coalescing/heterogeneous bubble flow regimes can be estimated by a slope change of the global gas holdups as a function of the gas superficial velocity (Krishna and Ellenberger, 1996; Krishna et al., 1991; Shaikh and Al-Dahhan, 2007), provided enough data is gathered. In dispersed flow and assuming proper gas distribution, gas holdup increases linearly as a function of the gas flow rate, where more bubbles of similar size occupy more volume in the column. Above the transition velocity, bubble coalescence increases the average rise velocity and reduces gas residence time in the column, hence decreasing the gas holdup versus gas velocity slope. Global gas holdups measured at atmospheric pressure, shown in Figure 3.7a, clearly demonstrate the slope change when transitioning from dispersed to coalesced bubble flow.

The impact of liquid velocity and operating pressure on bubble characteristics must also be considered when investigating global holdups. Liquid flow affected shear stresses acting on the bubbles as the liquid and gas both passed through the distributor plate concurrently. In addition, higher operating pressures enhanced bubble breakup and lowered the maximum stable bubble size due to a combination of the Kevin-Helmholtz instability between two fluids and the internal circulation of the gas. Fan et al. (1999) showed that the maximum stable bubble size was better estimated at lower pressures based on the Kevin-Helmholtz instability (Wilkinson and Dierendonck, 1990) while the internal circulation of gas model (Levich and Spalding, 1962) predicted the enhanced bubble break up at higher pressures. Figure 3.8 illustrates the impact of pressure on the bubble size in water. Increased liquid velocities and operating pressures therefore had complementary effects towards enhancing bubble breakup and thus impacting global gas holdups in the studied system.

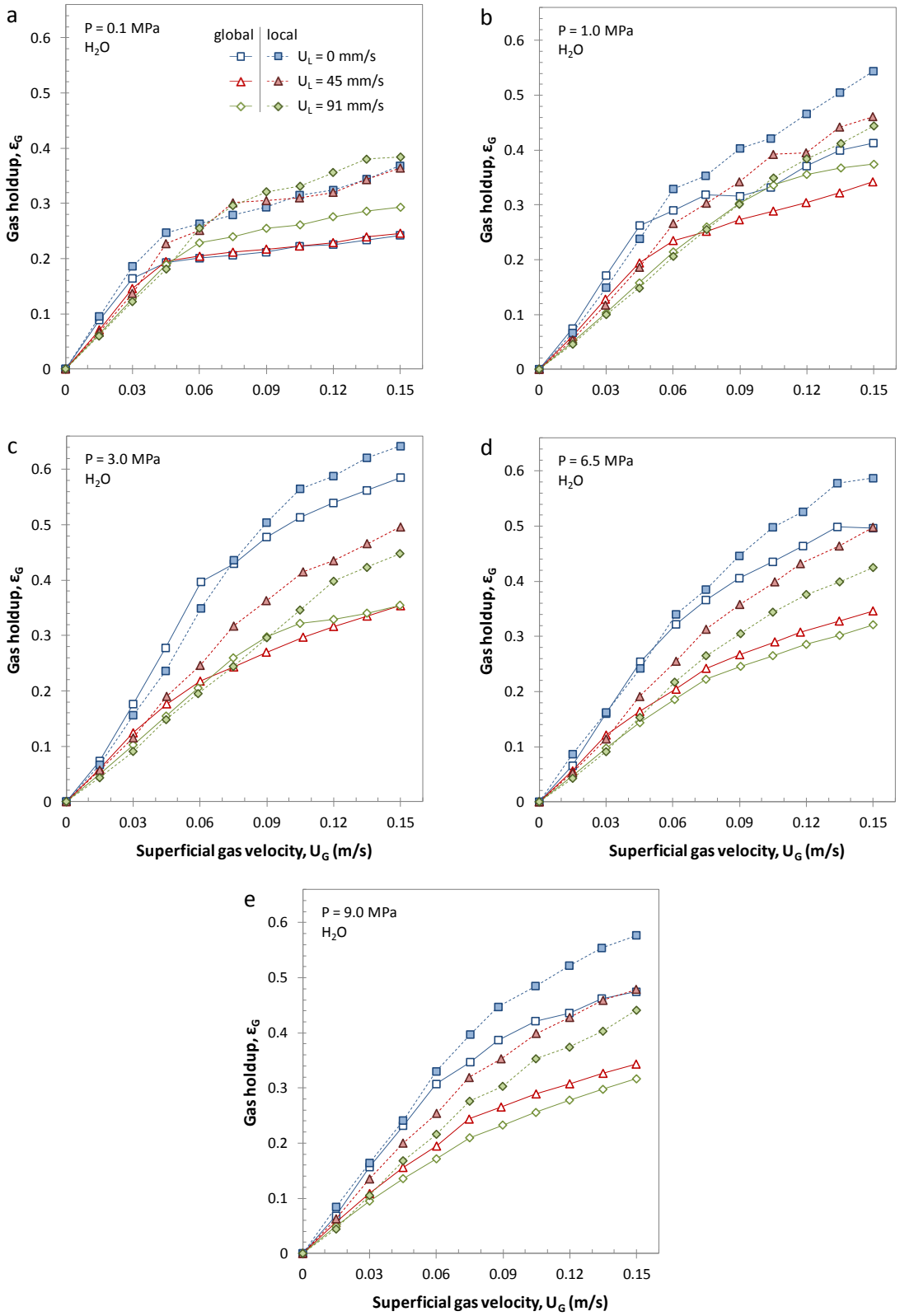

Figure 3.7. Local (r/R = 0) and global gas holdups in the water bubble column.

Figure 3.7a shows that dispersed to coalesced bubble flow transition velocities increased with the liquid velocity (approximately 35, 45 and 60 mm/s for U_L of 0, 45 and 91 mm/s, respectively). Furthermore, the highest studied liquid flow rate at 0.1 MPa resulted in the uppermost gas holdups, demonstrating that bubble breakup dominated over the potential increased bubble rise velocities due to greater liquid flow. Figure 3.7d conversely provides an example where pressure effects dominated as the highest void fractions were observed with no liquid flow. The combined effects of shearing due to liquid flow and pressure enabled the system to operate in the dispersed bubble flow regime at higher gas velocities.

Local gas holdups measured with the 1C optical probe followed expected trends when compared with global values. In dispersed bubble flow, local holdups at the center of the column were comparable to global values, where radial profiles for these conditions were shown to be relatively constant (refer to Figure 3.4). Following the transition to coalesced flow, probe measurements were greater than global values as larger/coalescing bubbles tend to rise at the center of the column. Comparisons between global and local measurements at $r/R = 0$ thus provided an additional method to establish the bubble flow regime. Bubble flow regime detection using local measurements has also been demonstrated by Shiea et al. (2013) using a dual tip resistivity probe.

Table 3.3 provides the proportion of fully detected bubbles for selected operating conditions to illustrate the impacts of pressure as well as gas and liquid superficial velocities. Fully detected bubbles indicate the fraction of successful measurements, where the signal reached the upper voltage threshold (refer to Figure 3.3). It was observed that the proportion of fully detected bubbles in water was not significantly affected by the selected gas and liquid flow rates and/or the operating pressure. As 90% or more of the bubbles were fully detected and based on the previous local and global measurement comparison, the 1C optical probe appeared to have satisfactorily measured local gas holdups in the water bubble column with/without liquid flow up to 9.0 MPa.

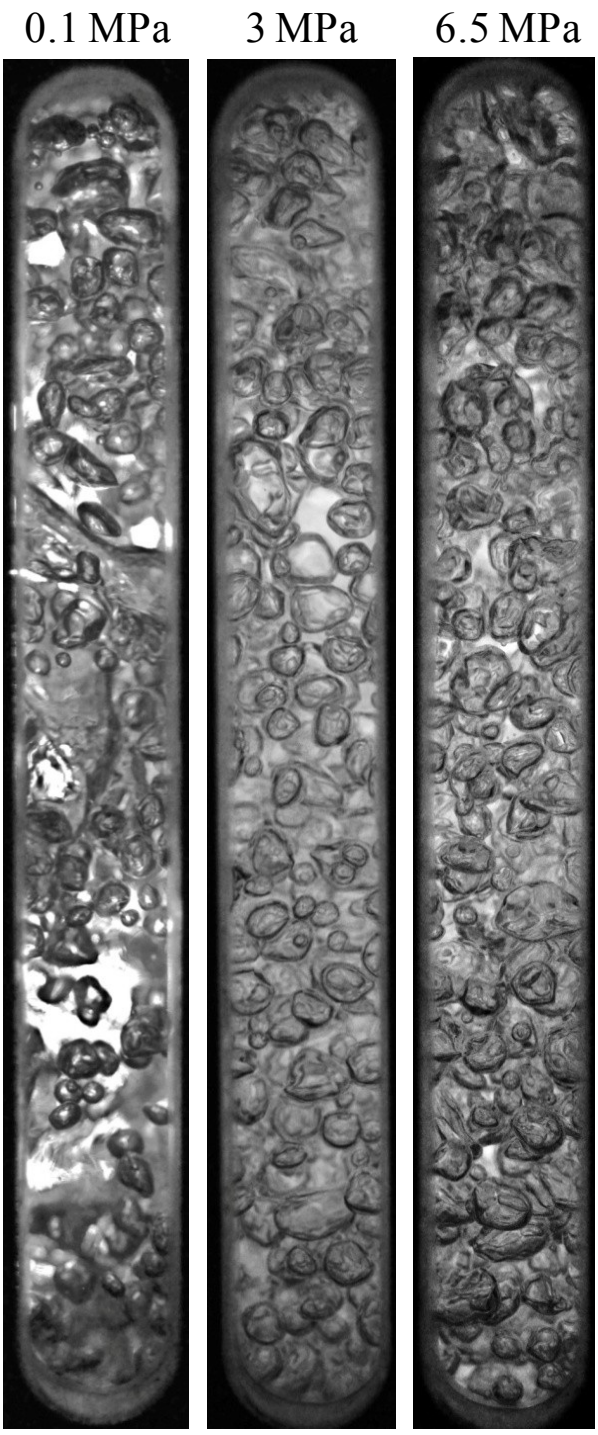

Figure 3.8. Photographic comparison of the water bubble column at U_L = 0 mm/s and U_G = 120 mm/s.

Table 3.3. Proportion of fully detected in the water bubble column (r/R = 0).

U_G (mm/s)	U_L (mm/s)	P (MPa)	Total detected bubbles	Fully detected signal (%)
30	0	0.1	2755	93.8
30	91	0.1	1689	92.5
120	0	0.1	3935	90.7
120	91	0.1	6870	93.4
30	0	6.5	2146	91.4
30	91	6.5	1905	93.3
120	0	6.5	10092	94.1
120	91	6.5	10093	93.5

Local and global gas holdups obtained in 0.5 wt.% aqueous ethanol are provided in Figure 3.9. Although measurements with no liquid flow were attempted, the entire column consisted of a foam head at relatively low gas velocities when the pressure was increased above 0.1 MPa. Surfactants generally have a polar and non-polar component, where added ethanol molecules were preferentially located at the bubble interface. The small fraction of added ethanol lowered the gas-liquid surface tension (0.072 N/m for water and 0.0685 N/m for 0.5 wt.% ethanol aqueous); however its main impact was bubble coalescence inhibition. As the hydrophilic components of the surfactant molecule cover the outer surface of a bubble, a repulsion force between polar heads is present between two approaching bubbles. Figure 3.9 clearly exhibits that ethanol addition increased global gas holdups compared to the water bubble column at equivalent operating conditions (refer to Figure 3.7), which was also observed in previous studies (Dargar and Macchi, 2006; Kelkar et al., 1983; Krishna et al., 2000).

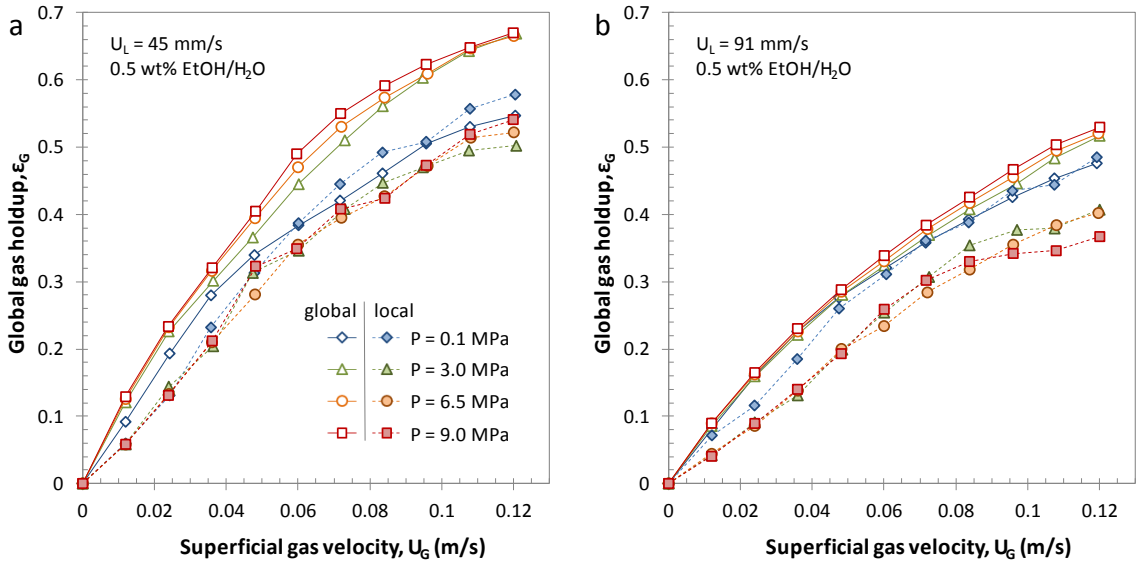

Figure 3.9. Local (r/R = 0) and global gas holdups in the 0.5 wt.% aqueous ethanol bubble column.

Pressure had a less significant effect when surfactant was added, particularly at the high liquid flow shown in Figure 3.9b. Shear stresses through the distributor and coalescence inhibition due to the ethanol addition resulted in a bubble size reduction, where Figure 3.10 visually demonstrates the significantly smaller bubbles obtained compared to water. Figure 3.9a nonetheless illustrates that pressure still had an impact on the global gas holdups. Bubble residence times in the column were reduced at the higher liquid velocity, shown by the global gas holdups reduction. Global behaviour in the surfactant system thus depended on the observed bubble breakup, either through increased pressure and shear stresses as well as the coalescence inhibition from the added surfactant.

Local gas holdups measured by the optical probe were below global values. As the probe was located at the center of the column, local bubble measurements struggled in the 0.5 wt.% aqueous ethanol solution. For both liquid flow rates, differences between local and global holdups increased with the operating pressure. Table 3.4 shows that the percentage of fully detected bubbles was lower at 6.5 MPa compared to atmospheric conditions. Although higher liquid flow rates improved the fraction of fully detected bubbles, it was considerably lower compared to water (refer to Table 3.3). The reduction of successful measurements is most likely due to smaller bubble sizes from increased pressure, as shown in Figure 3.10,

and/or surfactant addition, demonstrated in Figure 3.6. Based on the previous observations, the optical probe did not accurately measure local gas holdups under the studied high gas holdup conditions.

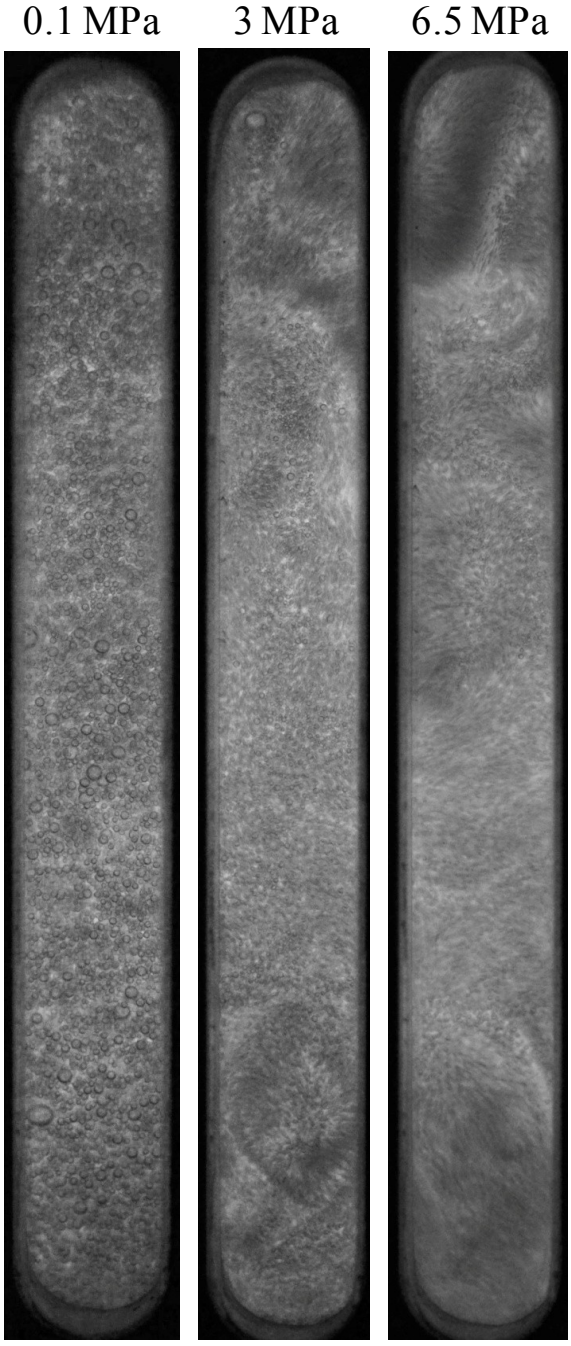

Figure 3.10. Photographic comparison of the 0.5 wt.% aqueous ethanol bubble column at U_L = 45 mm/s and U_G = 30 mm/s.

Table 3.4. Proportion of fully detected in the 0.5 wt.% aqueous ethanol bubble column (r/R = 0).

U_G (mm/s)	U_L (mm/s)	P (MPa)	Total detected bubbles	Fully detected signal (%)
24	45	0.1	9220	54.0
24	91	0.1	9431	51.6
120	45	0.1	25279	71.3
120	91	0.1	25435	66.6
24	45	6.5	18620	27.0
24	91	6.5	14711	21.8
120	45	6.5	30285	40.6
120	91	6.5	30806	33.9

3.4.3. Bubble rise velocity and chord length

For the operating conditions presented in section 3.4.2, bubble rise velocities and chord lengths were also measured using the 1C optical probe. Rise velocity and chord length cumulative distributions as a function of U_G, U_L and pressure provide useful information when attempting to predict or simulate bubble characteristics. Vejražka et al. (2010) demonstrated that the calculation of the bubble size distribution, which is dependent on the bubble residence time distribution, can be erroneous by assuming ideal probe behaviour. As local measurements under high gas holdup conditions have not yet been thoroughly investigated, the impacts of the varied operating conditions are discussed based on the chord length distributions. Although bubble properties of partially detected bubbles (i.e., when the signal does not reach the upper threshold) can be estimated, only fully detected bubbles were considered for this analysis.

For the water bubble column at constant liquid flow, the bubble rise velocity and chord length cumulative fractions, averages and standard deviations are provided in Figure 3.11 and Table 3.5. As shown with the cumulative fractions and average values, increasing

the gas flow rate at 0.1 MPa resulted in greater rise velocities and chord lengths at the center of the column. Cumulative chord length fractions presented in Figure 3.11b showed a larger portion of chord lengths above 5 mm for both U_G of 0.09 and 0.15 m/s. The previous agrees with the transition to coalesced flow at gas velocities above approximately 0.045 m/s (refer to Figure 3.7a). Above the transition gas velocity, chord length and rise velocity standard deviations increased due to the presence of smaller and larger bubbles. When operating at 6.5 MPa, average chord lengths were mostly reduced and standard deviations diminished due to more narrow bubble size distributions. Figure 3.11d shows that a negligible fraction of chord lengths were above 10 mm when elevating the pressure, in agreement with previously observed maximum stable bubble size reductions (Lin et al., 1998). Average values for the rise velocities showed little change when increasing the pressure to 6.5 MPa, nonetheless standard deviations were again reduced. The previous may be due to the higher global gas holdups, where the greater volume of gas in the column may have increased local liquid velocities.

Table 3.5. Mean and standard deviations of the rise velocity and chord lengths in the water bubble column at r/R = 0 when varying U_G.

Operating conditions			**Bubble rise velocity (mm/s)**		**Chord length (mm)**	
U_G (m/s)	**U_L (m/s)**	**Pressure (MPa)**	**Mean**	**Standard deviation**	**Mean**	**Standard deviation**
0.03	0.045	0.1	33.7	16.0	2.2	1.3
0.09	0.045	0.1	54.6	33.9	2.5	2.8
0.15	0.045	0.1	66.0	34.0	3.3	5.4
0.03	0.045	6.5	32.6	13.4	2.0	1.2
0.09	0.045	6.5	56.6	21.5	2.9	1.9
0.15	0.045	6.5	60.6	20.9	2.4	1.6

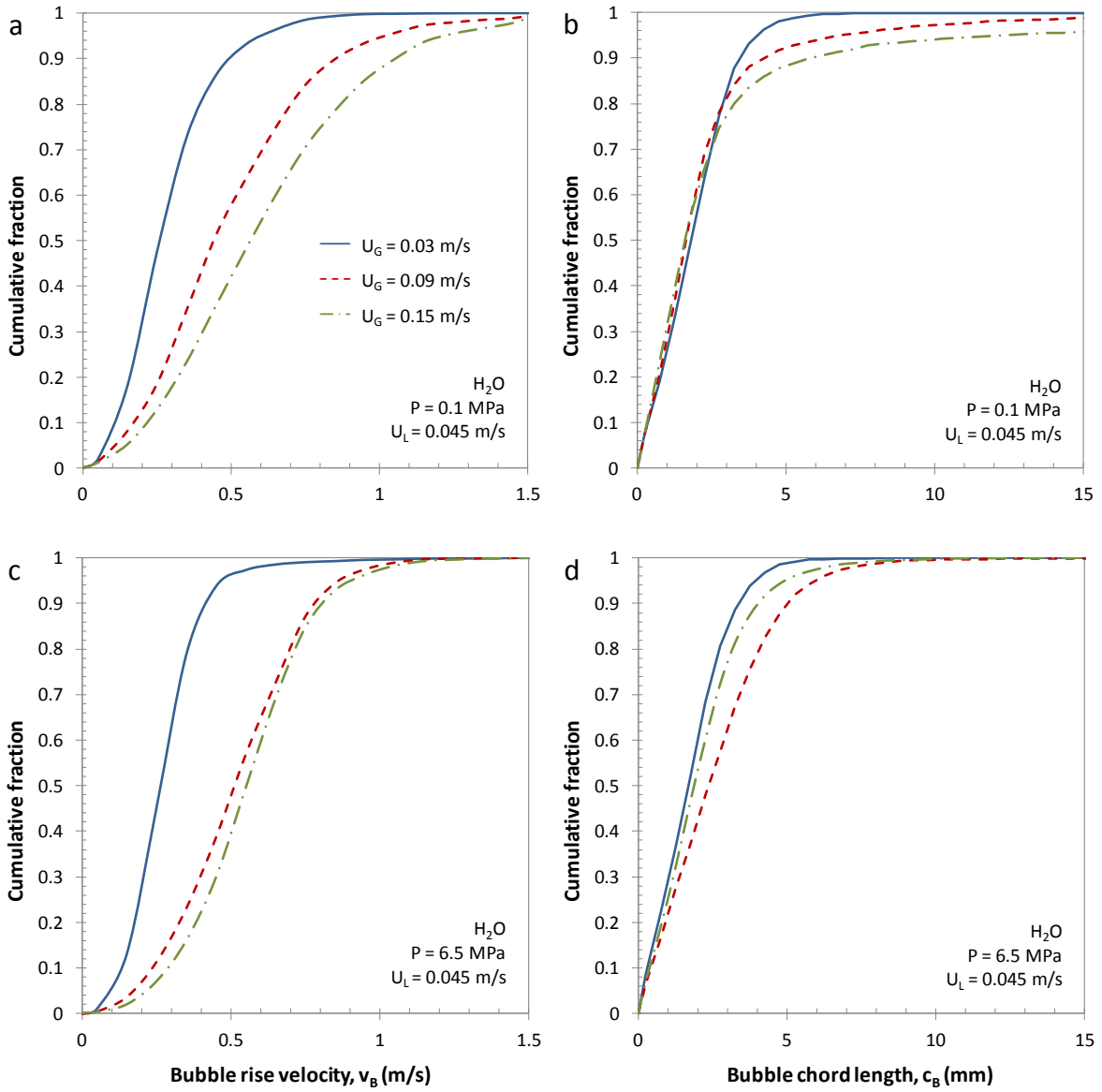

Figure 3.11. Effect of U_G on bubble rise velocity and chord length cumulative distributions in water at r/R = 0.

Figure 3.12 and Table 3.6 demonstrate the impact of liquid velocity in water. Figure 3.12a generally shows a counter-intuitive reduction in bubble rise velocity at atmospheric pressure with increased liquid flow. The corresponding chord length reduction shown in Figure 3.12b however justifies the previous trend and demonstrates the previously discussed bubble shearing through the distributor plate. Even though the system was in heterogeneous flow for the selected operating conditions (refer to Figure 3.7a), standard deviations were

also reduced with increased liquid flow. Figure 3.12a demonstrates the balance between the observed chord length reduction and reduced bubble residence times with higher liquid velocity. Between no liquid flow and a superficial liquid velocity of 0.045 m/s, bubble rise velocities dropped due to reduced chord lengths; however the increase to 0.091 m/s augmented the bubble rise velocities while detected chord lengths remained approximately constant. Operating at 6.5 MPa again diminished chord length and rise velocity standard deviations. When bubble breakup resulted due to increased pressure, Figure 3.12c demonstrates that rise velocities augmented with increased liquid flow.

Table 3.6. Mean and standard deviations of the rise velocity and chord lengths in the water bubble column at r/R = 0 when varying U_L.

Operating conditions			**Bubble rise velocity (mm/s)**		**Chord length (mm)**	
U_G (m/s)	**U_L (m/s)**	**Pressure (MPa)**	**Mean**	**Standard deviation**	**Mean**	**Standard deviation**
0.09	0	0.1	70.5	36.2	4.0	6.1
0.09	0.045	0.1	54.6	33.9	2.5	2.8
0.09	0.091	0.1	63.1	24.3	2.8	3.2
0.09	0	6.5	45.2	16.2	2.6	1.7
0.09	0.045	6.5	56.6	21.5	2.9	1.9
0.09	0.091	6.5	50.0	17.7	2.3	1.4

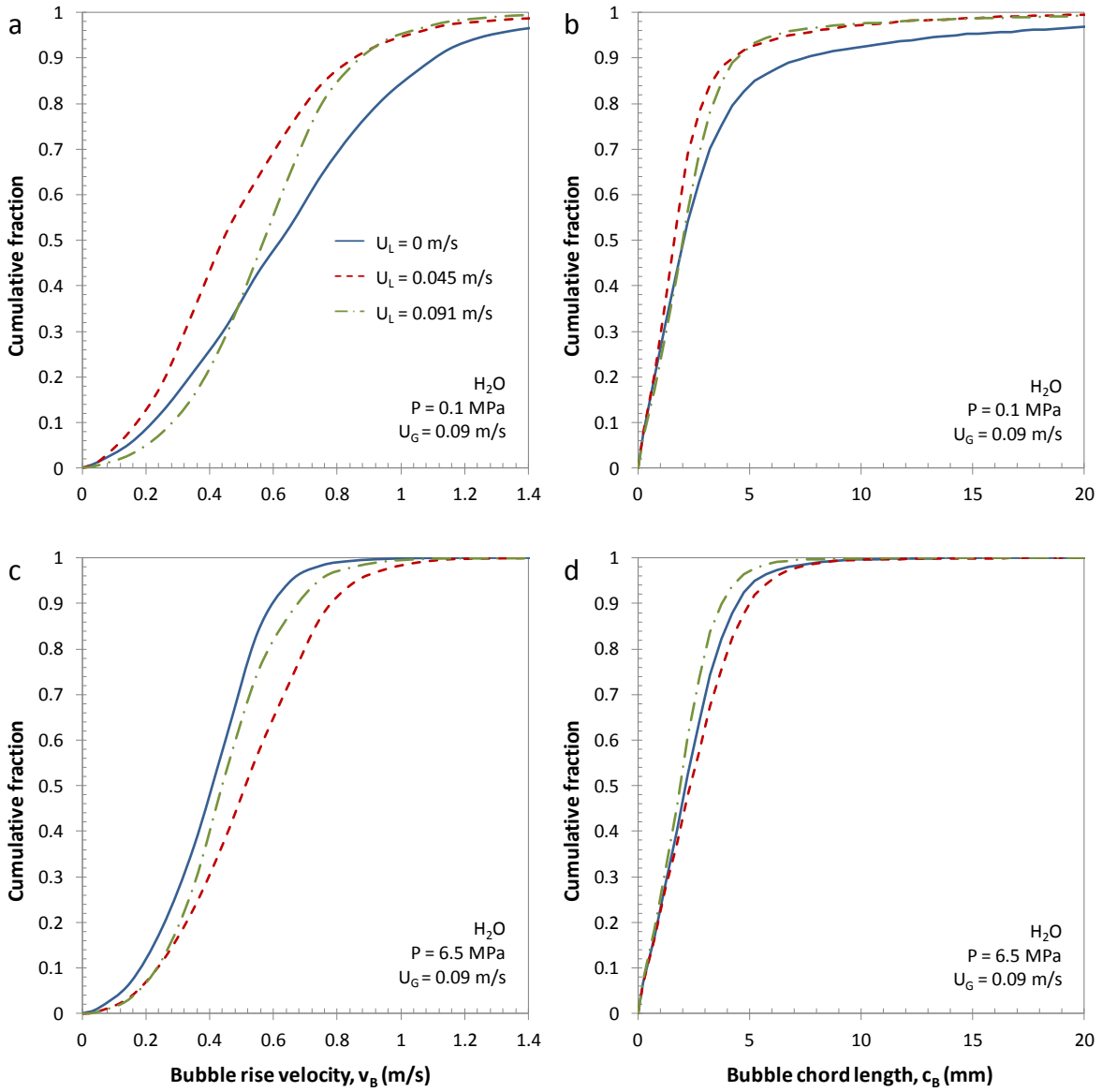

Figure 3.12. Effect of U_L on bubble rise velocity and chord length cumulative distributions in water at r/R = 0.

For 0.5 wt.% aqueous ethanol, measured bubble characteristic for a constant liquid flow followed the expected trends. Figure 3.13 shows that measured rise velocities and chord lengths both increased with greater gas flow rates. Compared to the water bubble column, measured chord lengths were significantly reduced with the added ethanol. It was previously shown that the 1C probe struggled to fully detect the smaller bubbles with the added surfactant (refer to Table 3.4). For all studied conditions, the lowest chord length measured

for a fully detected bubble was 0.13 mm, where the 1C probe can be considered physically limited by its sensing length ($L_S \approx 60$ μm). When referring to Figure 3.10 and the sight glass width (15.6 mm), it is consistent that a considerable portion of the bubbles were not being properly detected. Comparable trends were observed when the pressure was increased to 6.5 MPa, where one notable difference was the measured rise velocity reduction. Based on local holdups, chord length distributions, visual observations, bubble detection probabilities and probe physical limitations, local measurement in 0.5 wt.% aqueous ethanol are believed to have struggled due to the blinding effect resulting from significant bubble size reduction as well as modified bubble flow patterns, resulting in a greater distribution of impact angles. Due to the previous difficulties, reported average bubble rise velocity and chord length measurements for the 0.5 wt.% aqueous ethanol are believed to be inaccurate; however, overall bubble characteristic trends corresponded with those observed based on global measurements.

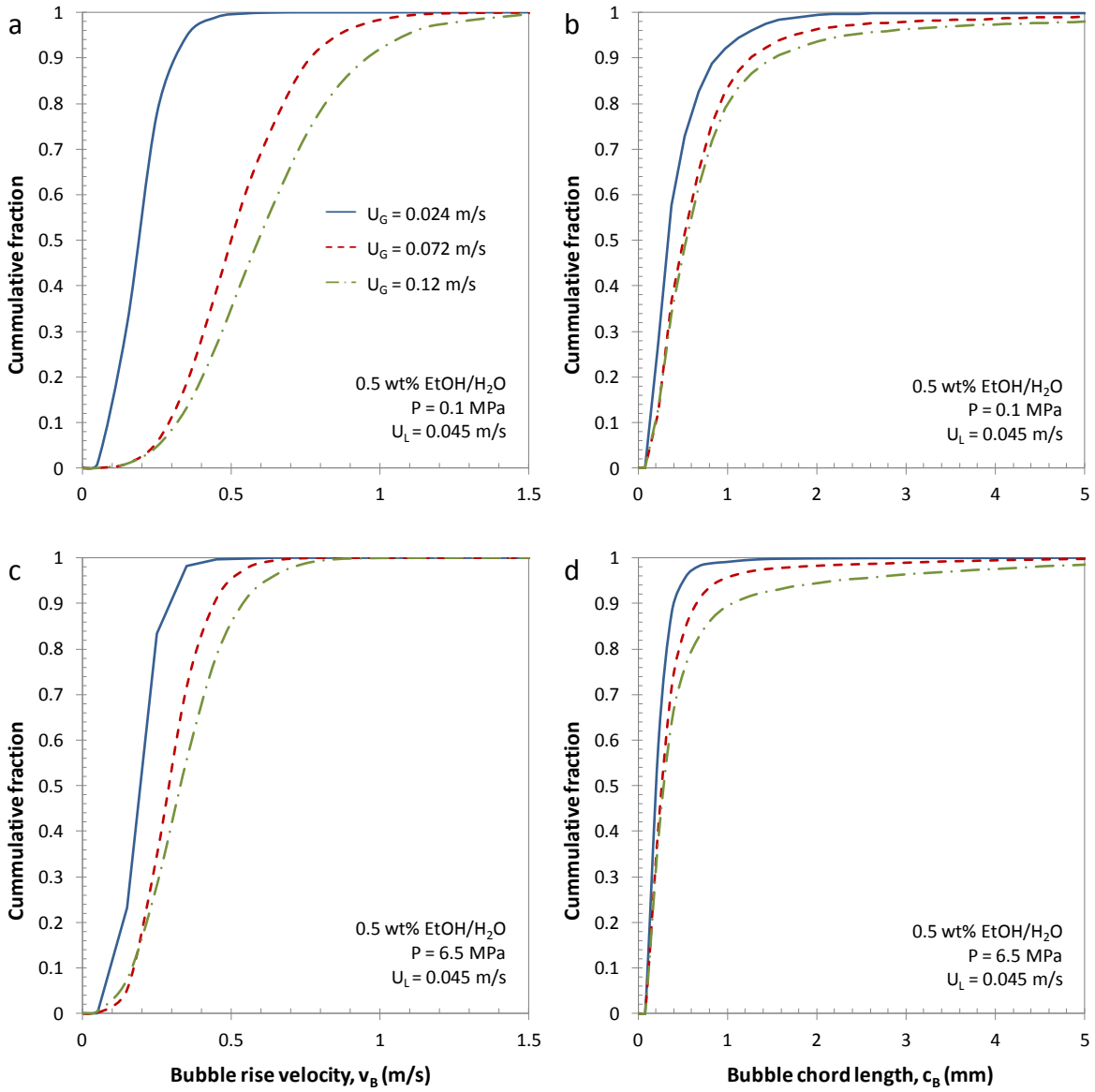

Figure 3.13. Effect of U_G on bubble rise velocity and chord length cumulative distributions in the 0.5 wt.% aqueous ethanol solution at r/R = 0.

3.5. Ebullated bed results

The probe was placed at the center of the column (r/R = 0) in the freeboard region above an ebullated bed containing 4 mm glass beads. Though bubble characteristics in the bed were of interest, the probe tip material could not withstand collisions with the studied glass beads. Mena et al. (2008) previously used a similar optical probe in three-phase flow using calcium alginate beads; however their studied particle density (1023 kg/m^3) and size

(d_P = 2.1 mm) minimized the likelihood of damaging the tip. The selected glass beads generally lead to a well dispersed bubble flow regime in the bed and a stable bed interface. The comparison between global and local gas holdups in the bubble column, bed and freeboard is provided in Figure 3.14 for all studied conditions.

Global gas holdups in the water bubble column and freeboard were similar in dispersed bubble flow, where deviations mostly occurred following the transition to coalesced bubble flow. Figure 3.14c and e show that the fluidized bed acted as an efficient gas-liquid distributor, enabling the freeboard to remain in dispersed flow for higher gas flow rates. Freeboard global gas holdups in the 0.5 wt.% aqueous ethanol were quite comparable to the equivalent bubble column. As bubble characteristics were already affected by shear stresses through the distributor, pressure effects and coalescence inhibition from the surfactant, the ebullated bed had a negligible impact on freeboard hydrodynamics. In the bed region, global gas holdups were generally lower compared to the freeboard due to the reduced available fluid volume.

Local gas holdups in the bubble column and freeboard were comparable for both water and 0.5 wt.% aqueous ethanol. Local measurements in the water column were similar following the transition to coalesced bubble flow, even though deviations between global values were observed. The previous is likely due to the placement of the probe at the center of the column and the shape of the radial profiles in the dispersed/coalescing bubble flow regimes (refer to Figure 3.4). Although it has been demonstrated that the optical probe struggled in the 0.5 wt.% aqueous ethanol, it is still interesting to note that local measurements were similar in the freeboard and bubble column.

Similarities between freeboard and bubble column gas holdups for both local and global measurements have some important implications for future studies regarding bubble characteristics under high gas holdup conditions. Assuming sufficient shear stresses, pressure effects and coalescence inhibition, the bubble column was representative of the studied ebullated bed freeboard region. Hence invasive techniques, such as the 1C optical probe, may be initially tested without the addition of particles, minimizing the chances of damaging the tip.

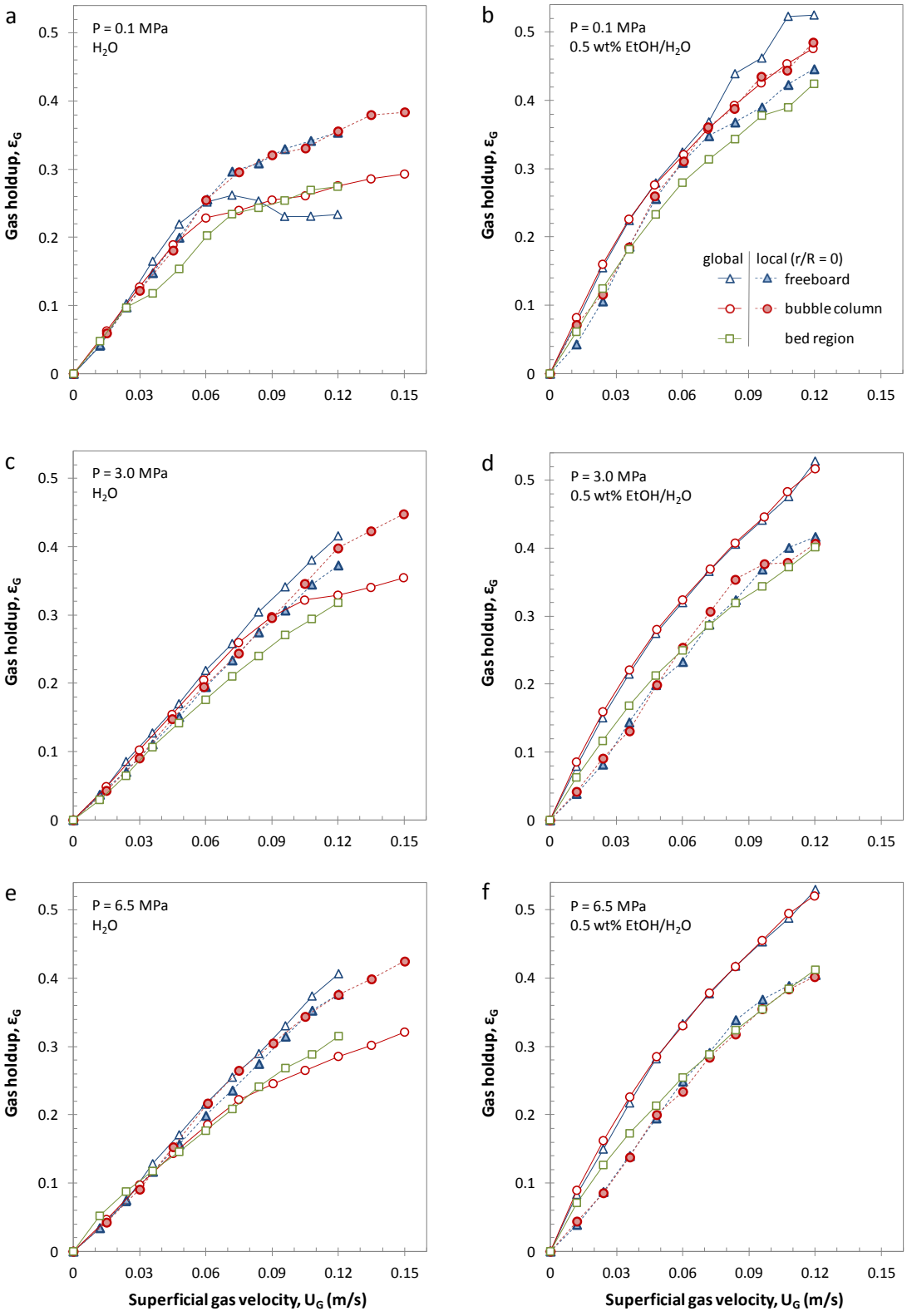

Figure 3.14. Global and local gas holdup comparisons at U_L = 91 mm/s for the bubble column and freeboard/bed regions of the ebullated bed.

3.6. Conclusions

A custom made monofibre optical probe was tested for the measurement of bubble characteristics in two phase flow under high gas holdup conditions, obtained via elevated pressures and/or the addition of a surfactant. Local gas holdup radial profiles were validated using global values obtained via the dynamic pressure drop. The average and maximum relative errors in water when integrating the profiles were 9% and 16%, respectively. Probe measurements also illustrated the modified profile curvature from enhanced bubble breakup due to shear stresses from the gas and liquid concurrently flowing through the distributor. With the added surfactant, estimated gas holdups based on local radial profiles underestimated the global measurements with average and maximum relative errors of 37% and 61%, respectively.

Comparing local measurements at the center of the column with global values, the probe successfully measured local gas holdups in water up to pressures of 9.0 MPa. In dispersed bubble flow, local gas holdups were comparable to the global values, as expected due to the relatively flat profiles. Following the transition to coalesced bubble flow, probe measurements at the column center were greater than global values. Increased operating pressures and the shearing through the distributor plate enhanced bubble break up in the system and led to dispersed bubble flow at higher gas velocities. The transition from dispersed to coalesced flow was less apparent in the 0.5 wt.% aqueous ethanol as the surfactant significantly inhibited bubble coalescence. Local gas holdups with the added ethanol were lower compared to global values, where the differences increased with pressure.

Local rise velocity and chords length cumulative fractions corresponded with global trends for both water and the 0.5 wt.% aqueous ethanol. Rise velocities and chord lengths cumulative fractions demonstrated the balance between pressure effects, shearing through the distributor and coalescence inhibition due to surface active compounds. Images captured through the system sight glass showed that chord length trends measured using the 1C probe corresponded with qualitatively observed bubble characteristics in water. Mean chord lengths with the added ethanol showed that a significant portion of bubbles were below 0.5 mm, in agreement with visual observations.

Freeboard gas holdups in water were generally higher compared to the bubble column operated at the same conditions. Enhanced bubble breakup when passing through the bed of particles allowed the system to operate in dispersed bubble flow for greater gas flow rates. For 0.5 wt.% aqueous ethanol, global and local holdups in the freeboard region were quite similar to results obtained in the bubble column at matching operating conditions. Future studies with an invasive device under high gas holdup conditions (i.e., high pressure, sufficient bubble shearing and coalescence inhibition) could be initially tested in a bubble column, minimizing the risk of damaging the device.

The 1C optical probe measurements were reliable in water up to operating pressures of 9.0 MPa and for the studied gas and liquid flow rates. For the 0.5 wt.% aqueous ethanol solution, the probe struggled to detect the smaller bubbles (below 0.5 mm in diameter). It is believed that the underestimated local gas holdups resulted from the blinding effect (improper tip dewetting) due to the significantly reduced bubble size. Visually observed back-mixing of the smaller bubbles with the added ethanol is also believed to have affected local measurements due to a wider distribution of impact angles with the probe tip. Selected operating conditions showed that the proportion of fully detected bubbles was considerably lower with the added ethanol (approximately 50 to 70% at 0.1 MPa and 20 to 40% at 6.5 MPa) compared to water (generally above 90%). For optical probe measurement technique under high gas holdup conditions, it is suggested to develop a smaller tip, and hence sensing length, to improve local measurements by increasing the proportion of fully detected bubbles.

Acknowledgments

The authors are grateful to Craig McKnight and Jason Wiens (Syncrude Canada Ltd.) as well as Stéphane Gluck and Nicolas Zuanon (A2 Photonic Sensors) for their valuable insights. The authors would like to acknowledge the Natural Sciences and Engineering Research Council of Canada, the Canadian Foundation for Innovation, the Ontario Innovation Trust and Syncrude Canada Ltd. for financial assistance.

Nomenclature

c_B	bubble chord length (m)
d_C	column inner diameter (m)
d_P	particle diameter (m)
g	gravitational acceleration (m/s^2)
h_B	bed height (m)
L_S	sensing length (μm)
m	mass of the particles (kg)
n	refractive index
P	pressure (Pa)
$-\Delta P$	dynamic pressure drop (Pa)
r	probe radial position (m)
R	column radius (m)
T	temperature (°C)
t_B	bubble residence time (s)
t_R	signal rise time (s)
t_T	total measurement time (s)
U_G , U_L	gas and liquid superficial velocities (m/s)
v_B	bubble rise velocity (m/s)
V_G, V_L	gas and liquid voltage levels (V)
Δz	vertical distance between differential pressure taps (m)

Greek symbols

β	impact angle (°)
ε_G , ε_L , ε_S	gas, liquid and solid phase holdups
μ_L	liquid dynamic viscosity (Pa s)
ρ_G , ρ_L , ρ_S	gas, liquid and solid densities (kg/m^3)

Chapter 4

Ebullated bed fluid dynamics relevant to industrial hydroprocessing

Dominic Pjontek[a], Craig A. McKnight[b], Jason Wiens[b], Arturo Macchi[a]

[a]*Centre for Catalysis Research and Innovation, Department of Chemical and Biological Engineering, University of Ottawa, 161 Louis Pasteur, Ottawa, Ontario, Canada, K1N 6N5*

[b]*Syncrude Canada Ltd., 9421-17 Avenue, Edmonton, Alberta, Canada, T6N 1H4*

Abstract

This study investigates the overall fluid dynamics of an ebullated bed operating at high gas holdup conditions to provide relevant observations for industrial residue hydroprocessors. Scaling approaches for three-phase fluidized beds were compared specifically for the scale-down of the industrially observed high gas holdup conditions. Five dimensionless groups, a binary approach for bubble coalescence behaviour in multi-component liquids, and geometric considerations are proposed to achieve dynamic similitude. Experiments were carried out in a 101.6 mm diameter co-current gas-liquid-solid fluidized bed operating at 0.1 and 6.5 MPa with liquids that do (e.g., 0.5 wt.% aqueous ethanol) and do not (e.g., tap water) significantly inhibit bubble coalescence. A comparison of the overall phase holdups for two sizes of cylindrical particles (d_{SV} of 1.6 and 3.9 mm) at matching dimensionless groups provided a preliminary verification of the proposed scaling approach. The impacts of increased liquid viscosity (e.g., greater vacuum distillation tower residue feed fraction), varying superficial gas velocity (e.g., inlet gas flow rate and gas entrainment in the liquid recycle line), and varying superficial liquid velocity (e.g., liquid recycle pump speed) were experimentally studied due to their relevance for industrial ebullated bed hydroprocessors. When increasing the liquid viscosity of the 0.5 wt.% aqueous ethanol, a fraction of the gas was entrained in the liquid recirculation, increasing gas holdups and exhibiting operational similarities to industrial hydroprocessors. The relation between freeboard and bed region gas holdups was studied for varying particle sizes and bubble coalescence behaviour. Experimental results at high gas holdups conditions were used to correlate the bed and freeboard phase holdups based on the proposed dimensionless groups.

***This manuscript has been submitted to:** Chemical Engineering Science

4.1. Introduction

The performance and optimization of industrial ebullated bed residue hydroprocessors, such as the LC-Finer[SM], are highly dependent on the overall fluid dynamic behaviour in the bed and freeboard regions. Discrepancies between industrial and typical experimental systems available in the literature generally arise from considerable differences in operating conditions, phase physical properties and column geometries. The high gas holdups observed in ebullated bed hydroprocessors at industrial operating conditions (McKnight et al., 2003) are difficult to predict or model due to the impacts of various interfacial phenomena and operating pressure. Experimental studies at industrially relevant fluid dynamic conditions are thus required to improve their design, optimization and regular operation. An appropriate scale-down method for the industrially observed high gas holdups must be identified, where scaling in general still presents an important challenge for gas-liquid-solid fluidized beds.

McKnight et al. (2003) discussed and identified key objectives to improve the LC-Finer[SM] performance, noting that minimizing the bed and freeboard gas holdups requires further investigation to maximize pitch conversion. Freeboard gas holdup measurements in the industrial hydroprocessor (approx. 50 to 60%) were considerably greater than predictions (approx. 15 to 25%) for comparable operating conditions based on selected correlations from the literature (Hughmark, 1967; Tarmy et al., 1984). Safoniuk et al. (1999) proposed a scale-down approach based on dynamic similitude using the following dimensionless groups:

$$M = \frac{g(\rho_L - \rho_G)\mu_L^{\,4}}{\rho_L^{\,2}\gamma_{G-L}^{\,3}},\quad Eo = \frac{g(\rho_L - \rho_G)d_P^{\,2}}{\gamma_{G-L}},\quad Re_{L-S} = \frac{\rho_L d_P U_L}{\mu_L},$$
$$\rho_P/\rho_L,\ U_G/U_L \qquad (4.1)$$

The method assumed that: (i) gas viscosity was negligible compared to the liquid viscosity, (ii) equilibrium interfacial properties were sufficient to characterize bubble coalescence behaviour, (iii) gas density was much lower than the liquid and solid densities, therefore it was only included in the buoyancy term, $g(\rho_L - \rho_G)$, and (iv) wall effects could be relaxed above a given column-to-particle size (d_C/d_p) ratio in the dispersed bubble flow regime. When attempting to match the proposed dimensionless groups for the LC-Finer[SM] using a

cold-flow experimental system with relaxed geometrical constraints, industrial freeboard gas holdups nearly doubled those obtained with the laboratory unit (McKnight et al., 2003). The significant discrepancy between industrial and cold-flow systems was attributed to the following possible reasons:

1. internal gas recycle via the liquid return line in the industrial unit,
2. inaccurate measurements of phase physical properties and holdups in the LC-Finer^{SM},
3. inadequate and/or missing dimensionless groups for the fluid dynamic scale-down.

Although the first and second considerations could have significantly influenced the comparison, the large gas holdup differences were also believed to be due to difficulties simulating the high gas holdup conditions in a cold-flow unit. The authors suggested based on other experimental studies that the influences of interfacial phenomena for multi-component liquids (Macchi et al., 2001a) and increased gas density due to elevated pressures (Luo et al., 1999; Macchi et al., 2003; Wilkinson et al., 1992) must be considered.

Ebullated bed experiments in a 29.4 mm diameter column using 1.7 mm glass beads, diesel fuel and nitrogen at pressures up to 15 MPa resulted in increased gas holdups and reduced minimum liquid fluidization velocities due to the modified bubble behaviour (R.S. Ruiz et al., 2004; Ruiz et al., 2005). However, the studied gas and liquid superficial velocities ranges for the previous studies (U_G and U_L < 20 mm/s) did not result in the high gas holdups observed in industrial units. Sanchez et al. (2008) investigated the Safoniuk et al. (1999) scaling approach by comparing the high pressure results of Luo et al. (1997) to an atmospheric system with matching dimensionless groups. Discrepancies in the bed porosities and gas holdups for both systems were generally less than 13% likely due to the differing pressures and foaming characteristics, where the gasoil used in the atmospheric system appeared to froth/foam even at low gas velocities.

The purpose of this work is to expand on previous fluid dynamic studies relevant to industrial ebullated bed hydroprocessors. A dimensional analysis that considers the effects of pressure and presence of surfactants is used to attempt dynamic similitude at the relevant high gas holdup conditions. The impact of a more viscous liquid on the overall fluid dynamics will also be examined as the hydroprocessing feed composition can be varied (Rana et al., 2007), where the vacuum distillation tower residue fraction may be increased

relative to the atmospheric tower residue. The relation between freeboard and bed region gas holdups is then discussed as the latter is difficult to estimate while the unit is operational due to uncertainties in catalyst inventory and density (McKnight et al., 2003). Finally, the proposed dimensionless groups are used to correlate the overall phase holdups under the high gas holdup conditions, where data from a previous study (Pjontek and Macchi, 2014) is also included.

4.2. Fluid dynamic scaling via dimensional analysis and similitude

Overall characteristics, such as global phase holdups, can have a significant impact on an industrial ebullated bed's performance by directly affecting major design parameters (e.g., bed region liquid holdup affects the reactant residence time and thus single-pass conversion). Other relevant characteristics such as the fluidized bed interface stability and particle mixing can depend on the local fluid dynamic behaviour. As such, scaling methodologies must attempt to match the overall and local fluid dynamics of the studied systems. The selected scaling approach in this study is based on the principle of dynamic similitude where geometric features (i.e., geometric similitude), the fluid flow regime (i.e., kinematic similarity), and a set of dimensionless groups are matched. This requires the identification of all physical parameters that have a significant impact on the fluid dynamics of the studied system. Failing to include a considerable variable can lead to inaccurate results, while the inclusion of an insignificant parameter may create unnecessary experiments which should eventually demonstrate that it is negligible.

Scale-up methods for bubble column and slurry bubble column reactors provide an initial assessment for ebullated beds as bubble characteristics impact the overall and local fluid dynamic behaviour in both systems. When reviewing previous bubble column scale-up attempts, Shaikh and Al-Dahhan (2013) noted that no method has yet been able to completely model the local and global behaviour. Nonetheless, the proposed methodologies provide an overview of relevant physical characteristics and general considerations when attempting to achieve dynamic similitude for a gas-liquid-solid fluidized bed.

Wilkinson et al. (1992) noted that previous gas holdup predictions in bubble columns struggled by not accounting for the transition between the dispersed and coalesced bubble

flow regimes. The authors therefore proposed a scale-up procedure based on the overall gas holdups in a bubble column by incorporating the dispersed-to-coalesced bubble flow gas transition velocity, similar to Krishna et al. (1991). Their experimental results showed that gas holdups were not considerably influenced by column geometry if the following conditions were met:

1. Column diameter larger than 0.15 m,
2. Column height-to-diameter ratio greater than 5,
3. Gas distributor holes diameter larger than 1 to 2 mm.

Wilkinson et al. (1992) proposed empirical correlations based on the following dimensionless groups: the capillary number ($v_B \mu_L \gamma_{G-L}^{-1}$), the Morton number assuming negligible gas density ($\gamma_{G-L}^{3} \rho_L g^{-1} \mu_L^{-4}$), and the liquid-gas density ratio ($\rho_L \rho_G^{-1}$). The average error of the correlations was approximately 10% with a maximum error of 40%. Fan et al. (1999) proposed an empirical correlation for bubble columns and slurry bubble columns based on three dimensionless numbers: the ratio of the superficial gas velocity over the rise velocity of the maximum stable bubble ($U_G v_{B,max}^{-1} \equiv U_G^{4} \rho_G \gamma_{G-L}^{-1} g^{-1}$), a modified Morton number for the slurry phase, and the gas-liquid density ratio. The average error for this correlation was 13% with a maximum error of 53%. Behkish et al. (2006) developed a correlation for slurry bubble columns that was not based on dimensionless groups, but still provides information on relevant physical properties. The correlation considered the following parameters: liquid density, gas density, solid density, liquid viscosity, gas-liquid surface tension, particle diameter, solid concentration in the slurry, superficial gas velocity, system pressure, vapour pressure of the liquid, column diameter, gas sparger type, and weight fraction of the primary liquid in a mixture. Differences between predicted and experimental values were within an average absolute relative error (AARE) of 20%.

It should be noted that these correlations were based on experiments with no liquid flow (i.e., batch liquid operation). The previous approaches focused on the overall fluid dynamics by examining global gas holdups, which inherently assumes that local characteristics will be similar if the previous can be achieved. However, experiments by Shaikh and Al-Dahhan (2010) have demonstrated that systems with similar overall gas

holdups can still differ in local characteristics such as radial profiles, mixing, and bubble properties. This also agrees with the observations of Macchi et al. (2001), where differences in the pressure power spectra indicated disparities in bubble coalescence behaviour at similar overall gas holdups for single and multi-component liquids. When considering the reported relative errors between correlated and experimental results, it is difficult to conclude whether the bubble coalescence behaviour in multi-component liquids is well predicted by such correlations.

For co-current gas-liquid-solid fluidized beds, Larachi et al. (2001) correlated the overall phase holdups using a combination of artificial neural networks and dimensional analysis (ANN-DA approach). The correlations were developed based on a large data set (20500 experimental phase holdup measurements for Newtonian liquids), where the following operating conditions and phase physical properties were considered: superficial liquid velocity, liquid density, liquid viscosity, gas-liquid surface tension, gas density, gas viscosity, superficial gas velocity, particle volume-equivalent diameter, particle sphericity, particle density, gravitational acceleration, column diameter, and a coalescence index (foaming or coalescing). Cross-correlation coefficients of the liquid gravity force, liquid viscous force, capillary force, as well as gas, liquid and solid inertial forces were examined for the gas holdup, liquid holdup and bed void fraction. Optimal assortments of dimensionless groups for the outputs were also provided. Compared to selected correlations in the literature, the ANN-DA approach of Larachi et al. (2001) resulted in reduced AAREs for the studied data bank (AAREs of 28%, 8.5% and 6% for the gas holdup, liquid holdup and bed void, respectively).

When scaling multiphase reactors, suitable fluid dynamic comparison between laboratory scale and industrial units of interest still appears to be a challenge. Although the previous correlations were based on data from various experimental studies, direct validations of scaling approaches by comparing industrial and laboratory systems are relatively scarce. Considering the average errors between predictions and experimental results, particularly for the gas holdup, it is difficult to conclude whether the previous correlations would result in suitable local and global fluid dynamic similitude under high gas holdup conditions. As discussed by Shaikh and Al-Dahhan (2013), scaling approaches for multiphase reactors are currently more of an art than science. It is nonetheless believed that

by considering the important geometric and fluid dynamic characteristics of a studied system, in this case the LC-Finer^{SM}, scaling between industrial and laboratory equipment using a dimensionless approach can still provide relevant observations.

4.2.1. Geometric similitude for high gas holdup conditions

Constraints towards strict geometrical similitude are discussed for the gas-liquid separation at the outlet, gas-liquid distribution into the ebullated bed, and wall effects due to column diameter and internal liquid recycle line. Gas entrainment in the LC-Finer^{SM} recycle pan must be considered as it may contribute to the observed high gas holdups in the freeboard region (McKnight et al., 2003). Conversely, the experimental system has a two stage gas-liquid separation, where experimental tests have demonstrated negligible gas entrainment when using a 0.5 wt.% aqueous ethanol solution to operate at high gas holdups (gas-liquid separation difficulties when increasing the liquid viscosity are discussed in the experimental results). The impact of gas entrainment in the industrial unit's liquid recycle can nonetheless be essentially simulated by increasing the experimental gas flow rate.

The gas-liquid distribution in the LC-Finer^{SM} must also be considered as the high gas holdups may be due to significant fluid shearing, resulting in enhanced bubble break-up. Gas distribution in bubble columns has been shown to have an influence when the initial bubble size is small relative to its maximum stable size and when the rate of bubble coalescence is low (Tarmy and Coulaloglou, 1992). The impact of the gas distributor is reduced at high rates of bubble coalescence as bubbles can reach their maximum stable size with a sufficient column aspect ratio (h_C/d_C). In the LC-Finer^{SM}, the feed liquid and gas are delivered in a horse-shoe/shroud distributor assembly and combined with the recycled liquid before passing through the risers and bubble caps located in the grid plate (McKnight et al., 2003). In the experimental system, the gas is therefore injected into the liquid using a porous pipe with openings of 10 μm below the distributor to resemble the shearing experienced by both fluids passing through the perforated plate. Moreover, local measurements have shown that increasing the liquid flow rate reduced bubble chord lengths and subsequently lowered bubble rise velocities due to enhanced bubble break-up (Pjontek et al., 2014).

Industrial hydroprocessors have relatively large column diameters, thus negating wall effects on the overall phase holdups when compared to laboratory scale systems. Shah et al. (1982) reported negligible wall effects on the gas holdups in a bubble column when the diameter is larger than 0.10 to 0.15 m, similar to the observations of Wilkinson et al. (1992). Kantarci et al. (2005) suggested that wall effects should generally be considered for bubble columns with a diameter below 0.1 m. In addition to the outer wall effects, the LC-Finer^{SM} uses an internal recycle line to recirculate the liquid following the gas-liquid separation. Experiments at high gas holdups by Fan et al. (1987) with an annular three-phase fluidized bed, where the inner-to-outer column diameter ratio was approximately 1:3, obtained comparable high gas holdups to Tarmy et al. (1984), which investigated coal liquefaction using a pilot scale system at high temperatures (450°C) and pressures (17MPa), at similar superficial velocities. Based on the previous observations and the experimental system column diameter of 0.1016 m, constraints for wall effects and the impact of an internal recycle line are relaxed due to the dispersed bubble flow regime and small bubble diameters obtained at high gas holdups.

4.2.2. Formation of dimensionless groups

The ANN-DA approach proposed by Larachi et al. (2001) can be used to provide initial considerations for relevant physical properties when attempting to scale-down the industrial high gas holdup conditions. The following variables are thus considered: liquid density (ρ_L), liquid viscosity (μ_L), gas-liquid surface tension (γ_{G-L}), gas density (ρ_G), gas viscosity (μ_G), particle volume equivalent diameter (d_V), particle sphericity (ϕ), particle density (ρ_S), superficial gas velocity (U_G), superficial liquid velocity (U_L), gravitational acceleration (g) and a coalescence index. Similar to Safoniuk et al. (1999), the impact of gas viscosity is assumed negligible as $\mu_G << \mu_L$. Particle shape is accounted for by using the volume equivalent diameter and particle sphericity. A previous study demonstrated that the overall hydrodynamics of spheres and cylinders with matching volume-to-surface area ratios (i.e., equal Sauter mean diameters) can be similar under high gas holdup conditions (Pjontek

and Macchi, 2014). At these conditions, the gas, liquid and solid holdup average absolute deviation (AAD) between both shapes were below 1.1%.

The inclusion of the gas-liquid equilibrium surface tension when scaling-down a system containing a multi-component liquid is problematic. The gas-liquid surface tension evidently impacts bubble characteristics (e.g., maximum stable bubble size and hence its rise velocity). For single component liquids, the rise velocity of a bubble can be represented by the Fan-Tsuchiya equation (Fan and Tsuchiya, 1990; Fan et al., 1999) while its maximum stable bubble size can be estimated based on the Davies-Taylor equation (Davies and Taylor, 1950), where the gas-liquid surface tension is required. In addition to the previous relations, bubble dynamics are often quantified using the Morton and Eötvös dimensionless numbers, which are again dependent on the gas-liquid surface tension.

Conflicting results have however been observed when investigating the impact of the gas-liquid surface tension on the overall fluid dynamics of bubble columns or gas-liquid-solid fluidized beds that contain multi-component liquids or surfactants. Kelkar et al. (1983) noted a gas holdup increase in a bubble column for various dilute aqueous aliphatic alcohol solutions, where the reduced equilibrium surface tension due to the added surfactants was not sufficient to explain the increase. Shah et al. (1985) observed a significant gas holdup increase in a bubble column for varying water-ethanol concentrations when compared to pure water (i.e., upper equilibrium surface tension) or pure ethanol (i.e., lowest equilibrium surface tension). Wilkinson et al. (1992) cautioned the use of equations developed using single-component liquids (or coalescing liquids) for liquid mixtures as this will generally underestimate the overall gas holdups. Gorowara et al. (1990) presented an approach to estimate the gas holdups in three-phase fluidized beds containing surfactants by grouping liquids into four categories based on the equilibrium and dynamic surface tensions. This approach was unsuccessful when Dargar and Macchi (2006) observed similar gas holdups in a bubble column and fluidized bed for aqueous solutions containing various surface-active compounds. For the previous conditions, the type and concentration of surfactant mainly affected the foam stability at the free surface. When discussing physical parameter selection for the ANN-DA approach, Larachi et al. (2001) noted that the impact of coalescence inhibitors on bubble break-up and coalescence behaviour in an ebullated bed was not yet well understood. The authors thus used a binary coalescence index to account for this

phenomenon, where the cross-correlation indicated that coalescence inhibition resulted in higher overall gas holdups.

Experiments with multi-component liquids in both bubble columns and three-phase fluidized beds thus suggest that once a liquid mixture sufficiently inhibits bubble coalescence, use of the equilibrium surface tension appears inappropriate to predict the resulting gas holdups. Since the goal of this study is to scale-down the fluid dynamics of an industrial ebullated bed containing a multi-component liquid, where high gas holdups measured in the freeboard were indicative of foaming (McKnight et al., 2003), the equilibrium gas-liquid surface tension will not be considered for the dimensionless groups. The addition of a surfactant that yielded high gas holdup conditions with the studied experimental system (Pjontek and Macchi, 2014) will instead be used to simulate the suspected bubble coalescence inhibition, consequently resulting in a binary approach for coalescing or coalescence inhibiting liquids.

The following variables are therefore selected when scaling gas-liquid-solid ebullated beds at high gas holdups: liquid density (ρ_L), gas density (ρ_G), particle density (ρ_S), liquid viscosity (μ_L), gravitational acceleration via the particle-liquid buoyancy term ($g(\rho_S - \rho_L)$), average particle size/shape using the Sauter mean diameter ($d_{SV} = d_V\phi$), gas superficial velocity (U_G), liquid superficial velocity (U_L), and a binary index for bubble coalescence behaviour (coalescing or coalescence inhibition). The particle Sauter mean diameter was chosen as the characteristic length and the fundamental dimensions used were mass, length, and time, resulting in the following dimensionless groups based on the Buckingham Pi theorem:

$$\mathrm{Re}_{L-S} = \frac{\rho_L\, d_{SV}\, U_L}{\mu_L},\ \mathrm{Ar}_{L-S} = \frac{\rho_L\, d_V{}^3\, g(\rho_S - \rho_L)}{\mu_L{}^2}$$
$$\frac{\rho_G}{\rho_L},\ \frac{\rho_S}{\rho_L},\ \frac{U_G}{U_L} \tag{4.2}$$

In addition to the dimensionless groups, this approach requires equivalent bubble coalescence behaviour for dynamic similarity (i.e., coalescing or significantly inhibiting coalescence). The previous dimensionless groups indicate that this scaling approach focuses

on matching inertial, viscous and buoyant forces between both systems. When examining the resulting dimensionless groups, systems with matching solid-liquid Reynolds and Archimedes numbers should exhibit equivalent liquid-solid fluidized bed voidage based on empirical correlations for the terminal particle settling velocity and n index parameter (Khan and Richardson, 1989) required for the well-known Richardson and Zaki (1954) correlation. As a result, the proposed scale-down approach matches the liquid-solid fluidized bed characteristics while the relevant high gas holdup behaviour for this study is accounted for by sufficiently inhibiting bubble coalescence, promoting bubble break-up, and matching the gas-liquid superficial velocity ratio.

If dynamic similitude between separate systems is achieved, equal dimensionless properties should be obtained. For example, both systems should have matching phase holdups as these are already dimensionless parameters. The ratio of the bubble diameter-to-characteristic length (i.e., Sauter mean particle diameter) should be also equal. By multiplying various dimensionless groups, it can be demonstrated that the bubble Reynolds number and gas-liquid Archimedes number will also match for both systems under dynamic similitude. Caution should be exercised when studying the local flow behaviour between matching laboratory and industrial scale systems as a reduced column diameter may impact the radial flow characteristics, especially in the heterogeneous/coalesced bubble flow regime. It is nonetheless believed that the previous has a less significant impact when investigating the overall phase holdups in the homogeneous/dispersed bubble flow regime, which are of interest for this study.

4.3. Experimental system

Experiments were carried out in a gas-liquid-solid fluidization system capable of reaching pressures up to 10 MPa. The column is made of stainless steel with an inner diameter of 101.6 mm and a maximum expanded bed height of 1.8 m. Three glass viewing windows are located above the distributor plate. The gas-liquid separation occurs via the expanded overflow section at the top of the column and then by conveying the liquid into a partitioned liquid storage tank for further degassing prior to being recycled to the bottom of the column. The system was pressurized using industrial grade nitrogen cylinders. Global

phase holdups were determined using a differential pressure transmitter. The reference pressure port for the dynamic pressure drop is located at 95 mm above the distributor plate and subsequent pressure ports are equally spaced by a distance of 146 mm. A centrifugal pump drives the liquid from the storage tank to the base of the column and a magnetic flow meter (Rosemount model: 8732CT12N0) measures the liquid flow rate. Gas was circulated via a single stage reciprocating compressor, where fluctuations in the gas flow are reduced by gas dampeners located at the compressor inlet and outlet. A differential pressure transducer and orifice plates of varying size, depending on the operating pressure, were used to measure the gas flow rate. Gas was sparged in the plenum chamber of the column (i.e., below the distributor plate) via a porous pipe with openings of 10 μm in diameter. The gas-liquid mixture then flowed into the bed through a perforated distributor plate with 23 holes of 3.175 mm diameter. A mesh was used to prevent particles from entering the plenum chamber. A schematic of the experimental system and additional details can be found in Pjontek and Macchi (2014).

Selected operating conditions and phase physical properties for this study were chosen to provide high gas holdup results relevant to the LC-Finer^{SM}. Table 4.1 summarizes the operating conditions, phase physical properties and ranges for the dimensionless groups used in this study. Uncertainties for the gas and liquid superficial velocities as well as operating pressure were estimated from fluctuations during experiments. Considering the binary approach for coalescing or coalescence inhibiting liquids, tap water or a 0.5 wt.% aqueous ethanol solution (that produces and effervescent foam at the free surface) were respectively selected. Uncertainties for the liquid density and viscosity were estimated based on repeated measurements, though experimental temperature variations were also considered for the viscosity. Aluminum cylindrical particles were selected to minimize particle density and size distribution effects, while also having a length-to-diameter ratio and particle-liquid density ratio relevant to hydroprocessing catalysts. Particle sizing uncertainties were estimated based on measurements for 100 particles and particle density uncertainties were based on repeated measurements. A carboxymethyl cellulose (CMC) sodium salt (low viscosity) was added to increase the liquid viscosity, where a 0.8 wt.% solution resulted in a viscosity of approximately 4.0 Pa·s (viscosity selection is further discussed in section 4.5.1).

It should be noted that measurements using a Anton Paar Physica MCR 301 Rheometer indicated that the studied CMC concentrations resulted in Newtonian rheological behaviour.

Table 4.1. Studied operating conditions, phase physical properties and dimensionless groups.

Parameter	Symbol	Range	Units
Superficial liquid velocity	U_L	75 to 123 (± 1%)	mm/s
Superficial gas velocity	U_G	0 to 140 (± 2%)	mm/s
Pressure	P	0.1 and 6.5 (± ~1%)	kPa
Column diameter	d_C	101.6	mm
Temperature	T	23 ± 2	°C
Liquid density	ρ_L	998 ± 2	kg/m^3
Liquid viscosity (H_2O)	μ_L	$(0.95 \pm 0.4) \times 10^{-3}$	Pa · s
Liquid viscosity (0.8 wt.% CMC in H_2O)	μ_L	$(4.0 \pm 0.3) \times 10^{-3}$	Pa · s
Gas density	ρ_G	1.15 ± 0.03 and 73.7 ± 0.7	kg/m^3
Particle density	ρ_S	2711 ± 8	kg/m^3
Particle diameter	d_p	3.16 ± 0.03	mm
Particle length	L_P	7.5 ± 0.4	mm
Sphericity	ϕ	0.81 ± 0.05	-
Sauter mean diameter	d_{SV}	3.9 ± 0.2	mm
Particle-liquid Reynolds number	Re_{S-L}	61 to 450	-
Particle-liquid Archimedes number	Ar_{S-L}	$(0.12 \text{ to } 2.14) \times 10^6$	-
Gas-liquid density ratio	ρ_G/ρ_L	0.0015 and 0.0740	-
Solid-liquid density ratio	ρ_S/ρ_L	2.505 and 2.716	-
Gas-liquid superficial velocity ratio	U_G/U_L	0 to 2.0	-

4.4. Global phase holdups measurements

Global phase holdups were calculated by measuring the dynamic pressure drop, where the hydrostatic head of liquid is subtracted, throughout the bed and freeboard regions. The bed height (h_B) was estimated from the intersection of the bed and freeboard dynamic pressure axial profiles, obtained by linear regression. Visual observations of the bed height were recorded when possible to corroborate the bed height obtained by the pressure drop method. Solid holdups (ε_S) were calculated knowing the mass of solids in the fluidized bed (m).

$$\varepsilon_S = \frac{4\,m}{\pi\, d_C^{\,2}\, h_B\, \rho_S} \tag{4.3}$$

Neglecting frictional drag on the wall and accelerations of the phases in the vertical direction, gas holdups in the bed region (ε_G) were measured based on the bed region dynamic pressure axial profile.

$$\varepsilon_G = \frac{(\Delta P/\Delta z)g^{-1} + (\rho_S - \rho_L)\varepsilon_S}{\rho_L - \rho_G} \tag{4.4}$$

Liquid holdups in the bed region (ε_L) were calculated knowing that the sum of phase holdups must give unity. Gas holdups in the freeboard region (ε_{G-FB}) were measured based on the dynamic pressure axial profile above the bed.

$$\varepsilon_{G-FB} = \frac{(\Delta P/\Delta z)g^{-1}}{\rho_L - \rho_G} \tag{4.5}$$

Phase holdups standard deviations were estimated to provide additional insight on the fluid dynamic behavior of the bed and freeboard regions. Bars presented in the figures of this study provide the estimated standard deviations for the overall phase holdups based on the method presented in Pjontek and Macchi (2014).

4.5. Experimental results and discussion

4.5.1. Dynamic similitude test via particle size

The proposed scaling method was used to compare the overall fluid dynamic behaviour of two systems with differing particles sizes but matching dimensionless groups. Experimental runs from a previous study (Pjontek and Macchi, 2014) using smaller cylindrical aluminum particles (ρ_S = 2649 ± 9 kg/m^3, d_{SV} = 1.6 ± 0.2 mm, and ϕ = 0.80 ± 0.08) in water and 0.5 wt.% aqueous ethanol were compared to larger aluminum cylinders, where modified liquid properties and operating conditions resulted in matching dimensionless groups. For the larger cylinders, the liquid viscosity was increased by adding 0.8 wt.% CMC ($\mu_L \approx$ 0.004 Pa·s) to approximately match the particle-liquid Archimedes number (Ar_{L-S}) of the smaller cylinders.

4.5.1.1. Liquid-solid fluidized bed

Figure 4.1 presents the solid holdups in the liquid-solid fluidized beds as a function of the particle Reynolds number (Re_{L-S}) for both sizes. Horizontal bars in the previous figure were included to illustrate the estimated Re_{L-S} uncertainty, where deviations were mainly due to the particle Sauter mean diameters and liquid viscosities. Solid holdups for both particle sizes compared relatively well when considering the Re_{L-S} uncertainty and Ar_{L-S} differences.

Experimental data was fitted to a modified-dimensionless form of the well-known Richardson and Zaki (1954) empirical correlation:

$$\ln Re_{L-S} = n \ln(1-\varepsilon_S) + \ln(Re_{L-S,T}) \tag{4.6}$$

Where the intercept provides the Reynolds number at the terminal settling velocity of a particle accounting for wall effects ($Re_{L-S,T}$) and the slope estimates the n index. The least squares fit for the experimental liquid-solid fluidized bed results gave n ≈ 2.7 and $Re_{L-S,T} \approx$ 290. The estimated n index (2.4 < n < 4.7) and Reynolds number at the terminal free settling

velocity ($0.2 < Re_{L-S,T} < 500$) indicated the transition between the Stokes (viscous forces dominating) and Newton (inertial forces dominating) settling flow regimes.

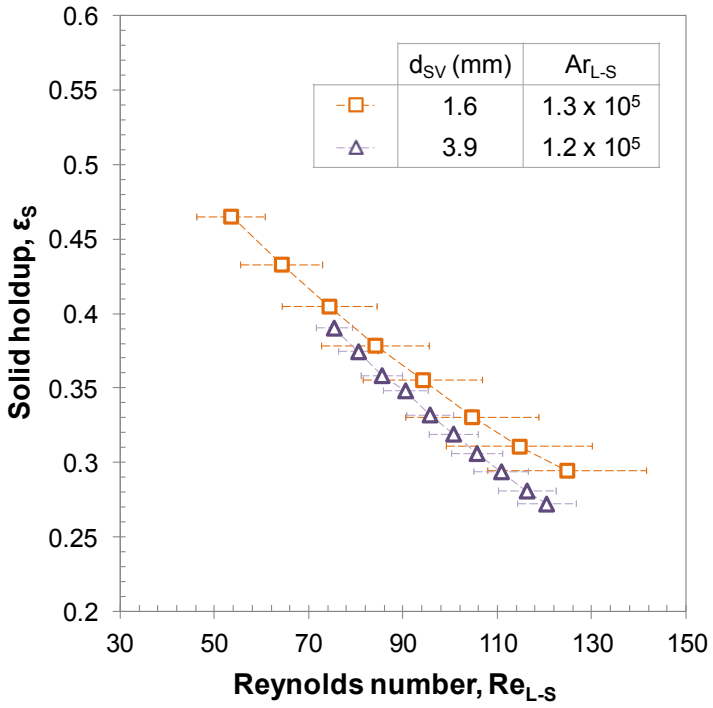

Figure 4.1. Solid holdup as a function of particle-liquid Reynolds number for smaller and larger aluminum cylinders in a liquid-solid fluidized bed with matching dimensionless groups.

4.5.1.2. Gas-liquid-solid fluidized bed

Figure 4.2 compares the ebullated bed phase holdups and freeboard gas holdups for both particle sizes at matching Ar_{L-S} and Re_{L-S} as a function of the gas-liquid superficial velocity ratio. The open data points depict water as the solvent (i.e., coalescing system) while the closed data points represent the 0.5 wt.% aqueous ethanol as the solvent (i.e., coalescence inhibition system). A liquid superficial velocity of 0.075 m/s for the larger cylinders was required to match the particle Reynolds number ($Re_{L-S} = 74$) of the smaller aluminum cylinders ($U_L = 0.045$ m/s). It should be noted that measurements for the smaller cylinders were not carried out at elevated pressures due to operating difficulties at these conditions,

such as significant bed expansions leading to partial blocking of the liquid return line (Pjontek and Macchi, 2014). The comparison was thus carried out at atmospheric pressure to match the ρ_G/ρ_L ratio.

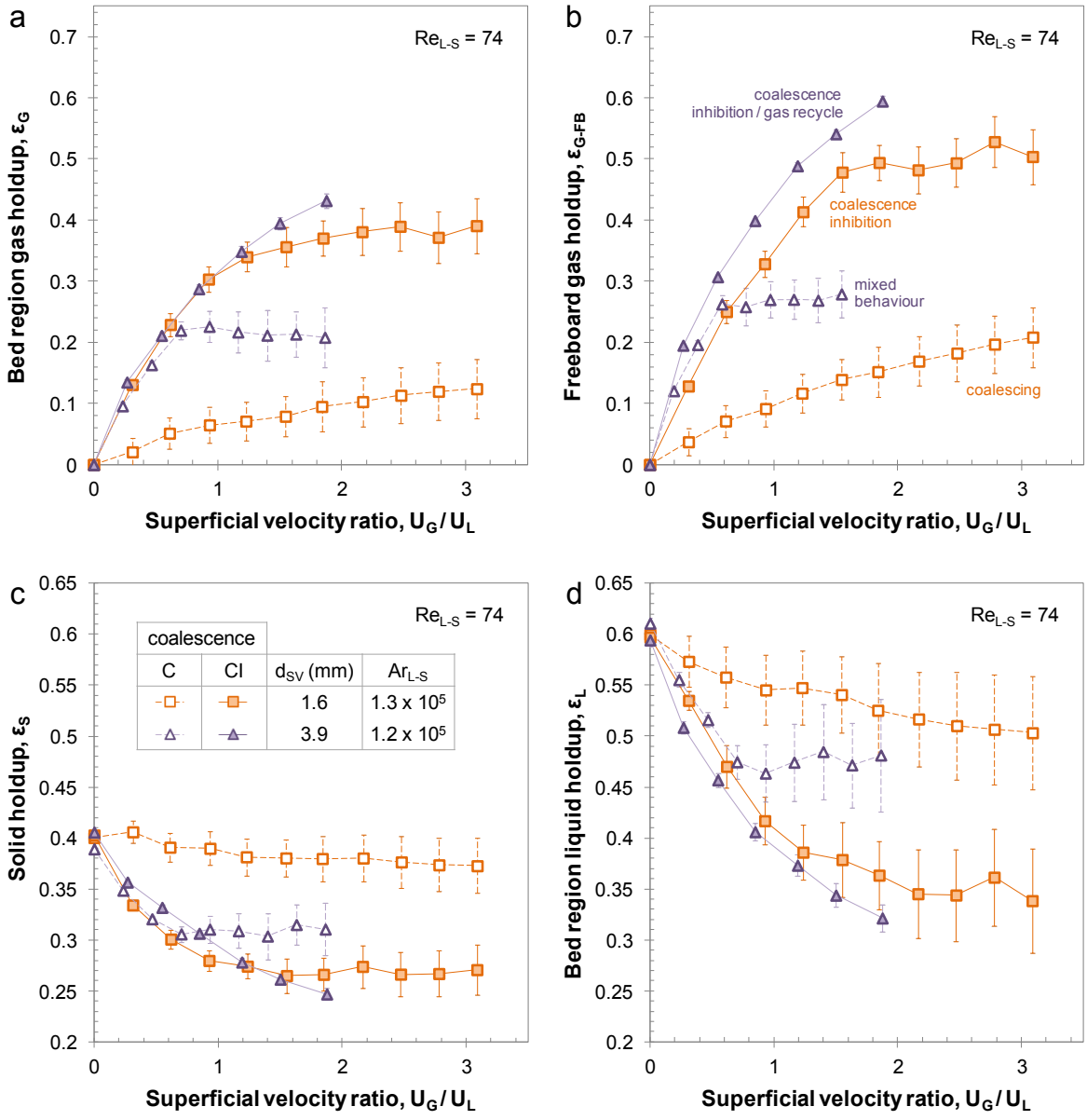

Figure 4.2. Ebullated bed and freeboard phase holdups as a function of gas-liquid superficial velocity ratio for smaller and larger aluminum cylinders in water (i.e., coalescing / mixed behaviour (C) systems) and 0.5 wt.% aqueous ethanol (i.e., coalescence inhibition (CI) systems) at P = 0.1 MPa.

During the experiments, it was observed that adding CMC to water resulted in interfacial phenomena that inhibited bubble coalescence at the lower gas velocities. Bubbles readily coalesced at the higher gas velocities, although small/micro-bubbles were still present giving the liquid a froth-like appearance. The transition from dispersed to coalesced bubble flow can be readily observed based on the gas holdups in Figure 4.2a. The resulting behaviour of the 0.8 wt.% aqueous CMC solution thus prevented a suitable comparison to the smaller aluminum cylinders in water since the proposed scaling approach is based on a binary consideration for bubble coalescence behavior (i.e., comparisons must be made between systems that do or do not significantly inhibit bubble coalescence, whereas mixed behaviour is difficult to quantify).

During the experiments using the 0.5 wt.% aqueous ethanol and added CMC, it was observed that a fraction of the gas was being recycled with the liquid recirculation (readily observed after stopping the inlet gas flow). It is believed that the gas recycle resulted from the addition of a second surface-active component and/or the reduced film drainage rate between two adjacent bubbles as it is inversely proportional to the liquid viscosity (Sagert and Quinn, 1978, 1977). The resulting foam at the free surface consequently did not entirely dissipate in the two gas-liquid separation stages (i.e., expanded overflow section and partitioned recycle tank) prior to being recycled to the bottom of the ebullated bed. The superficial velocity ratios presented in Figure 4.2 had to be adjusted to account for the increased gas and reduced liquid superficial velocities due to the gas recycle. The gas fraction in the liquid recycle was experimentally estimated by measuring the dynamic pressure drop in the freeboard region shortly after gas shut-off while maintaining liquid flow. At the highest superficial gas velocity shown in Figure 4.2, the fluid recirculation in the experimental system had a volumetric gas fraction of approximately 17%. The volumetric fraction of gas in the liquid recirculation was approximated based on measurements taken at multiple gas velocities. It is important to note that the magnetic flow meter on the liquid recycle line measures the volumetric fluid flow rate independently of fluid density. The superficial velocity ratios presented in Figure 4.2 were adjusted based on the estimated gas fractions in the liquid recycle line, thus providing an estimate of the actual gas and liquid flow rates in the ebullated bed.

Following the corrections to the gas and liquid superficial velocities due to the gas recycle, phase holdups in the ebullated bed were relatively comparable for both coalescence inhibition systems in dispersed bubble flow. Discrepancies can be observed for the coalescence inhibition systems at higher gas flow rates ($U_G/U_L > 1.55$) as the smaller cylinders transitioned to coalesced bubble flow (Pjontek and Macchi, 2014). The previous demonstrated the importance of matching the fluid flow regimes (i.e., kinematic similarity) for the scaling approach. Bearing in mind the differences in particle size (d_{SV} of 1.6 and 3.9 mm), superficial liquid velocities (U_L of 45 and 75 mm/s), and liquid viscosities (μ_L of 9.5 x 10^{-4} and 4.0 x 10^{-3} Pa·s) for both systems, the similar overall phase holdups trends in the ebullated bed provided a preliminary confirmation of the proposed dimensionless scaling approach for similar bubble coalescence behaviours. Freeboard gas holdups observed with the larger particles were however greater than those obtained with the smaller cylinders. Improved measurements of the gas fraction in the liquid recirculation are required to confirm this trend.

4.5.2. Effect of increased liquid viscosity

Measurements at high gas holdup conditions relevant to industrial ebullated bed hydroprocessors (i.e., coalescence inhibition using the 0.5 wt.% aqueous ethanol, before and after CMC addition) were carried out to study the following parameters:

1. increased liquid viscosity due to higher vacuum distillation tower residue feed fraction,
2. varying superficial gas velocity due to the gas feed flow rate or gas recycle fraction,
3. varying superficial liquid velocity due to the liquid feed flow rate or liquid recycle.

Similar to the results discussed in the previous section, gas entrainment in the liquid recirculation was observed when adding CMC to the coalescence inhibition system (0.5 wt.% aqueous ethanol as the solvent). The superficial velocity ratios presented in Figure 4.3 and Figure 4.5 were therefore adjusted to account for the increased gas and reduced liquid superficial velocities due to the gas recycle (refer to the method described in section 4.5.1.2).

Although not representative of the high gas holdup behaviour in industrial ebullated beds, data is also presented for the coalescing and mixed behaviour systems (i.e., water and 0.8 wt.% aqueous CMC, respectively) for comparison purposes. A system that does not inhibit bubble coalescence provides a lower bound for the gas holdups at matching dimensionless groups. Unfortunately, the observed surface-active characteristics following CMC addition in water prevented the isolated investigation of increased liquid viscosity in a coalescing system.

4.5.2.1. Varying inlet gas flow rate

Ebullated bed and freeboard phase holdups before and after CMC addition in 0.5 wt.% aqueous ethanol (coalescence inhibition systems) and water (coalescing / mixed behaviour systems) are presented in Figure 4.3 and Figure 4.4, respectively, where the inlet gas flow was varied while maintaining the liquid flow rate. The effects of bubble coalescence behaviour and operating pressure with respect to the overall phase holdups have already been discussed for the studied particles in water and 0.5 wt.% aqueous ethanol in a previous study (Pjontek and Macchi, 2014). Increasing the pressure allowed the coalescing system to remain in dispersed bubble flow for higher gas superficial velocities (refer to Figure 4.4a). The addition of CMC to water again resulted in some coalescence inhibition at low gas velocities whereas bubble coalescence occurred at increased gas flow rates, indicated by the greater phase holdup standard deviations (Figure 4.4) due to the formation of larger bubbles. Elevated pressures had a less significant impact for the aqueous ethanol systems (refer to Figure 4.3a), where bubble break-up via the gas-liquid distribution system considerably reduced the average bubble size based on visual observations. Photographs at comparable operating conditions in the experimental system can be found elsewhere (Pjontek et al., 2014). Elevated pressure following CMC addition to the 0.5 wt.% aqueous ethanol was not investigated as the foam layer stability would have likely resulted in liquid entering the gas compressor, where the polymer characteristics of CMC could have damaged the internals.

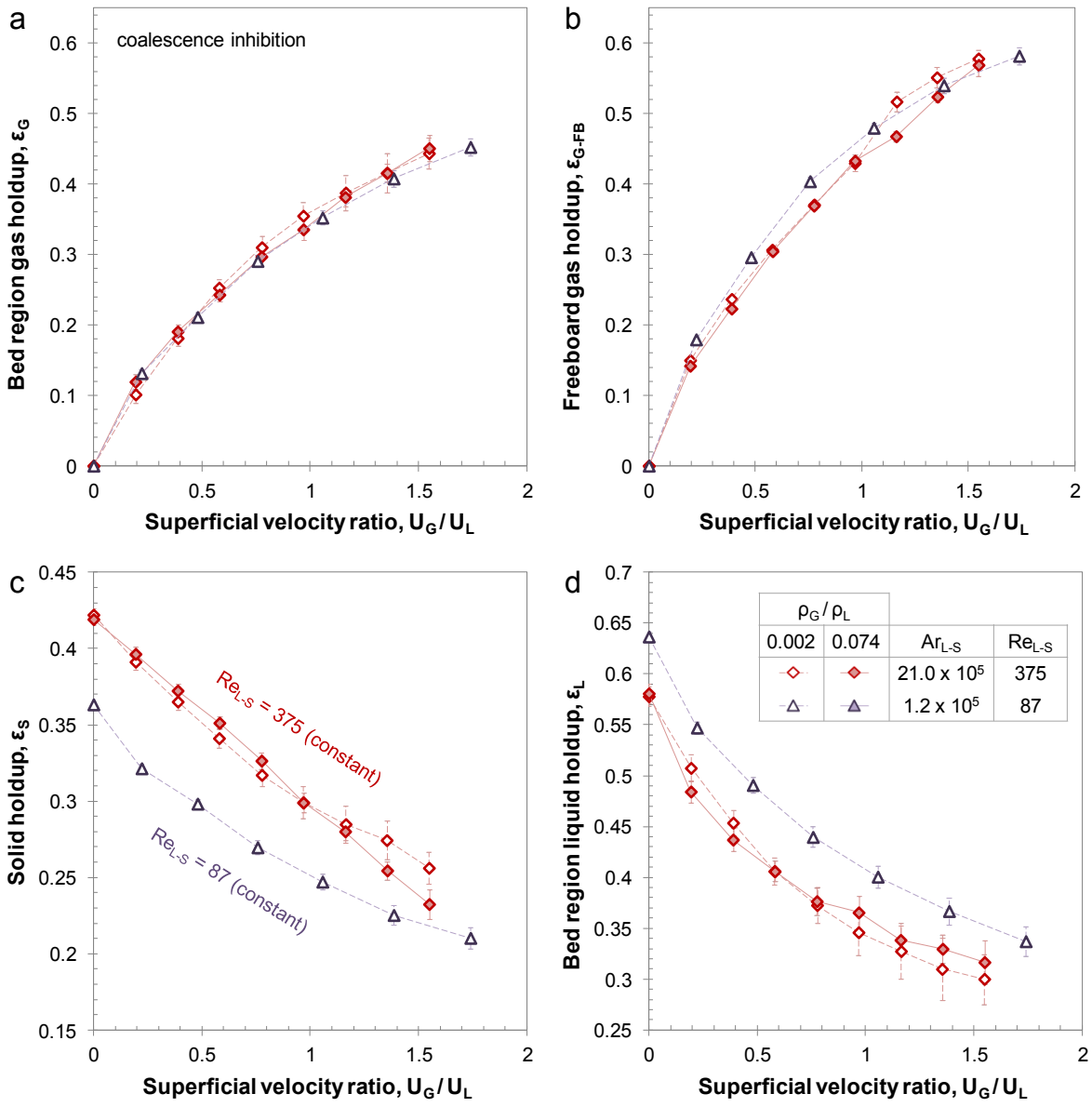

Figure 4.3. Ebullated bed phase holdups for the coalescence inhibition systems at varying gas flow rates and liquid viscosity.

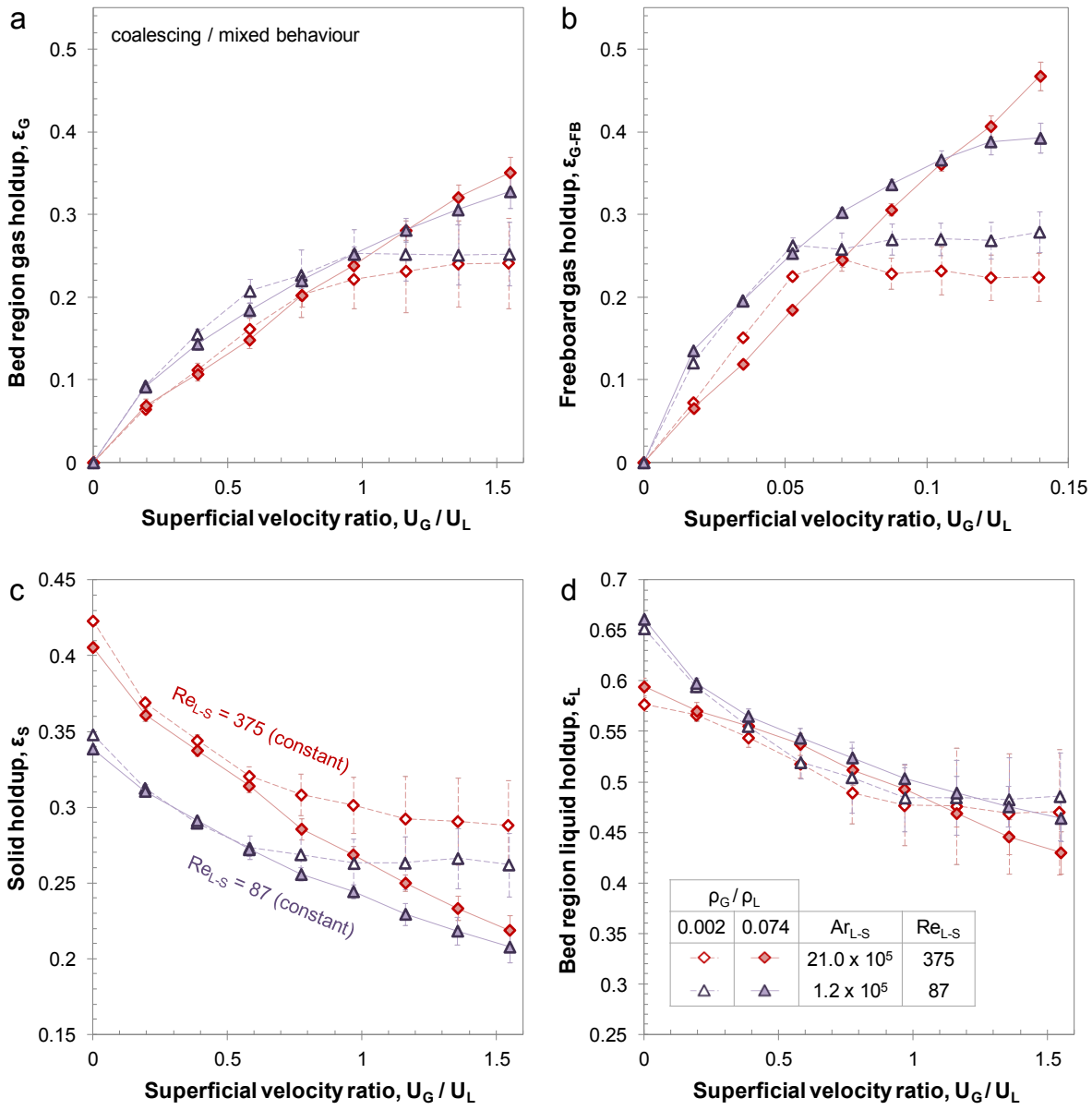

Figure 4.4. Ebullated bed phase holdups for the coalescing (water) and mixed behavior (0.8 wt.% aqueous CMC) systems at varying gas flow rates and liquid viscosity.

Bed region gas holdups trends indicated operation in the dispersed bubble flow regime for the 0.5 wt.% aqueous ethanol (e.g., rate of increase of ε_G versus U_G/U_L and relatively low phase holdup standard deviations shown in Figure 4.3a). Figure 4.3 demonstrates that the bed and freeboard gas holdups were not significantly affected by the increased liquid viscosity. McKnight et al. (2003) reported freeboard gas holdups ranging

from approximately 50% to 60% in the industrial hydroprocessor, where similar values were obtained in the coalescence inhibiting system (refer to Figure 4.3b). Measurements yielded a gas fraction of approximately 20 vol.% in the liquid recirculation at the highest gas superficial velocity shown in Figure 4.3. Freeboard gas holdups at the previous conditions increased by approximately 10 vol.% with gas entrainment when comparing equal inlet gas flow rates (i.e., without adjusting for gas entrainment in the liquid recirculation). Gas fractions in the liquid recirculation increased at higher inlet gas flow rates, where a similar trend in the industrial unit has been previously observed (McKnight et al., 2003).

Comparing 0.5 wt.% aqueous ethanol (Figure 4.3d) and water (Figure 4.4d), it is apparent that the high gas holdup conditions resulted in lower overall bed region liquid phase holdup, therefore reducing the liquid residence time. Figure 4.3c demonstrates that increasing the liquid viscosity mainly reduced the solid holdups (i.e., greater bed expansion) due to the relative gain in viscous forces compared to particle inertial (Re_{L-S} reduction) and gravitational (Ar_{L-S} reduction) forces. Experimental liquid-solid fluidized bed results for the studied particles before and after CMC addition gave $Re_{L-S,T} \approx 1400$ (Pjontek and Macchi, 2014) and $Re_{L-S,T} \approx 280$, respectively. The estimated Reynolds number at the terminal free settling velocity ($Re_{L-S,T}$) indicated that increasing the liquid viscosity transitioned the particles from the Newton ($Re_{L-S,T} > 500$, inertial forces dominate) to the intermediate ($0.2 < Re_{L-S,T} < 500$) settling flow regimes, where increased liquid viscosity will have a greater impact.

4.5.2.2. Varying liquid recirculation rate

Figure 4.5 and Figure 4.6 present the ebullated bed and freeboard phase holdups for the 0.5 wt.% aqueous ethanol (coalescence inhibition) and water (coalescing / mixed behaviour) systems, respectively, when varying the liquid recirculation flow rate while the inlet gas flow rate was constant. Increasing the liquid superficial velocity thus reduced the gas-liquid superficial velocity ratio (U_G/U_L) and augmented the particle Reynolds numbers (Re_{L-S}), as illustrated in Figure 4.5c. For the 0.5 wt.% aqueous ethanol prior to CMC

addition, bed region gas holdups decreased at higher liquid superficial velocities (Figure 4.5a), where a reduction of 3.7 vol.% was observed for the studied Re_{L-S} range. CMC addition to the coalescence inhibition system increased the gas-liquid superficial velocity ratio due to gas entrainment (approx. 15 vol.%) in the liquid recirculation (i.e., higher gas and reduced liquid flow rates in the ebullated bed for equivalent inlet gas and fluid recirculation flow rates), subsequently increasing U_G/U_L as well as the bed and freeboard gas holdups. Bed region gas holdups for the coalescing system (Figure 4.6a) increased for higher liquid flow rates at atmospheric pressure (ρ_G/ρ_L = 0.002), likely due to increased bubble break-up in the ebullated bed, while they remained relatively constant at elevated pressure (ρ_G/ρ_L = 0.074). Once more, significant bubble coalescence inhibition (Figure 4.5d) resulted in lower ebullated bed liquid phase holdups when compared to the coalescing system (Figure 4.6d).

When comparing Figure 4.3c and Figure 4.5c, it is apparent that solid holdup trends are dependent on both U_G/U_L and Re_{L-S}. For a constant Re_{L-S} and hence constant liquid superficial velocity (shown in Figure 4.3c), the ebullated bed expanded when increasing U_G/U_L due to the increased volumetric gas fraction. However, the opposite trend was observed when reducing the liquid superficial velocity for a constant gas flow rate (shown in Figure 4.5c), again increasing U_G/U_L, as the lower Re_{L-S} resulted in bed contraction.

The decreasing freeboard gas holdup trends observed with the 0.5 wt.% aqueous ethanol prior to CMC addition were expected when increasing Re_{L-S} (Figure 4.5b) as the rise velocities of the considerably smaller bubbles are more dependent on the superficial liquid velocity. An improved measurement technique for the gas entrainment in the liquid recirculation would be required to confirm the freeboard gas holdup trend observed following CMC addition (Figure 4.5b), where a reduction at higher liquid flow rates was initially expected. For the coalescing and mixed behaviour systems at atmospheric pressure, the observed bed and freeboard gas holdups increase at higher superficial liquid velocities (Figure 4.6a and Figure 4.6b) were likely due to greater shearing on the bubbles when flowing through the distributor plate and ebullated bed, consequently enhancing bubble break-up.

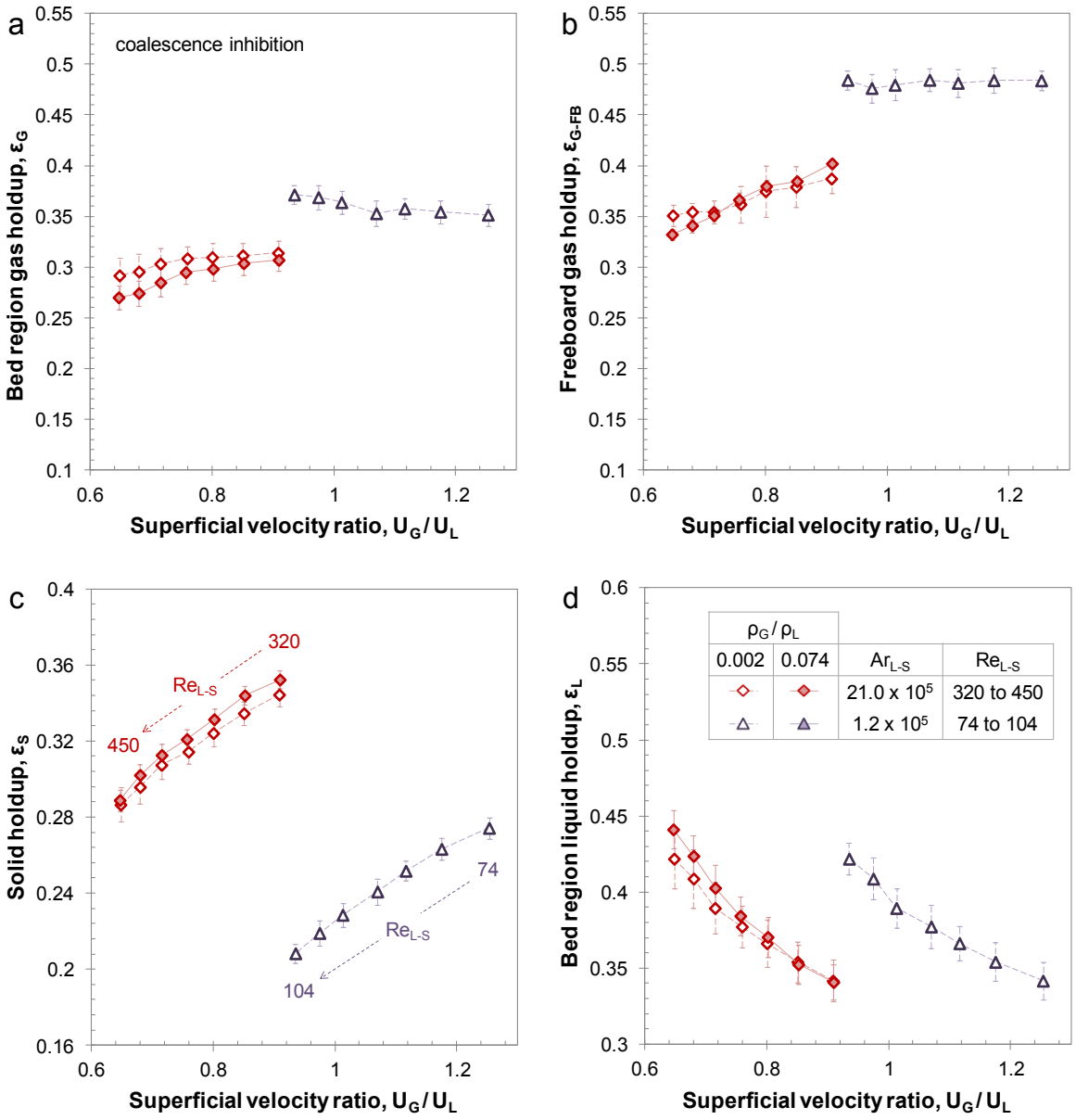

Figure 4.5. Ebullated bed phase holdups for the coalescence inhibition systems at varying liquid flow rates and liquid viscosity.

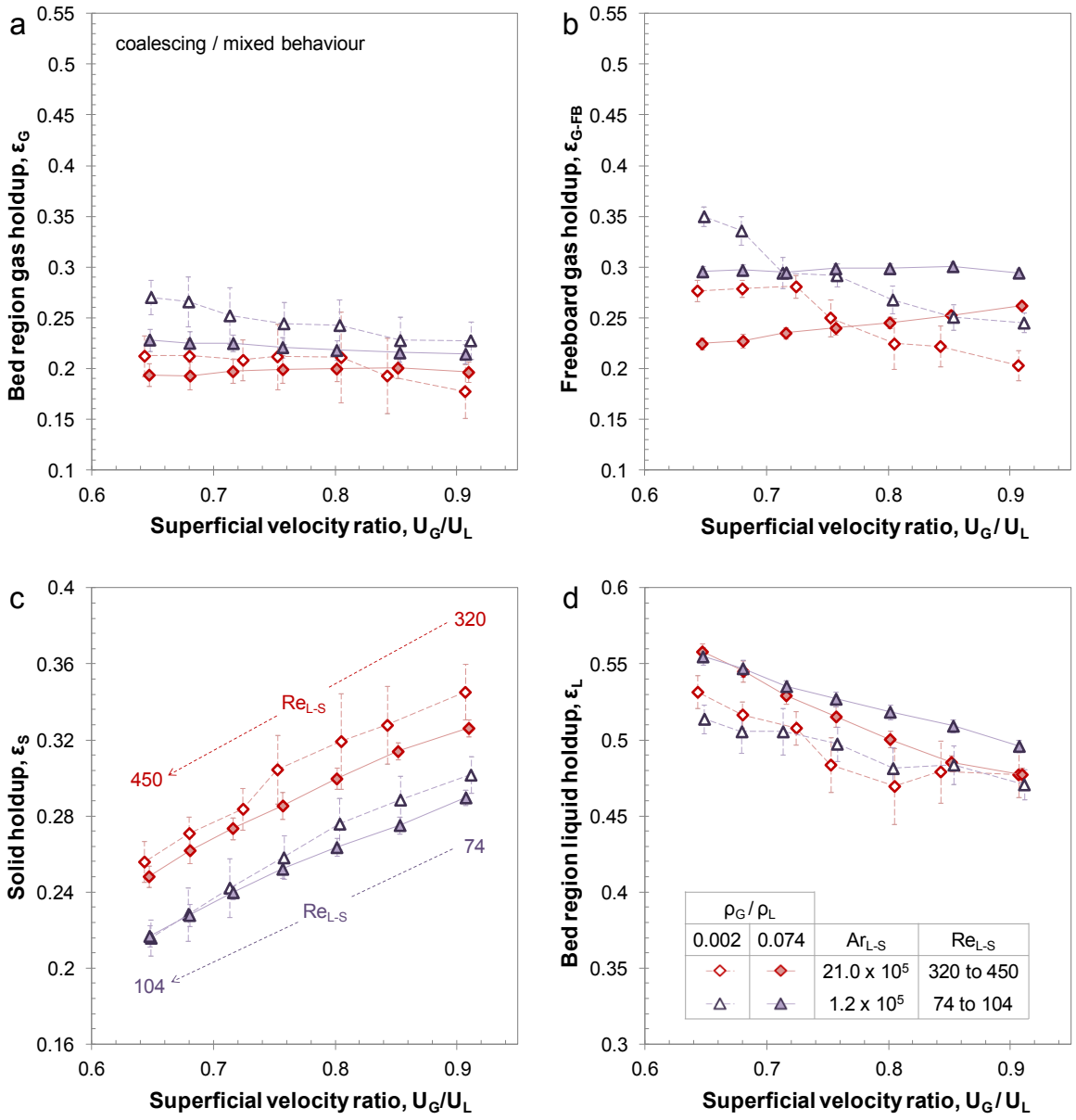

Figure 4.6. Ebullated bed phase holdups for the coalescing (water) and mixed behavior (0.8 wt.% aqueous CMC) systems at varying liquid flow rates and liquid viscosity.

4.5.2.3. Relation between bed and freeboard gas holdups

Gas holdup measurements in the LC-Finer[SM] are limited to the freeboard region as estimates in the bed region are sensitive to changes in the catalyst inventory and density, which are not well known while the unit is operational (McKnight et al., 2003). For the coalescing and coalescence inhibition systems, freeboard gas holdups presented in this study were on average 23% and 28% greater than their associated ebullated bed gas holdups, respectively.

If bubble characteristics were to remain constant between the ebullated bed and freeboard regions, the bed region gas holdups on a solids-free basis should be comparable to the freeboard measurements. Using data from this study as well as from Pjontek and Macchi (2014), Figure 4.7 compares the solids-free gas holdups in the ebullated bed (i.e., $\varepsilon_G/(1-\varepsilon_S)$) to the freeboard gas holdups in water and 0.5 wt.% aqueous ethanol. The AAREs were 61% and 29% for the coalescing and coalescence inhibition systems, respectively. For the coalescing system, the smaller particles ($d_{SV} \approx 1.5$ mm) led to coalesced bubble flow in the ebullated bed due to the particle size and density, where bed contraction at the introduction of gas was observed. Upon exiting the ebullated bed, bubbles have been visually observed to break-up, likely due to the change in apparent viscosity between the bed and freeboard regions. Figure 4.7a demonstrates that the solids-free gas holdups at these conditions underestimated the freeboard gas holdup, in agreement with the bubble break-up when exiting the ebullated bed. The size and density of the larger particles ($d_{SV} \approx 4$ mm) resulted in the dispersed bubble flow regime in water. At these conditions, the solids-free gas holdup overestimated the freeboard gas holdup, suggesting that bubble break-up in the ebullated bed due to particle inertia is non-negligible. Similar results were observed in coalescence inhibition systems (Figure 4.7b), though the solids-free estimate approached the freeboard gas holdups when the fluidized bed was sufficiently dilute at higher gas holdups.

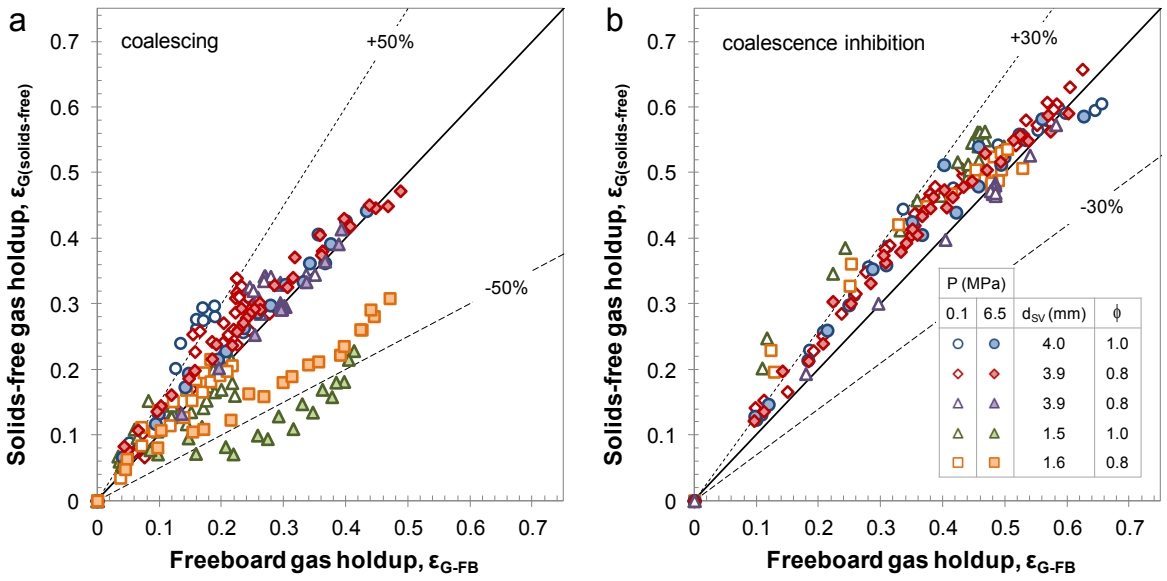

Figure 4.7. Comparison of solids-free and freeboard gas holdups for (a) water and (b) 0.5 wt.% aqueous ethanol. Additional data taken from Pjontek and Macchi (2014).

4.5.3. Phase holdup correlations in the coalescence inhibition systems

Overall phase holdups in the bed and freeboard regions were correlated for high gas holdup conditions in the coalescence inhibition systems. Data from a previous study (Pjontek and Macchi, 2014) was included with the current results, consequently using spherical and cylindrical particles with Sauter mean diameters of approximately 4 mm in 0.5 wt.% aqueous ethanol. The correlations were also based on the following considerations:

- Gas injection into the liquid using a porous pipe prior to both phases passing through the distributor plate and subsequent flow through the ebullated bed contributed to the high gas holdups by enhancing bubble break-up. This combined with the presence of surfactants led to negligible pressure effects on phase holdups in the ebullated bed. The gas-liquid density ratio was thus not included in the correlations.
- Due to the limited range of particle-liquid density ratios studied at high gas holdups, this dimensionless group was not included.
- High gas holdups resulted from the dispersed bubble flow observed at relatively high superficial gas velocities. Similar to the approach of Wilkinson et al. (1992), the provided correlations are specific to the dispersed bubble flow regime.

Table 4.1 provides the ranges for the dimensionless groups used to develop the correlations. Gas holdups in the ebullated bed were correlated using a power-law based on the relevant dimensionless groups. Freeboard gas holdups in a system with significant bubble coalescence inhibition and enhanced bubble break-up should not be affected by the particle properties in the ebullated bed. Experiments at such conditions have shown similar gas holdups between the freeboard region and a bubble column at equal gas and liquid superficial velocities (Pjontek et al., 2014). Freeboard gas holdups were therefore correlated based on the gas-liquid superficial velocity ratio. It should again be noted that the gas and liquid superficial velocities were adjusted to account for gas entrainment in the liquid recirculation (refer to the method described in section 4.5.1.2), thus estimating the actual flow rates in the ebullated bed. The bed (ε_G) and freeboard (ε_{G-FB}) region gas holdups correlations are:

$$\frac{\varepsilon_G}{1-\varepsilon_G} = 0.62\left(U_G/U_L\right)^{0.94} Re_{L-S}^{\ 0.26}\, Ar_{L-S}^{\ -0.12} \tag{4.7a}$$

$$\frac{\varepsilon_{G-FB}}{1-\varepsilon_{G-FB}} = 0.79\left(U_G/U_L\right)^{1.12} \tag{4.7b}$$

Figure 4.8 compares the predicted and experimental gas holdups in the bed and freeboard regions (AARE of 7.0% and 4.7%, AAE of 0.016 and 0.015, respectively). Eq. (4.7a) and (4.7b) thus provided a satisfactory representation of the gas holdups in the bed and freeboard regions at the selected high gas holdup conditions.

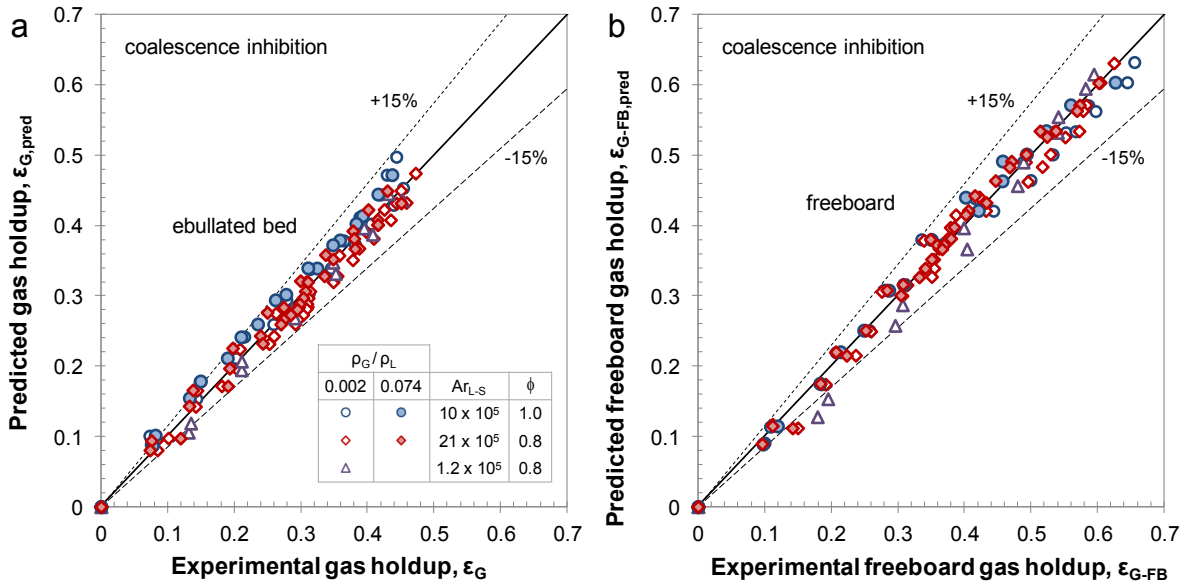

Figure 4.8. Correlated versus experimental gas holdups in the (a) bed and (b) freeboard regions. Additional data taken from Pjontek and Macchi (2014).

The solid holdup was correlated by modifying the well-known Richardson and Zaki (1954) relationship (refer to Eq. (4.6)) to include the suggested dimensionless groups for ebullated bed scaling. The Archimedes number, which is related to the Reynolds number at the terminal settling velocity of a particle, and the particle-liquid Reynolds are accounted for by the Richardson and Zaki expression. Since ρ_S/ρ_L and ρ_G/ρ_L are being excluded based on the prior discussion, the gas-liquid superficial velocity ratio was included as follows:

$$1-\varepsilon_S = \left(\frac{U_L}{k\,U_{LT\infty}}\right)^{\frac{1}{n}}\left(1+0.22\left(\frac{U_G}{U_L}\right)^{0.92}\right) \tag{4.8}$$

Coefficients for the U_G/U_L dimensionless group were determined using the experimentally determined terminal settling velocities ($U_{LT} = k\,U_{LT\infty}$) and n index from the liquid-solid fluidized beds. Empirical correlations for U_{LT} and n were nonetheless compared to the experimentally determined values (refer to Table 4.2) to investigate the robustness of Eq. (4.8). The n index for spheres and cylinders was calculated using (Khan and Richardson, 1989):

$$\frac{4.8-n}{n-2.4} = 0.043 Ar_{L-S}^{0.57}\left[1-1.24\left(d_V/d_C\right)^{0.27}\right] \tag{4.9}$$

Wall effects were estimated based on the relation provided by Khan and Richardson (1989) for spheres and the correlation proposed by Chhabra (1995) for cylinders when $L_P/d_P < 10$:

$$\text{spheres: } k = 1-1.15\left(d_V/d_C\right)^{0.6} \tag{4.10}$$

$$\text{cylinders: } k = 1-1.33\, d_V/d_C \tag{4.11}$$

The free settling velocity of spherical particles was estimated using the correlation of Turton and Clark (1987), shown to provide adequate predictions (Brown and Lawler, 2003). The cylindrical terminal free settling velocity was estimated using the Haider and Levenspiel (1989) empirical correlation for isometric non-spherical particles.

$$\text{spheres: } U_{LT\infty} = \frac{\mu_L}{d_V\ \rho_L} Ar_L^{1/3}\left[\left(\frac{18}{Ar_{L-S}^{2/3}}\right)^{0.824} + \left(\frac{0.321}{Ar_{L-S}^{1/3}}\right)^{0.412}\right]^{-1.214} \tag{4.12}$$

$$\text{cylinders: } U_{LT\infty} = \frac{\mu_L}{d_V\ \rho_L} Ar_{L-S}^{1/3}\left(\frac{18}{Ar_{L-S}^{2/3}} + \frac{2.335-1.744\phi}{Ar_{L-S}^{1/6}}\right)^{-1} \tag{4.13}$$

Table 4.2. Particle settling parameters determined experimentally and using correlations.

	Parameter	spheres	cylinders (μ_L = 0.001 Pa s)	cylinders (μ_L = 0.004 Pa s)
Experimental	n	2.39	2.45	2.64
	U_{LT} (m/s)	0.33	0.34	0.28
Correlations	n	2.44	2.43	2.55
	k	0.83	0.94	0.94
	$U_{LT\infty}$ (m/s)	0.40	0.31	0.29

Figure 4.9 compares the predicted and experimental solids holdups using both the experimental and correlated particle settling parameters (AARE of 2.0% and 9.7%, AAE of 0.006 and 0.031, respectively). The experimentally determined settling parameters (Figure 4.9a) provided an adequate fit for the solid holdups while the correlated parameters (Figure 4.9b) resulted in a deviation for the aluminum cylinders at a liquid viscosity of 0.001 Pa s. Table 4.2 demonstrates that the predicted free settling velocity for the previous conditions underestimated the experimentally determined value, in agreement with the observed solid holdup deviation (shown in Figure 4.9b). It is consequently recommended to use experimentally determined liquid-solid fluidized bed settling parameters when possible. The proposed correlations thus appeared to adequately represent the bed and freeboard gas holdups as well as solid holdups for a system operating at high gas holdups and that satisfies the discussed reactor geometric and bubble coalescence characteristics.

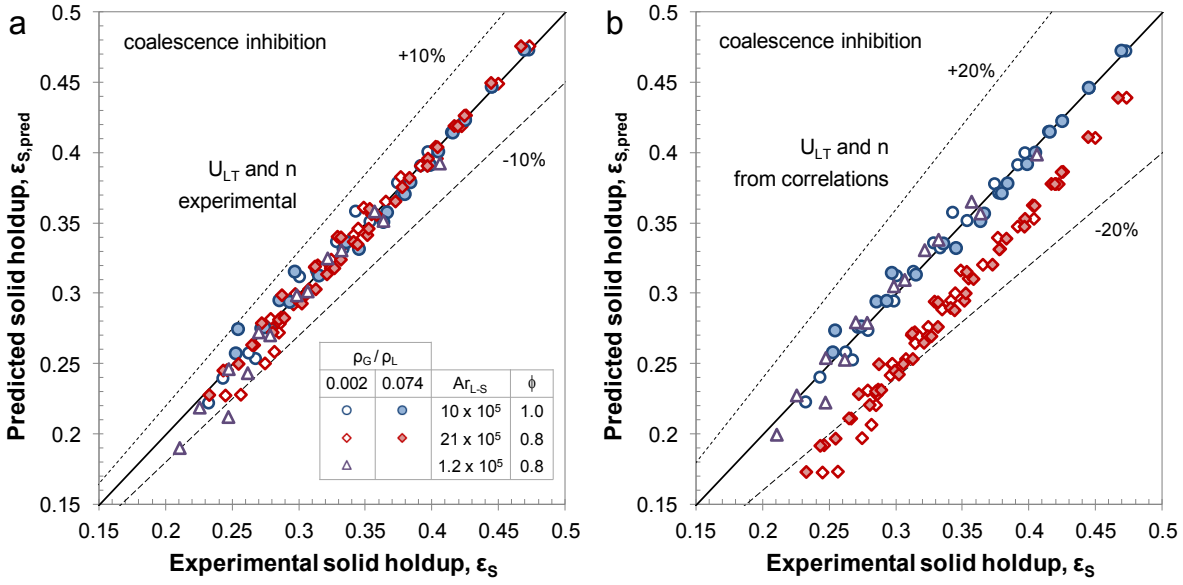

Figure 4.9. Correlated versus experimental solid holdups based on particle settling parameters determined (a) experimentally and (b) from literature correlations. Additional data taken from Pjontek and Macchi (2014).

4.6. Conclusions

Dynamic similitude was assumed when matching five dimensionless groups, at equal bubble coalescence behaviour based on a binary consideration (e.g., coalescing or coalescence inhibition), and relaxing important geometric considerations (e.g., gas injection method and gas-liquid distribution) for systems at high gas holdups. This approach was tested by comparing the overall phase holdups for separate cylindrical particles (d_{SV} of 1.6 and 3.9 mm) at matching dimensionless groups, where results were comparable when bubble coalescence was consistently and sufficiently inhibited. Unfortunately, the comparison could not be carried out in a coalescing system as CMC addition to water resulted in some surface-active characteristics that affected the overall phase holdups, particularly at low gas velocities.

The combined effects of enhanced bubble break-up (i.e., gas injection, gas-liquid distribution method, and/or elevated pressure) and significant bubble coalescence inhibition (i.e., surfactant addition) were required to achieve the desired high gas holdup conditions. The effects of increased liquid viscosity, varying superficial gas velocity and varying superficial liquid velocity were therefore studied at relevant fluid dynamic conditions for industrial hydroprocessors. When increasing the liquid viscosity in the 0.5 wt.% aqueous ethanol, a fraction of the gas was entrained in the liquid recirculation due to inadequate foam dissipation at the free-surface. Gas entrainment up to approximately 20 vol.% at the highest studied gas flow rates resulted in similar gas holdups when compared to industrial measurements.

For the coalescing and coalescence inhibition systems, freeboard gas holdups were on average 23% and 28% greater than bed region gas holdups, respectively. When attempting to estimate the freeboard gas holdup based on a solids-free basis in the ebullated bed in the water and 0.5 wt.% aqueous ethanol systems, the AAREs were 61% and 29%, respectively. Developed bed and freeboard gas holdup correlations provided an adequate fit at the high gas holdup conditions (AARE of 8.9% and 5.4%, respectively). Solids holdups were correlated based on a modified Richardson and Zaki (1954) expression which also provided an acceptable fit (AARE of 2.0%), particularly when the particle terminal settling velocity and n index were determined from experimental liquid-solid fluidized bed results.

Acknowledgments

The authors are grateful to Dr. Jules Thibault for allowing the use of the Anton Paar Physica MCR 301 Rheometer. The authors would like to acknowledge the Natural Sciences and Engineering Research Council of Canada, the Canadian Foundation for Innovation, the Ontario Innovation Trust and Syncrude Canada Ltd. for financial support.

Nomenclature

AARE	average absolute relative error
Ar_{L-S}	particle-liquid Archimedes number, $Ar_{L-S} = \rho_L d_V^3 (\rho_S - \rho_L) g / \mu_L^2$
CMC	carboxymethyl cellulose
d_C	column inner diameter (m)
d_P	particle diameter (m)
d_{SV}	Sauter mean diameter (m)
d_V	volume equivalent diameter (m)
Eo	Eötvös number, $Eo = g(\rho_L - \rho_G) d_P^2 / \gamma_{G-L}$
g	gravitational acceleration (m/s^2)
h_B	fluidized bed height (m)
h_C	column height (m)
k	wall effect for bed expansion correlation
L_P	particle length (m)
m	mass of the particles (kg)
M	M-group, $M = g(\rho_L - \rho_G) \mu_L^4 / \rho_L^2 \gamma_{G-L}^3$
n	index for bed expansion correlation
P	pressure (Pa)
$-\Delta P$	dynamic pressure drop (Pa)
Re_{L-S}	particle-liquid Reynolds number, $Re_{L-S} = U_L \rho_L d_{SV} / \mu_L$
$Re_{L-S,T}$	particle-liquid Reynolds number based on terminal free settling velocity and accounting for wall effects, $Re_{L-S,T} = U_{LT} \rho_L d_{SV} / \mu_L$
T	temperature (°C)

U_G , U_L	gas and liquid superficial velocities (m/s)
U_{LT}	terminal settling velocity of a particle, accounting for wall effects (m/s)
$U_{LT\infty}$	terminal free settling velocity of a particle (m/s)
v_B	bubble rise velocity (m/s)
Δz	vertical distance between differential pressure taps (m)

Greek symbols

γ_{G-L}	gas-liquid surface tension (N/m)
ε_G , ε_L , ε_S	gas, liquid and solid holdups in the bed region
ε_{G-FB}	freeboard gas holdup
μ_G , μ_L	gas and liquid dynamic viscosity (Pa s)
ρ_G , ρ_L , ρ_S	gas, liquid and solid densities (kg/m^3)
ϕ	sphericity

Subscripts

FB	freeboard
G	gas
L	liquid
P	particle
S	solid

Chapter 5

Effect of a dispersed immiscible liquid phase on the hydrodynamics of a bubble column and ebullated bed

Dominic Pjontek[a], Jérôme Landry[a], Craig A. McKnight[b], Larry P. Hackman[b], Arturo Macchi[a]

[a]*Chemical and Biological Engineering Department, University of Ottawa, 161 Louis Pasteur, Ottawa, Ontario, Canada, K1N 6N5*

[b]*Syncrude Canada Ltd.,9421-17 Avenue, Edmonton, Alberta, Canada, T6N 1H4*

Abstract

Secondary undesired reactions in ebullated bed resid hydroprocessors can generate an additional dispersed liquid phase, referred as mesophase, which is denser and more viscous than the continuous liquid phase and affects the operation and transport phenomena of the fluidized bed. This study investigates the effect of a dispersed immiscible liquid phase on the overall phase holdups, bubble properties, and fluidization behaviour in a bubble column and ebullated bed. The experimental system consisted of biodiesel as the continuous liquid phase, glycerol as the dispersed liquid phase, 1.3 mm diameter glass beads, and nitrogen. The addition of dispersed glycerol reduced the gas holdups in the bubble column for the studied gas and liquid superficial velocities. Dynamic gas disengagement profiles reveal a rise in the large bubble population and reductions to the small and micro bubble holdups when increasing the glycerol concentration. Liquid-liquid-solid bed expansions at various liquid flow rates confirm particle agglomeration in the presence of a more viscous dispersed liquid phase. Overall phase holdups in a gas-liquid-liquid-solid ebullated bed were obtained while varying the gas and liquid flow rates as well as the glycerol concentration. A coalesced bubble flow regime was observed in the bed region without glycerol whereas the addition of glycerol resulted in the dispersed bubble flow regime due to particle clustering and a greater apparent particle size. The resulting bubble flow regime increased the bed and freeboard region gas holdups due to enhanced bubble break-up. Observations of the fluidized bed behaviour following the addition of the dispersed glycerol are also discussed.

***This manuscript has been published**: D. Pjontek, L.P. Hackman, J. Landry, C.A. McKnight, A. Macchi, 2011. Effect of a dispersed immiscible liquid phase on the hydrodynamics of a bubble column and ebullated bed, Chem. Eng. Sci. 66, 2224–2231.

5.1. Introduction

Hydroprocessing a heavy feedstock can generate mesophase, a dispersed immiscible liquid phase, as occasionally observed in industrial ebullated beds such as the LC-Finer^{SM} operated by Syncrude Canada Ltd. Mesophase is formed due to undesired secondary reactions and can be characterized as polar, denser and more viscous compared to the continuous liquid phase (Srinivasan and McKnight, 1994). This additional liquid phase is believed to affect the operation and transport phenomena of the fluidized bed reactor (McKnight et al., 2003).

Ebullated beds and slurry bubble columns are gas-liquid-solid fluidized bed configurations commonly used in residue hydroprocessing. In an ebullated bed, the liquid and gas flow co-currently through a bed of particles, where the particle diameter is in the millimeter range. Due to the particle size, fluidization is achieved mostly by the liquid flow. In a slurry bubble column, the gas flows through a liquid containing particles in the 100 μm range, where the superficial liquid velocity is lower than the gas. Because of the smaller particle size, fluidization occurs due to local liquid flow primarily induced by the faster rising bubbles.

Bubble columns and gas-liquid-solid fluidized beds have been the subject of numerous studies. Nonetheless, gas-liquid-liquid and gas-liquid-liquid-solid systems have not yet been thoroughly investigated. The few gas-liquid-liquid bubble column studies have generally focused on interphase mass transfer (Kaur et al., 2007) due to the additional phase's potential to increase the gas absorption rate. The production of tertiary carboxylic acids using the Koch synthesis is an example of a gas-liquid-liquid system in which mass transfer parameters are crucial (Brilman et al., 1999) as the reactants consists of carbon monoxide, alkenes and water in the gas, organic liquid and aqueous liquid phases, respectively. Hydrodynamic studies on liquid-liquid-solid fluidized beds have examined the dispersed liquid drop properties, pressure fluctuations, interphase mass transfer coefficients and overall phase holdups (Chiu et al., 1987; Dakshinamurty et al., 1979; Kyu and Kwang, 1986; Rao and Setty, 2000; Roszak and Gawroński, 1979; Song et al., 2005).

Previously studied gas-liquid-liquid-solid systems consisted of slurry bubble columns where the solids used were in the order of 100 microns in diameter (Argüelles et al., 1993;

Siquier et al., 1991). These experiments explored the effect of the second immiscible liquid phase on solids and gas axial holdup profiles using kerosene and water as the continuous and dispersed liquid phases, respectively.

A recent review on the role of a dispersed liquid phase in gas-liquid reactions concluded the need for additional research due to the complexities in the hydrodynamic and mass transfer behaviour associated with two immiscible liquid phases (Kaur et al., 2007). A better understanding of bubble columns and ebullated beds containing a dispersed immiscible liquid phase would thus benefit the optimization and control of ebullated bed hydroprocessors. This study therefore investigates the hydrodynamic behaviour of gas-liquid-liquid, liquid-liquid-solid and gas-liquid-liquid-solid systems with an organic continuous liquid phase and a denser and more viscous polar dispersed liquid phase.

5.2. Material and methods

5.2.1. Phases selection

Biodiesel and glycerol were respectively selected as the continuous and dispersed liquid phases, where the glycerol concentration was varied from 0 to 15 wt.%. The physical properties at 20°C for biodiesel are: $\rho_{L,C}$ = 880 kg/m^3, $\mu_{L,C}$ = 0.0056 Pa·s, σ_{G-L} = 30.6 mN/m; and for glycerol: $\rho_{L,D}$ = 1250 kg/m^3, $\mu_{L,D}$ = 1.5 Pa·s, σ_{G-L} = 62.4 mN/m. The gas-liquid surface tensions were measured with a K12 Krüss Tensiometer by averaging the values obtained using the Ring and Plate methods. The liquid-liquid interfacial tension for the biodiesel-glycerol mixture was measured as σ_{L-L} = 50.7 mN/m using the Plate method.

The choice of experimental liquids was based on the characteristics of liquids likely encountered during mesophase formation in a resid hydroprocessor such as the LC-Finer^{SM}. Asphaltenes molecules are believed to be at the root of the mesophase formation reaction (Srinivasan and McKnight, 1994). The physical properties of asphaltenes were compared with those of the reacting liquid mixture to obtain approximate viscosity, density and surface tension ratios. Biodiesel was selected as it is an organic liquid with foaming tendencies as well as an appropriate viscosity and lower density. Glycerol was chosen to simulate the denser and more viscous polar mesophase. Both liquids were also selected based on health

and safety concerns. An additional advantage of biodiesel is its color which makes it possible to differentiate from the glycerol in the acrylic column, facilitating visual observations.

Density and viscosity estimates of the studied biodiesel-glycerol emulsions are provided in Table 5.1. The emulsion densities were required for the phase holdup calculations and were determined using the following relation:

$$\rho_{L,E} = \left(1 - \varepsilon_{L,D}/\varepsilon_{L,E}\right)\rho_{L,C} + \left(\varepsilon_{L,D}/\varepsilon_{L,E}\right)\rho_{L,D} \tag{5.1}$$

Table 5.1. Estimated emulsion densities and viscosities using Equations 1 and 2.

Dispersed phase mass fraction	Dispersed phase volume fraction	$\rho_{L,E}$ (kg/m^3)	$\mu_{L,E}$ (Pa·s)
0.00	0.000	880	0.0055
0.03	0.021	888	0.0061
0.08	0.058	901	0.0073
0.15	0.111	921	0.0092

The emulsion viscosity was estimated using the cell-model approach developed by Yaron and Gal-Or (1972), which is valid for moderately concentrated Newtonian emulsions at low capillary numbers. These conditions were met as the highest volumetric fraction of the dispersed glycerol was $\varepsilon_{L,D}/\varepsilon_L = 0.11$ and the droplets were visually observed to be considerably small due to sufficient liquid shearing when passing through the centrifugal pump. This estimation was selected as it has been experimentally shown to reasonably predict the viscosity of Newtonian emulsions without requiring adjustable parameters (Pal, 2000; Yaron and Gal-Or, 1972). The model is provided below:

$$\frac{\mu_{L,E}}{\mu_{L,C}} = 1 + \frac{5.5\lambda^3\left[4\lambda^7 + 10 - (84/11)\lambda^2 + (4/\kappa)\left(1-\lambda^7\right)\right]}{10\left(1-\lambda^{10}\right) - 25\lambda^3\left(1-\lambda^4\right) + (10/\kappa)\left(1-\lambda^3\right)\left(1-\lambda^7\right)} \tag{5.2a}$$

$$\lambda = \sqrt[3]{\varepsilon_{L,D}/\varepsilon_L} \tag{5.2b}$$

$$\kappa = \frac{\mu_{L,D}}{\mu_{L,C}} \tag{5.2c}$$

The solid phase consisted of uniformly sized glass beads with a mean diameter of 1.3 mm and a density of 2500 kg/m^3. The particle size was selected to approach the surface-to-volume ratio of the cylindrical particles used in the LC-Finer^{SM}. Nitrogen was used as the gas phase to reduce the potential for biodiesel vapours combustion.

5.2.2. Experimental setup

Experiments were performed at atmospheric conditions in an acrylic column with a height of 2.75 m and an inner diameter of 0.152 m, sufficiently large to minimize wall effects on phase holdups (Wilkinson et al., 1992). The gas and liquid were introduced into the bed separately, but at the same level. This facilitates uniform spatial distribution of the fluids. The liquid distributor was a perforated plate with 80 holes of 4.0 mm diameter, while the gas was introduced via 26 holes of 0.8 mm diameter. At the top of the column, an overflow tank separated the gas from the liquid stream. The exiting gas was directed to an exhaust system to remove entrained biodiesel droplets whereas the liquid was directed to a storage tank and then recycled to the column. Rotameters monitor the liquid and gas flow rates. All data were obtained for superficial gas and liquid velocity ranges of 0 to 0.25 m/s and 0 to 27 mm/s, respectively. The fluidized bed aspect ratio (h_B/d_C) was always greater than 5. Pressure taps are mounted along the height of the column at 0.1016 m intervals and are connected to a differential pressure transducer; model PX750-DI from Omega.

When dealing with a mixture of two immiscible liquids, the homogeneity of the mixture is vital to have an approximately equal distribution of the dispersed phase throughout the column. The LC-Finer^{SM} would produce a pseudo-homogeneous liquid mixture due to the liquid recycle ratio, sufficient liquid shearing from the recycle pump and flow through the grid. Manual mixing was thus applied to the liquid storage tank during the experiments to ensure that no glycerol settled below the liquid outlet. The liquid residence time in the overflow tank was insufficient for liquid-liquid separation. Since the centrifugal

pump applies significant shearing to the liquids, the emulsion entering the column consisted of evenly dispersed glycerol in the continuous biodiesel.

5.2.3. Measurement techniques

5.2.3.1. Phase holdups

Overall phase holdups were determined by measuring the dynamic pressure drop along the column at several heights. The bed height and resulting solid holdup were determined from the intersection of the bed and freeboard pressure drop lines, each obtained by linear regression. Visual observations of the bed height were also recorded to corroborate the bed height obtained by the pressure drop method. The bed heights obtained by linear regression were within ± 6% of the visual observed heights, where the greater differences were observed at higher glycerol concentrations. Knowing the bed height, the averaged solid holdup in the bed is calculated from a mass balance on the particles:

$$\varepsilon_S = \frac{4\,m}{\pi\, d_C^{\,2}\, h_B\, \rho_S} \tag{5.3}$$

Neglecting the frictional drag on the wall and accelerations of the phases in the vertical direction, the gas holdup can be related to the dynamic pressure drop. In order to account for the dispersed immiscible liquid phase in the column, the pressure tap lines were only filled with biodiesel, allowing the gas holdup in the bed region to be determined from the following:

$$\varepsilon_G = \frac{\dfrac{\Delta P}{g\Delta z} + (\rho_S - \rho_{L,E})\,\varepsilon_S + \rho_{L,E} - \rho_{L,C}}{(\rho_{L,E} - \rho_G)} \tag{5.4}$$

The liquid holdup can then be obtained knowing that the sum of phase holdups must give unity. Duplicate runs were completed in the bubble column and the relative differences in the gas holdups were within ± 3%.

5.2.3.2. Dynamic gas disengagement technique

The gas phase structure in a bubble column can be studied using the dynamic gas disengagement (DGD) technique. The gas holdup is monitored after the gas flow rate is abruptly stopped. For the dispersed bubble flow regime, the gas holdup decreases linearly with time due to the uniform bubble size distribution. In the coalesced bubble flow regime however, there is a wider bubble size distribution resulting in a more complex DGD profile. In such case, bubbles are generally lumped into separate classes. Immediately after the gas is stopped, larger bubbles escape the column rapidly followed by a slower disengagement rate for the smaller dispersed bubbles. As biodiesel is a foaming liquid, an additional class of micro bubbles is defined and these are the last to completely disengage from the column. An example of a DGD profile for the studied system is presented in Figure 5.1.

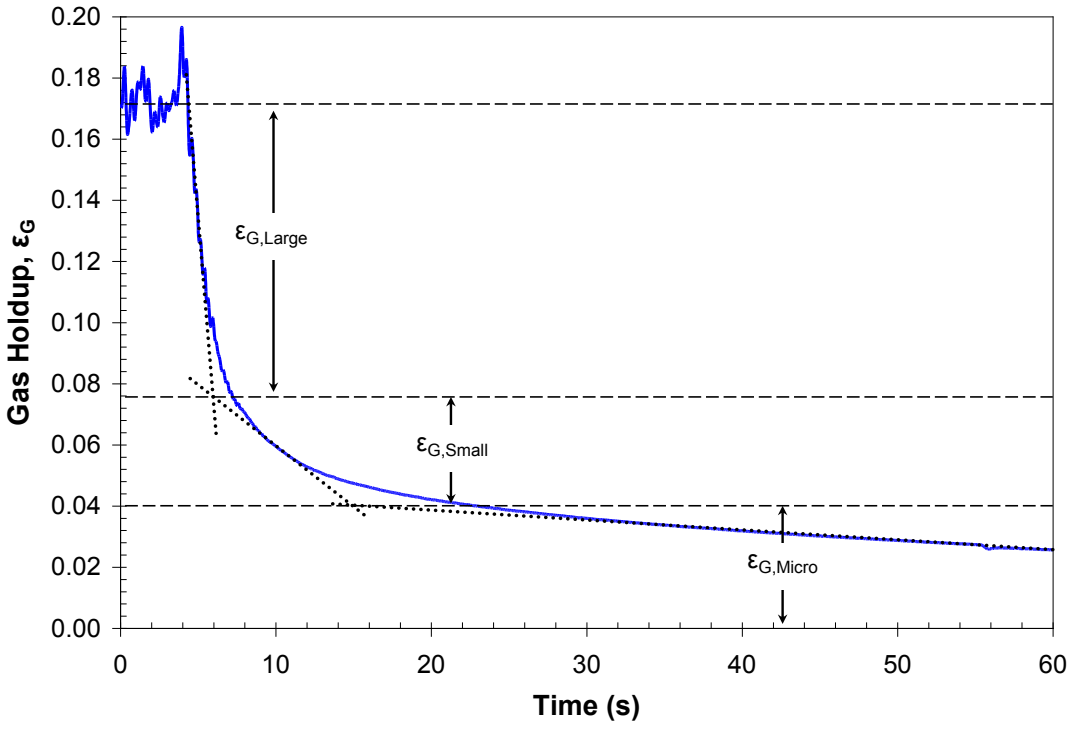

Figure 5.1. Dynamic gas disengagement profile for an 8 wt.% glycerol bubble column at U_G = 0.122 m/s.

For this study, it is assumed that the disengagement rate of each bubble class is sequential, the gas holdups are independent of axial position when gas flow is stopped, and there is no bubble coalescence or break up during gas disengagement (Camarasa et al., 1999; Jordan et al., 2003; Lee et al., 1999). These assumptions simplify the analysis of the DGD data as its purpose here is to analyze relative trends rather than accurate numerical values.

5.3. Results and discussion

5.3.1. Bubble column

The bubble column experiments investigated the effect of dispersed glycerol on the gas holdups. The dynamic gas disengagement technique was used to investigate the large, small and micro bubble holdups with no liquid flow at varying glycerol concentrations.

5.3.1.1. Gas phase holdups

Figure 5.2 compares the gas holdups obtained for the pure biodiesel bubble column with the highest studied glycerol concentration. Gas holdups in both the dispersed and coalesced bubble flow regime were reduced in the presence of dispersed glycerol, where the drop is greater at higher gas flow rates. Kundu et al. (2003) also observed decreased gas holdups in a bubble column with various organic liquid phases dispersed in water. Higher liquid velocities resulted in lower gas holdups with no glycerol present due to increased bubble rise velocities. At the highest studied glycerol concentration however, the liquid velocity had no observable effect on the gas holdups. Changes in the liquid flow rate had a greater impact on the small and micro bubble rise velocities, and the addition of dispersed glycerol reduced these bubble classes, as discussed in section 5.3.1.2.

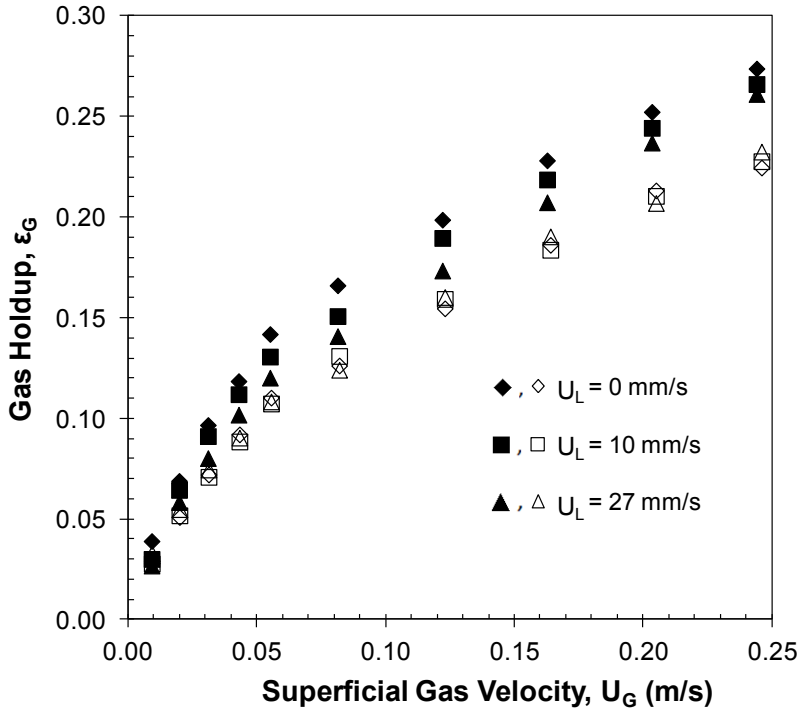

Figure 5.2. Gas holdup in a bubble column as a function of gas and liquid superficial velocities with pure biodiesel (filled-in symbols) and 15 wt.% glycerol (open symbols).

Figures 5.3a and b show decreased gas holdups following the addition of dispersed glycerol for all superficial gas velocities. Experiments by Arguelles et al. (1993) obtained comparable results using kerosene and water as the continuous and dispersed liquid phases, respectively. The higher apparent liquid viscosity of the biodiesel-glycerol emulsion is believed to have enhanced bubble coalescence. Increasing the liquid viscosity has been previously observed to reduce the gas holdup in a bubble column (Schäfer et al., 2002; Urseanu et al., 2003) due to a larger mean bubble size (O'Connor et al., 1990). Gas holdups in the dispersed bubble flow regime were less impacted by the glycerol at the highest liquid flow rate, as shown in Figure 5.3c. The gas holdup reductions in the coalesced bubble flow regime at a superficial liquid velocity of 22 mm/s are similar for all studied glycerol concentrations.

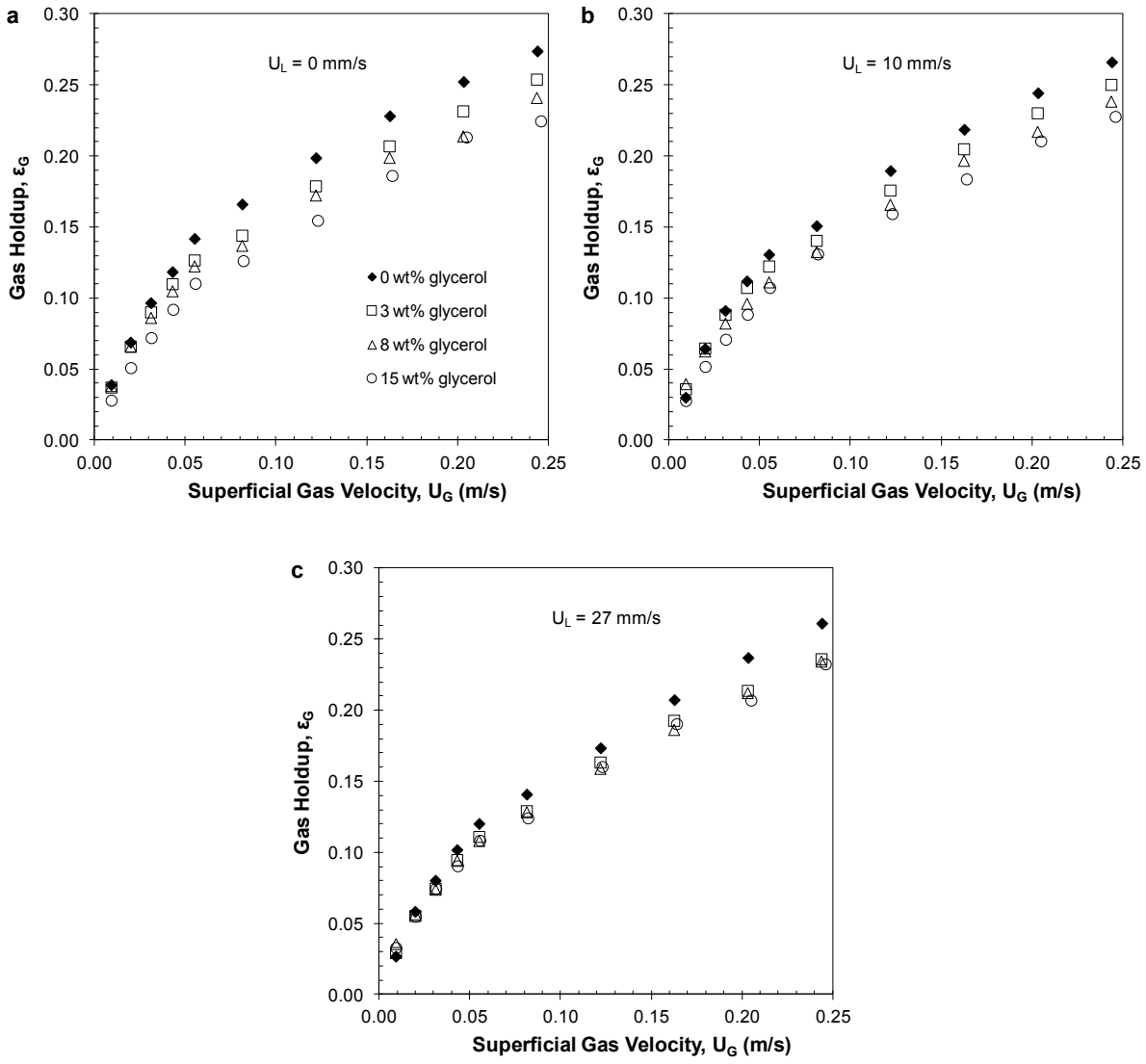

Figure 5.3. Gas holdup as a function of superficial gas velocity and glycerol concentrations at (a) U_L = 0 mm/s, (b) U_L = 10 mm/s, and (c) U_L = 27 mm/s.

5.3.1.2. Large, small and micro bubble holdups

Figure 5.4 presents the large, small and micro bubble holdups as a function of gas superficial velocity and glycerol concentration. The small and micro bubble holdups increased linearly in the dispersed flow regime. Beyond the dispersed-to-coalesced flow transition velocity of approximately 50 mm/s, the small bubble holdups dropped and then remained constant, as observed in Figure 5.4b. In the coalesced bubble flow regime, increases to the gas flow rate mainly resulted in the formation of large bubbles, where the

large bubble holdups increased linearly as a function of the superficial gas velocity. Similar observations regarding the small and large bubble holdups in the dispersed and coalesced bubble flow regimes were obtained by Macchi (2002). The micro bubble holdups rate of increase was reduced in the coalesced regime due to smaller residence times from the larger bubble wakes.

The large bubble holdups, presented in Figure 5.4a, increased following the addition of glycerol for all studied gas flow rates, where the increase was independent of the quantity of glycerol added. Figure 5.4b shows a reduction of the small bubble holdups as a function of the glycerol added to the bubble column, particularly in the coalesced bubble flow regime. In dispersed bubble flow, the micro bubble holdups presented in Figure 5.4c were less affected by the addition of glycerol. The previous trends agree with the belief that the increased apparent viscosity of the biodiesel-glycerol emulsion enhanced the bubble coalescence in a bubble column. The effect of the glycerol became more apparent in the coalesced flow regime where the micro bubble holdups decreased based on the amount glycerol added. The transition from the dispersed to the coalesced bubble flow regime occurred at similar superficial gas velocities regardless of the quantity of glycerol added to the column.

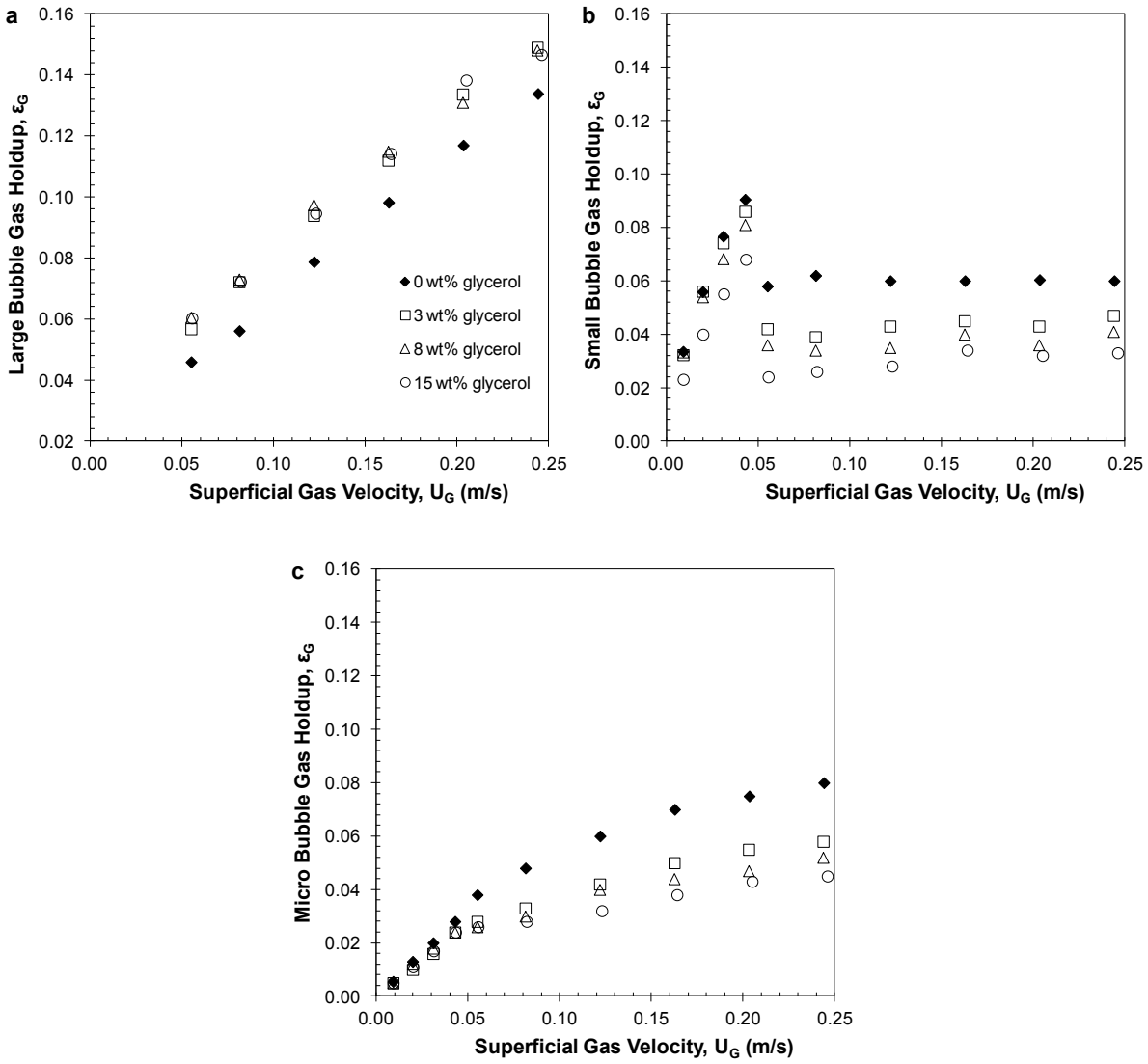

Figure 5.4. Gas holdup for (a) large, (b) small and (c) micro bubbles in a bubble column with no liquid flow as a function of the gas superficial velocity and glycerol concentration.

5.3.2. Fluidized bed

The bed expansion of the liquid-liquid-solid fluidized bed was studied to characterize particle agglomeration in the presence of glycerol. The ebullated bed experiments examined the overall phase holdups at varying glycerol concentrations. Observations of the fluidization behaviour and operational issues at high glycerol concentrations are discussed.

5.3.2.1. Liquid-liquid-solid phase holdups

The solid holdups as a function of liquid velocity and glycerol concentration for the liquid-liquid-solid fluidized beds are presented in Figure 5.5. The solid holdup increased as glycerol was added to the column, which is equivalent to a reduction in the bed height for a given quantity of particles. Based on Eq. (5.2), the biodiesel-glycerol emulsion has a higher liquid viscosity compared to pure biodiesel. Neglecting particle interaction due to the dispersed liquid phase, the fluidized bed should expand with a more viscous liquid at the same operating conditions. The observed opposite trend indicates an increased apparent particle size due to agglomeration. Experiments by Siquier et al. (1991) have reported the formation of particle agglomerates in a kerosene-water slurry bubble column with 110 micron particles. The agglomerate sizes in the previous study were observed to reach up to 5 mm in diameter where the larger particles could be found at the bottom of the column.

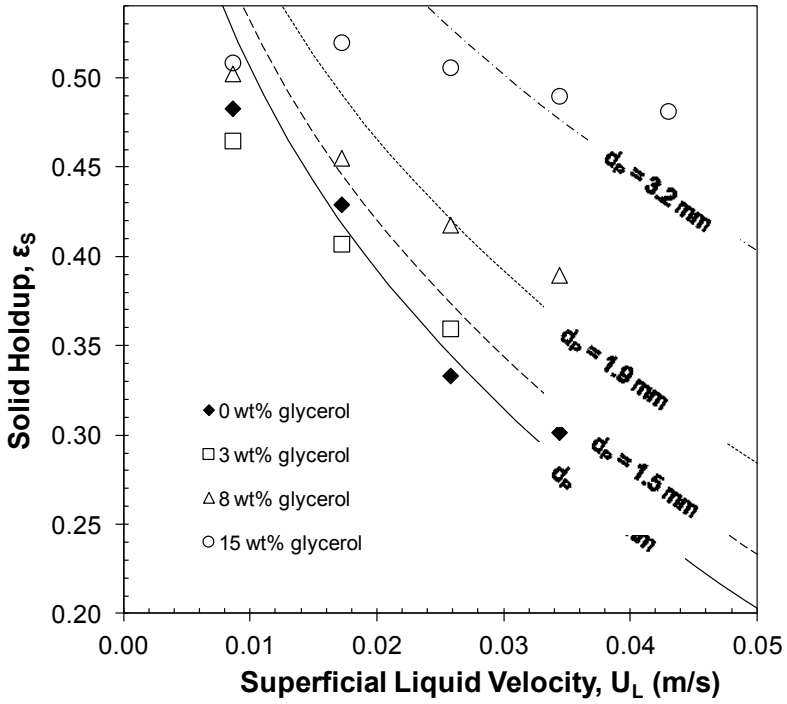

Figure 5.5. Solid holdup as a function of liquid superficial velocity for a biodiesel-glycerol-1.3 mm glass beads fluidized bed at varying glycerol concentrations. Predicted holdups were determined using correlations provided in Khan and Richardson (1989).

Liquid-solid bed expansion correlations (Khan and Richardson, 1989) were used to estimate the agglomerate sizes at various glycerol concentrations. The solid holdup can be related to the superficial liquid velocity and the particle terminal velocity in the column using the following correlation:

$$1-\varepsilon_S=\left(\frac{U_L}{U_{Lt}}\right)^{\frac{1}{n}} \tag{5.5}$$

The index n and the particle terminal velocity in the column can be approximated using the following correlations (Khan and Richardson, 1989):

$$\frac{4.8-n}{n-2.4}=0.043Ar_L^{\,0.57}\left[1-1.24\left(d_P/d_C\right)^{0.27}\right] \tag{5.6}$$

$$U_{Lt\infty}=\frac{\mu_L}{\rho_L d_p}\left(2.33Ar_L^{\,0.018}-1.53Ar_L^{\,-0.016}\right)^{13.3} \tag{5.7a}$$

$$U_{Lt}=U_{Lt\infty}\left[1-1.15\left(d_P/d_C\right)^{0.6}\right] \tag{5.7b}$$

The predicted solid holdups for the pure biodiesel fluidized bed are within ± 8% of the experimental values, where the predictions improve at higher liquid velocities. When glycerol is added to the column, the predictions do not match the experimental values using a particle diameter of 1.3 mm. To improve the fit, larger particles should be assumed based on visual observations. Figure 5.5 shows the required increases in particle size for the studied glycerol concentrations. The particle diameter was adjusted to fit at the higher liquid velocities as the predictions were more accurate in this range for the biodiesel fluidized bed. It is clear that the correlations are not applicable with dispersed glycerol. Based on the correlations, a better fit would be obtained assuming smaller particles at lower liquid velocities. It is thus believed that the particle agglomerates increase in size as a function of rising liquid velocity.

5.3.2.2. Gas-liquid-liquid-solid phase holdups

Figures 5.6, 5.7 and 5.8 present the effects of glycerol concentration on the ebullated bed phase holdups. Figure 5.6 shows that the addition of glycerol results in higher gas

holdups at lower gas flow rates. For the pure biodiesel ebullated bed, bubbles in the bed region were in the coalesced flow regime for all studied gas flow rates. When glycerol was added however, particle agglomeration resulted in the dispersed bubble flow regime in the ebullated bed at lower gas velocities. Bubble break up due to particle clustering produced higher gas holdups. The dispersed and coalesced bubble flow regimes in the bed region can be distinguished based on the respective slopes at lower and higher gas velocities. At higher gas flow rates, the gas holdups with dispersed glycerol decreased below the pure biodiesel bed values. This can be explained based on the bubble column results where the dispersed glycerol reduced the small and micro bubble populations, especially in the coalesced bubble flow regime. Based on Figure 5.6, the addition of glycerol increased the gas holdup required to transition from the dispersed to the coalesced flow regime in the bed region.

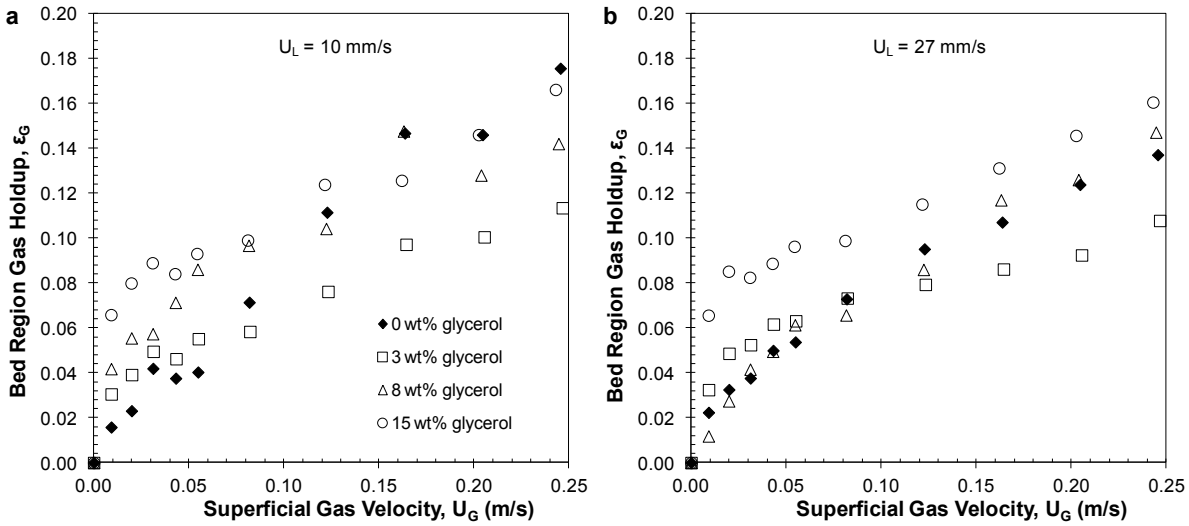

Figure 5.6. Bed region gas holdup as a function of superficial gas velocity and glycerol concentration for a nitrogen-biodiesel-glycerol-1.3 mm glass beads ebullated bed where (a) U_L = 10 mm/s and (b) U_L = 27 mm/s.

Figure 5.7 shows that with no glycerol, the fluidized bed contracted at the introduction of gas for both liquid flow rates. Bed contraction has been observed using similar particles with water and a water-ethanol (0.5 wt.%) solution (Dargar and Macchi, 2006). The bed contraction, characterized by a higher solid holdup, generally increased at

higher superficial gas velocities. The bed however expanded with the introduction of gas in the presence of dispersed glycerol due to bubble break-up from particle agglomerates. Figure 5.7 demonstrates that bed height remained approximately constant at low gas flow rates for the 8 and 15 wt.% glycerol concentrations. However, once the gas flow rate was sufficiently raised, bed expansion was observed.

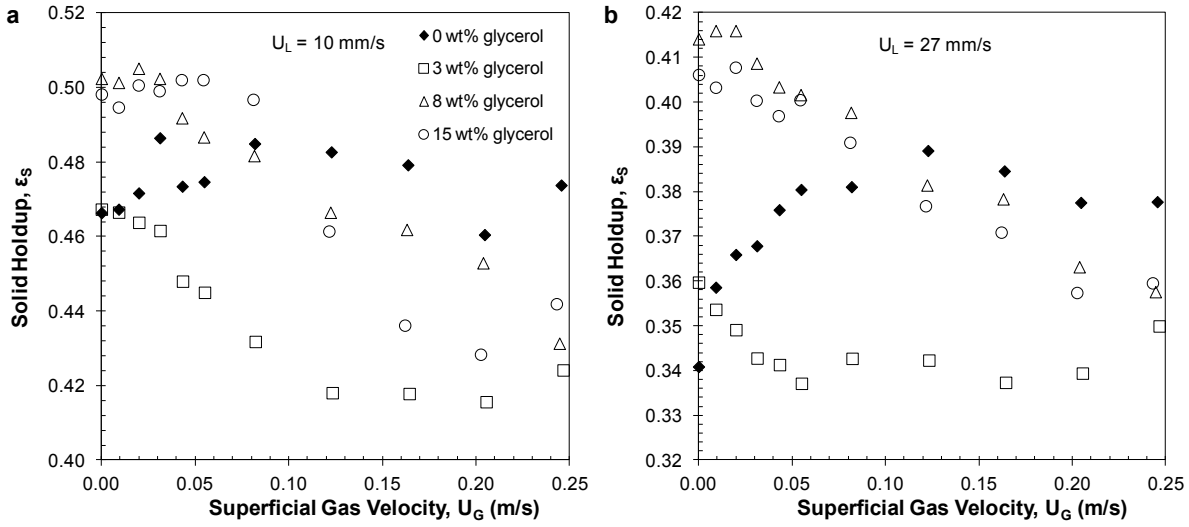

Figure 5.7. Solid holdup as a function of superficial gas velocity and glycerol concentration for a nitrogen-biodiesel-glycerol-1.3 mm glass beads ebullated bed where (a) U_L = 10 mm/s and (b) U_L = 27 mm/s.

Figure 5.8 presents the effect of the dispersed glycerol on the bed region liquid holdups. In the pure biodiesel ebullated bed, liquid holdups naturally decreased as a function of the gas flow rate as both the gas and solids holdups increased. When the dispersed glycerol was added, the liquid holdups still decreased as a function of gas flow rate, but at reduced rate as the solids holdups actually increased and the rise in gas holdups is lower. The liquid holdup reduction was proportional to the glycerol concentration.

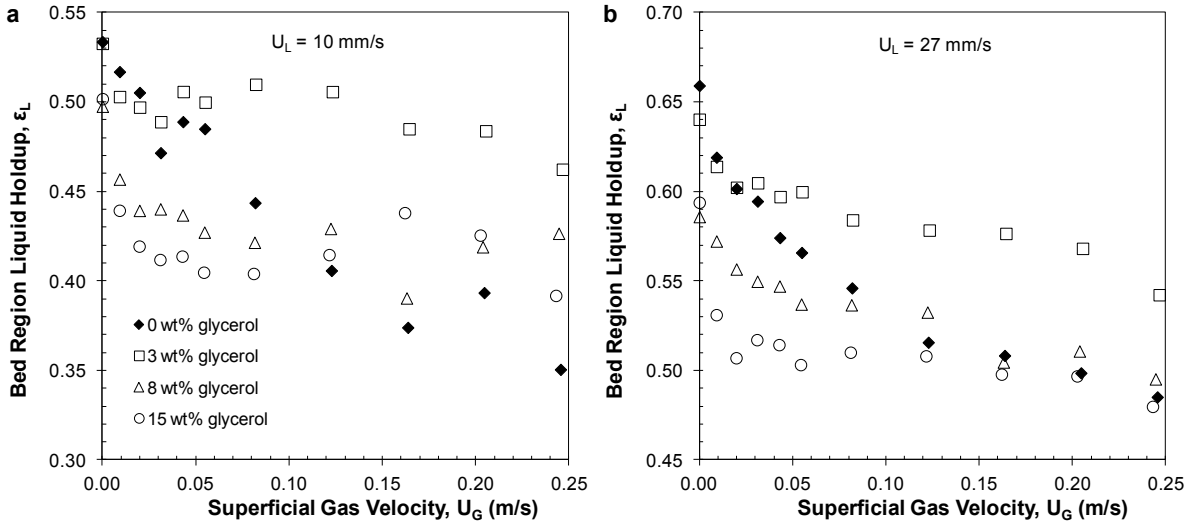

Figure 5.8. Liquid holdup as a function of superficial gas velocity and glycerol concentration for a nitrogen-biodiesel-glycerol-1.3 mm glass beads ebullated bed where (a) U_L = 10 mm/s and (b) U_L = 27 mm/s.

The freeboard gas holdups presented in Figure 5.9 generally increased, particularly at lower gas velocities, when dispersed glycerol was added to the system. As previously described, dispersed bubble flow in the bed region was obtained when glycerol was added to the column. The resulting bubble break-up occurring through the bed region generated smaller bubbles flowing into the freeboard region, increasing the gas holdups. For both liquid flow rates, a glycerol concentration of 15 wt.% resulted in similar or lower freeboard gas holdups compared to the pure biodiesel fluidized bed as well as the other glycerol concentrations. This is likely due to the competing effects of bubble break up in the bed region from particle clustering, increasing the freeboard gas holdup, and a reduction of the small and micro bubble holdups, discussed in section 5.3.1.2.

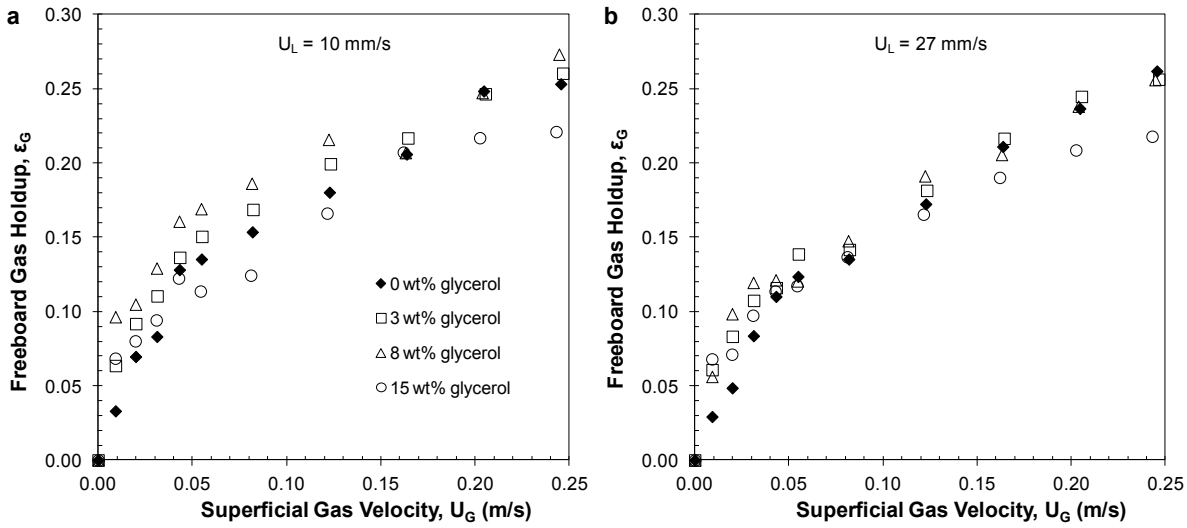

Figure 5.9. Freeboard region gas holdup as a function of superficial gas velocity and glycerol concentration for a nitrogen-biodiesel-glycerol-1.3 mm glass beads ebullated bed where (a) U_L = 10 mm/s and (b) U_L = 27 mm/s.

5.3.2.3. Fluidization behaviour

The experimental plan originally included tests to determine the effect of dispersed glycerol on the minimum liquid fluidization velocity while varying the gas flow rate. The minimum liquid fluidization velocity with no gas flow of the pure biodiesel system was experimentally determined to be 3.9 mm/s. The predicted U_{lmf} value using the gas-perturbed liquid model (Zhang et al., 1998) is 3.4 mm/s. The introduction of gas reduced the U_{lmf} of a similar magnitude as predicted by the gas-perturbed liquid model.

Unfortunately, the fluidized bed behaviour following the addition of glycerol prevented the use of conventional measurement techniques. Usually, the pressure drop along a fixed height interval is measured at varying liquid flow rates while maintaining the gas velocity. When the bed is not fluidized, an increased liquid flow rate results in a higher pressure drop. Once the bed becomes fluidized, the pressure drop no longer increases. When adding glycerol, the bed would be considered fluidized with no liquid flow even at low gas velocities. It was visually observed that the high glycerol concentrations caused the bed to behave as sludge. In addition, the agglomerate sizes varied as a function of the superficial liquid velocity, further complicating the conventional measurement technique. Future studies

on the minimum liquid fluidization velocity at elevated glycerol concentrations will require alternate measurement techniques.

The presence of a denser and more viscous liquid phase in an ebullated bed significantly affected the hydrodynamic behaviour. With no gas flowing, the agglomerate size distribution was relatively wide, where the larger agglomerates were found towards the bottom of the column. It was observed that at high liquid flow rates and no gas, groups of smaller agglomerates at the top of the bed occasionally jetted out, which could be problematic if particle carry over is a concern. The introduction of gas resulted in a more narrow agglomerate size distribution likely due to increased shearing and improved mixing in the bed region. At low liquid flow rates, the agglomerate sizes varied approximately from 10 to 20 mm for the large clusters at the bottom and 4 to 10 mm for the smaller clusters rising at the top of the bed.

The moving packed bed phenomenon has been previously observed at the startup of a liquid-solid fluidized bed (Fan et al., 1999). The previous phenomenon is due to the displacement of a layer of fine bubbles between the packed particles. Once the bed is properly degassed, the moving packed bed collapses. A similar phenomenon was also observed in the liquid-liquid-solid fluidized bed. With no gas present and after sufficient mixing to properly disperse the glycerol, the liquid flow would be stopped. Following a sufficient amount of time, the liquid velocity was slowly increased which resulted in a moving packed bed. As there is no gas present in the column, the phenomenon is solely due to particle adhesion from the glycerol. The moving packed beds eventually collapsed due to gravitational forces.

Finally, pressure effects could not be studied with the experimental apparatus. Elevated pressures impact the bubble properties for the studied operating conditions. As the purpose of the study was to provide insight to the hydrodynamics of high pressure ebullated bed hydroprocessors, future experiments will look into pressure effects with an immiscible dispersed liquid phase.

5.4. Conclusions

The effects of dispersed glycerol on the hydrodynamics in a bubble column and ebullated bed while varying the gas and liquid superficial velocities were studied. The addition of glycerol reduced the gas holdups in a bubble column, particularly at high gas flow rates with no liquid flow. At the highest glycerol concentration of 15 wt.%, the studied superficial liquid velocity range had no observable effect on the gas holdups. The DGD technique was used to study the effects of a dispersed liquid phase on individual bubble populations. The large bubble holdups increased when glycerol was added, though the increase was constant for the studied glycerol concentrations. The small and micro bubble holdups were reduced as the glycerol concentration was raised, especially in the coalesced flow regime.

The liquid-liquid-solid and gas-liquid-liquid-solid fluidized bed behaviour was significantly affected by the presence of dispersed glycerol. The liquid-liquid-solid bed expansions show that although the overall liquid viscosity increased with the addition of glycerol, the solid holdups increased due to particle agglomeration. With no glycerol present, the coalesced bubble flow regime was obtained in the gas-liquid-solid ebullated bed for all studied gas and liquid flow rates. The addition of glycerol resulted in particle clustering, increasing the apparent particle size which yielded the dispersed bubble flow regime. As a result of the increased bubble break-up, bed and freeboard region gas holdups were greater.

Acknowledgments

The authors are grateful to Marten Ternan for valuable insights and to the Natural Sciences and Engineering Research Council of Canada and Syncrude Canada Ltd. for financial assistance.

Nomenclature

Ar_L	liquid Archimedes number $= \rho_L(\rho_S - \rho_L) g\, d_P^{\,3} / \mu_L^{\,2}$
d_C	column inner diameter (m)
d_P	particle diameter (m)
g	gravitational acceleration (m/s^2)
h_B	bed height (m)
m	mass of the particles (kg)
n	index n in Eq. (5.5) and Eq. (5.6)
$-\Delta P$	dynamic pressure drop (Pa)
U_G, U_L	gas and liquid superficial velocities (m/s)
U_{lmf}	minimum liquid fluidization velocity (m/s)
U_{Lt}	particle terminal velocity in the column (m/s)
$U_{Lt\infty}$	particle terminal velocity in a large vessel [$d_P/d_C < 0.001$] (m/s)
Δz	vertical distance between differential pressure taps (m)

Greek symbols

ε_G, ε_L, ε_S	gas, liquid and solid phase holdups
κ	ratio of dispersed phase viscosity to continuous phase viscosity
λ	cubic root of the dispersed phase volumetric fraction in the emulsion
μ_L	liquid dynamic viscosity (Pa s)
$\mu_{L,C}$, $\mu_{L,D}$	continuous and dispersed phase liquid dynamic viscosity (Pa s)
$\mu_{L,E}$	emulsion dynamic viscosity (Pa s)
$\rho_{L,C}$, $\rho_{L,D}$	continuous and dispersed phase liquid densities (kg/m^3)
$\rho_{L,E}$	emulsion density (kg/m^3)
ρ_G, ρ_L, ρ_S	gas, liquid and solid densities (kg/m^3)
σ_{G-L}	gas-liquid surface tension (N/m)
σ_{L-L}	liquid-liquid interfacial tension (N/m)

Chapter 6

Particle agglomeration in gas-liquid-solid fluidized beds with a dispersed immiscible liquid: study on particle size, shape and material

Dominic Pjontek[a], Valois Parisien[a], Connor Farrell[a], Craig McKnight[b], Jason Wiens[b], Arturo Macchi[a]

[a]*Centre for Catalysis Research and Innovation, Department of Chemical and Biological Engineering, University of Ottawa, 161 Louis Pasteur, Ottawa, Ontario, Canada, K1N 6N5*

[b]*Syncrude Canada Ltd.,9421-17 Avenue, Edmonton, Alberta, Canada, T6N 1H4*

Abstract

The formation of a denser and more viscous secondary liquid phase may impact the fluid dynamic behaviour of industrial ebullated bed reactors such as hydroprocessors. This study investigates the effects of particle size, shape and material on the global fluid dynamic behaviour of gas-liquid-liquid-solid fluidized beds subject to particle agglomeration. Ebullated bed experiments were carried out in a 152.4 mm diameter column at atmospheric conditions with biodiesel as the continuous liquid, 5 wt.% of glycerol as the denser and more viscous dispersed liquid, and nitrogen. Glass spheres with diameters of 4 and 1.5 mm were compared to aluminum cylinders with equivalent volume to surface area ratios, where the sphericity of both larger and smaller cylinders was approximately 0.8. In a liquid-solid fluidized bed, the previous particles were in the intermediate settling flow regime ($0.2 < Re_{LT\infty} < 500$) in biodiesel; nonetheless, coalescing and dispersed bubble flow regimes were obtained with the smaller and larger particles, respectively, at the introduction of gas. Liquid-liquid-solid fluidized bed results established that particle size, shape and material had considerable impacts on agglomeration behaviour. In the gas-liquid-liquid-solid ebullated bed, the 1.5 mm glass beads transitioned from coalesced to dispersed bubble flow due to increased particle inertia from agglomeration. Larger glass beads experienced a reduced bed expansion due to agglomeration since the bubble flow regime remained constant. The studied aluminum cylinders did not agglomerate to the same extent as the glass beads due to differing material wetting properties, where negligible clustering occurred with the larger cylinders and an axial agglomerate size distribution was observed with the smaller cylinders. Preliminary experiments in a slurry bubble column using 100 to 150 μm glass beads were inoperable at a relatively low glycerol concentration of 0.7 wt.% due to considerable sedimentation on the distributor. Interparticle forces relevant to gas-liquid-liquid-solid fluidized beds are discussed, with an emphasis on the relation between fluid and particle properties with respect to attractive forces due to liquid bridging.

***This manuscript has been published**: Pjontek, D., Parisien, V., Farrell, C., McKnight, C. A., Wiens, J., Macchi, A., 2014. Particle agglomeration in gas-liquid-solid fluidized beds with a dispersed immiscible liquid: Study on particle size, shape and material. Powder Technol. 266, 45–60.

6.1. Introduction

Ebullated bed hydroprocessors operate as gas-liquid-solid fluidized beds to promote contact between the gas (mostly hydrogen), liquid (resid feed and converted fractions) and solid (alumina supported catalyst) phases. Hydroprocessing combines thermal cracking at elevated temperatures (~ 440°C) and hydrogenation at elevated operating pressure (~ 11.7 MPa) to convert the heavier liquid feed material to lighter fractions (McKnight et al., 2003). LC-Finer^{SM} ebullated bed resid upgraders operate with co-current flow of gas and liquid through a bed of cylindrical heterogeneous catalyst particles sized in the mm range. The catalyst bed is fluidized mainly due to the liquid flow, where an internal liquid recycle line increases the liquid residence time and controls the catalyst bed expansion. Another resid hydroprocessing configuration is the slurry bubble column (e.g., VEBA-combi-cracking, M-coke technology, HDH technology, and UOP Uniflex^{TM}) which uses dispersed unsupported catalysts in the μm range, where catalysts are primarily suspended from local liquid flow induced by the wakes of rising bubbles.

Upgrading heavier feeds can lead to coke formation in hydroprocessors, largely due to accelerated thermal cracking at elevated temperatures, which can cause reactor/downstream equipment fouling and reduced catalytic activity (Gray, 1994). Coke is generally defined as toluene insoluble materials and is believed to originate from the asphaltene fraction in the feedstock (Srinivasan and McKnight, 1994). An intermediate phase between the heavier liquid fraction and solid coke, commonly referred as carbonaceous mesophase, was initially identified by its optical anisotropy when observed under polarized light (Brooks and Taylor, 1965). Some potential formation mechanisms have been discussed by previous authors (Bagheri et al., 2012; Gray and McCaffrey, 2002; Marsh and Latham, 1986; Wiehe, 1994), where the intermediate phase is believed to form due to an increased rate of thermal cracking relative to the rate of hydrogenation. If the cracking rate of alkyl chains from polyaromatics cores increases relative to the rate of aromatic core hydrogenation, resulting planar polyaromatic cores may oligomerize/coalesce to form initial mesophase domains. A recent study by Bagheri et al. (2012) observed the in-situ formation of both small and large mesophase domains with areas below and above 2000 μm^2, respectively, in a stirred hot-stage reactor at 440°C and 4.8 MPa. Larger mesophase domains, which resulted from the coalescence of smaller domains, were minimized with the addition

of a proprietary catalyst as the particles attached themselves to the mesophase outer surface. Although it is difficult to know whether carbonaceous mesophase is present in industrial ebullated beds and/or its approximate concentration, mounds of agglomerated catalysts and coke have been previously found above the grid during shutdowns (McKnight et al., 2003).

Mesophase may impact the fluidization behaviour of ebullated bed and slurry hydroprocessors, particularly if the additional phase leads to particle clustering. Few studies are currently available in the open literature with regards to the effect of an additional immiscible liquid in ebullated beds and/or slurry bubble columns. Mass transfer parameters in bubble columns with an additional liquid phase have been previously studied (Brilman et al., 1999; Kaur et al., 2007) due to the dispersed liquid's potential to increase gas absorption. Studies on liquid-liquid-solid fluidized beds have investigated dispersed drop properties, pressure fluctuations and interphase mass transfer coefficients mostly for liquid-liquid extractions as the particles can improve the contact between both liquid phases (Chiu et al., 1987; Dakshinamurty et al., 1979; Kyu and Kwang, 1986; Rao and Setty, 2000; Roszak and Gawroński, 1979; Song et al., 2005). Siquier et al. (1991) and Argüelles et al. (1993) studied the solid and gas axial holdup profiles in slurry bubble columns, where the continuous and dispersed liquid phases were kerosene and water, respectively.

Particle agglomeration is also relevant to fluid coking, a complementary process for resid upgrading, where the liquid feed is injected in a gas-solid fluidized bed of coke particles. Although different from ebullated beds and slurry bubble columns, agglomeration studies in gas-solid fluidized beds provide an initial comparison for clustering behaviour. The stability of prepared agglomerates, using water as the liquid and glass beads or silica sand as the solid, was investigated in a gas-solid fluidized bed (Weber et al., 2006) while a subsequent study examined the effects of agglomerate size/density, liquid viscosity, binder concentration and gas velocity (Weber et al., 2008). Agglomerates were also examined using coke particles and oil to better represent the industrial particle properties (Weber et al., 2011). Artificial agglomerates made of polyurethane foam, magnets and RFID tags were employed to study the stability of spherical (Parveen et al., 2013a) and cylindrical shapes (Parveen et al., 2013b). McMillan et al. (2013) discuss the cohesive forces between particles in fluidized beds operated in the bubbling and fast fluidization regimes as well as when liquid jets are introduced. They used FCC catalyst, glass beads and sand, where the particle

sizes were in the range of 70 to 220 μm. High speed video and image analysis demonstrated significant particle clustering, particularly due to cohesive bridging when a liquid was injected. Effects of selected liquid properties in a cold-model gas-solid fluidized were studied by Mohagheghi et al. (2014), where the liquid viscosity and contact angle had a considerable impact on particle cohesiveness and agglomerate formation.

An initial ebullated bed study investigated the impact of a dispersed immiscible liquid phase on the overall phase holdups and fluidization behaviour in a cold-flow non-simulating system using biodiesel as the continuous liquid phase, glycerol as the dispersed liquid phase, 1.3 mm diameter glass beads, and nitrogen (Pjontek et al., 2011). It is important to note that the previous experimental conditions were not representative of the industrially observed high gas holdup conditions in ebullated bed hydroprocessors (McKnight et al., 2003). Bubble column experiments demonstrated that added glycerol reduced the gas holdups, where dynamic gas disengagement profiles revealed an increased large bubble population and reductions to the small and micro bubble holdups. Conversely, glycerol addition changed the bubble characteristics and fluidization behaviour in the ebullated bed from coalescing to dispersed bubble flow due to an increased apparent particle size via agglomeration.

The purpose of this study is to expand on the previous study by qualitatively and quantitatively investigating the impact of particle size, shape and material on agglomeration tendencies in an ebullated bed using two sets of spheres and cylinders with equivalent Sauter mean diameters. Liquid-liquid-solid fluidized bed results are used as an initial indicator of agglomeration tendencies and to estimate the change in cluster size due to increased liquid flow. Ebullated bed results study the impact of gas and liquid flow rates on the fluidization behaviour with particle agglomeration. Preliminary experiments in a slurry bubble column further demonstrate the impact of particle size relative to particle clustering. As the measurements are carried out in a non-simulating system, the experimental results thus provide fluid dynamic trends following particle agglomeration in gas-liquid-solid fluidized beds. Lastly, the discussion focuses on interparticle forces, particularly liquid bridging, which can lead to agglomeration in gas-liquid-liquid-solid fluidized beds.

6.2. Materials and methods

6.2.1. Experimental system

Experiments were performed at ambient temperature and pressure in a clear polyvinyl chloride column with a maximum expanded bed height of 2.7 m and an inner diameter of 0.1524 m, adequately large to minimize wall effects on phase holdups (Wilkinson et al., 1992). A schematic of the experimental setup is provided in Figure 6.1. The gas and liquid were separately introduced to the bottom of the fluidized bed to facilitate uniform spatial distribution of the fluids. The gas-liquid distributor was a perforated plate with 62 holes of 4.0 mm diameter for liquid flow, while gas was introduced via 32 holes of 0.8 mm diameter. A mesh placed on top of the distributor was used to prevent particles from entering the plenum chamber. At the top of the column, an expanded overflow section acted as the primary gas-liquid separation. Exiting gas passed through an oil mist filter to remove any entrained biodiesel droplets prior to being exhausted. Liquid was conveyed from the overflow tank to a conical bottom storage tank for further degassing before being recycled to the bottom of the column. A centrifugal pump designed for organic liquids was used to circulate the liquid while gas was introduced via industrial grade nitrogen cylinders. Various liquid drains were added to the system to facilitate the separation of immiscible liquids. Global phase holdups were determined using a differential pressure transmitter (model PX750-30DI from Omega), where the reference pressure port was located 70 mm above the distributor and subsequent pressure ports were equally spaced by 101.6 mm.

The experimental operating condition ranges for this study are summarized in Table 6.1. Uncertainties in the operating conditions were estimated based on rotameter precision and fluctuations during experiments. Liquid superficial velocities (U_L) for the ebullated bed runs were selected based on liquid-solid fluidized bed results to ensure suitable bed expansions (e.g., potential bed contraction for the equivalent 1.5 mm particles with the introduction of gas, further discussed in section 6.2.3). Gas superficial velocities (U_G) were selected based on the previous study (Pjontek et al., 2011) to observe the transition from dispersed to coalesced bubble flow with the larger particles. The ebullated bed aspect ratio (h_B/d_C) was always greater than 5 for all studied operating conditions to reduce the impact of entrance effects in the bed region.

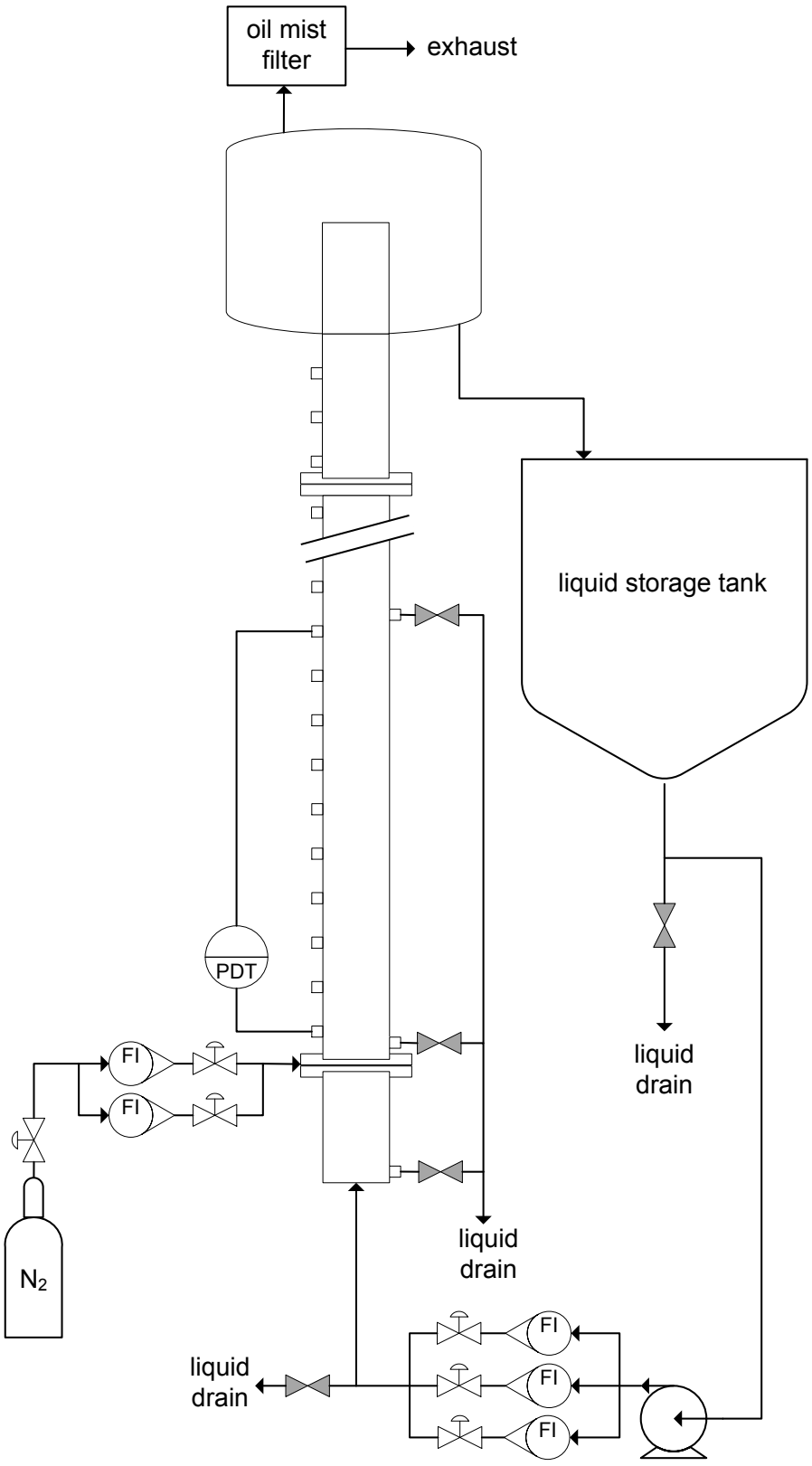

Figure 6.1. Schematic of the fluidization column for organic liquids.

Table 6.1. Experimental operating conditions.

Parameter	Symbol	Range	Units
superficial liquid velocity	U_L	0 to 121 (± ~ 2%)	mm/s
superficial gas velocity	U_G	0 to 130 (± ~ 2%)	mm/s
pressure	P	106 (± 1)	kPa
column diameter	d_C	152.4	mm
temperature	T	24 ± 2	°C

When dealing with two immiscible liquids, the homogeneity of the mixture is vital to ensure proper distribution of the dispersed phase throughout the system. A hydroprocessor (e.g., the LC-Finer^{SM}) would likely produce a pseudo-homogeneous emulsion due its internal liquid recycle, liquid shearing from the recycle pump, and subsequent flow through the grid. The conical bottom of the liquid storage tank (refer to Figure 6.1) ensured that any settled glycerol would be recycled back to the column. As the centrifugal pump applied significant shearing to the liquids, the emulsion entering the column consisted of finely dispersed glycerol droplets in the continuous biodiesel.

6.2.2. Fluid properties

Relevant fluid properties for this study are provided in Table 6.2, where uncertainties for the liquid properties were estimated from repeated measurements. Gas-liquid surface tensions were measured with a K12 Krüss Tensiometer by averaging the values obtained using the ring and plate methods, while the liquid-liquid interfacial tension for biodiesel-glycerol was measured using only the plate method. Continuous and dispersed liquids were chosen based on selected characteristics of those encountered in a resid hydroprocessor following mesophase formation. Biodiesel was selected as it is a relatively low viscosity organic liquid with foaming tendencies. Glycerol was chosen to simulate the polar, denser, and more viscous mesophase. In addition, both liquids were selected to minimize health and safety concerns while nitrogen was used as the gas phase to reduce the potential of biodiesel

vapour combustion. Furthermore, the biodiesel color allows the differentiation of glycerol in the experimental system, thus facilitating visual observations. Based on the previous study which investigated the impact of the dispersed liquid concentration (Pjontek et al., 2011), a glycerol concentration of 5 wt.% was selected as this was shown to sufficiently impact the fluidization behaviour.

Table 6.2. Fluid properties for the continuous liquid, dispersed liquid, and gas.

Parameter	Symbol	Value	Units
biodiesel density	$\rho_{L,C}$	877 ± 0.2	kg/m^3
glycerol density	$\rho_{L,D}$	1250 ± 1	kg/m^3
nitrogen density	ρ_G	1.20 ± 0.02	kg/m^3
biodiesel viscosity	$\mu_{L,C}$	5.0 x 10^{-3}	Pa · s
glycerol viscosity	$\mu_{L,D}$	1.5	Pa · s
biodiesel-air surface tension	$\gamma_{Air-L,C}$	30.6	mN/m
glycerol-air surface tension	$\gamma_{Air-L,D}$	62.4	mN/m
biodiesel-glycerol surface tension	$\gamma_{L,C-L,D}$	50.7	mN/m

Estimates of the biodiesel-glycerol emulsion density and viscosity were required for phase holdup calculations and to predict the liquid-liquid-solid fluidized bed expansion. The emulsion density ($\rho_{L,E}$) in a given region was determined using the following relation:

$$\rho_{L,E} = \left(1 - \varepsilon_{L,D}/\varepsilon_{L,E}\right)\rho_{L,C} + \left(\varepsilon_{L,D}/\varepsilon_{L,E}\right)\rho_{L,D} \tag{6.1}$$

The volumetric fraction of the dispersed phase in the emulsion ($\varepsilon_{L,D}/\varepsilon_{L,E}$) was estimated experimentally based on the liquid-liquid-solid fluidized bed measurements (further discussed in section 6.3.1). The emulsion viscosity was estimated using the cell-

model approach developed by Yaron and Gal-Or (1972), which is valid for moderately concentrated Newtonian emulsions:

$$\frac{\mu_{L,E}}{\mu_{L,C}} = 1 + \frac{5.5\lambda^3\left[4\lambda^7 + 10 - (84/11)\lambda^2 + (4/\kappa)(1-\lambda^7)\right]}{10(1-\lambda^{10}) - 25\lambda^3(1-\lambda^4) + (10/\kappa)(1-\lambda^3)(1-\lambda^7)} \tag{6.2a}$$

$$\lambda = \sqrt[3]{\varepsilon_{L,D}/\varepsilon_{L,E}} \tag{6.2b}$$

$$\kappa = \frac{\mu_{L,D}}{\mu_{L,C}} \tag{6.2c}$$

These conditions were met based on the studied volumetric fractions of dispersed glycerol and as droplets were visually observed to be considerably small due to sufficient liquid shearing via the centrifugal pump. This estimation was also selected as it has been experimentally shown to reasonably predict the viscosity of Newtonian emulsions without requiring adjustable parameters (Pal, 2000; Yaron and Gal-Or, 1972). It should be noted that a considerable portion of the added glycerol was located in the ebullated bed when particle agglomeration occurred (discussed in greater detail in section 6.3.1).

6.2.3. Particle properties

Particles were selected to study the expansion or collapse of an ebullated bed at the introduction of gas, which depend on the particle properties, fluid properties and operating conditions (Epstein, 1976; Muroyama and Fan, 1985). Pjontek and Macchi (2014) compared the fluid dynamic behaviour of spheres and cylinders with matching Sauter mean diameters under high gas holdup conditions. Overall holdup discrepancies due to particle shape were mainly observed when the bed contracted in the coalescing bubble flow regime. Glass beads with diameters of 4 mm and 1.5 mm were hence selected to compare the clustering in both coalescing and dispersed bubble flow regimes.

Since glass beads were previously shown to agglomerate in the biodiesel-glycerol emulsion (Pjontek et al., 2011), cylindrical particles were selected to minimize particle density and size distribution effects while attempting to match the spherical properties. Preferably, spheres and cylinders would have been manufactured using the same material to

isolate shape effects. Limitations due to the cost and manufacturing of cylindrical particles, however, led to the material selection of aluminum. Properties of the spheres and cylinders used in this study are provided in Table 6.3 and a visual comparison is shown in Figure 6.2. Sizing uncertainties for the cylindrical particles were estimated based on measurements for 100 particles, uncertainties for the glass beads were based on the manufacturer specifications, and density uncertainties were estimated from repeated measurements. Aluminum wire diameters were chosen to match the Sauter mean diameter of the spheres while maintaining a desired length/diameter ratio of approximately 2.5, resulting in a sphericity of 0.8.

Table 6.3. Physical properties of spherical and cylindrical particles.

Parameter	**L spheres**	**L cylinders**	**S spheres**	**S cylinders**
material	borosilicate glass	aluminum 1100	borosilicate glass	aluminum 5356
density, ρ_S (kg/m^3)	2500 ± 9	2711 ± 8	2502 ± 4	2649 ± 9
diameter, d_P (mm)	4.0 ± 0.2	3.2 ± 0.03	1.5 ± 0.2	1.2 ± 0.07
length, L_P (mm)	-	7.5 ± 0.4	-	3.1 ± 0.1
d_V (mm)	-	4.9 ± 0.1	-	1.9 ± 0.1
d_{SV} (mm)	4.0 ± 0.3	3.9 ± 0.2	1.5 ± 0.2	1.6 ± 0.2
sphericity, ϕ	1.0 ± ~ 0	0.81 ± 0.05	1.0 ± ~ 0	0.80 ± 0.08

Figure 6.2. Visual comparison of the L spheres (a), L cylinders (b), S spheres (c), and S cylinders (d).

Although the aluminum density is a somewhat higher compared to the glass spheres, this mainly affects the bed expansion behaviour in a predictable manner. The impact of particle size on particle clustering can thus be quantitatively compared using particles of the same material, while material and shape effects can be qualitatively compared between equivalent spheres and cylinders. It should be noted that particle material will affect the wettability of the dispersed and continuous liquids, and hence impact the clustering behaviour (further discussed in section 6.4.2).

6.2.4. Measurement techniques

6.2.4.1. Global phase holdups

Global phase holdups were calculated by measuring the dynamic pressure drop throughout the bed and freeboard regions, where the hydrostatic head of the continuous liquid phase is subtracted. Bed heights (h_B) were estimated from the intersection of the bed and freeboard dynamic pressure profiles via linear regression. Visual estimates of the bed height were recorded to corroborate the values obtained via the pressure drop method with the average and maximum relative differences being 1.5% and 4.9%, respectively. Solid holdups (ε_S) were calculated knowing the fluidized mass of particles (m) in the bed.

$$\varepsilon_S = \frac{4\,m}{\pi\, d_C{}^2\, h_B\, \rho_S} \tag{6.3}$$

Neglecting frictional drag on the wall and accelerations of the phases in the vertical direction, gas holdups in the bed region (ε_G) were measured via bed region dynamic pressure profiles. In order to account for the dispersed immiscible liquid in the column, pressure tap lines were only filled with biodiesel, allowing the gas holdup in the bed region to be determined as follows:

$$\varepsilon_G = \frac{(\Delta P/\Delta z)g^{-1} + (\rho_S - \rho_{L,E})\varepsilon_S + \rho_{L,E} - \rho_{L,C}}{\rho_{L,E} - \rho_G} \tag{6.4}$$

Bed region liquid holdups (ε_L) were calculated knowing that the sum of phase holdups must give unity. Gas holdups in the freeboard region (ε_{G-FB}) were measured based on the dynamic pressure profile above the bed.

$$\varepsilon_{G-FB} = \frac{(\Delta P/\Delta z)g^{-1} + \rho_{L,E} - \rho_{L,C}}{\rho_{L,E} - \rho_G} \tag{6.5}$$

6.2.4.2. Statistical analysis

Global phase holdup standard deviations were estimated to provide additional insight on the fluid dynamic behaviour of the bed and freeboard regions. Bars presented on the figures in this study provide the estimated standard deviations based on the method discussed in this section. Dynamic pressure drops were measured for 20 seconds with a sampling rate of 20 Hz at multiple pressure ports. Pooled variances ($s_P{}^2$) were estimated for the bed and freeboard regions as follows:

$$s_P{}^2 = \frac{\sum_{i=1}^{N}(m_i - 1)s_i{}^2}{\sum_{i=1}^{N}(m_i - 1)} \tag{6.6}$$

Where m_i is the number of data points for a given measurement and N is the number of dynamic pressure drop mean values in the bed or freeboard. Phase holdups depend on the intercept (β_0) and slope (β_1) of the dynamic pressure profiles in the bed and freeboard region, where standard deviations were estimated as follows:

$$s_{\beta_0} = \sqrt{\frac{s_P^{\,2} N}{N \cdot \left(\sum_{i=1}^{N} \Delta z_i^{\,2}\right) - \left(\sum_{i=1}^{N} \Delta z_i\right)^2}} \tag{6.7}$$

$$s_{\beta_1} = \sqrt{\frac{s_P^{\,2} \left(\sum_{i=1}^{N} \Delta z_i^{\,2}\right)}{N \cdot \left(\sum_{i=1}^{N} \Delta z_i^{\,2}\right) - \left(\sum_{i=1}^{N} \Delta z_i\right)^2}} \tag{6.8}$$

Bed heights were estimated via the intersection of the bed and freeboard region pressure profiles, where the bed height standard deviation (s_{h_B}) was approximated using the following relation:

$$s_{h_B} = \sqrt{\left(\frac{s_{\beta_0-FB}}{\beta_{1-B} - \beta_{1-FB}}\right)^2 + \left(\frac{s_{\beta_0-B}}{\beta_{1-B} - \beta_{1-FB}}\right)^2 + \left(\frac{\beta_{0-FB} \cdot s_{\beta_1-B}}{\beta_{1-B} - \beta_{1-FB}}\right)^2 + \left(\frac{\beta_{0-B} \cdot s_{\beta_1-FB}}{\beta_{1-B} - \beta_{1-FB}}\right)^2} \tag{6.9}$$

Finally, the standard deviations of the solid (s_{ε_S}), gas (s_{ε_G}) and liquid (s_{ε_L}) holdups in the bed region were estimated as follows:

$$s_{\varepsilon_S} = \frac{4m}{\pi d_C^{\,2} \rho_S h_B^{\,2}} s_{h_B} \tag{6.10}$$

$$s_{\varepsilon_G} = \sqrt{\left(\frac{s_{\beta_1-B}}{g\left(\rho_{L,E} - \rho_G\right)}\right)^2 + \left(\frac{\rho_S - \rho_{L,E}}{\rho_{L,E} - \rho_G} s_{\varepsilon_S}\right)^2} \tag{6.11}$$

$$s_{\varepsilon_L} = \sqrt{s_{\varepsilon_G}^{\,2} + s_{\varepsilon_S}^{\,2}} \tag{6.12}$$

For the gas holdup standard deviation, it was assumed that the emulsion density was constant as measurements were taken at steady state. In the freeboard, gas holdup standard deviations were estimated using Eq. (6.11), where the solid holdup standard deviation is equal to zero.

6.3. Experimental Results

6.3.1. Liquid-liquid-solid fluidized bed

Experiments were first carried out in a liquid-liquid-solid (L-L-S) fluidized bed to investigate the agglomeration behaviour of each particle type prior to the ebullated bed runs. Solid holdups in the L-L-S fluidized bed for the 1.5 mm and 4 mm equivalent particles are presented in Figure 6.3.

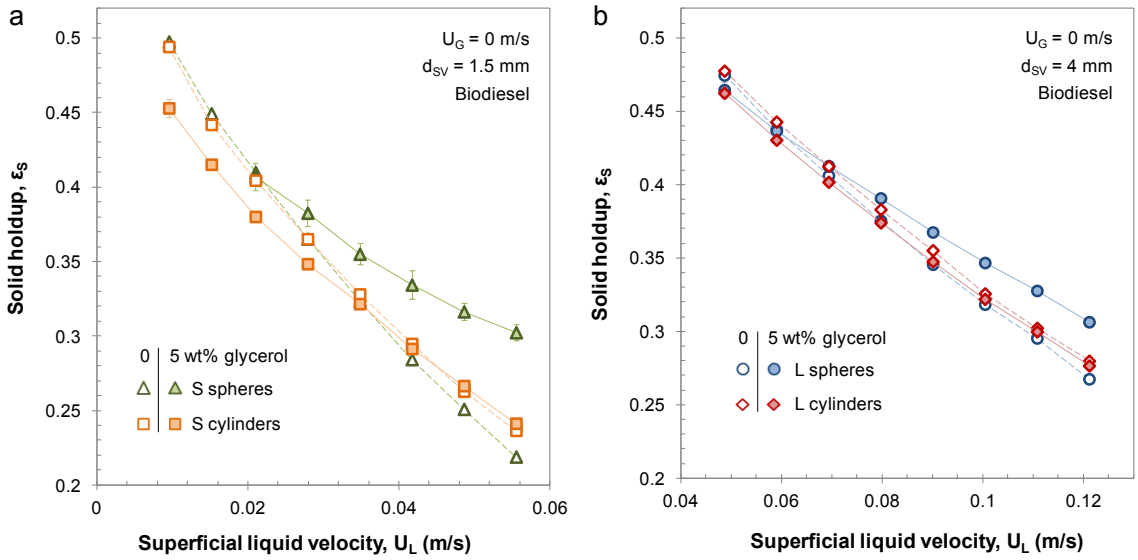

Figure 6.3. Solid holdups in the liquid-liquid-solid fluidized for (a) 1.5 mm and (b) 4 mm equivalent particles.

The fluid dynamic behaviour during the dispersed phase addition was also investigated, where the total volume of glycerol was poured into the liquid storage tank while attempting to maintain a relatively constant liquid flow. This was completed to qualitatively study the L-L-S fluidized bed contraction at the onset of agglomeration due to a secondary liquid phase that wets the particles. As glycerol was added upstream from the centrifugal pump, it was assumed that shearing through the impeller sufficiently dispersed the immiscible liquid. When monitoring the L-L-S fluidized bed height, the onset of agglomeration differed based on the studied particles. For example, 1.5 mm glass beads agglomerated more readily while changes to the behaviour of the 4 mm aluminum cylinders

were negligible. Agglomeration however required a longer period of time than initially anticipated. Within approximately 1 to 3 minutes following the glycerol addition, minor agglomeration was observed for most particles. Nevertheless, within 5 to 10 minutes clusters were readily distinguishable. The time between the formation/addition of a secondary liquid phase to particle clustering is believed to be dependent on the binding liquid/solid interfacial energy, particle characteristics, and liquid viscosity (refer to section 6.4.3). These results demonstrated the importance of allowing the system to reach steady state before gathering data and provided some insight to the bed dynamics in the advent of a process upset due to increased mesophase fraction.

Experimental L-S fluidized bed results were fitted to a linearized form of the Richardson and Zaki (1954) bed porosity empirical relation.

$$\ln U_L = n \ln \varepsilon + \ln(U_{LT}) \tag{6.13}$$

The slope provides the n index and the intercept estimates the particle settling velocity accounting for wall effects (U_{LT}). Corrections to terminal settling velocities in an infinitely large vessel ($U_{LT\infty}$) were calculated based on approximated wall effects for spherical (Khan and Richardson, 1989) and cylindrical (Chhabra, 1995) particles in a cylindrical column as follows:

$$\text{spheres: } k = 1 - 1.15\,(d_V/d_C)^{0.6} \tag{6.14}$$

$$\text{cylinders: } k = 1 - 1.33(d_V/d_C) \tag{6.15}$$

Table 6.4 presents the fitted parameters for the studied particles in biodiesel. Liquid-particle Reynolds numbers at the terminal free settling velocity ($Re_{LT\infty}$) thus provided additional information on the fluidization behaviour in the L-S bed. The n index is typically between 2.3 and 2.4 for spherical particles in the Newton flow regime ($Re_{LT\infty} > 500$), where particle inertial forces dominate (Khan and Richardson, 1989); however, when liquid viscous forces dominate in the Stokes flow regime ($Re_{LT\infty} < 0.2$), the n index is generally between 4.6 and 4.8. It can be observed in Table 6.4 that the larger and smaller particles in the L-S fluidized bed appeared to be in the transition between the Stokes and Newton flow regions, indicating that particle motion was dependent on both particle inertia and fluid viscous forces.

Table 6.4. Estimated Richardson and Zaki (1954) parameters based on the L-S fluidized bed experiments.

Parameter	L spheres	L cylinders	S spheres	S cylinders
n	2.78	2.77	3.82	4.27
U_{LT} (m/s)	0.292	0.301	0.150	0.184
k	0.87	0.85	0.93	0.92
$Re_{LT\infty}$	235	268	42	62
AAE (%)	0.09	0.14	0.58	0.53

The volumetric fraction of glycerol in the bed region and its standard deviations can be estimated based on the dynamic pressure profiles in the L-L-S fluidized bed and calculated solid holdups obtained with Eq. (6.3).

$$\varepsilon_{L,D} = \frac{(\Delta P/\Delta z)g^{-1} + (\rho_S - \rho_{L,C})\varepsilon_S}{\rho_{L,C} - \rho_{L,D}} \tag{6.16}$$

$$s_{\varepsilon_{L,D}} = \sqrt{\left(\frac{s_{(\Delta P/\Delta z)}}{g(\rho_{L,C} - \rho_{L,D})}\right)^2 + \left(\frac{\rho_S - \rho_{L,C}}{\rho_{L,C} - \rho_{L,D}} s_{\varepsilon_S}\right)^2} \tag{6.17}$$

For the studied emulsion system, 130 L of biodiesel were used as the continuous liquid while approximately 5 litres of glycerol were added, resulting in a total dispersed phase concentration of 5 wt.%. Estimated glycerol holdups in the L-L-S bed region are provided in Figure 6.4 for each particle. It should be noted that the estimated volume of glycerol in the bed region, based on the glycerol volumetric fraction and fluidized bed volume, was lower than the total volume added to the system for all studied operating conditions of the L-L-S fluidized bed.

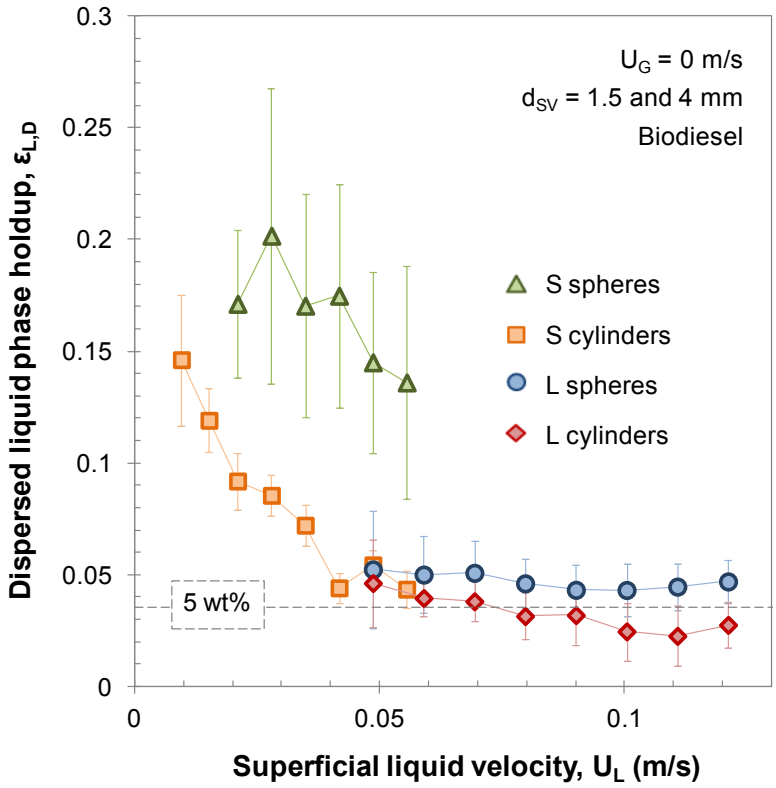

Figure 6.4. Dispersed liquid (glycerol) phase holdups in the liquid-liquid-solid fluidized bed.

Figure 6.3 shows comparable solid holdups for the 1.5 mm and 4 mm equivalent particles prior to adding glycerol, where similar results were obtained in a previous study using water and a 0.5 wt.% aqueous ethanol solution (Pjontek and Macchi, 2014). Theoretical predictions of Yaron and Gal-Or (1972) indicate that the emulsion viscosity should be greater than the pure biodiesel viscosity. The resulting greater drag on the particles, could potentially expand the fluidized bed; however, solid holdups for both sets of glass beads at a total glycerol concentration of 5 wt.% were greater when compared to pure biodiesel. The visually observed agglomerates thus required a higher liquid flow rate to achieve the same bed expansion obtained prior to adding glycerol. Increased bed region glycerol holdups for the 4 mm glass beads (Figure 6.4) corroborate the particle clustering at the studied conditions. The highest estimated dispersed phase holdups were for the 1.5 mm glass beads. The previous particles clustered the most based on deviations between solid holdups before and after adding glycerol and visual observations.

The fluid dynamic behaviour of the aluminum cylinders after the glycerol addition differed when compared to the glass beads. The larger aluminum cylinders (d_{SV} of 4 mm) did not appear to agglomerate based on observations and exhibited comparable bed expansions for the studied liquid flow rates. Solid holdups were marginally reduced at lower liquid velocities compared to the biodiesel system, likely due to the increased emulsion viscosity. For a non-clustering well mixed system, the initial glycerol volumetric fraction of 3.6 % (equivalent to 5 wt.% for the studied emulsion) would be expected in the bed region. The previous was approximately observed with the larger aluminum cylinders, accounting for the standard deviation of the data, in agreement with the lack of agglomeration.

The fluidization behaviour of the smaller aluminum cylinders (d_{SV} of 1.5 mm) diverged from the other particles as an agglomerate size distribution along the axial length of the column was observed, where larger clusters were located at the bottom of the fluidized bed. Figure 6.5 provides a comparison of the clustering behaviour at a relatively high superficial liquid velocity, where agglomerates of approximately 3 to 6 cylinders can be observed at the bottom of the fluidized bed while agglomeration was negligible near the bed/freeboard interface. Compared to the other studied particles, estimated bed region glycerol holdups for the 1.5 mm aluminum cylinders (Figure 6.4) were reduced at increasing superficial liquid velocities. Glycerol holdups for the other studied particles remained approximately constant for the studied liquid flow rates, where greater fractions in the bed region were indicative of more extensive agglomeration. Conversely, reduced solid holdups for the smaller aluminum cylinders at lower liquid velocities, shown in Figure 6.3a, indicate bed expansion following glycerol addition. The previous observations initially appear contradictory as agglomerate formation due to higher glycerol content typically contracted the fluidized bed, while bed expansion following glycerol addition could be associated to an increased liquid/emulsion viscosity. The particle wettability with respect to the dispersed glycerol in continuous biodiesel (further discussed in section 6.4.2) must be considered alongside the energy dissipation when flowing through the fluidized bed. Although aluminum particles did not appear to be preferentially wetted by the glycerol in a static system, it is believed that the glycerol droplet shearing when flowing through the fluidized bed of aluminum cylinders impacted the wetting characteristics and resulted in the higher bed region glycerol holdups at lower liquid velocities. When increasing the liquid flow rate

and further expanding the fluidized bed, glycerol holdups were reduced as the bed void increased, thus allowing the dispersed phase to flow more easily between the fluidized particles. The previous explanation appears to be in agreement with the results in Figure 6.4 as the bed region glycerol holdups for the smaller cylinders approached the values of the larger cylinders at higher liquid flow rates.

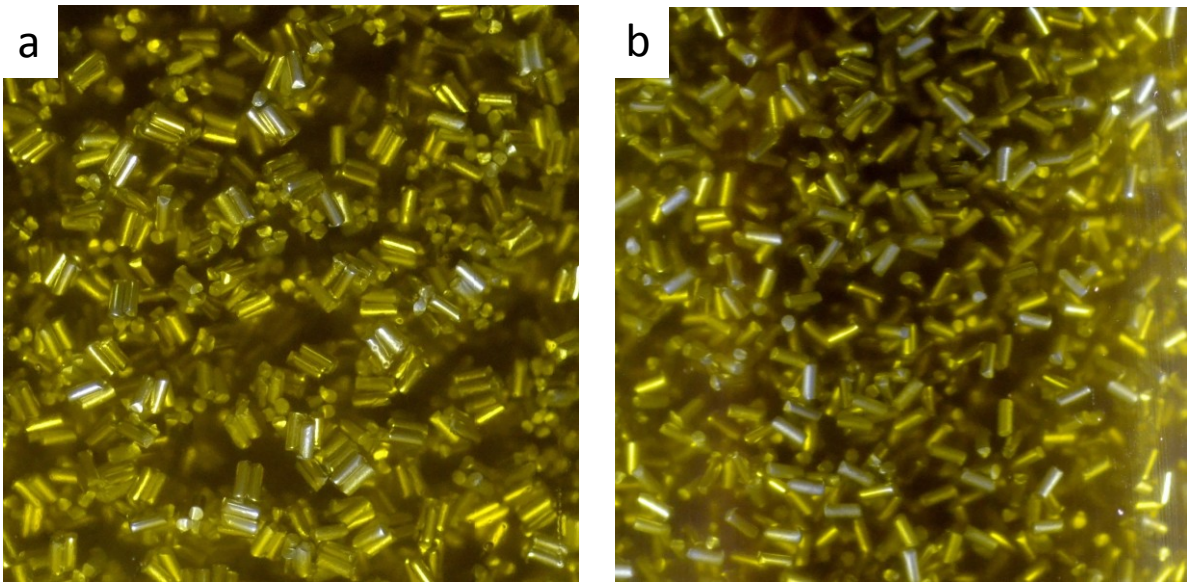

Figure 6.5. Clustering behaviour comparison at (a) the bottom of the fluidized bed and (b) near the bed/freeboard interface for the S cylinders (U_L = 0.08 m/s, U_G = 0 m/s, and overall glycerol concentration of 5 wt.%).

An attempt was made to quantify the change in apparent particle size for the 1.5 mm and 4 mm glass beads based on theoretical predictions for the n index (Khan and Richardson, 1989) and terminal settling velocity (Turton and Clark, 1987):

$$\frac{4.8-n}{n-2.4} = 0.043 Ar_L^{\,0.57}\left[1-1.24\left(d_V/d_C\right)^{0.27}\right] \tag{6.18}$$

$$Re_{LT\infty} = \frac{d_V\, U_{LT\infty}\, \rho_L}{\mu_L} = Ar_L^{\,1/3}\left[\left(\frac{18}{Ar_L^{\,2/3}}\right)^{0.824} + \left(\frac{0.321}{Ar_L^{\,1/3}}\right)^{0.412}\right]^{-1.214} \tag{6.19}$$

Increasing deviations between pure biodiesel and emulsion runs for the smaller and larger glass beads at higher liquid flow rates (refer to Figure 6.3) suggested that larger agglomerates were obtained. The average absolute error (AAE) when comparing the theoretical predictions using the previous correlations with Eq. (6.13) to the experimental results in biodiesel for the 1.5 mm and 4 mm glass beads were 3.8 % and 3.2 %, respectively, where experimental values were consistently lower. Predictions were previously shown to be more erroneous in the intermediate region between Stokes and Newton flow (Khan and Richardson, 1989), likely causing the minor discrepancy between predicted and experimental results.

It was assumed that predicted trends for Richardson and Zaki parameters could be used to estimate the average volume-equivalent agglomerate diameter based on the experimentally determined values, provided in Table 6.4. Theoretical predictions for the emulsion system, where the agglomerate diameter could be varied, were compared to predictions for the pure biodiesel system, for which all physical properties were known. Emulsion densities and viscosities were approximated using Eqs. (6.1) and (6.2a), respectively, based on the bed region glycerol holdups shown on Figure 6.4. Experimentally determined Richardson and Zaki parameters (Table 6.4) were then multiplied by the ratio of the predicted parameters for the emulsion over those for pure biodiesel, where the agglomerate volume equivalent diameter was varied to match the solid holdups at 5 wt.% glycerol (refer to Figure 6.3).

The estimated agglomerate volume equivalent diameter, shown in Figure 6.6, increased with greater superficial liquid velocities, in agreement with the deviations shown in Figure 6.3. Figure 6.6 also indicates relatively larger agglomerates for the 1.5 mm glass beads, corroborating the glycerol holdups in the bed region (Figure 6.4) and visual observations. However, the estimated agglomerate volume equivalent diameters are believed to underestimate the observed agglomerates during the experiments, likely due to assumptions used for the calculations. Even so, the experimental results and predictions based on the Richardson and Zaki parameters both indicated increasing agglomerate size at higher liquid flow rates.

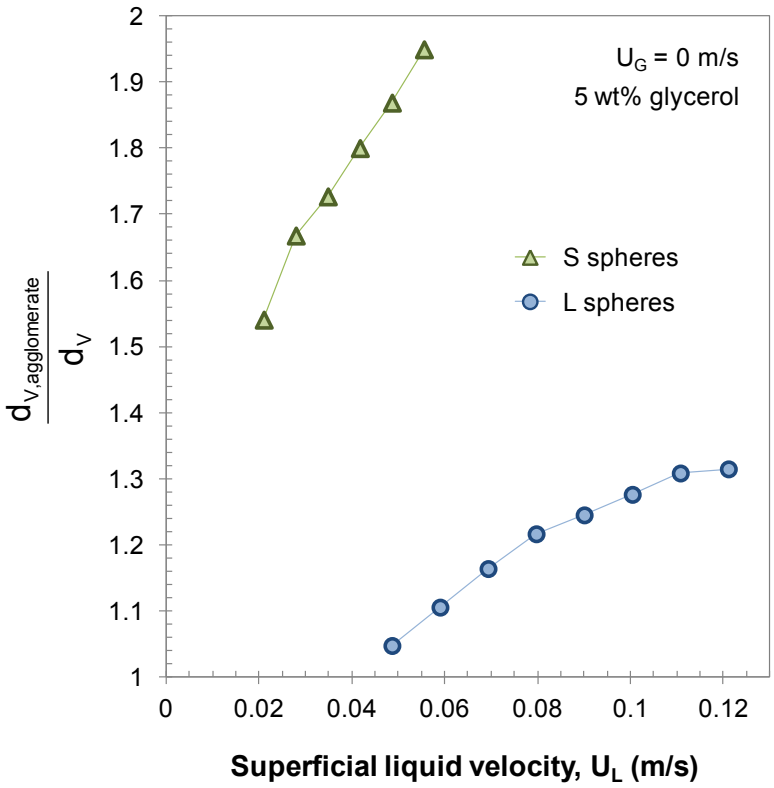

Figure 6.6. Estimated volume-equivalent agglomerate diameter and single particle diameter ratio for the 1.5 mm and 4 mm glass beads.

The L-L-S fluidized bed results established that the studied particle size, shape, and material have a considerable impact on agglomeration behaviour. An important consideration for particle clustering is the wettability/contact angle of the dispersed liquid phase with respect to the solid while submerged in the continuous liquid, since liquid bridging between particles appeared to be the main cohesive force (refer to section 6.4.1). The smaller and larger glass beads were shown to readily cluster as the glycerol wetted the particles in the continuous biodiesel. The 1.5 mm glass beads exhibited the most agglomeration in the L-L-S fluidized bed, demonstrating the effect of particle size. The studied aluminum particles did not agglomerate to the same extent when compared to the equivalent glass beads, likely due to reduced particle wettability with respect to the dispersed liquid (discussed in section 6.4.2). It was nonetheless observed that reducing the Sauter mean diameter of the aluminum cylinders from 4 mm to 1.5 mm resulted in some particle clustering, demonstrating that

particle inertia should be considered alongside particle wettability when investigating agglomeration in a fluidized bed (refer to section 6.4.3).

6.3.2. Gas-liquid-liquid-solid ebullated bed

Following the L-L-S fluidized bed measurements, ebullated bed fluid dynamics were investigated before and after glycerol addition. The emulsion density in the bed and freeboard regions had to be estimated prior to calculating gas holdups using Eq. (6.4). It was assumed that estimated glycerol holdups for the L-L-S fluidized beds (Figure 6.4) provided an adequate estimate of the bed region emulsion composition for the ebullated beds. Dispersed liquid phase holdups for the glass beads were straightforward as they were relatively constant for the studied liquid flow rates, where the average glycerol holdups in the L-L-S fluidized bed were used. To account for the glycerol holdup trend obtained with the smaller aluminum cylinders (Figure 6.4), glycerol holdups at matching superficial liquid velocities in the L-L-S fluidized bed runs were assumed for the ebullated bed calculations. Glycerol holdups in the freeboard, required for the gas holdup calculation, were estimated by subtracting the resulting glycerol volume in the bed region from the total glycerol in the system. Table 6.5 provides the estimated glycerol holdups in the ebullated bed and freeboard for each particle.

Table 6.5. Estimated dispersed liquid phase holdups at for the ebullated bed and freeboard.

$\varepsilon_{L,D}$	**L spheres**	**L cylinders**	**S spheres**	**S cylinders**
Ebullated bed region	0.047	0.036	0.167	0.103
Freeboard region	0.034	0.036	0.017	0.027

6.3.2.1. Impact of superficial gas velocity

Ebullated bed phase holdups while varying the gas flow rate for the 1.5 mm equivalent particles are presented in Figure 6.7. Prior to adding glycerol, coalesced bubble flow was observed in the bed region for both spheres and cylinders, resulting in the relatively large holdup standard deviations. Figure 6.7c shows an immediate increase in the solid holdups (i.e., bed contraction) for both spheres and cylinders following the introduction of gas in the fluidized bed. This behaviour has been previously noted for particles in this size range (Han et al., 1990), where entrained liquid in the wake of large/coalescing bubbles reduces the effective amount of liquid in the bed and thus liquid flow available for fluidization. Coalesced bubble flow can also be deduced by comparing the bed (Figure 6.7a) and freeboard (Figure 6.7b) gas holdups, where large bubbles in the bed region tended to breakup when entering the freeboard due to the reduced apparent fluid viscosity, resulting in higher gas holdups.

Fluid dynamic behaviour in the ebullated bed differed considerably after adding glycerol. An increased apparent particle size for the 1.5 mm glass beads was previously observed in the L-L-S fluidized bed due to agglomeration. Contrary to the G-L-S system, the introduction of gas resulted in bed expansion for the emulsion system, shown in Figure 6.7c, where further expansion was observed at higher gas flow rates. Agglomeration of the glass beads increased the particle inertia and resulted in bubble breakup in the bed region, hence the smaller wakes of dispersed bubbles were insufficient to produce the previously observed bed contraction. Fluid dynamics of the 1.5 mm aluminum cylinders did not deviate as significantly compared to the glass beads; nonetheless, glycerol addition still reduced the previously observed bed contraction. Similar to the L-L-S fluidized bed runs, an agglomerate size distribution was visually observed; however, the gas flow provided some mixing and reduced axial segregation based on agglomerate size. Gas holdups for both particles were similar before and after glycerol addition where differences may have resulted from the assumed glycerol holdups in the bed region. Freeboard gas holdups for both spheres and cylinders were higher in the emulsion due to the enhanced bubble breakup in the bed region.

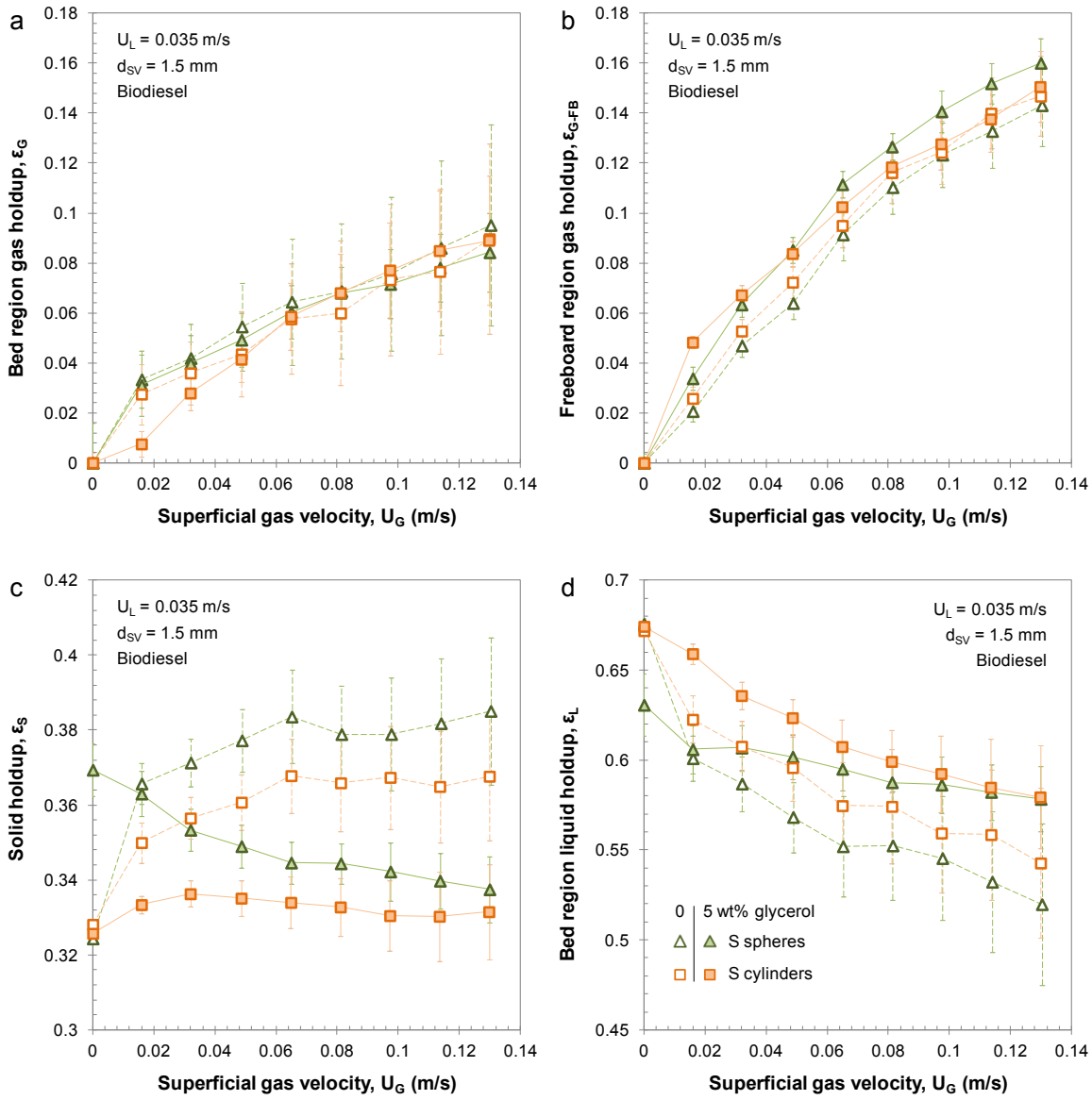

Figure 6.7. Effect of gas flow rate on the phase holdups in the gas-liquid-liquid-solid ebullated bed for the 1.5 mm equivalent particles.

The phase holdups as a function of gas flow rate for the 4 mm equivalent particles before and after glycerol addition are presented in Figure 6.8. When increasing the gas flow rate, the 4 mm particles initially resulted in dispersed bubble flow and eventually transitioned to coalescing flow. The previous was confirmed by the following observations: (i) bed expansion at the introduction and further increase of gas flow, (ii) slope reduction for the gas holdup as a function of superficial gas velocity (Figure 6.8a) due to the transition to

coalesced flow, and (iii) larger phase holdup standard deviations at higher gas flow rates due to the larger/coalescing bubbles. Prior to glycerol addition, the L spheres and L cylinders exhibited similar phase holdups for the studied range of operating conditions, in agreement with a previous study (Pjontek and Macchi, 2014).

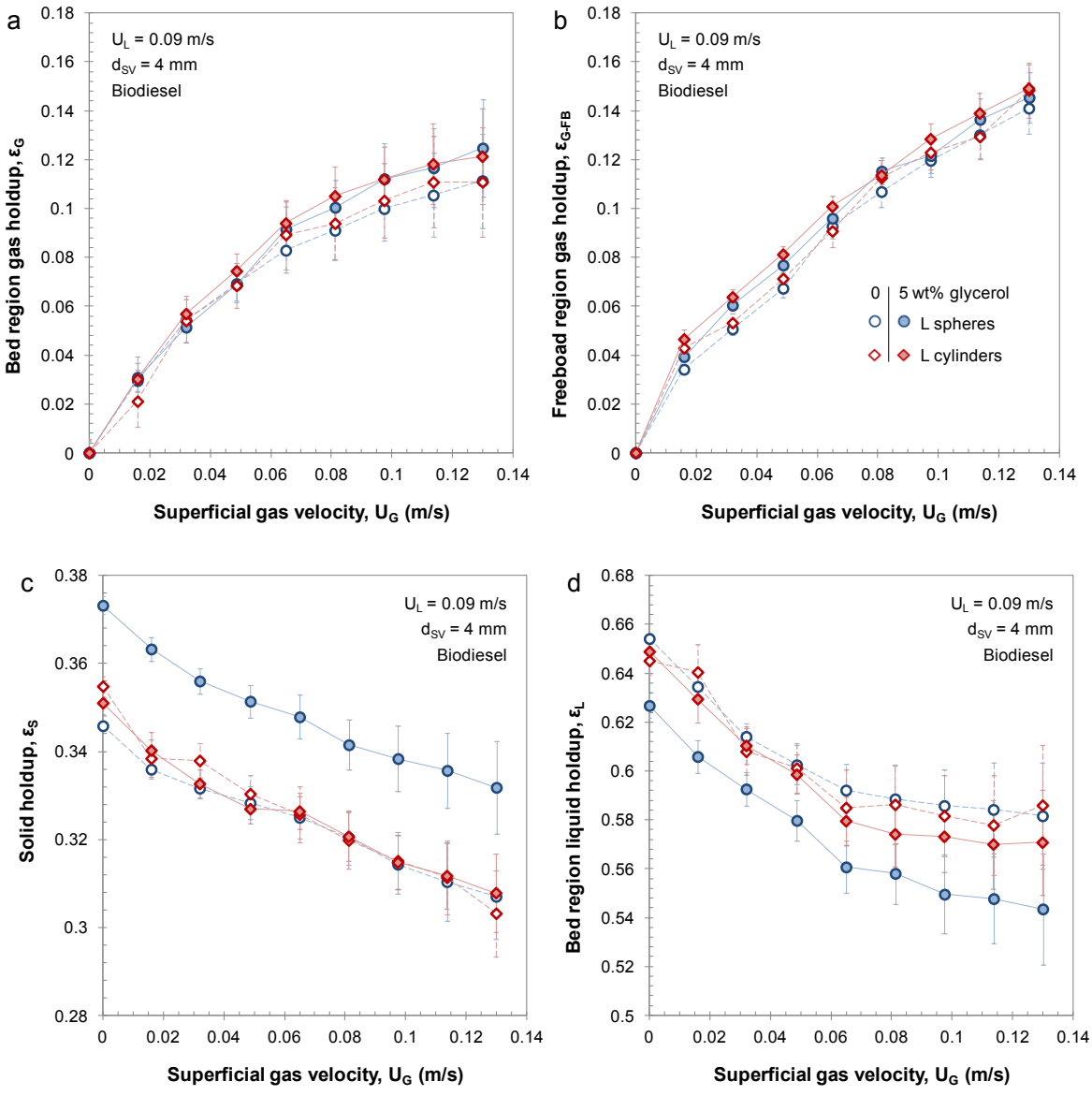

Figure 6.8. Effect of gas flow rate on the phase holdups in the gas-liquid-liquid-solid ebullated bed for the 4 mm equivalent particles.

Glycerol addition had a less considerable impact with the 4 mm equivalent particles when compared to the smaller particles. Similar to the L-L-S fluidized bed experiments, the L cylinder phase holdups, shown in Figure 6.8, were comparable before and after glycerol addition due to negligible agglomeration. The L spheres, however, were shown to agglomerate in the L-L-S fluidized bed. As dispersed bubble flow was obtained in the G-L-S ebullated bed with the 4 mm glass beads, the increased apparent particle size due to agglomeration mainly led to the reduced bed expansions shown in Figure 6.8c. Gas holdups were similar with or without particle agglomeration as the bubble flow regime did not significantly change. Bed region liquid holdups were reduced as a consequence of the bed contraction due to glycerol addition.

6.3.2.2. Impact of superficial liquid velocity

Figure 6.9 and Figure 6.10 present the effect of liquid flow on phase holdups for the 1.5 mm and 4 mm equivalent particles, respectively. The observed solid holdup reductions with increasing superficial liquid velocity were expected as greater drag on the particles resulted in increased bed expansion. This increased the void volume available for gas and liquid flow, where liquid holdups were consistently higher at greater liquid flow rates. The impact of liquid flow on bed region gas holdups was less intuitive. Figure 6.9b shows a minor gas holdup reduction in the freeboard with increasing liquid flow, indicating a bubble residence time reduction due to greater absolute rise velocities. Gas holdups in the ebullated bed for the 1.5 mm (Figure 6.9a) and 4 mm (Figure 6.10a) equivalent particles remained relatively constant and in some cases showed a slight increase with higher liquid flow. The previous demonstrated that gas holdup trends for the studied system were difficult to anticipate when varying the superficial liquid velocity as the subsequent bed expansion impacted interstitial fluid velocities and likely the bubble characteristics. By estimating the interstitial liquid velocities in the bed region, based on superficial liquid velocities and bed region liquid holdups, the local liquid velocities increased in the bed. It is thus believed that smaller bubble resulted due to increased liquid shearing, maintaining bed region gas holdups at the studied operating conditions.

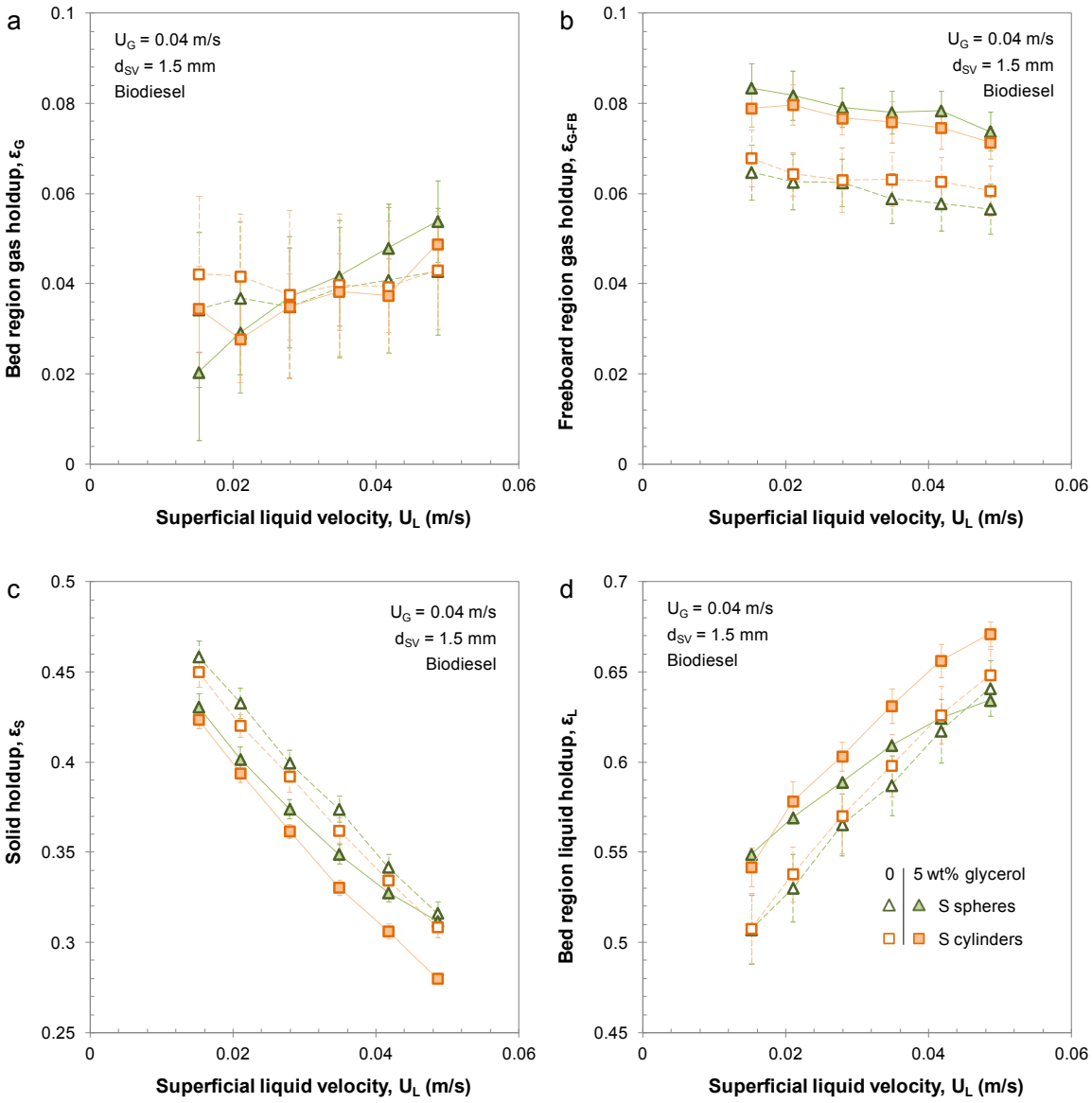

Figure 6.9. Effect of liquid flow rate on the phase holdups in the gas-liquid-liquid-solid ebullated bed for the 1.5 mm equivalent particles.

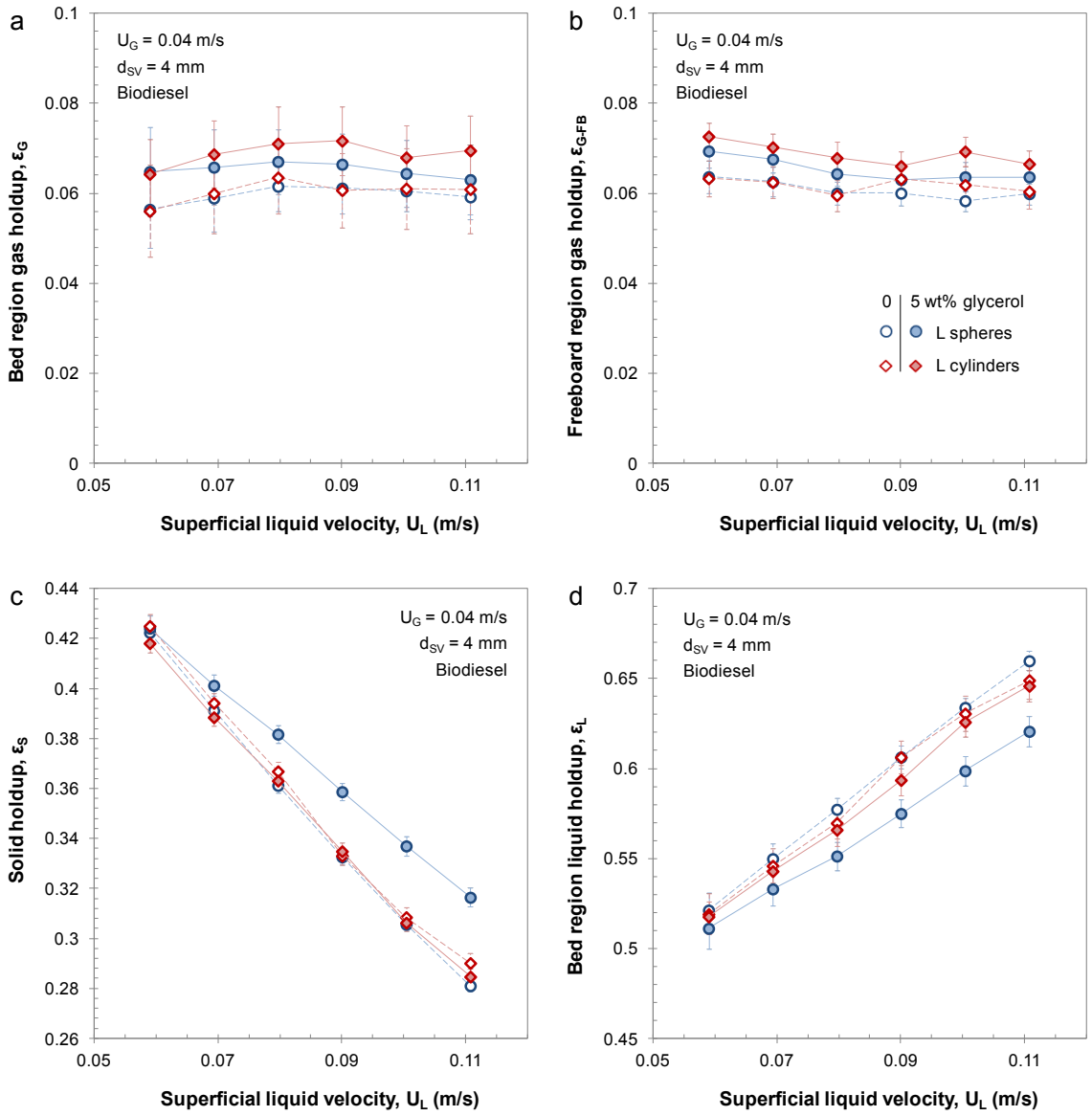

Figure 6.10. Effect of liquid flow rate on the phase holdups in the gas-liquid-liquid-solid ebullated bed for the 4 mm equivalent particles.

Effects of glycerol addition for the 1.5 mm and 4 mm equivalent particles were analogous to the previous section (refer to 6.3.2.1). It is interesting to note that Figure 6.10c shows an increasing deviation between the L spheres solid holdups before and after glycerol addition at higher liquid flow rates, similar to the L-L-S fluidized bed runs (shown in Figure 6.3b). The previous again demonstrated that agglomerate/apparent particle size likely increased at greater liquid flow rates. Agglomerate size estimates for the 1.5 mm equivalent

particles from the solid holdups were less evident due to the bed contraction or expansion observed at the introduction of gas before and after glycerol addition, respectively.

6.3.3. Gas-liquid-liquid-solid slurry bubble column

Measurements in a G-L-L-S slurry bubble column were carried out in the experimental system using glass beads of 100 to 150 μm in diameter to further study the impact of particle size on agglomeration. Axial solid holdup profiles were measured while the fluid dynamic behaviour was qualitatively observed. The quantity of slurry particles added to the system was selected to obtain a well mixed global solid holdup of approximately 0.04 (i.e., solid concentration of 100 kg/m^3) to ease particle suspension at the distributor. The quantity of glycerol added for these runs was based on preliminary tests in small containers which demonstrated that relatively small quantities of glycerol (volumetric concentrations lower than 1 wt.%) resulted in considerable clustering of the slurry glass beads.

Gas holdups in the slurry bubble column were calculated based on visual estimates of the slurry height at a given gas flow rate compared to the static liquid height. Figure 6.11 shows that gas holdups at two glycerol concentrations were comparable for the studied range of gas flow rates. Axial solid holdup profiles were estimated from the dynamic pressure profile:

$$\varepsilon_S = \frac{-\left(\Delta P/\Delta z\right)g^{-1} + \left(\rho_{L,C} - \rho_G\right)\varepsilon_G + \left(\rho_{L,C} - \rho_{L,D}\right)\varepsilon_{L,D}}{\rho_S - \rho_{L,C}} \tag{6.20}$$

Where glycerol holdups ($\varepsilon_{L,D}$) were assumed constant throughout the slurry bubble column. Although this assumption may be inaccurate, its impact on local solid holdups was negligible due to the low glycerol holdups of the studied system.

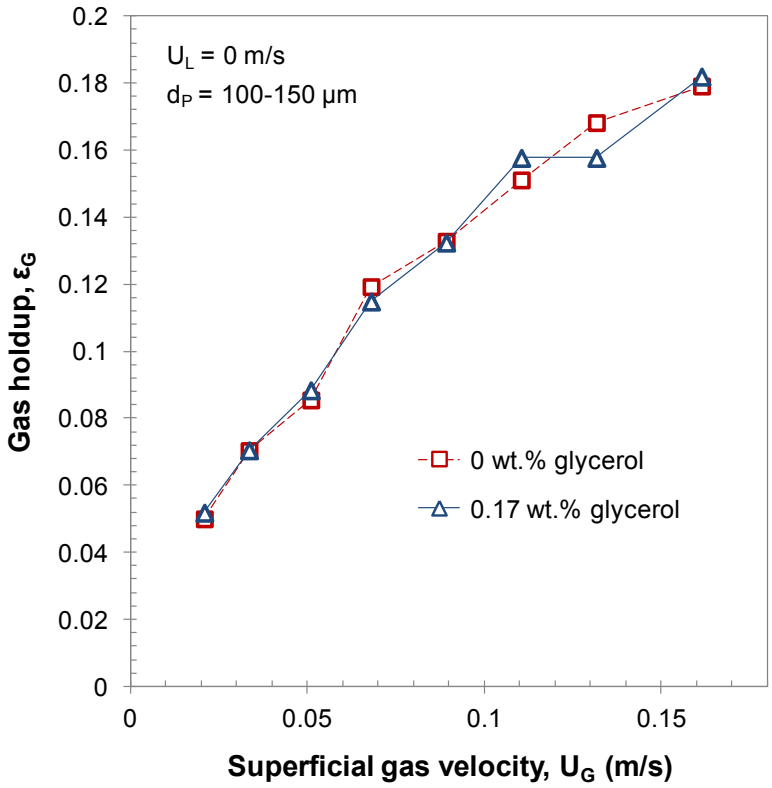

Figure 6.11. Gas holdups in the slurry bubble column as a function of superficial gas velocity.

Figure 6.12 compares the axial solid holdup profiles with no glycerol and for a total concentration of 0.17 wt.%. As the gas distributor (described in section 6.2.1) had an equal diameter to the column, suspension of the slurry particles was entirely dependent on gas flow through the particle bed at the bottom of the column. The slurry was fully suspended (i.e., no observable quantity of settled particles on the distributor) above a gas superficial velocity of approximately 0.016 m/s in pure biodiesel, similar to a prediction of 0.013 m/s based on the correlation provided by Koide et al. (1984). With 0.17 wt.% glycerol, partial sedimentation was observed at superficial gas velocities below approximately 0.07 m/s. Prior to glycerol addition, local solid holdups showed a somewhat decreasing trend along the axial length of the column, where the average was comparable to the concentration initially added to the system. Axial solid holdup profiles at 0.17 wt.% glycerol showed a greater decrease as a function of column height, indicating particle segregation based on agglomerate size. Although not presented, comparable results were obtained at other studied gas velocities

ranging from 0.07 to 0.16 m/s. Figure 6.13 demonstrates that agglomerates were readily observed after the gas flow was shut off for a total glycerol concentration of 0.17 wt.%.

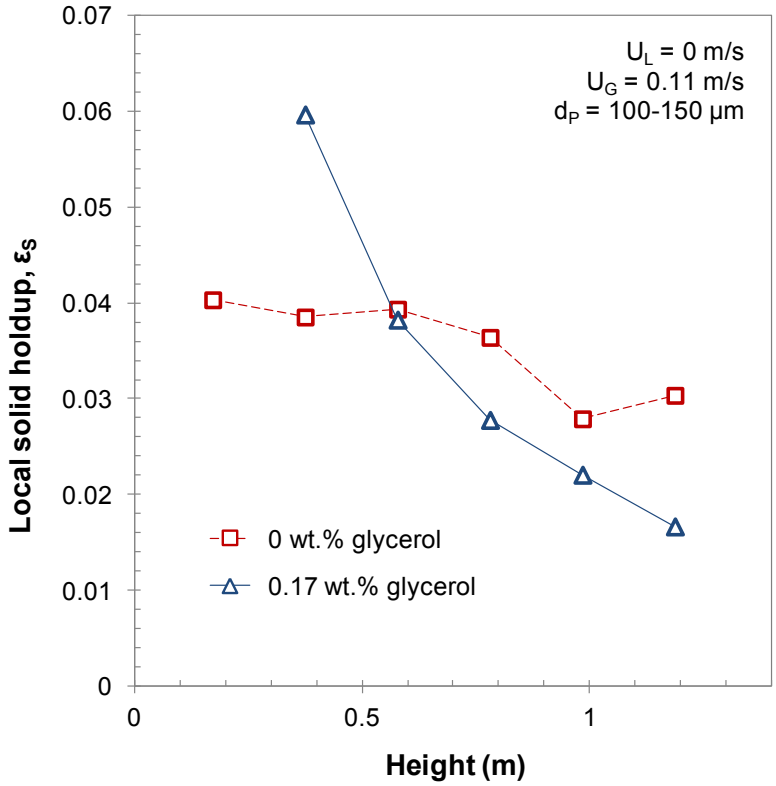

Figure 6.12. Axial solid holdup profile example in the slurry bubble column.

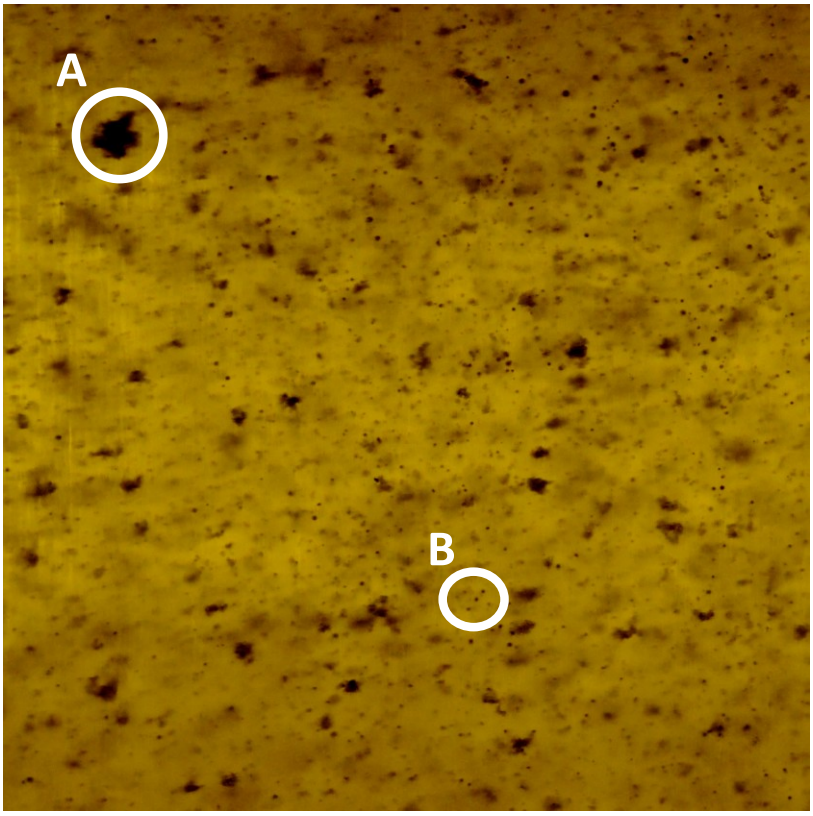

Figure 6.13. Photograph after gas shut off in the slurry bubble column (d_P: 100 to 150 μm, total glycerol concentration: 0.17 wt.%). (A) is a slurry agglomerate and (B) shows individual particles.

Glycerol addition considerably impacted the slurry particle suspension, as even at the lowest studied glycerol concentration (0.17 wt.%), high gas flow rates were required to initially suspend the slurry. Supplementary glycerol was added to the system up to a concentration of 0.7 wt.%; however, the slurry could not be properly suspended even at a relatively high gas flow rate ($U_G \approx 0.25$ m/s) for the studied system, shown in Figure 6.14. The previous was partly due to the flat distributor used in this study, where a conical geometry can be used in slurry bubble columns and may improve these issues by minimizing stagnant areas above the distributor. It should also be noted that local solid holdups at a column height of 0.17 m could not be estimated following glycerol addition as the lowest pressure port could not be properly drained due to particle agglomeration; the following port was thus used as a reference for the dynamic pressure drop measurements.

Figure 6.14. Particle sedimentation at $U_G \approx 0.25$ m/s for a total glycerol concentration of 0.7 wt.%.

6.4. Discussion on agglomeration

The experimental results in this study demonstrated that particle agglomeration due to a secondary immiscible liquid phase had a considerable impact on the fluid dynamics of gas-liquid-solid fluidized beds. Physical properties and/or operating conditions that enhance or inhibit particle agglomeration must be further examined. Relevant interparticle forces are discussed while the impacts of particle size, shape, material, as well as fluid properties are examined with respect to clustering behaviour. It should be noted that most equations provided in this section are based on the L-L-S system.

6.4.1. Interparticle forces

Particle agglomeration for the studied gas-liquid-liquid-solid fluidized beds can result from Van der Waals forces, electrostatic/Coulombic forces, and/or liquid bridging. Agglomeration from Van der Waals forces may occur at the microscopic scale due to attractive interactions between permanent dipoles (Keesom forces), permanent and induced dipoles (Debye forces), and dispersion forces of non-polar molecules (London dispersion

forces). Hamaker (1937) demonstrated that attractive forces would result for particles of the same material when submerged in a liquid. Van der Waals forces can have an impact on particles in the micron range, typically for diameters lower than 10 μm (Simons, 1996), where the slurry bubble column data demonstrated agglomeration mainly occurred after glycerol addition for 100 to 150 μm diameter particles. For particles in the mm range, differences between interparticle and intermolecular distances as well as surface irregularities render Van der Waals forces negligible compared to other interparticle interactions. Although these forces are always present, dispersion forces were not the cause of the experimentally observed agglomeration as the biodiesel-only system did not exhibit substantial clustering behaviour.

Electrostatic charges in fluidized beds can arise from triboelectrification, ion collection, thermionic emission, and frictional charging (Park and Fan, 2007), where charges in gas-solid fluidized beds are mainly generated from friction between the gas, particles, and reactor wall (Park et al., 2002; Sowinski et al., 2010). The attractive force between particles with dissimilar charge can be characterized by Coulomb's law. Park and Fan (2007) observed particle agglomeration due to electrostatic charging in a gas-liquid-solid fluidized bed consisting of air, Norpar15, and high density polyethylene (HDPE) particles with an average diameter of 4.1 μm. Interestingly, when 15 wt.% of a fine glass powder with an average diameter of 26.2 μm was added to the system, the initial static charge was reduced up to 72% within a few minutes. Similar to the Van der Waals forces, electrostatic charges were not the primary contributor to the agglomeration for this study as the behaviour was not observed prior to glycerol addition.

The collision of two particles which are surrounded by a layer of wetting liquid can lead to the formation of a liquid bridge between both particles. Interparticle attractive forces in a static system result from the liquid surface tension acting at the liquid-solid boundary and a difference in hydrostatic pressure due to the liquid bridge curvature (Simons et al., 1994). Buoyancy and gravitational effects on the liquid bridges can be considered depending on the particle size and liquid volume. The interfacial tensions and wetting characteristics of the fluid phases relative to the solid surfaces impact the relative strength of the static liquid bridges (Simons, 1996). In addition to the forces in a static system, dynamic forces must also be considered when particles bound by a liquid bridge are separated at a given relative

velocity due to viscous effects. For this study, the addition of a dispersed immiscible liquid led to the experimentally observed particle agglomeration, thus liquid bridging will be further discussed.

6.4.2. Particle wettability

The secondary dispersed liquid phase must first wet the particles in order for a liquid bridge to form. Wetting and spreading characteristics can be interpreted based on the contact angle (θ_C) of the dispersed liquid (L,D) on a solid surface (S) submerged in the continuous liquid (L,C), where the Young-Laplace equation for such a system is defined as follows:

$$\gamma_{S-L,C} = \gamma_{S-L,D} + \gamma_{L,D-L,C} \cos\theta_{C(L,D-L,C-S)} \tag{6.21}$$

Relative surface energies (γ) of the three phase system based on the contact angles indicate which phase preferentially wets the solid, and hence the likelihood of a dispersed liquid film on the particles. If the contact angle defined in Eq. (6.21) is below 90°, indicating that the dispersed liquid phase readily wets the static solid surface, this implies that more energy is needed to remove the liquid-solid interface than is required to create it. It should however be noted that a contact angle above 90° implies that additional energy would be required for the dispersed phase to wet the particle surface, where energy dissipation due to liquid and gas flow in an ebullated bed may influence the wetting characteristics.

6.4.2.1. Contact angles for the studied system

As the primary interparticle force leading to the experimentally observed agglomeration resulted from liquid bridging, the liquid-liquid-solid surface energies are a suitable initial consideration. The formation of liquid bridges between particles requires that the dispersed liquid phase is capable of wetting the particle surface. Contact angles for the L-L-S systems were approximated by measuring the biodiesel and glycerol contact angles in air on non-porous borosilicate glass and aluminum 1100 surfaces using a VCA Optima (AST Products) instrument (examples are provided in Figure 6.15). Based on the gas-liquid and liquid-liquid surface tensions (refer to Table 6.2) as well as G-L-S contact angle

measurements, the L-L-S contact angles were estimated by combining Eq. (6.21) for G-L-S and L-L-S systems:

$$\theta_{C(L,D-L,C-S)} = \cos^{-1}\left(\frac{\gamma_{Air-L,D}\cos\theta_{C(L,D-Air-S)} - \gamma_{Air-L,C}\cos\theta_{C(L,C-Air-S)}}{\gamma_{L,C-L,D}}\right) \tag{6.22}$$

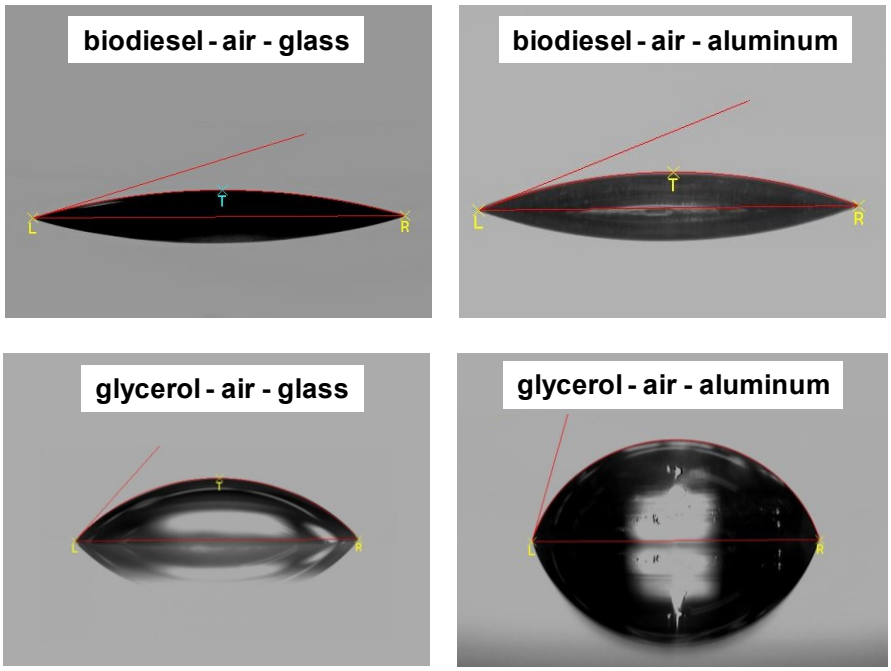

Figure 6.15. Examples of biodiesel and glycerol contact angle measurements in air on borosilicate glass and aluminum 1100.

Table 6.6 provides the contact angles for the studied experimental system, where uncertainties were estimated from repeated measurements. The estimated glycerol contact angle on glass submerged in biodiesel was lower than 90° based on the Sessile drop method, indicating that liquid bridges were likely formed. This estimate corroborates the fluidized bed experimental results as the glass beads agglomerated to a greater extent compared to the aluminum cylinders (demonstrated in Figure 6.4). Since the estimated glycerol contact angle on the aluminum 1100 surface was approximately 103°, it could be initially considered that liquid bridging would not occur, as observed with the larger aluminum cylinders. Agglomeration nonetheless occurred with the smaller aluminum cylinders, though to a lesser

extent when compared to the 1.5 mm glass beads. Estimated contact angles for the aluminum surface suggest that additional energy (e.g., shearing due to particle contact through the fluidized bed and via gas/liquid flow) could have resulted in the glycerol wetting the particles. The previous is believed to have been observed with the smaller aluminum cylinders in the L-L-S fluidized bed (Figure 6.4) as the higher bed region glycerol holdups observed at lower liquid flow rates are thought to have resulted from the droplet shearing when flowing through the fluidized bed. Relative surface energies between the continuous liquid, dispersed liquid and solid in a static system thus provide initial physical characteristics to consider for particle agglomeration; nonetheless, differences between static and dynamic systems must be considered when investigating a fluidized bed as a dynamic system may still exhibit agglomeration for contact angles above 90°.

Table 6.6. Measured and estimated contact angles for biodiesel and glycerol on glass and aluminum surfaces.

Contact angle	Borosilicate glass	Aluminum 1100
$\theta_{C(L,C-Air-S)}$	16.8 ± 0.6°	20.9 ± 1.6°
$\theta_{C(L,D-Air-S)}$	47.4 ± 2.9°	74.4 ± 2.0°
$\theta_{C(L,D-L,C-S)}$	75.2 ± 1.1°	103.4 ± 2.4°

6.4.3. Liquid bridging

Binding forces due to the formation of liquid bridges between particles are typically characterized based on two equally sized spheres in a static system (Seville et al., 2000; Simons et al., 1994), while unequal spheres have also been investigated (Lian et al., 1998). Figure 6.16 illustrates some of the relevant geometric parameters to estimate the static liquid bridge force (F_{static}) based on the sum of the liquid-solid surface tension forces as well as the hydrostatic pressure reduction (ΔP) at the center of the liquid bridge (Seville et al., 2000):

$$F_{static} = 2\pi r_2 \gamma_{L,C-L,D} + \pi r_2^{\,2} \Delta P \tag{6.23}$$

The curvature of the liquid bridge, related to r_1 and r_2, must satisfy the Young-Laplace equation:

$$\Delta P = \gamma_{L,C-L,D}\left(\frac{1}{r_1}+\frac{1}{r_2}\right) \tag{6.24}$$

The static liquid bridge force is thus dependent on the simultaneous solution of Eqs. (6.23) and (6.24), where r_1 and r_2 are variables related to the liquid volume of the bridge. The attractive force originates from the deformation of the liquid surface, which should be flat in the absence of particles. Larger interfacial deformations between particles indicate stronger capillary interactions (Birdi, 2008), as liquid bridge curvature is related to wetting properties at the solid surfaces (i.e., increased curvature is associated with a lower contact angle). Solutions incorporating the liquid bridge curvature can be found in the literature (Lian et al., 1998; Pitois et al., 2000; Simons et al., 1994); however, the provided relations are sufficient for this discussion as fluid and particle properties impacting agglomeration in the ebullated bed are qualitatively examined.

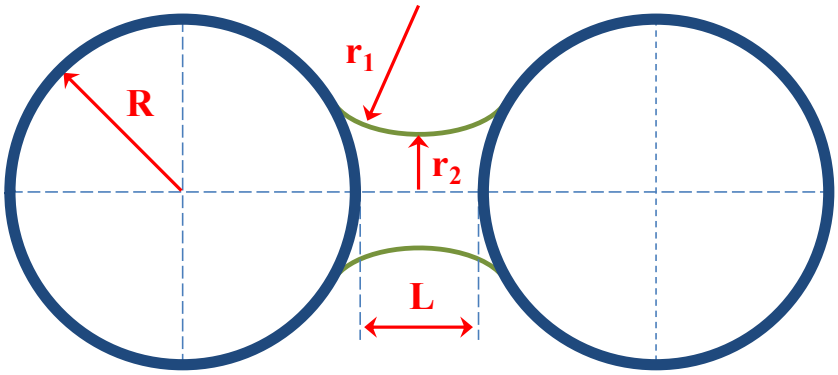

Figure 6.16. Geometric parameters for liquid bridging between two equally sized spheres.

An expression for the viscous forces ($F_{dynamic}$) acting on the spheres, which opposes the relative movement between particles, has been previously estimated based on the pressure generated in a liquid relative to the displacement of two solids, assuming an infinite liquid (Cameron, 1966; Pitois et al., 2000):

$$F_{dynamic} = \frac{3}{2}\pi\mu_{L,D} R^2 \frac{1}{L}\frac{dL}{dt} \tag{6.25}$$

Increasing the dispersed phase viscosity ($\mu_{L,D}$) thus results in a greater dynamic binding force for a liquid bridge. Mazzone et al. (1987) showed that increasing the binder viscosity for a given relative velocity (dL/dt) can result in viscous forces up to 200 times that of the liquid bridging static forces.

Eqs. (6.23), (6.24) and (6.25) demonstrate that attractive forces due to liquid bridging for static and dynamic systems are primarily dependent on the surface tension and dispersed liquid viscosity, respectively. Another important consideration for liquid bridging is the likelihood that a particle collision, where both particles are coated with the dispersed liquid, would result in the formation of a cluster. Ennis et al. (1991) established that viscous forces dominated under these circumstances, justifiably as the system is dynamic, and related the particle agglomeration for two equally sized spheres to a viscous Stokes number (St_v) which is dependent on the solid density (ρ_S), collision velocity (v_C), particle radius (R) and dispersed liquid viscosity ($\mu_{L,D}$):

$$St_v = \frac{8\rho_S v_C R}{9\mu_{L,D}} \tag{6.26}$$

The viscous Stokes number can then be compared to a critical viscous Stokes number (St_v^*) which is related to the particle coefficient of restitution (e), dispersed liquid phase layer thickness (δ) and characteristic length of surface asperities (h_a).

$$St_v^* = \left(1+\frac{1}{e}\right)\ln\left(\frac{\delta}{h_a}\right) \tag{6.27}$$

Three granulation regimes were defined based on the comparison of St_v and St_v^* (Simons and Fairbrother, 2000):

(i) non-inertial regime ($St_v << St_v^*$) : all collisions result in agglomeration.

(ii) inertial regime ($St_v \approx St_v^*$) : some collisions result in agglomeration.

(iii) coating regime ($St_v >> St_v^*$) : collisions do not result in agglomeration.

It is challenging to appropriately carry out the previous comparison as many of the parameters are difficult to estimate for the studied gas-liquid-liquid-solid fluidized beds (e.g., dispersed liquid phase layer thickness, collision velocity, and characteristic length of surface asperities). Nonetheless, it allows for a qualitative analysis of the fluid properties, particle characteristics and operating conditions for this study.

6.4.3.1. Relevant experimental properties for liquid bridging

Eqs. (6.23) and (6.24) indicate that a lower contact angle for the dispersed phase (i.e., increased liquid bridge curvature) would increase the binding force of static liquid bridges, confirming the increased agglomeration of the glass beads compared to the aluminum cylinders. The impacts of the dispersed liquid phase viscosity and particle size must then be considered for a dynamic system such as a gas-liquid-solid fluidized bed. The dispersed liquid viscosity increases the probability of forming agglomerates as well as the resistance to particle separation once a liquid bridge has been formed. Greater liquid binder viscosity reduces the viscous Stokes number, shown in Eq. (6.26), thus increasing the probability that colliding particles will agglomerate based on a comparison with the critical viscous Stokes number. The liquid bridge viscous force that opposes the separation of agglomerated particles, expressed in Eq. (6.25), is also proportional to the dispersed liquid viscosity. The dynamic liquid bridge force due to the separation of agglomerated particles is believed to cause the increased apparent particle size observed with greater liquid flow rates.

Increasing the particle size, and hence the particle mass, results in greater inertia, augmenting the viscous Stokes number and lowering the probability of agglomerate formation. Experimental results agreed with the previous theoretical prediction as indicated by the estimated bed region glycerol holdups (Figure 6.4) as well as the particle sedimentation in the slurry bubble column at relatively low glycerol concentrations (Figure 6.14). Although Eq. (6.25) indicates that a larger particle radius would increase the liquid

bridge viscous force, it should be noted that the previous expression assumes an infinite liquid, where the dispersed liquid loading must also be considered.

The impact of particle shape on clustering unfortunately could not be directly investigated with the experimental results of this study. The particle density was selected to study both the dispersed and coalescing bubble flow regimes for particles in the range of 1 to 4 mm, limiting material selection for spheres and cylinders of equivalent Sauter mean diameter. Varying wetting characteristics for both materials thus had a more considerable impact on agglomeration tendencies compared to spherical or cylindrical shapes. Based on theoretical predictions, the maximum static liquid bridge force occurs at particle contact due to the toroidal approximation proposed by Fisher (1926), where r_1 is assumed constant for the liquid bridge. In addition, studies in the literature that have developed relations for the binding force between two cylinders with a liquid bridge (Shinto et al., 2007; Urso et al., 1999; Virozub et al., 2009) express the force (summation of the interfacial tension and asymmetrical hydrostatic pressure) per unit length of the liquid bridge. It is also interesting to note that Virozub et al. (2009) predicted that cylinders would align themselves due to torque from the liquid bridge, which was experimentally observed (shown in Figure 6.5). Based on the previous theoretical predictions, it is thus believed that cylindrical particles would have a greater tendency to agglomerate compared to spheres of the same material primarily due the increased contact area between cylinders.

6.5. Conclusions

The impact of particle size on agglomeration was investigated with 4 and 1.5 mm diameter glass spheres in an ebullated bed as well as with 100 to 150 μm in diameter glass beads in a slurry bubble column. Particle shape and material effects were qualitatively studied via comparison with aluminum cylinders of equivalent Sauter mean diameters (d_{SV} of 1.5 and 4 mm). Fluid properties (wetting characteristics of both liquids), particle properties (size, shape, and material) and operating conditions (relative particle velocities) were shown to impact the agglomeration behaviour in gas-liquid-liquid-solid fluidized beds.

Estimated bed expansion parameters in a L-S fluidized bed with biodiesel indicated that the 1.5 mm and 4 mm equivalent particles were in the intermediate settling flow regime

($0.2 < Re_{LT\infty} < 500$), demonstrating competing effects between particle inertia and fluid viscous forces. For the 1.5 mm glass beads ($Re_{LT\infty} = 42$), glycerol holdups in the bed region were estimated up to approximately 25 wt.%, in agreement with the experimentally observed bed contraction due to increased apparent particle size. The 4 mm glass beads ($Re_{LT\infty} = 235$) agglomerated to a lesser extent compared to the smaller glass beads, indicating an influence of particle inertia. An axial agglomerate size distribution was observed with the smaller aluminum cylinders ($Re_{LT\infty} = 62$), while the larger aluminum cylinders ($Re_{LT\infty} = 268$) did not exhibit clustering. The reduced agglomeration behaviour of aluminum particles was attributed to the reduced wettability of the material with respect to the dispersed glycerol.

In the gas-liquid-liquid-solid ebullated bed, the 1.5 mm glass beads transitioned from coalesced to dispersed bubble flow after glycerol addition due to increased particle inertia from clustering. Dispersed bubble flow was obtained with the 4 mm glass beads prior to the addition of glycerol; the ebullated bed expansion was thus reduced due to particle clustering while gas holdups remained approximately constant. The 100 to 150 μm diameter glass bead slurry bubble column was inoperable at a relatively low glycerol concentration of 0.7 wt.%, further illustrating the impact of particle size. Similar to the L-L-S fluidized bed, the larger aluminum cylinders did not agglomerate in the G-L-L-S ebullated bed. For the 1.5 mm equivalent aluminum cylinders, gas flow reduced the previously observed axial agglomerate size distribution.

Experimental results and associated literature indicated that attractive forces due to liquid bridging between fluidized particles led to the observed particle agglomeration. Relative surface energies (i.e., contact angles) between the solid, dispersed liquid, and continuous liquid were found to be an initial indicator for particle agglomeration. For a system where the dispersed phase can wet the particles, liquid bridging in a static system is mainly related to the interfacial tensions acting between the binding liquid and solid surfaces, while viscous forces which oppose the separation of agglomerated particles may have a significant impact in dynamic systems.

Acknowledgments

The authors are grateful to Pellets LLC for manufacturing the aluminum cylindrical particles. The authors would like to acknowledge the Natural Sciences and Engineering Research Council of Canada, the Canadian Foundation for Innovation, the Ontario Innovation Trust and Syncrude Canada Ltd. for financial support.

Nomenclature

AAE	average absolute error, $AAE = (1/n)\sum_{i=1}^{n}\left\|y_{i,pred} - y_{i,exp}\right\|$
Ar_L	liquid Archimedes number, $Ar_L = \rho_L(\rho_S - \rho_L)g\,d_P^{\,3}/\mu_L^{\,2}$
d_C	column inner diameter (m)
d_P	particle diameter (m)
d_{SV}	Sauter mean diameter (m)
d_V	volume equivalent diameter (m)
e	coefficient of restitution
F_{static}	static liquid bridge force (N)
$F_{dynamic}$	dynamic liquid bridge force (N)
g	gravitational acceleration (m/s^2)
h_a	characteristic length of surface asperities (m)
h_B	bed height (m)
k	wall effect for bed expansion correlation
L	particle separation distance (m)
L_P	particle length (m)
m	fluidized mass of particles (kg)
m_i	number of data points in the i'th measurement
n	index for bed expansion correlation
N	number of dynamic pressure drop mean values in the bed or freeboard
P	pressure (Pa)
r_1	liquid bridge meridional radius of curvature (m)
r_2	liquid bridge neck radius (m)

R	particle radius (m)
$Re_{LT\infty}$	liquid-particle Reynolds number based on terminal free settling velocity, $Re_{LT\infty} = U_{LT\infty} \rho_L d_P / \mu_L$
s	standard deviation
s_P^2	pooled variance
St_v	viscous stokes number
St_v^*	critical viscous stokes number
T	Temperature (°C)
U_G, U_L	gas and liquid superficial velocities (m/s)
U_{LT}	terminal settling velocity of a particle, accounting for wall effects (m/s)
$U_{LT\infty}$	terminal free settling velocity of a particle (m/s)
v_C	collision velocity (m/s)
Δz	vertical distance between differential pressure taps (m)

Greek symbols

β_0	dynamic pressure profile intercept
β_1	dynamic pressure profile slope
γ	interfacial tension (N/m)
δ	dispersed liquid phase layer thickness (m)
ε	bed void fraction
ε_G, ε_L, ε_S	gas, liquid and solid holdups in the bed region
ε_{G-FB}	freeboard gas holdup
θ_C	contact angle (°)
κ	ratio of dispersed phase viscosity to continuous phase viscosity
λ	cubic root of the dispersed phase volumetric fraction in the emulsion
$\mu_{L,C}$, $\mu_{L,D}$	continuous and dispersed liquid viscosity (Pa · s)
$\mu_{L,E}$	emulsion viscosity (Pa · s)
$\rho_{L,C}$, $\rho_{L,D}$	continuous and dispersed liquid densities (kg/m^3)
$\rho_{L,E}$	emulsion density (kg/m^3)

ρ_G , ρ_S	gas and solid densities (kg/m^3)
ϕ	sphericity

Subscripts

B	bed
C	continuous
D	dispersed
E	emulsion
FB	freeboard
G	gas
L	liquid
S	solid

Chapter 7

Conclusions and recommendations

Ebullated bed hydroprocessing fluid dynamics are difficult to investigate on-site due to their operating conditions (i.e., require materials that can withstand elevated temperatures and pressures) and restricted measurement techniques (i.e., conventional methods are typically not suitable and required properties such as the solid inventory and/or density are not well-known during operation). The main objective of this doctoral thesis was to investigate the fluid dynamics of an ebullated bed hydroprocessor following an increased vacuum distillation tower bottoms feed fraction. Studies were therefore carried out in an experimental system by first scaling-down the high gas holdup conditions based on relevant phase physical properties and operating conditions. Dynamic similarity for the previous conditions was assumed for systems which shared important geometric characteristics (i.e., gas-liquid distribution into the ebullated bed and gas-liquid separation in the freeboard), had equivalent fluid flow regimes (i.e., dispersed bubble flow via enhanced bubble break-up and significant bubble coalescence inhibition), and matched the following dimensionless groups:

- particle-liquid Reynolds number $(Re_{S-L} = \rho_L \, d_{SV} \, U_L / \mu_L)$
- particle-liquid Archimedes number $(Ar_{S-L} = \rho_L \, d_V \, g(\rho_S - \rho_L) / \mu_L^{\,2})$
- gas-liquid density ratio (ρ_G / ρ_L)
- solid-liquid density ratio (ρ_S / ρ_L)
- gas-liquid superficial velocity ratio (U_G / U_L)
- binary bubble coalescence behaviour (coalescing or coalescence inhibition)

Base-case simulation conditions resulted in an ebullated bed of nitrogen, 0.5 wt.% aqueous ethanol, and aluminum cylinders (Sauter mean particle diameter (d_{SV}) of 3.9 mm and sphericity of 0.8) operating at a pressure of 6.5 MPa and a gas-to-liquid superficial velocity ratio of 0.78.

When comparing 4 mm and 1.5 mm glass spheres to aluminum cylinders with equivalent Sauter mean diameters, liquid-solid fluidized bed porosities indicated similar

hydrodynamic behaviour. The larger equivalent spheres and cylinders showed comparable gas-liquid-solid fluidized bed phase holdups in water (phase holdup average absolute deviation (AAD) < 2.6%) and in 0.5 wt.% aqueous ethanol (phase holdup AAD < 1.1%), validating the use of the Sauter mean particle diameter to account for particle shape effects at the simulation conditions (i.e., high gas holdups). Discrepancies were observed for the 1.5 mm equivalent spheres and cylinders in water (phase holdup AAD < 5.5%) due to the larger/coalescing bubbles in the bed region and differing bed contraction behaviour at the introduction of gas. As expected, particle shape did not have a significant effect on the freeboard gas holdups. The experimental operating conditions of the particle shape study included the LC-Finer^{SM} base-case simulation conditions, resulting in the following overall phase holdups:

- Bed region gas, liquid, and solid holdups of 0.28, 0.40, and 0.32, respectively.
- Freeboard region gas and liquid holdups of 0.36 and 0.64, respectively.

High gas holdup conditions were achieved with satisfaction, particularly when considering that the previous conditions do not consider gas entrainment in the recycle pan.

Local bubble characteristics at the simulation conditions were then investigated using a custom made monofibre optical probe, suitable for gas-liquid flow at elevated pressures. A comparison between local radial profiles and global gas holdups confirmed the probe measurements in water (average and maximum relative errors of 9% and 16%, respectively), while measurements at the center of the column validated its use up to 9.0 MPa. Experiments demonstrated that increased operating pressure and gas-liquid shearing through the distributor plate enhanced bubble break-up, leading to dispersed bubble flow at higher gas velocities in water (i.e., coalescing system). Conversely, the surfactant addition required for the simulation conditions hindered the optical probe measurements, where local radial profiles underestimated global gas holdups (average and maximum relative errors of 37% and 61%, respectively). It is believed that the probe struggled in the 0.5 wt.% aqueous ethanol due to the blinding effect (improper tip dewetting) from significantly reduced bubble sizes. For the previous system, visually observed back-mixing of the smaller bubbles is also believed to have hindered local measurements due to a wider distribution of impact angles with the probe tip. Nonetheless, local rise velocity and chord length cumulative fractions

corresponded with global trends for both water and 0.5 wt.% aqueous ethanol, demonstrating the impact of operating pressure, fluid shearing through the distributor, and coalescence inhibition from surfactant addition when simulating high gas holdup conditions.

The scaling approach was investigated by comparing the overall phase holdups for smaller and larger cylindrical particles (d_{SV} of 1.6 and 3.9 mm) at matching dimensionless groups. Results were comparable when bubble coalescence was consistently and sufficiently inhibited; however, the comparison was inconclusive for a coalescing system as the carboxymethyl cellulose addition to water resulted in some surface-active characteristics. When increasing the liquid viscosity of the 0.5 wt.% aqueous ethanol, a fraction of the gas was entrained in the liquid recirculation due to inadequate foam dissipation at the free-surface. It is interesting to note that the freeboard gas holdups obtained with the gas recirculation (i.e., freeboard gas holdup of 0.48 for a gas entrainment of approx. 15 vol.%) were comparable to industrial measurements provided by McKnight et al. (2003). Freeboard gas holdups for the coalescing and coalescence inhibition systems were on average 23% and 28% greater than bed region gas holdups, respectively. When estimating the freeboard gas holdup from a solids-free basis in the ebullated bed, the average absolute relative errors for water and 0.5 wt.% aqueous ethanol were 61% and 29%, respectively, due to enhanced bubble break-up or coalescence from the presence of particles. Correlations for the bed and freeboard phase holdups were developed based on the proposed dimensionless groups, providing satisfactory predictions at the simulation conditions.

The potential impact of mesophase formation in an ebullated bed hydroprocessor was investigated in a non-simulating system using nitrogen, biodiesel (continuous liquid), glycerol (dispersed liquid), and various particles. Glycerol addition in a bubble column reduced the overall gas holdups, where dynamic gas disengagement profiles indicated increased large bubble holdups while the small and micro bubble holdups were reduced. Liquid-liquid-solid fluidized bed expansions were reduced following particle agglomeration due to interparticle liquid bridging, contrasting the impact of increased overall liquid viscosity. Estimated glycerol holdups in an ebullated bed (total system concentration of 5 wt.%) were higher for 1.5 mm glass spheres (approx. 25 wt.%) when compared to 4 mm glass beads (approx. 6.5 wt.%), indicating an influence of particle inertia on agglomeration tendencies. Coalesced bubble flow in the ebullated bed was initially observed with the

smaller glass beads (1.3 and 1.5 mm); however, glycerol addition resulted in dispersed flow due to increased particle inertia from clustering. When qualitatively investigating the impacts of particle shape and material, an axial agglomerate size distribution was observed with the smaller aluminum cylinders (d_{SV} = 1.6 mm) whereas the larger aluminum cylinders (d_{SV} = 3.9 mm) did not cluster. The agglomeration tendencies of the aluminum cylinders was lower compared to the glass spheres, which was attributed to the lower material wettability with respect to dispersed glycerol when submerged in biodiesel. Relative surface energies between the solid, dispersed liquid, and continuous liquid were consequently found to be an initial indicator for particle agglomeration in ebullated beds. Interparticle liquid bridging in static systems is mainly related to the interfacial tensions between the binding liquid and solid surfaces, while viscous forces, which oppose the separation of agglomerated particles, may considerably affect dynamic systems.

7.1. Recommendations and future work

McKnight et al. (2003) identified gas holdup reduction in the LC-Finer^{SM} as a key objective to improve the unit performance. Experimental observations indicated that the inlet hydrogen flow rate should be kept as low as possible since the gas holdup was highly dependent on the superficial gas velocity at the simulation conditions. The impact of varying liquid flow on the overall gas holdups was less straightforward at the simulation condition, where it must considered that the liquid recycle pump speed maintains the bed height in the industrial unit. Experiments demonstrated that increased liquid flow can result in higher liquid holdups, assuming complete gas-liquid separation, due to the ensuing gas and solid holdup reductions. However, when gas recirculation was observed in the experimental unit, increased liquid flow resulted in a negligible change to the bed and freeboard gas holdups as the gas-liquid separation efficiency was reduced. Measurements in the industrial unit indicated a similar trend when increasing the recycle pump speed (McKnight et al., 2003).

The gas-liquid separation above the ebullated bed consequently has a significant impact on the overall gas and liquid holdups in the industrial ebullated bed. Recycle pan improvements will be studied in the future using a combination of local bubble measurements in the experimental system and computational fluid dynamic (CFD) studies.

Unfortunately, the studied monofibre optical probe could not accurately measure the desired bubble properties at the simulation conditions due to the significantly reduced bubble sizes. A modified optical probe with a smaller tip diameter could improve the measurements at high gas holdups as the probe may have been limited by its physical dimensions. It is also important to note that experiments at high gas holdups demonstrated that global and local holdups above an ebullated bed were similar to results obtained in the bubble column at matching operating conditions. Invasive devices could therefore be initially tested at these conditions in a bubble column, minimizing the risk of damaging the device. In addition, the dynamic gas disengagement method could be combined with local measurements to further study the bubble size and rise velocity relationship, required to validate CFD simulations.

Experiments demonstrated that an increased vacuum distillation tower bottoms feed fraction would mostly impact the fluidization behaviour and gas-liquid separation in the freeboard. The modified liquid properties (i.e., increased liquid viscosity) could lead to an ebullated bed expansion. However, since catalyst addition and withdrawal rates are manipulated to maintain the desired recycle pump speed and bed position, reduced solid holdups in the industrial unit (i.e., diluted bed) could be observed for a more viscous liquid feed. Potential issues arising from bed dilution may be improved by studying and modifying the catalyst properties. An increased vacuum residue feed fraction may also hinder the recycle pan separation efficiency (e.g., liquid drainage rate between two adjacent bubbles is inversely proportional to the liquid viscosity). As such, the impact of the modified liquid properties on the gas-liquid separation could be investigated experimentally and/or using CFD simulations.

The mesophase studies provided interesting fluid dynamics trends following the formation of interparticle liquid bridges in an ebullated bed. Considerable mesophase formation, possibly due to a temperature increase in the reactor, could lead to a collapse of the ebullated bed, assuming the additional liquid phase results in particle agglomeration. Future research could investigate whether mesophase readily wets the alumina catalyst at industrially relevant conditions, possibly using an experimental setup similar to Bagheri et al. (2012). In addition, the impact of other relevant particle properties (e.g., porosity, pore size and size distribution, particle size distribution, and particle density distribution) could be

investigated to better understand the forces related to agglomerate size and stability in an ebullated bed.

Lastly, the fundamental understanding and/or identification of physical properties to characterize bubble coalescence and break-up mechanisms in multi-component liquids and industrial relevant operating conditions should be further studied. Although the binary consideration (i.e., coalescing or significant coalescence inhibition) resulted in the desired high gas holdup conditions, these mechanisms have a major impact on the design and optimization of many multiphase systems.

References

Abel, R., Resch, F.J., 1978. A method for the analysis of hot-film anemometer signals in two-phase flows. Int. J. Multiph. Flow 4, 523–533.

Ancheyta, J., Speight, J.G., 2007. Hydroprocessing of Heavy Oils and Residua CRC Press.

Argüelles, C., Yépez, M.M., Sáez, A.E., 1993. Hydrodynamics of Bubble Columns with Two Immiscible Liquid Phases. Chem. Eng. Commun. 122, 201–212.

Bagheri, S.R., Gray, M.R., Shaw, J.M., McCaffrey, W.C., 2012. In Situ Observation of Mesophase Formation and Coalescence in Catalytic Hydroconversion of Vacuum Residue Using a Stirred Hot-Stage Reactor. Energy & Fuels 26, 3167–3178.

Barrau, E., Rivière, N., Poupot, C., Cartellier, A., Riviere, N., 1999. Single and double optical probes in air-water two-phase flows: real time signal processing and sensor performance. Int. J. Multiph. Flow 25, 229–256.

Begovich, J.M., Watson, J.S., 1978. Hydrodynamic characteristics of Three-Phase Fluidized Beds, in: Fluidization. Cambridge University Press, pp. 190–195.

Behkish, A., Lemoine, R., Oukaci, R., Morsi, B.I., 2006. Novel correlations for gas holdup in large-scale slurry bubble column reactors operating under elevated pressures and temperatures. Chem. Eng. J. 115, 157–171.

Behkish, A., Lemoine, R., Sehabiague, L., Oukaci, R., Morsi, B.I., 2007. Gas holdup and bubble size behavior in a large-scale slurry bubble column reactor operating with an organic liquid under elevated pressures and temperatures. Chem. Eng. J. 128, 69–84.

Birdi, K.S., 2008. Handbook of surface and colloid chemistry. CRC Press, Boca Raton, FL.

Boyer, C., Duquenne, A.-M.M., Wild, G., 2002. Measuring techniques in gas–liquid and gas–liquid–solid reactors. Chem. Eng. Sci. 57, 3185–3215.

Briens, L.A., Briens, C.L., Margaritis, A., Hay, J., 1997. Minimum liquid fluidization velocity in gas-liquid-solid fluidized beds. AIChE J. 43, 1180–1189.

Brilman, D.W.F., Van Swaaij, W.P.M., Versteeg, G.F., 1999. Gas-liquid-liquid reaction engineering: The Koch synthesis of pivalic acid from iso- and tert-butanol; Reaction kinetics and the effect of a dispersed second-liquid phase. Chem. Eng. Sci. 54, 4801–4809.

Broering, S., Fischer, J., Korte, T., Sollinger, S., Luebbert, A., 1991. Flow structure of the dispersed gasphase in real multiphase chemical reactors investigated by a new ultrasound-doppler technique. Can. J. Chem. Eng. 69, 1247–1256.

Brooks, J.D., Taylor, G.H., 1965. The formation of graphitizing carbons from the liquid phase. Carbon N. Y. 3, 185–193.

Brown, P.P., Lawler, D.F., 2003. Sphere Drag and Settling Velocity Revisited. J. Environ. Eng. 129, 222–231.

Camarasa, E., Vial, C., Poncin, S., Wild, G., Midoux, N., Bouillard, J., 1999. Influence of coalescence behaviour of the liquid and of gas sparging on hydrodynamics and bubble characteristics in a bubble column. Chem. Eng. Process. Process Intensif. 38, 329–344.

Cameron, A., 1966. The principles of lubrication. Longmans, London.

CAPP, 2014. The Facts on: Oil Sands. Can. Assocation Pet. Prod.

Cartellier, A., 1992. Simultaneous void fraction measurement, bubble velocity, and size estimate using a single optical probe in gas–liquid two-phase flows. Rev. Sci. Instrum. 63, 5442.

Cartellier, A., Barrau, E., 1998a. Monofiber optical probes for gas detection and gas velocity measurements: optimised sensing tips. Int. J. Multiph. Flow 24, 1265–1294.

Cartellier, A., Barrau, E., 1998b. Monofiber optical probes for gas detection and gas velocity measurements: conical probes. Int. J. Multiph. Flow 24, 1265–1294.

Chabot, J., de Lasa, H.I., 1993. Gas holdups and bubble characteristics in a bubble column operated at high temperature. Ind. Eng. Chem. Res. 32, 2595–2601.

Chabot, J., Farag, H., De Lasa, H., 1998. Fluid dynamics of bubble columns at elevated temperature modelling and investigation with refractive fiber optic sensors. Chem. Eng. J. 70, 105–113.

Chaouki, J., Larachi, F., Dudukovic, M.P., 1997. Non-invasive monitoring of multiphase flows. Elsevier Science.

Chaudhari, R.V., Hofmann, H., 1994. Coalescence of gas bubbles in liquids. Rev. Chem. Eng. 10, 131–190.

Chaumat, H., Billet-Duquenne, A.M., Augier, F., Mathieu, C., Delmas, H., 2007. On the reliability of an optical fibre probe in bubble column under industrial relevant operating conditions. Exp. Therm. fluid Sci. 31, 495–504.

Chhabra, R.P., 1995. Wall effects on free-settling velocity of non-spherical particles in viscous media in cylindrical tubes. Powder Technol. 85, 83–90.

Chhabra, R.P., Agarwal, L., Sinha, N.K., 1999. Drag on non-spherical particles: an evaluation of available methods. Powder Technol. 101, 288–295.

Chiu, T.-M., Hoh, Y.-C., Wang, W.-K., 1987. Dispersed-Phase Hydrodynamic Characteristics and Mass Transfer in Three-Phase (Liquid-Liquid) Fluidized Beds. Ind. Eng. Chem. Res. 26, 712–718.

Dakshinamurty, P., Veerabhadrarao, K., Venkatarao, A.B., 1979. Bed Porosities in Three-Phase (Liquid-Liquid) Fluidized Beds. Ind. Eng. Chem. Process Des. Dev. 18, 638–640.

Dargar, P., Macchi, A., 2006. Effect of surface-active agents on the phase holdups of three-phase fluidized beds. Chem. Eng. Process. Process Intensif. 45, 764–772.

Davies, R.M., Taylor, G., 1950. The Mechanics of Large Bubbles Rising through Extended Liquids and through Liquids in Tubes. Proc. R. Soc. A Math. Phys. Eng. Sci. 200, 375–390.

Eastwood, J., Matzen, E.J.P., Young, M.J., Epstein, N., 1969. Random loose porosity of packed beds. Brit. Chem. Eng 14, 1542–1545.

Ennis, B.J., Tardos, G., Pfeffer, R., 1991. A microlevel-based characterization of granulation phenomena. Powder Technol. 65, 257–272.

Enrique Juliá, J., Harteveld, W.K., Mudde, R.F., Van den Akker, H.E. a., 2005. On the accuracy of the void fraction measurements using optical probes in bubbly flows. Rev. Sci. Instrum. 76, 035103.

Epstein, N., 1976. Criterion for initial contraction or expansion of three-phase fluidized beds. Can. J. Chem. Eng. 54, 259–263.

Epstein, N., 2003. Liquid-Solids Fluidization, in: Handbook of Fluidization and Fluid-Particle Systems. CRC press.

Ergun, S., 1952. Fluid flow through packed columns. Chem. Eng. Prog. 48, 89–94.

Ermakova, A., Ziganshin, G.K., Slin'ko, M.G., 1970. Hydrodynamics of a gas-liquid reactor with a fluidized bed of solid matter. Theor. Found. Chem. Eng 4, 84–89.

Fan, L.-S., 1989. Gas-Liquid-Solid Fluidization Engineering. Butterworths Publishers.

Fan, L.-S., Bavarian, F., Gorowara, R., Kreischer, B.E., Buttke, R.D., Peck, L.B., 1987. Hydrodynamics of gas—liquid—solid fluidization under high gas hold-up conditions. Powder Technol. 53, 285–293.

Fan, L.-S., Tsuchiya, K., 1990. Bubble wake dynamics in liquids and liquid-solid suspensions. Butterworth-Heinemann Stoneham.

Fan, L.-S., Yang, G., 2003. Gas-Liquid-Solid Three-Phase Fluidization, in: Handbook of Fluidization and Fluid-Particle Systems. CRC press.

Fan, L.-S., Yang, G.Q., Lee, D.J., Tsuchiya, K., Luo, X., 1999. Some aspects of high-pressure phenomena of bubbles in liquids and liquid–solid suspensions. Chem. Eng. Sci. 54, 4681–4709.

Fisher, R.A., 1926. On the capillary forces in an ideal soil; correction of formulae given by W. B. Haines. J. Agric. Sci. 16, 492.

Fouda, A.E., Capes, C.E., 1977. Hydrodynamic particle volume and fluidized bed expansion. Can. J. Chem. Eng. 55, 386–391.

Gabitto, J., Tsouris, C., 2008. Drag coefficient and settling velocity for particles of cylindrical shape. Powder Technol. 183, 314–322.

Gorowara, R.L., Fan, L.S., Gorowarat, R.L., 1990. Effect of surfactants on three-phase fluidized bed hydrodynamics. Ind. Eng. Chem. Res. 29, 882–891.

Gray, M.R., 1994. Upgrading petroleum residues and heavy oils. CRC press.

Gray, M.R., McCaffrey, W.C., 2002. Role of chain reactions and olefin formation in cracking, hydroconversion, and coking of petroleum and bitumen fractions. Energy & Fuels 16, 756–766.

Haider, A., Levenspiel, O., 1989. Drag coefficient and terminal velocity of spherical and nonspherical particles. Powder Technol. 58, 63–70.

Hamaker, H.C., 1937. The London—van der Waals attraction between spherical particles. Physica 4, 1058–1072.

Han, J.H., Wild, G., Kim, S.D., 1990. Phase holdup characteristics in three phase fluidized beds. Chem. Eng. J. 43, 67–73.

Hughmark, G.A., 1967. Holdup and Mass Transfer in Bubble Columns. Ind. Eng. Chem. Process Des. Dev. 6, 218–220.

Ishibashi, H., Onozaki, M., Kobayashi, M., Hayashi, J. -i., Itoh, H., Chiba, T., 2001. Gas holdup in slurry bubble column reactors of a 150t/d coal liquefaction pilot plant process. Fuel 80, 655–664.

Jiang, P., Luo, X., Lin, T.-J., Fan, L.-S., 1997. High temperature and high pressure three-phase fluidization—bed expansion phenomena. Powder Technol. 90, 103–113.

Jin, H., Yang, S., Zhang, T., Tong, Z., 2004. Bubble Behavior of a Large-Scale Bubble Column with Elevated Pressure. Chem. Eng. Technol. 27, 1007–1013.

Jordan, U., Saxena, A.K., Schumpe, A., 2003. Dynamic Gas Disengagement in a High-Pressure Bubble Column. Can. J. Chem. Eng. 81, 491–498.

Kantarci, N., Borak, F., Ulgen, K.O., 2005. Bubble column reactors. Process Biochem. 40, 2263–2283.

Kaur, R., Ramakrishna, M., Nigam, K.D.P., 2007. Role of dispersed phase in gas-liquid reactions: A review. Rev. Chem. Eng. 23, 247–300.

Kelkar, B.G., Godbole, S.P., Honath, M.F., Shah, Y.T., Carr, N.L., Deckwer, W., 1983. Effect of addition of alcohols on gas holdup and backmixing in bubble columns. AIChE J. 29, 361–369.

Khan, A.R., Richardson, J.F., 1987. The Resistance to Motion of a Solid Sphere in a Fluid. Chem. Eng. Commun. 62, 135–150.

Khan, A.R., Richardson, J.F., 1989. Fluid-Particle Interactions and Flow Characteristics of Fluidized Beds and Settling Suspensions of Spherical Particles. Chem. Eng. Commun. 78, 111–130.

Koide, K., Horibe, K., Kawabata, H., Ito, S., 1984. Critical gas velocity required for complete suspension of solid particles in solid-suspended bubble column with draught tube. J. Chem. Eng. Japan 14, 368–374.

Krishna, R., Ellenberger, J., 1996. Gas holdup in bubble column reactors operating in the churn-turbulent flow regime. AIChE J. 42, 2627–2634.

Krishna, R., Urseanu, M.., Dreher, A.., 2000. Gas hold-up in bubble columns: influence of alcohol addition versus operation at elevated pressures. Chem. Eng. Process. Process Intensif. 39, 371–378.

Krishna, R., Wilkinson, P.M., Van Dierendonck, L.L., 1991. A model for gas holdup in bubble columns incorporating the influence of gas density on flow regime transitions. Chem. Eng. Sci. 46, 2491–2496.

Kundu, A., Dumont, E., Duquenne, A.M., Delmas, H., 2003. Mass transfer characteristics in gas-liquid-liquid system. Can. J. Chem. Eng. 81, 640–646.

Kyu, K.B., Kwang, K., 1986. The behaviour of the dispersed phase in liquid-liquid extraction in fluidized beds. Chem. Eng. Commun. 41, 101–120.

Larachi, F., Belfares, L., Iliuta, I., Grandjean, B.P. a., 2001. Three-Phase Fluidization Macroscopic Hydrodynamics Revisited. Ind. Eng. Chem. Res. 40, 993–1008.

Lau, R., Hassan, M.S., Wong, W., Chen, T., 2010. Revisit of the Wall Effect on the Settling of Cylindrical Particles in the Inertial Regime. Ind. Eng. Chem. Res. 49, 8870–8876.

Lee, D., Epstein, N., Grace, J.R., 2003. The Variable-Voidage Effect on Modeling the Minimum Liquid Fluidization Velocity of Gas-Liquid Fluidized Beds. J. Chem. Eng. Japan 36, 1111–1115.

Lee, D.J., Luo, X., Fan, L.-S., 1999. Gas disengagement technique in a slurry bubble column operated in the coalesced bubble regime. Chem. Eng. Sci. 54, 2227–2236.

Levich, V.G., Spalding, D.B., 1962. Physicochemical hydrodynamics. Prentice-Hall Englewood Cliffs, NJ.

Lian, G., Thornton, C., Adams, M.J., 1998. Discrete particle simulation of agglomerate impact coalescence. Chem. Eng. Sci. 53, 3381–3391.

Lin, T.-J., Tsuchiya, K., Fan, L.S., 1998. Bubble flow characteristics in bubble columns at elevated pressure and temperature. AIChE J. 44, 545–560.

Luo, X., Jiang, P., Fan, L.-S., 1997. High-Pressure Three-Phase Fluidization: Hydrodynamics and Heat Transfer. AIChE J. 43, 2432–2445.

Luo, X., Lee, D.J., Lau, R., Yang, G., Fan, L.-S., 1999. Maximum stable bubble size and gas holdup in high-pressure slurry bubble columns. AIChE J. 45, 665–680.

Macchi, A., 2002. Dimensionless hydrodynamic simulation of high pressure multiphase reactors subject to foaming. Dep. Chem. Biol. Eng.

Macchi, A., Bi, H., Grace, J.R., McKnight, C.A., Hackman, L., 2001a. Dimensional hydrodynamic similitude in three-phase fluidized beds. Chem. Eng. Sci. 56, 6039–6045.

Macchi, A., Bi, H., Grace, J.R., McKnight, C.A., Hackman, L., 2003. Effect of Gas Density on the Hydrodynamics of Bubble Columns and Three-Phase Fluidized Beds. Can. J. Chem. Eng. 81, 846–852.

Macchi, A., Grace, J.R., Bi, H., 2001b. Use of ultrasound for phase holdup measurements in multiphase systems. Can. J. Chem. Eng. 79, 570–578.

Magaud, F., Souhar, M., Wild, G., Boisson, N., 2001. Experimental study of bubble column hydrodynamics. Chem. Eng. Sci. 56, 4597–4607.

Marsh, H., Latham, C.S., 1986. The chemistry of mesophase formation. Pet. Deriv. Carbons 1–28.

Mazzone, D.N., Tardos, G.I., Pfeffer, R., 1987. The behavior of liquid bridges between two relatively moving particles. Powder Technol. 51, 71–83.

McKnight, C.A., Hackman, L.P., Grace, J.R., Macchi, A., Kiel, D., Tyler, J., 2003. Fluid Dynamic Studies in Support of an Industrial Three-Phase Fluidized Bed Hydroprocessor. Can. J. Chem. Eng. 81, 338–350.

McMillan, J., Shaffer, F., Gopalan, B., Chew, J.W., Hrenya, C., Hays, R., Karri, S.B.R., Cocco, R., 2013. Particle cluster dynamics during fluidization. Chem. Eng. Sci. 100, 39–51.

Mena, P.C., Rocha, F.A., Teixeira, J.A., Sechet, P., Cartellier, A., 2008. Measurement of gas phase characteristics using a monofibre optical probe in a three-phase flow. Chem. Eng. Sci. 63, 4100–4115.

Mizushima, Y., Sakamoto, A., Saito, T., 2013. Measurement technique of bubble velocity and diameter in a bubble column via single-tip optical-fiber probing with judgment of the pierced position and angle. Chem. Eng. Sci. 100, 98–104.

Mohagheghi, M., Hamidi, M., Briens, C., Berruti, F., McMillan, J., 2014. The effects of liquid properties and bed hydrodynamics on the distribution of liquid on solid fluidized particles in a cold-model fluidized bed. Powder Technol. 256, 5–12.

Moujaes, S.F., 1990. Testing of a spherical dual-tipped optical fiber probe for local measurements of void fraction and gas velocity in two-phase flows. Can. J. Chem. Eng. 68, 504–510.

Muroyama, K., Fan, L.-S., 1985. Fundamentals of gas-liquid-solid fluidization. AIChE J. 31, 1–34.

O'Connor, C.T., Randall, E.W., Goodall, C.M., 1990. Measurement of the effects of physical and chemical variables on bubble size. Int. J. Miner. Process. 28, 139–149.

Pal, R., 2000. Shear Viscosity Behavior of Emulsions of Two Immiscible Liquids. J. Colloid Interface Sci. 225, 359–366.

Park, A.-H., Fan, L.-S., 2007. Electrostatic charging phenomenon in gas–liquid–solid flow systems. Chem. Eng. Sci. 62, 371–386.

Park, A.-H.A., Bi, H.T., Grace, J.R., Chen, A., 2002. Modeling charge transfer and induction in gas–solid fluidized beds. J. Electrostat. 55, 135–158.

Parveen, F., Berruti, F., Briens, C., McMillan, J., 2013a. Effect of fluidized bed particle properties and agglomerate shape on the stability of agglomerates in a fluidized bed. Powder Technol. 237, 46–52.

Parveen, F., Berruti, F., Briens, C., McMillan, J., 2013b. Effect of particle size, liquid content and location on the stability of agglomerates in a fluidized bed. Powder Technol. 237, 376–385.

Pitois, O., Moucheront, P., Chateau, X., 2000. Liquid Bridge between Two Moving Spheres: An Experimental Study of Viscosity Effects. J. Colloid Interface Sci. 231, 26–31.

Pjontek, D., Hackman, L.P., Landry, J., McKnight, C.A., Macchi, A., 2011. Effect of a dispersed immiscible liquid phase on the hydrodynamics of a bubble column and ebullated bed. Chem. Eng. Sci. 66, 2224–2231.

Pjontek, D., Macchi, A., 2014. Hydrodynamic comparison of spherical and cylindrical particles in a gas–liquid–solid fluidized bed at elevated pressure and high gas holdup conditions. Powder Technol. 253, 657–676.

Pjontek, D., Parisien, V., Macchi, A., 2014. Bubble characteristics measured using a monofibre optical probe in a bubble column and freeboard region under high gas holdup conditions. Chem. Eng. Sci. 111, 153–169.

Rana, M.S., Sámano, V., Ancheyta, J., Diaz, J.A.I., 2007. A review of recent advances on process technologies for upgrading of heavy oils and residua. Fuel 86, 1216–1231.

Rao, N.S., Setty, Y.P., 2000. Total liquid holdup in a liquid-liquid-solid fluidized bed. J. Inst. Eng. Chem. Eng. Div. 81, 18–20.

Richardson, J.F., Zaki, W.N., 1954. Sedimentation and fluidisation, Part 1. Trans Instn Chem Engrs 32, 357–362.

Roszak, J., Gawroński, R., 1979. Cocurrent liquid-liquid extraction in fluidized beds. Chem. Eng. J. 17, 101–109.

Rudkevitch, D., Macchi, A., 2008. Hydrodynamics of a high pressure three-phase fluidized bed subject to foaming. Can. J. Chem. Eng. 86, 293–301.

Ruiz, R.S., Alonso, F., Ancheyta, J., 2004. Effect of high pressure operation on overall phase holdups in ebullated-bed reactors. Catal. Today 98, 265–271.

Ruiz, R.S., Alonso, F., Ancheyta, J., 2004. Minimum Fluidization Velocity and Bed Expansion Characteristics of Hydrotreating Catalysts in Ebullated-Bed Systems. Energy & Fuels 18, 1149–1155.

Ruiz, R.S., Alonso, F., Ancheyta, J., 2005. Pressure and temperature effects on the hydrodynamic characteristics of ebullated-bed systems. Catal. Today 109, 205–213.

Safoniuk, M., Grace, J.R., Hackman, L., McKnight, C.A., 1999. Use of dimensional similitude for scale-up of hydrodynamics in three-phase fluidized beds. Chem. Eng. Sci. 54, 4961–4966.

Sagert, N.H., Quinn, M.J., 1977. Influence of high-pressure gases on the stability of thin aqueous films. J. Colloid Interface Sci. 61, 279–286.

Sagert, N.H., Quinn, M.J., 1978. Surface viscosities at high pressure gas-liquid interfaces. J. Colloid Interface Sci. 65, 415–422.

Sanchez, J., Ruiz, R.S., Alonso, F., Ancheyta, J., Sánchez, J.L., 2008. Evaluation of the hydrodynamics of high-pressure ebullated beds based on dimensional similitude. Catal. Today 130, 519–526.

Schäfer, R., Merten, C., Eigenberger, G., 2002. Bubble size distributions in a bubble column reactor under industrial conditions. Exp. Therm. Fluid Sci. 26, 595–604.

Seville, J.P.K., Willett, C.D., Knight, P.C., 2000. Interparticle forces in fluidisation: a review. Powder Technol. 113, 261–268.

Shah, Y.T., Joseph, S., Smith, D.N., Ruether, J.A., 1985. On the behavior of the gas phase in a bubble column with ethanol-water mixtures. Ind. Eng. Chem. Process Des. Dev. 24, 1140–1148.

Shah, Y.T., Kelkar, B.G., Godbole, S.P., Deckwer, W.-D.D., 1982. Design Parameters Estimations for Bubble Column Reactors. AIChE J. 28, 353–379.

Shaikh, A., Al-Dahhan, M., 2010. A new methodology for hydrodynamic similarity in bubble columns. Can. J. Chem. Eng. 88, 503–517.

Shaikh, A., Al-Dahhan, M., 2013. Scale-up of Bubble Column Reactors: A Review of Current State-of-the-Art. Ind. Eng. Chem. Res. 52, 8091–8108.

Shaikh, A., Al-Dahhan, M.H., 2007. A Review on Flow Regime Transition in Bubble Columns. Int. J. Chem. React. Eng. 5.

Shiea, M., Mostoufi, N., Sotudeh-Gharebagh, R., 2013. Comprehensive study of regime transitions throughout a bubble column using resistivity probe. Chem. Eng. Sci. 100, 15–22.

Shinto, H., Komiyama, D., Higashitani, K., 2007. Lattice Boltzmann study of capillary forces between cylindrical particles. Adv. Powder Technol. 18, 643–662.

Simons, S.J.R., 1996. Modelling of agglomerating systems: from spheres to fractals. Powder Technol. 87, 29–41.

Simons, S.J.R., Fairbrother, R.J., 2000. Direct observations of liquid binder–particle interactions: the role of wetting behaviour in agglomerate growth. Powder Technol. 110, 44–58.

Simons, S.J.R., Seville, J.P.K., Adams, M.J., 1994. An analysis of the rupture energy of pendular liquid bridges. Chem. Eng. Sci. 49, 2331–2339.

Sinha, V.T., Butensky, M.S., Hyman, D., 1986. Comparison of cylinders and spheres in three-phase fluidization. Ind. Eng. Chem. Process Des. Dev. 25, 321–324.

Siquier, S., Yépez, M.M., Sáez, A.E., 1991. Solid distribution in a slurry bubble column with two immiscible liquid phases. AIChE J. 37, 466–469.

Song, G.-H., Bavarian, F., Fan, H.-S., Buttke, R.D., Peck, L.B., 1989. Hydrodynamics of three-phase fluidized bed containing cylindrical hydrotreating catalysts. Can. J. Chem. Eng. 67, 265–275.

Song, P.S., Lee, C.G., Kang, S.H., Son, S.M., Kang, Y., Kim, S.D., 2005. Drop properties and pressure fluctuations in liquid-liquid-solid fluidized-bed reactors. Chem. Eng. Process. Process Intensif. 44, 1296–1305.

Soong, Y., Harke, F.W., Gamwo, I.K., Schehl, R.R., Zarochak, M.F., 1997. Hydrodynamic study in a slurry-bubble-column reactor. Catal. Today 35, 427–434.

Soung, W.Y., 1978. Bed expansion in three-phase fluidization. Ind. Eng. Chem. Process Des. Dev. 17, 33–36.

Sowinski, A., Miller, L., Mehrani, P., 2010. Investigation of electrostatic charge distribution in gas–solid fluidized beds. Chem. Eng. Sci. 65, 2771–2781.

Srinivasan, N.S., McKnight, C.A., 1994. Mechanism of coke formation from hydrocracked Athabasca residuum. Fuel 73, 1511–1517.

Steinour, H.H., 1944. Rate of sedimentation. Suspensions of uniform-size angular particles. Ind. Eng. Chem 36, 840–847.

Subramanian, P., Arunachalam, V., 1980. A simple device for the determination of sphericity factor. Ind. Eng. Chem. Fundam. 19, 436–437.

Tarmy, B.L., Chang, M., Coulaloglou, C.A., Ponzi, P.R., 1984. Three Phase Hydrodynamic Characteristics of the EDS Coal Liquefaction Reactors: Their Development and Use in Reactor Scaleup. Inst. Chem. Eng. Symp. Ser. 87, 303–317.

Tarmy, B.L., Coulaloglou, C.A., 1992. Alpha-omega and beyond industrial view of gas/liquid/solid reactor development. Chem. Eng. Sci. 47, 3231–3246.

Turton, R., Clark, N., 1987. An explicit relationship to predict spherical particle terminal velocity. Powder Technol. 53, 127–129.

Urseanu, M.I., Guit, R.P.M., Stankiewicz, A., van Kranenburg, G., Lommen, J.H.G.M., 2003. Influence of operating pressure on the gas hold-up in bubble columns for high viscous media. Chem. Eng. Sci. 58, 697–704.

Urso, M., Lawrence, C., Adams, M., 1999. Pendular, Funicular, and Capillary Bridges: Results for Two Dimensions. J. Colloid Interface Sci. 220, 42–56.

Utiger, M., Guy, C., Stuber, F., Duquenne, A., Delmas, H., 1999. Local measurements for the study of external loop airlift hydrodynamics. Can. J. Chem. Eng. 77, 375–382.

Vejražka, J., Večeř, M., Orvalho, S., Sechet, P., Ruzicka, M.C., Cartellier, A., 2010. Measurement accuracy of a mono-fiber optical probe in a bubbly flow. Int. J. Multiph. Flow 36, 533–548.

Virozub, A., Haimovich, N., Brandon, S., 2009. Three-dimensional simulations of liquid bridges between two cylinders: forces, energies, and torques. Langmuir 25, 12837–42.

Weber, S., Briens, C., Berruti, F., Chan, E., Gray, M., 2006. Agglomerate stability in fluidized beds of glass beads and silica sand. Powder Technol. 165, 115–127.

Weber, S., Briens, C., Berruti, F., Chan, E., Gray, M., 2008. Effect of agglomerate properties on agglomerate stability in fluidized beds. Chem. Eng. Sci. 63, 4245–4256.

Weber, S., Briens, C., Berruti, F., Chan, E., Gray, M., 2011. Stability of agglomerates made from fluid coke at ambient temperature. Powder Technol. 209, 53–64.

Wen, C.Y., Yu, Y.H., 1966. A generalized method for predicting the minimum fluidization velocity. AIChE J. 12, 610–612.

Wiehe, I.A., 1994. The pendant-core building block model of petroleum residua. Energy & Fuels 8, 536–544.

Wild, G., Poncin, S., 1996. Hydrodynamics, in: Nigam, K.D.P., Shumpe, A. (Eds.), Three-Phase Sparged Reactors. Gordon and Breach, Netherlands, pp. pp. 11–112.

Wilkinson, P.M., Dierendonck, L.L. v., 1990. Pressure and gas density effects on bubble break-up and gas hold-up in bubble columns. Chem. Eng. Sci. 45, 2309–2315.

Wilkinson, P.M., Spek, A.P., van Dierendonck, L.L., 1992. Design parameters estimation for scale-up of high-pressure bubble columns. AIChE J. 38, 544–554.

Xue, J., Al-Dahhan, M., Dudukovic, M.P., Mudde, R.F., 2003. Bubble Dynamics Measurements Using Four-Point Optical Probe. Can. J. Chem. Eng. 81, 375–381.

Xue, J., Al-Dahhan, M., Dudukovic, M.P., Mudde, R.F., 2008. Four-point optical probe for measurement of bubble dynamics: Validation of the technique. Flow Meas. Instrum. 19, 293–300.

Yang, G.Q., Du, B., Fan, L.S., 2007. Bubble formation and dynamics in gas–liquid–solid fluidization—A review. Chem. Eng. Sci. 62, 2–27.

Yang, X.L., Euzen, J.P., Wild, G., 1993. Study of liquid retention in fixed-bed reactors with upward flow of gas and liquid. Int. Chem. Eng. (A Q. J. Transl. from Russ. East. Eur. Asia);(United States) 33.

Yaron, I., Gal-Or, B., 1972. On viscous flow and effective viscosity of concentrated suspensions and emulsions - Effect of particle concentration and surfactant impurities. Rheol. Acta 11, 241–252.

Zhang, J.P., Epstein, N., Grace, J.R., 1998. Minimum fluidization velocities for gas-liquid-solid three-phase systems. Powder Technol. 100, 113–118.

Zou, R.P., Yu, A.B., 1996. Evaluation of the packing characteristics of mono-sized non-spherical particles. Powder Technol. 88, 71–79.